

# *3D porous sponges from electrospun polymer fibers and their applications*

## DISSERTATION

zur Erlangung des akademischen Grades einer Doktorin/  
eines Doktors der Naturwissenschaften (Dr. rer. nat.)  
an der Bayreuther Graduiertenschule für Mathematik und  
Naturwissenschaften (BayNAT) der Universität Bayreuth

vorgelegt von

***Gaigai Duan***

*Geboren in Ye county, Henan Province, China*

Bayreuth 2017



This doctoral thesis was prepared at the Chair of Macromolecular Chemistry II at the University of Bayreuth from 10/2012 until 02/2017 and was supervised by Prof. Dr. Andreas/Greiner. (with first child and take care of my son: from 10/2015 until 11/2016).

This is a full reprint of the dissertation submitted to obtain the academic degree of Doctor of Natural Sciences (Dr. Rer. nat.) and approved by the Bayreuth Graduate School of Mathematical and Natural Sciences (BayNAT) of the University of Bayreuth.

Date of submission: 06.03.2017

Date of defense: 26.07.2017

Acting director: Prof. Dr. Stephan Kümmel

Doctoral committee:

Prof. Dr. Andreas Greiner           (1st reviewer)

Prof. Dr. Ruth Freitag           (2nd reviewer)

Prof. Dr. Birgit Weber           (chairman)

Prof. Dr. Peter Strohriegl

(3<sup>rd</sup> reviewer: Prof. Dr. Rudolf Zentel)



## Table of content

<b>Table of content</b> .....	1
<b>List of Figures</b> .....	3
<b>List of Tables</b> .....	8
<b>List of symbols and abbreviations</b> .....	9
<b>Summary/Zusammenfassung</b> .....	13
Summary .....	13
Zusammenfassung.....	15
<b>1 Introduction</b> .....	19
1.1 Motivation.....	19
1.2 Submicrometer fibers by electrospinning.....	19
1.2.1 Solution, melt and emulsion electrospinning.....	20
1.2.2 Materials for electrospinning .....	21
1.2.3 Morphology of electrospun fibers.....	23
1.2.4 Short electrospun fibers .....	25
1.2.5 Assembly of electrospun fibers .....	27
1.2.6 Applications of electrospun materials.....	31
1.3 Ultralight porous 3D materials .....	41
1.3.1 Carbon-based ultralight porous 3D materials .....	41
1.3.2 Polymer-based ultralight porous 3D materials .....	43
1.3.3 Inorganic ultralight porous 3D materials.....	45
1.3.4 Hybrid-based ultralight porous 3D materials .....	47
1.3.5 Modifications on ultralight porous 3D materials .....	48
1.4 References.....	49
<b>2 Cumulative part of dissertation</b> .....	65
2.1 Ultralight, soft polymer sponges by self-assembly of short electrospun fibers in colloidal dispersions .....	67
2.2 Ultralight open cell polymer sponges with advanced properties by PPX CVD coating.....	72
2.3 Highly efficient reusable sponge-type catalyst carriers based on short electrospun fibers .....	76

2.4 Polymeric fibrous sponge as drug-delivery system with ultra-high drug loading capacity and retarded release of Artemisone.....	80
2.5 Spongy gels by a top-down approach from polymer fibrous sponges .....	85
<b>3 Publications</b> .....	<b>89</b>
3.1 Ultralight, soft polymer sponges by self-assembly of short electrospun fibers in colloidal dispersions .....	90
3.2 Ultralight open cell polymer sponges with advanced properties by PPX CVD coating.....	106
3.3 Highly efficient reusable sponge-type catalyst carriers based on short electrospun fibers .....	114
3.4 Polymeric fibrous sponge as drug-delivery system with ultra-high drug loading capacity and retarded release of Artemisone.....	128
3.5 Spongy gels by a top-down approach from polymer fibrous sponges .....	136
<b>4 Outlook</b> .....	<b>149</b>
<b>5 Acknowledgements</b> .....	<b>150</b>
<b>6 List of publications</b> .....	<b>152</b>

## List of Figures

<b>Figure 1-1.</b> Schematic drawing of solution (a), melt (b) and emulsion (c) electrospinning. ....	21
<b>Figure 1-2.</b> Electrospun fibers with porous structure of PLA (a) (Reprinted with permission from ref. [48]. Copyright 2010, Springer) and PS (b) (Reprinted with permission from ref. [49]. Copyright 2004, American Chemical Society), necklace-like (c) (Reprinted with permission from ref. [50]. Copyright 2010, American Chemical Society), firecracker-shaped (d) (Reprinted with permission from ref. [51]. Copyright 2011, Royal Society of Chemistry), rice grain-shaped (e) (Reprinted with permission from ref. [52]. Copyright 2011, Royal Society of Chemistry), ribbon-like and branched (f and g) (Reprinted with permission from ref. [53]. Copyright 2001, John Wiley and Sons), and barbed (h) morphologies (Reprinted with permission from ref. [54]. Copyright 2008, John Wiley and Sons). ....	23
<b>Figure 1-3.</b> Core-sheath (a) (Reprinted with permission from ref. [19]. Copyright 2003, John Wiley and Sons), hollow (b) (Reprinted with permission from ref. [55]. Copyright 2004, American Chemical Society), triaxial (c) (Reprinted with permission from ref. [28]. Copyright 2014, American Chemical Society), Janus (d) (Reprinted with permission from ref. [56]. Copyright 2014, John Wiley and Sons), spring (e) (Reprinted with permission from ref. [9]. Copyright 2009, John Wiley and Sons), nanowire-in-microtube (f) (Reprinted with permission from ref. [58]. Copyright 2010, American Chemical Society), and multi-channel tubular (g-j) (Reprinted with permission from ref. [57]) structures of electrospun fibers obtained by the modification of spinnerets.....	24
<b>Figure 1-4.</b> Short electrospun fibers. (a) Polymethylsilsesquioxane (PMSQ) (Reprinted with permission from ref. [59]. Copyright 2011, Springer), (b) cellulose acetate (Reprinted with permission from ref. [60]. Copyright 2014, Springer), (c) cellulose/TiO <sub>2</sub> (Reprinted with permission from ref. [61]. Copyright 2014, Elsevier), (d) UV cross-linked polymer (Reprinted with permission from ref. [62]. Copyright 2008, John Wiley and Sons), (e) glass (Reprinted with permission from ref. [63]. Copyright 2015, John Wiley and Sons), (f) PS (Reprinted with permission from ref. [64]. Copyright 2013, Elsevier), (g) carbon (Reprinted with permission from ref. [65]. Copyright 2015, Elsevier), (h) Co/P(MMA-c-VA) (Reprinted with permission from ref. [66]. Copyright 2007, John Wiley and Sons), (i) nylon-6 (Reprinted with permission from ref. [67]. Copyright 2013, Elsevier), (j) polyimide (PI) (Reprinted with permission from ref. [68]. Copyright 2013, Elsevier), (k) poly(lactide-co-ethylene oxide) (Reprinted with permission from ref. [69]. Copyright 2009, John Wiley and Sons), and (l) cross-linked poly(MA-MMA-MABP) ([70]. Open access, John Wiley and Sons).....	26
<b>Figure 1-5.</b> Comparison of specific strength and specific energy to failure of as-spun PAN nanofibers (diamonds) with typical values for commercial and developmental fibers and materials. The arrow density indicates approximate values of nanofiber diameters (see scale bar). The colored area represents the strength/toughness region occupied by traditional materials. (Reprinted with permission from ref. [74]. Copyright 2013, American Chemical Society). ....	28

- Figure 1-6.** 2D electrospun fiber assembly. (a) Randomly (Reprinted with permission from ref. [5]. Copyright 2007, John Wiley and Sons), (b) (Reprinted with permission from ref. [77]. Copyright 2015, Royal Society of Chemistry) and (c) aligned (Reprinted with permission from ref. [78]. Copyright 2007, American Chemical Society), (d) (Reprinted with permission from ref. [82]. Copyright 2004, John Wiley and Sons) and (e) (Reprinted with permission from ref. [79]. Copyright 2007, John Wiley and Sons) weaved, (f) fan-shape (Reprinted with permission from ref. [80]. Copyright 2008, Royal Society of Chemistry) and (g) grid-patterned (Reprinted with permission from ref. [81]. Copyright 2007, John Wiley and Sons). .....29
- Figure 1-7.** 3D electrospun fibrous porous materials. (a) zein electrospun scaffolds (Reprinted with permission from ref. [88]. Open access, American Chemical Society), (b) 3D fibrous tubes with different shapes (Reprinted with permission from ref. [89]. Copyright 2008, American Chemical Society), (c) poly(lactic acid-co-glycolic acid) (PLGA) (Reprinted with permission from ref. [90]. Copyright 2007, John Wiley and Sons), (d) hyaluronic acid/collagen/salt hybrid scaffold (Reprinted with permission from ref. [92]. Copyright 2008, Elsevier), (e) PLLA (Reprinted with permission from ref. [91]. Copyright 2011, Elsevier), (f) carbon (Reprinted with permission from ref. [86]. Copyright 2011, Royal Society of Chemistry), (g) cross-linked poly(MA-co-MMA-co-ABP) (Reprinted with permission from ref. [70]. Open access, John Wiley and Sons), (h) PAN/SiO<sub>2</sub> (Reprinted with permission from ref. [71]. Copyright 2014, Nature Publishing Group) and (i) PCL (Reprinted with permission from ref. [93]. Copyright 2015, John Wiley and Sons).....31
- Figure 1-8.** Electrospun PA6 nanofiber membranes with different mean fiber diameters of (a) 100 nm, (b) 430 nm and (c) 730 nm, and their pressure drop (d) and filtration efficiency (e) performance for filtration application (Reprinted with permission from ref. [98]. Copyright 2008, Springer). .....32
- Figure 1-9.** Schematics of preparation of 3D PA66 nanofiber/nets on nonwoven PP scaffold and their filtration process (a-c) (Reprinted with permission from ref. [106]. Copyright 2011, Royal Society of Chemistry), transparent polymeric nanofibers on fiber glass wire mesh with different optical transparency of 85, 75, 55, 30 and 10% (d) and optical microscopy images on in-situ study of PM capture at different time (e) (Reprinted with permission from ref. [107]. Copyright 2015, Nature Publishing Group). .....33
- Figure 1-10.** Electrospun PVDF fiber membrane for particle separation (a) (Reprinted with permission from ref. [108]. Copyright 2006, Elsevier), grain proteins/PEO composite fiber membrane for bacteria filtration (b) (Reprinted with permission from ref. [115]. Copyright 2016, Royal Society of Chemistry) and cellulose acetate electrospun fibers mat before (c) and after (d) Cu(II) adsorption (Reprinted with permission from ref. [118]. Copyright 2011, Elsevier). .....34
- Figure 1-11.** A schematic showing the electrospun membrane for oil/water separation. (a) Electrospinning process, (b) a schematic of separation process, (c) SEM images with high and low magnifications, (d) A photograph showing superoleophilic and superhydrophobic PS nanofiber membrane, and (e) The real scale as-prepared PS nanofiber membrane attached to the stainless mesh, whose size is compared with a

coin (Reprinted with permission from ref. [121]. Copyright 2013, American Chemical Society).....	35
<b>Figure 1-12.</b> Electrospun PET nanofibers from recycled PET bottles (a), fiber mats before (b) and after (c) smoke filtration testing (1.0 mm diameter), IR-spectroscopy (e) of a clean fiber mat compared to that of smoke-exposed fiber mats with different fiber diameters (Reprinted with permission from ref. [136]. Open access, Royal Society of Chemistry).....	36
<b>Figure 1-13.</b> Effect of electrospun fiber alignment on the grow of cells (Reprinted with permission from ref. [153]. Copyright 2015, Elsevier). ....	37
<b>Figure 1-14.</b> (a) ECNF supported electroactive biofilm for microbial fuel cells (Reprinted with permission from ref. [162]. Copyright 2011, Royal Society of Chemistry), (b) platinum clusters deposited on ECNFs for catalyzing methanol oxidation (Reprinted with permission from ref. [164]. Copyright 2008, Elsevier) and (c) electrospun Bi <sub>2</sub> O <sub>3</sub> fibers for photodegradation of thevorganic pollutant Rhodamine B (Reprinted with permission from ref. [171]. Copyright 2009, Elsevier). ....	39
<b>Figure 1-15.</b> A monolithic CNT sponge with a bulk density of 7.5 mg/cm <sup>3</sup> (a), cross-sectional SEM image of (a) showing a porous morphology and overlapped CNT (b), illustration of the sponge consisting of CNT piles (black lines) as the skeleton and open pores (c), images of the fabrication process of the graphene aerogel (d), an image of an original aerogel (left) and a flame treated aerogel (right) sitting on a green bristlegrass (e), SEM image of the cellulose fibers in raw cotton (f), SEM image of the carbon fibers in carbon fiber aerogel (g), photograph of a water droplet supported on a carbon fiber aerogel (h) and mirror-reflection can be observed when a carbon fiber aerogel was immersed into water, which is convincing evidence for the hydrophobicity of the TCF aerogel (i). (a-c) (Reprinted with permission from ref. [207]. Copyright 2009, John Wiley and Sons), (d, e) (Reprinted with permission from ref. [211]. Copyright 2013, Royal Society of Chemistry) and (f-i) (Reprinted with permission from ref. [212]. Copyright 2013, John Wiley and Sons). ....	42
<b>Figure 1-16.</b> (a) Compressed cross-linked native cellulose nano/micro fibrillar cellulose aerogels with fast recovery properties in water (Reprinted with permission from ref. [219]. Copyright 2012, Royal Society of Chemistry), (b) ultra-flyweight hydrophobic poly(m-phenylenediamine) aerogel with compression recovery for 50 cycles (Reprinted with permission from ref. [232]. Copyright 2014, Royal Society of Chemistry), (c) PVDF sponges loaded with amoxicillin for drug release (Reprinted with permission from ref. [233]. Copyright 2011, Elsevier), and (d) electrospun polymer nanofibers for cell culture (green: live cells; red: dead cells) (Reprinted with permission from ref. [70]. Open access, John Wiley and Sons).....	44
<b>Figure 1-17.</b> Loading (a) and release (b) profiles of ketoprofen from hydrophilic and hydrophobic silica aerogels of different densities in 0.1N HCl at 37 °C (Reprinted with permission from ref. [240]. Copyright 2004, Elsevier). ....	45
<b>Figure 1-1-18.</b> Silica aerogel sample with refractive index (n) = 1.045 and size of 18 × 18 × 2 cm <sup>3</sup> (a) and UV-Vis spectra of 20 mm thick aerogel tiles with n = 1.045 and n = 1.055, respectively (b) (Reprinted with permission from ref. [245]. Copyright 2016, Elsevier).....	46

<b>Figure 1-19.</b> 3D porous boron nitride foam with thermal stability to 850 oC, mechanical recovery and low dielectric constant (Reprinted with permission from ref. [253]. Copyright 2013, American Chemical Society).....	47
<b>Figure 1-20.</b> A schematic illustration of the preparation of 3D porous Fe <sub>2</sub> O <sub>3</sub> /graphene oxide hybrid aerogel (a), SEM image showing the 3D macroporous structure (b) and the discharge curves at the current density of 100 mA/g between 0.01 and 3.0 V in the first, second, fifth and 50 <sup>th</sup> cycle (Reprinted with permission from ref. [264]. Copyright 2013, American Chemical Society). ....	48
<b>Figure 2-1.</b> Preparation of fibrous and porous sponge from short electrospun fibers and the porous structure of the sponge. ....	69
<b>Figure 2-2.</b> Digital photos of the reversibly compressive and bendable sponge (a), compression stress-strain curves of the sponges with different densities (b), and Ashby plot of the compression stress vs density with comparison to other porous materials. (1) boron nitride, (2) carbon nanotube, (3) carbon aerogel, (4) cellulose fiber, (5) cross-linked polystyrene, (6) polyolefin (closed cell), (7) polyethylene (closed cell), (8) polyimide, (9) polyethylene (50% strain), (10) silk fibroin, (11) melamine-formaldehyde (rigid), (12) tannin-based (rigid), (13) PDLLA/Bioglass composite, (14) latex rubber, (15) PAN-microspheres and fibers, (16) rigid polyurethane, (17) PVC (cross-linked), (18) epoxy-boroxine, (19) bio-based macroporous polymers, (20) silicon oxycarbide ceramic, (21) aluminum foams. ....	70
<b>Figure 2-3.</b> Weight gain of liquids (mineral oil, cyclohexane and petroleum ether) (a) and reversible sorption and desorption of cyclohexane (b) from the porous sponge; Jurkat cells colonized on a sponge (c); and 3D confocal images of Jurkat cells incubation for 13, 20 and 30 days in the sponges (d), where green and red color indicated the live and dead cells. ....	71
<b>Figure 2-4.</b> Digital photo of PPX-coated sponge (a); SEM images of original sponge (b, c) with density of 5.16 mg/cm <sup>3</sup> , and the corresponding sponge after PPX coating with 1000 nm (d, e); Typical water contact angle of sponges with different PPX coating thicknesses (f). ....	73
<b>Figure 2-5.</b> Compression stress-strain curves of the sponges with different densities and different PPX coating thicknesses. The densities for the sponges without PPX coating of (a), (b), (c) and (d) are 4.34, 5.16, 7.43 and 8.42 mg/cm <sup>3</sup> , respectively. ....	74
<b>Figure 2-6.</b> Solvent resistance of the sponges without (a) and with (b) 280 nm PPX coating.....	75
<b>Figure 2-7.</b> Procedure of the preparation of Au-sponges.....	77
<b>Figure 2-8.</b> SEM image of Au-sponge <sub>3.56</sub> (a), EDX spectra of AuNP-immobilized fibers (b), TEM images of AuNPs on the sponge (c), and cyclic compression measurement of Au-sponge <sub>3.56</sub> (d).....	78
<b>Figure 2-9.</b> UV-Vis spectra to monitor the reduction of 4-nitrophenol using Au-sponge <sub>0.29</sub> (a) and Au-sponge <sub>3.56</sub> (b) as catalysts, and Ashby plot of the comparison of normalized rate constant ( $K_{nor}$ ) versus the amount of AuNPs on the different kinds of supports. ....	79
<b>Figure 2-10.</b> Procedure of the preparation of drug-loaded sponge. ....	81
<b>Figure 2-11.</b> SEM images of as-prepared sponge (3.5 mg/cm <sup>3</sup> , SG <sub>3.5</sub> ) (a), sponge (6	

---

mg/cm <sup>3</sup> , SG6) loading with drug Artemisone (b, c), drug-loaded SG6 after coating with PPX thickness of 150 nm (d) and 423 nm (e), and the corresponding EDX mapping of Artemisone distribution in the sponges by monitoring the sulfur element (f). ....	82
<b>Figure 2-12.</b> Drug loading capacity of sponges with comparison to other supporters. ....	83
<b>Figure 2-13.</b> Drug release profile of drug-loaded sponges with densities of 3.5 and 6 mg/cm <sup>3</sup> and PPX coating thicknesses of 0, 88, 150, 423 and 1000 nm.....	84
<b>Figure 2-14.</b> Sponge made from electrospun fibers (a) and the spongy gel after uptake of mineral oil. ....	86
<b>Figure 2-15.</b> Dynamic oscillatory shear rheological properties of spongy gel loaded with ethylene glycol as functions of strain (a), temperature (b), and frequency at 25 (c) and 50 °C (d).....	87
<b>Figure 2-16.</b> Evaporation of water and ethanol from sponges of P-SG1 and P-SG2....	88

## List of Tables

**Table 1-1.** Summary of typical polymers and solvents for electrospinning.....22

## List of symbols and abbreviations

°C	degree Celsius
1D	one dimensional
2D	two dimensional
3D	three dimensional
AcOH	acetic acid
AIBN	2,2'-azobis(isobutyronitrile)
AuNPs	Gold nanoparticles, Au nanoparticles
C	concentration
cm <sup>3</sup>	cubic centimeter
CNTs	carbon nanotubes
CVD	chemical vapor deposition
d	day
DMAc	dimethylacetamide
DMF	dimethylformamide
DMSO	dimethyl sulfoxide
ECNFs	electrospun carbon nanofibers
EDX	energy-dispersive X-ray spectroscopy
FA	formic acid
g	gram
h	hour
HFIP	1,1,1,3,3,3-hexafluoro-2-propanol
K	Kelvin
K <sub>nor</sub>	normalized reaction rate constant

Pa	Pascal
V	volt
L	length
m	meter
MA	methylacrylate
MABP	methacryloyloxybenzophenone
min	minute
mL	milliliter
MMA	methyl methacrylate
MOF	metal organic framework
P2VP	poly(2-vinyl pyridine)
P4VP	poly(4-vinyl pyridine)
PA1010	polyamide-1010, nylon-1010
PA6	polyamide-6, nylon-6
PA66	polyamide-66, nylon-66
PAA	poly(amic acid)
PAN	polyacrylonitrile
PBI	polybenzimidazole
PC	polycarbonate
PCL	polycarprolactone
PDLLA	Poly(D,L-lactic acid)
PEO	poly(ethylene oxide)
PET	poly(ethylene terephthalate)
PI	polyimide
PLA	poly(lactic acid)

PLGA	poly(lactic-co-glycolic acid)
PM2.5	particulate matter with particle size below 2.5 $\mu\text{m}$
PMMA	poly(methyl methacrylate)
PPX	poly( <i>p</i> -xylylene)
PSA	Poly(sulfone amide)
PU	polyurethane
PVA	poly(vinyl alcohol)
PVC	poly(vinyl chloride)
PVDF	Poly(vinylidene fluoride)
PVP	polyvinylpyrrolidone
r	radius
s	second
SEM	scanning electron microscopy
T	temperature
TEM	Transmission electron microscopy
TFE	2,2,2-trifluoroacetic acid
$\mu$ -CT	micro-computer tomography
UV	ultraviolet
UV-Vis	ultraviolet-visible
V	volume
W	watt
WCA	water contact angle
wt	weight
wt%	weight percent

$\varepsilon$	porosity
$\phi_c$	volume fraction

# Summary/Zusammenfassung

## Summary

The aim of this thesis was to develop porous sponges with a three dimensional (3D) interconnected network, ultralow density, high porosity, and hierarchical pore structure for various applications. The underlying concept was to freeze-dry a dispersion of short electrospun fibers to remove the solvent and to form the fibrous porous structures by self-assembly. Further modifications of the fibrous sponges provided more functionalities, e.g. enhanced mechanical properties, or tunable wetting behavior, which can be used for different applications in liquid absorption, cell growth, catalysis, drug release and many more. Furthermore the copolymerization with 2-vinyl pyridine also allowed the immobilization of metal particles.

The major challenge of this thesis was to prepare the 3D porous sponges from electrospun fibers. In **Section 2.1**, dispersions of short electrospun fibers were produced for the preparation of 3D sponges by self-assembly. The preparation of the sponge involved the synthesis of the UV cross-linkable polymer, electrospinning of the polymer, UV cross-linking, cutting the fibers to a short fiber dispersion and freeze-drying the dispersion to 3D sponges. The highly porous structure of the sponges was investigated by scanning electron microscopy and micro-CT. The sponges had superior compression elasticity that the sponges could be performed with cyclic compression and bending. The highly porous structures granted the sponges an excellent liquid absorption. The hydrophobicity of the sponges made them applicable to absorb oil from water. Besides, the sponges also showed good compatibility with cells and the cells could survive and colonize in the sponges. This investigation on cell growth opens great opportunities of fibrous sponges for applications in tissue engineering.

The sponges introduced in **Section 2.1** showed many distinguished properties and applications, but they exhibit disadvantages of relatively low compression strength (<1 kPa) and poor solvent resistance. In **Section 2.2**, a novel strategy was applied to solve these problems. An additional polymer layer of poly(*p*-xylylene) (PPX) with different thickness was coated onto the whole surface of the sponge. This additional layer, which possessed excellent mechanical properties, thermal stability, and chemical resistance, generated junctions between the fibers due to film formation and

enhanced the stability of the sponges. By controlling the density of the neat sponges and the coating thickness of the PPX layer, sponges with densities in the range of 4.83-22.59 mg/cm<sup>3</sup>, and water contact angles in the range of 114-156° were obtained. The compression strength of the PPX coated sponges at 50% compression strain could be increased up to 12.1 kPa, which was ten times more than that of the sponges without PPX coating. Due to the improved chemical and mechanical stability, the PPX coated sponges could keep their structure integrity in different solvents even after intense shaking.

**Section 2.3** and **2.4** present two applications of the fibrous 3D sponges. In **Section 2.3**, the porous fibrous sponges were used to immobilize gold nanoparticles (AuNPs) as a catalyst carrier for the reduction of 4-aminophenol. Firstly, copolymer with the functional group of 2-vinylpyridine (2-VP) was synthesized and electrospun into fibers for immobilization of very small amounts of AuNPs. Then the AuNP immobilized fibers were mechanically cut to produce a short fiber dispersion and freeze-dried into 3D sponge (Au-sponge) as catalyst support. The prepared Au-sponges exhibited small specific surface areas but a very high pore volume, which could efficiently facilitate the mass transfer of educts and products. In comparison to other AuNPs immobilized catalyst systems, the Au-sponge offered a very high normalized reaction rate constant. The Au-sponge also showed reversible compression stability, which is in favor for the cyclic use of the Au-sponge as catalyst. In **section 2.4**, the fibrous sponges were loaded with drugs to examine the controllable drug release. The high pore volume of the sponges provided a large drug loading capacity, which was achieved on the use of 1 vol% of the pore volume of the sponges. This small portion of usage of the pore volume suggested the promising improvement on drug loading capacity in the future. PPX coating with various coating thicknesses on the drug-loaded sponges led to a controllable drug release. Thicker PPX layers resulted in slower drug release. The drug release performance could be controlled by the diffusion barrier behavior of the PPX layer and the changing wetting between PPX layer and the liquid medium.

Traditional organogels are usually formed by a bottom-up approach from the self-assembly of low- or high-molecular weight molecules. In **Section 2.5**, a novel top-down approach to prepare gels from polymer fibrous sponges was developed. The spongy gels were formed from a pre-formed 3D fibrous sponge followed with filling of apolar liquid. The spongy gels exhibited the same features as an organic gel, such as a liquid phase, a 3D network, and essentially no flow, but also possessed their distinct advantages of fine control over the nature and structure of the 3D fibrous network, no

shrinkage, no sensitivity to impurities on gel formation and provide a wide range of possibilities for functionalization owing to the wealth of modification of electrospun fibers. These spongy gels were mechanically stable and the evaporation of both wettable and nonwettable solvents from the spongy gels could be considered as shrinking-in-time blobs. These spongy gels could be found many promising applications in bioengineering, sensors, templates, oil recovery, lubrication, catalyst, and drug delivery.

The future work and challenges on 3D fibrous sponges are (1) exploring a green technique to produce the sponges without solvents or only with environmental friendly solvents like water and ethanol; (2) producing the sponges in large scale; (3) thoroughly investigating of the wetting behavior between the sponges and a liquid; and (4) providing sponges with more functionalities to enable access to different kinds of applications.

In conclusion, the 3D sponges with hierarchical pore structures have been successfully prepared with electrospun fibers. The densities, compression properties, water contact angle, and solvent resistance of the sponges could be improved by an additional PPX coating. The functionalized sponges with pre-immobilization of AuNPs were successfully applied as catalyst supporter and possessed superior normalized reaction rate constant. Due to the large pore volume, the sponges had very high drug loading capacity based on the use of 1 vol% of the pores in the sponges. An additional PPX coating on the drug-loaded sponges could effectively provide the controllable drug release. Development on spongy gels based on fibrous porous sponges is initiated and shows bright future on the gel field.

## **Zusammenfassung**

Das Ziel dieser Arbeit war die Entwicklung poröser Schwämme mit einem dreidimensionalen (3D) miteinander verbundenem Netzwerk, sehr geringer Dichte, hoher Porosität und hierarchischer Porenstruktur für verschiedene Anwendungen. Das zugrundeliegende Konzept war das Gefriertrocknen einer Dispersion aus elektrogesponnenen Kurzschnittfasern zur Entfernung des Lösungsmittels und zur Bildung der porösen Struktur durch Selbstanordnung der Fasern. Modifikationen der Schwämme lieferten zusätzliche Funktionalitäten wie verbesserte mechanische Eigenschaften oder ein einstellbares Benetzungsverhalten, welche für unterschiedliche Anwendungen in der Absorption von Flüssigkeiten, Zellwachstum,

Katalyse, Medikamentenfreisetzung und vielen mehr eingesetzt werden könnten. Des Weiteren erlaubte die Copolymerisation von 2-Vinylpyridin die Immobilisierung von Metallpartikeln.

Die größte Herausforderung dieser Arbeit war die Herstellung der porösen 3D Schwämme aus elektrogesponnenen Fasern. In Abschnitt 2.1 wurden Dispersionen von elektroversponnenen Kurzschnittfasern hergestellt, welche für die Darstellung von Schwämmen durch deren Selbstanordnung verwendet wurden. Die Anfertigung der Schwämme umfasste die Synthese eines UV-vernetzbares Polymers, das Verspinnen dieses Polymers, die UV-Vernetzung, das Schneiden der Fasern zu einer Kurzschnittfaser-Dispersion und das Gefriertrocknen der Dispersion zum Schwamm. Die hochporöse Struktur der Schwämme wurde mittels Rasterelektronenmikroskopie und Mikro-CT überprüft. Die Schwämme hatten eine überdurchschnittliche Kompressionselastizität, welche durch zyklisches Zusammenpressen und Biegen gezeigt werden konnte. Die hochporöse Struktur erlaubte die Absorption von Flüssigkeiten. Durch die Hydrophobizität der Schwämme eigneten sich diese für die selektive Absorption von Öl aus Wasser. Des Weiteren zeigten die Schwämme eine gute Biokompatibilität und Zellen konnten im Schwamm angesiedelt werden. Durch den Nachweis des Zellwachstums bieten sich Anwendungsmöglichkeiten der Faserschwämme im Bereich des Tissue Engineerings.

Die in Abschnitt 2.1 eingeführten Schwämme zeigten viele herausragende Eigenschaften und Anwendungsmöglichkeiten, allerdings auch Nachteile wie eine relativ niedrige Druckfestigkeit ( $<1$  kPa) und schlechte Lösungsmittelbeständigkeit. In Abschnitt 2.2 wurde ein neues Konzept für die Lösung dieser Probleme eingeführt. Die gesamte Oberfläche des Schwammes wurde mit einer zusätzlichen Poly(p-xylylen) (PPX) Polymerschicht unterschiedlicher Dicken beschichtet. Diese Schicht, welche exzellente mechanische Eigenschaften, thermische Stabilität und Chemikalienbeständigkeit aufweist, bildete Vernetzungspunkte zwischen den Fasern durch Filmbildung und verbesserte die Stabilität der Schwämme. Durch die Kontrolle der Dichte des Schwammes und der Beschichtungsdicke des PPX konnten Schwämme mit Dichten von  $4.83$ - $22.59$   $\text{mg}/\text{cm}^3$  und Kontaktwinkel von  $114$ - $156^\circ$  erhalten werden. Die Druckfestigkeit der PPX-beschichteten Schwämme bei einer Stauchung von 50% konnte auf  $12.1$  kPa erhöht werden, was dem Zehnfachen im Vergleich zum unbeschichteten Schwamm entspricht. Aufgrund der verbesserten Chemikalienbeständigkeit und mechanischen Stabilität behielten die beschichteten Schwämme ihre Form nach dem Einlegen in verschiedene Lösungsmittel auch nach

intensivem Schütteln.

In Abschnitt 2.3 und 2.4 wurden zwei Anwendungen für die Schwämme vorgestellt. In Abschnitt 2.3 wurden die Schwämme für die Immobilisierung von Goldnanopartikeln (AuNPs) verwendet, welche als Katalysatoren zur Reduktion von 4-Aminophenol dienen. Dazu wurde zuerst ein Copolymer mit 2-Vinylpyridin synthetisiert und versponnen, sodass sehr kleine Mengen von AuNPs auf den Fasern immobilisiert werden konnten. Anschließend wurden die Fasern maschinell zerschnitten um eine Kurzschnittfaser-Dispersion zu erhalten, welche gefriergetrocknet wurde, um einen Schwamm (Au-Schwamm) als Katalysatorträger zu erhalten. Der Schwamm wies eine kleine spezifische Oberfläche bei gleichzeitig sehr großem Porenvolumen auf, welches den Massentransfer der Edukte und Produkte erleichtern könnte. Im Vergleich zu anderen Immobilisierungssystemen für AuNP, boten die Au-Schwämme eine sehr hohe normalisierte Reaktionsgeschwindigkeitskonstante. Außerdem zeigten die Schwämme eine reversible Kompressionsstabilität was vorteilhaft für die wiederholte Nutzung der Schwämme als Katalysator war. In Abschnitt 2.4 wurden die Schwämme mit Medikamenten beladen, um das kontrollierte Freisetzungverhalten zu untersuchen. Das große Porenvolumen der Schwämme lieferte reichlich Kapazität für die Medikamentenbeladung, welche bereits bei einer Nutzung von 1% des Volumens erreicht wurde. Dieser kleine verwendete Teil des Porenvolumens deutet die vielversprechenden Perspektiven der Medikamentenbeladungskapazitäten für die Zukunft an. PPX-Beschichtungen der beladenen Schwämme mit unterschiedlichen Schichtdicken führten zur kontrollierten Freisetzung der Medikamente. Dickere PPX-Schichten bewirkten eine langsamere Freisetzung. Das Freisetzungverhalten konnte durch die Barriereigenschaften der PPX-Schichten und dem wechselnden Benetzungsverhalten kontrolliert werden.

Konventionelle Organogele werden im Allgemeinen über einen Bottom-up-Ansatz ausgehend von der Selbstanordnung nieder- oder hochmolekularer Verbindungen hergestellt. In Abschnitt 2.5 wurde ein neuer Top-down-Zugang für die Herstellung von Gelen über Faserschwämme entwickelt. Diese schwammartigen Gele wurden durch Beladung eines vorgeformten 3D Faserschwammes mit apolaren Flüssigkeiten hergestellt. Sie besaßen die gleichen Eigenschaften wie ein Organogel, zum Beispiel eine flüssige Phase, ein 3D Netzwerk und nahezu keinen Fluss. Weiterhin zeigten sie eindeutige Vorteile wie die Feinsteuerung der Natur und Struktur des 3D Netzwerks, keinen Schrumpf, keine Empfindlichkeit gegen Verunreinigungen bei der Gelherstellung und sie eröffneten einen breiten Bereich für Funktionalisierungen

aufgrund der Vielzahl der Modifikationsmöglichkeiten von elektrogewebenen Fasern. Die hier vorgestellten schwammartigen Gele waren mechanisch stabil und das Abdampfen sowohl benetzender als auch unbenetzender Lösungsmittel aus den Gelen kann als zeitabhängiges Schrumpfen eines Tropfens beschrieben werden. Die schwammartigen Gele besitzen viele potentielle Anwendungen in der Biotechnologie, in Sensoren, als Template, zur Rückgewinnung von Ölen, für Schmiermittel, in der Katalyse und zur Freisetzung von Medikamenten.

Die weiteren Arbeiten und Herausforderungen zu Faserschwämmen sind (1) Entwicklung einer „grünen“ Herstellung der Schwämme ohne oder mit Verwendung umweltfreundlicher Lösungsmittel wie Wasser und Ethanol; (2) die Herstellung im größeren Maßstab; (3) die umfassende Untersuchung des Benetzungsverhaltens und (4) die Entwicklung neuer Eigenschaften, um neue Anwendungen zu finden.

Die 3D Schwämme mit einer hierarchischen Porenstruktur wurden erfolgreich aus elektrogewebenen Fasern hergestellt. Die Dichten, Kompressionseigenschaften, Kontaktwinkel zu Wasser und Lösungsmittelbeständigkeit der Schwämme konnten durch eine zusätzliche PPX-Beschichtung verbessert werden. Die funktionalisierten Schwämme mit einer vorgelagerten AuNP-Immobilisierung wurden erfolgreich als Katalysatorträger eingesetzt und zeigten eine verbesserte Reaktionsgeschwindigkeitskonstante. Aufgrund des großen Porenvolumens war die Medikamentenbeladungskapazität schon bei der Verwendung von einem Prozent des Porenvolumens sehr hoch. Eine weitere PPX-Beschichtung der beladenen Schwämme sorgte für eine kontrollierte Freisetzung. Die Entwicklung von schwammartigen Gelen basierend auf Faserschwämmen wurde begonnen und eröffnet eine strahlende Zukunft im Bereich der Gele.

# 1 Introduction

## 1.1 Motivation

Electrospinning is an efficient method to form fibers with diameters in the range of nanometers to micrometers and with dimensions from one dimensional (1D) single fiber, two dimensional (2D) fibrous membranes and even three dimensional (3D) fibrous constructs. The interests on the 1D single fiber focus on the original mechanical properties of electrospun fibers, where size effect on the tensile strength, Young's modulus and toughness have been demonstrated. The research on mechanical properties of 1D single fiber provides the basic data for the applications of electrospun fibers. 2D electrospun fibrous membranes can be obtained by directly assembling the 1D fibers during electrospinning process. Till now, most applications on electrospun fibers are based on the 2D membranes. The 2D electrospun fibrous membranes have found applications in textile industry, filtration, tissue engineering, composites, catalysts, and drug release.

Compared to 1D single fiber and 2D fibrous membranes, 3D fibrous constructs possesses unique characteristics, such as 3D connected networks, ultra-light weight, high porosity and hierarchical pore structures. The pioneer work on 3D constructs by electrospinning is to increase the thickness to form the third dimension. These 3D constructs are usually used as scaffolds for tissue engineering applications. However, this kind of 3D constructs have disadvantages like weak mechanical properties, unstable 3D structure, which limited their applications in other areas. Therefore, how to get stable and mechanically strong 3D constructs from electrospun fibers and explore the applications of these 3D constructs, become an interesting and important topic that attracts more and more attention in the last few years. Till now, only countable reports are available in this topic. For this quite new field of mechanical strong and stable 3D constructs from electrospun fibers, more studies regarding the preparation and applications are highly required, which are highlighted in the present thesis.

## 1.2 Submicrometer fibers by electrospinning

Conventional fibers have fiber diameters no smaller than 2  $\mu\text{m}$  [1]. However, fibrous

materials with scale in the nanometer and sub micrometer play an important role in various fields [2, 3]. Electrospinning is such a facile and versatile method to produce fibrous materials with fiber diameter in the range from several nanometers to a few micrometers [4-6]. It is considered as the simplest and lowest cost method for preparation of nanofibers [7]. Depending on the feeding materials, electrospinning can be divided into solution electrospinning, melt electrospinning and emulsion electrospinning. In the following sections, a brief introduction on the development of electrospinning including the electrospinning classifications, the materials, assembly of electrospun fibers, and the morphology of electrospun fibers will be given.

### **1.2.1 Solution, melt, and emulsion electrospinning**

Depending on the form of the feeding materials, electrospinning can be divided into three main types of solution, melt, and emulsion electrospinning. All the three electrospinning types use a similar set-up, which contains four parts: a high voltage supply, a collector, a syringe pump and a syringe filled with feeding materials (**Figure 1-1**). However, there are also some differences between them. First, the types of the feeding materials are different as polymer solutions, polymer melts, and emulsions are used respectively. Solution electrospinning requires a viscous polymer solution where polymers are dissolved in proper solvents, melt electrospinning requires that the polymers have a melting point or glass transition temperature, and emulsion electrospinning requires that the emulsions are mixed with some other spinnable polymers. Second, the set-up for melt electrospinning differs from the other two electrospinning techniques that an external heating set-up is mounted around the syringe. The heating approach can be realized from electricity or hot gas. Solution electrospinning is the earliest and highly developed to produce very fine fibers with sizes from tens of nanometers to 1 micrometer. Melt electrospinning usually results in much larger fibers with fiber diameter in micrometer range. Emulsion electrospinning typically produces as-spun fibers with matrix polymer and the emulsion particles.

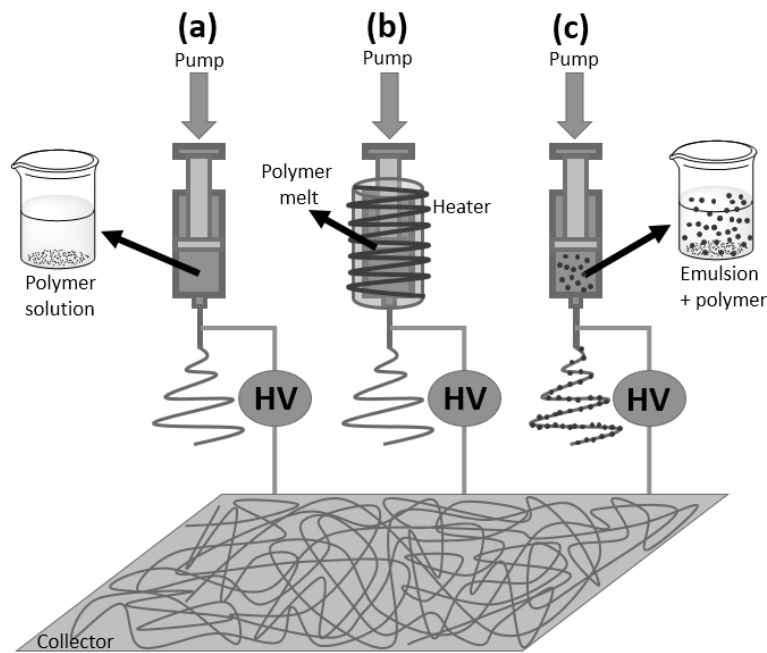


**Figure 1-1.** Schematic drawing of solution (a), melt (b) and emulsion (c) electrospinning.

### 1.2.2 Materials for electrospinning

Since 2000 electrospinning technology experienced a burst development and hundreds of materials are processed into fibers by electrospinning. The materials used for electrospinning can be polymers, inorganic materials, and bioactive materials [4-6]. **Table 1-1** summarizes the typical polymers and the solvents for electrospinning. The polymers used for electrospinning can be liquid crystalline polymers (nomex, Polybenzimidazole (PBI), Polysulfone amide (PSA)) [8-11], water soluble polymers (Polyethylene oxide (PEO), Polyvinyl alcohol (PVA)) [12, 13], polyamides (PA6, PA66, PA1010) [14-16], textile fabric polymers (PAN) [17], biodegradable polymers (Polylactic acid (PLA), Polycaprolactone (PCL), silk) [18-22], rubber (polybutadiene, polyisobutylene-isoprene, and silicon rubber) [23], natural polymer (cellulose) [24, 25] and other polymers (Polyamic acid (PAA), Polyurethanes (PU), Polycarbonate (PC), Polyvinylpyrrolidone (PVP), Poly(methyl methacrylate) (PMMA), Polystyrene (PS), Polyvinylidene fluoride (PVDF)) [26-38]. Depending on the polymers, different kinds of solvents are used for electrospinning. Generally, the solvents used for polymer electrospinning should have a good solubility for the polymers and should not possess too high boiling point. Dimethylacetamide (DMAc), dimethylformamide (DMF), formic acid (FA), acetic acid (AcOH), 2,2,2-trifluoroacetic acid (TFE), 1,1,1,3,3,3-hexafluoro-2-propanol (HFIP), chloroform, dichloromethane, ethanol, and methanol are mostly

used organic solvents while water is considered as an environmentally-friendly solvent for solution electrospinning. Inorganic materials including metals, metal oxides, ceramics, and their precursors can also be directly used for electrospinning to produce functional inorganic fibers [39-43]. In addition, bioactive materials, such as bacteria [44], virus [45], DNA [46], and enzymes [47], can also be incorporated in the electrospinning solution for electrospinning. These bioactive materials give electrospun fibers many biofunctionalities and can be used for biocatalysts, biomedicine, and biosensor.

**Table 1-1.** Summary of typical polymers and solvents for electrospinning.

<b>Materials</b>	<b>Solvent</b>	<b>References</b>
Nomex	DMAc+LiCl	[8, 9]
Polybenzimidazole (PBI)	DMAc+LiCl	[10, 11]
Polysulfone amide (PSA)	DMF	[8]
Polyethylene oxide (PEO)	water	[12]
Polyvinyl alcohol (PVA)	water	[13]
Polyamide (PA6, PA66, PA1010)	FA+AcOH, TFE, HFIP	[14-16]
Polyacrylonitrile (PAN)	DMF	[17]
Polylactic acid (PLA)	HFIP, chloroform	[18, 19]
Polycaprolactone (PCL)	chloroform/DMF, chloroform/methanol	[20, 21]
silk	HFIP, water	[18, 22]
Rubber	THF/DMF	[23]
Cellulose	acetone, AcOH, DMAc, DMAc+LiCl	[24, 25]
Polyamic acid (PAA)	DMF, DMAc	[26, 27]
Polyurethanes (PU)	DMF	[28]
Polycarbonate (PC)	dichloromethane, chloroform+THF+DMF, THF+DMF	[29-31]
Polyvinylpyrrolidone (PVP)	DMF, ethanol	[32, 33]

PMMA	DMF, chloroform, dichloromethane	[34, 35]
Polystyrene (PS)	DMF, chloroform, 1,2-dichloroethane	[28, 36]
PVDF	DMF, DMAc	[37, 38]

### 1.2.3 Morphology of electrospun fibers

In most cases, electrospun fibers with smooth surface and beads-free are required to guarantee the mechanical properties of the fibers/mats for their further applications. However, the various electrospinning parameters provide a great diversity of electrospun fiber morphologies (**Figure 1-2**). Porous electrospun fibers can be produced by controlling the humidity and the evaporation of solvents during electrospinning process due to the phase separation [48, 49]. Necklace-like structures can be achieved from the electrospinning of the blend of PVA and Silica particles in water by adjusting the weight ratio of PVA/SiO<sub>2</sub>/water and the applied voltage [50]. Interesting fiber shapes with firecracker-shape and rice grain-shape are fabricated by combining electrospinning and post-treatment [51, 52]. Koombhongse *et al.* reported ribbon-like and branched fibers, which are formed from the thin skin of the rapid evaporation of solvent and by the ejection of smaller jets from the surface of the primary jets, respectively [53]. In another report, Holzmeister *et al.* presented a “barbed” shaped fiber from electrospinning by carefully controlling the concentration of PVA solutions [54].

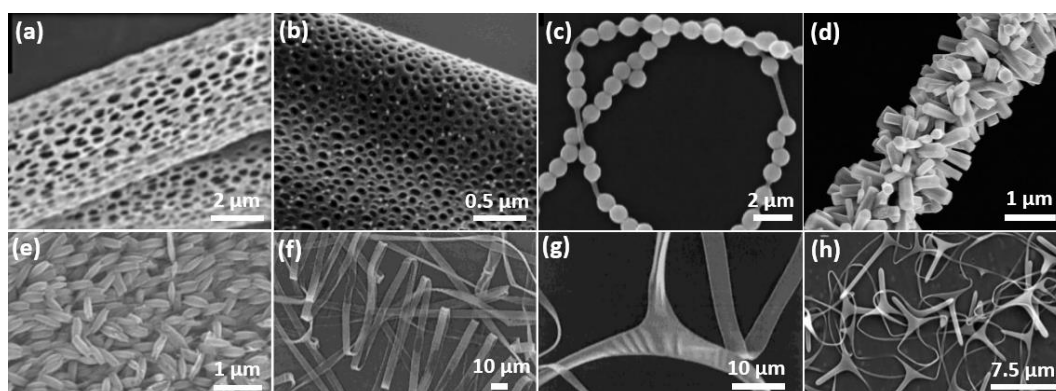


**Figure 1-2.** Electrospun fibers with porous structure of PLA (a) (Reprinted with permission from ref. [48]. Copyright 2010, Springer) and PS (b) (Reprinted with permission from ref. [49]. Copyright 2004, American Chemical Society), necklace-like

(c) (Reprinted with permission from ref. [50]. Copyright 2010, American Chemical Society), firecracker-shaped (d) (Reprinted with permission from ref. [51]. Copyright 2011, Royal Society of Chemistry), rice grain-shaped (e) (Reprinted with permission from ref. [52]. Copyright 2011, Royal Society of Chemistry), ribbon-like and branched (f and g) (Reprinted with permission from ref. [53]. Copyright 2001, John Wiley and Sons), and barbed (h) morphologies (Reprinted with permission from ref. [54]. Copyright 2008, John Wiley and Sons).

The spinnerets used for electrospinning also plays an important role to the fiber morphologies (**Figure 1-3**). The well-known core-shell and hollow structures can be achieved by the coaxial spinneret [19, 55]. Further modifying the spinneret into triaxial shape, then the fibers exhibit triaxial structures with three different layers [28]. Janus fibers [56] can be produced by side-by-side electrospinning with two different polymer solutions. With the same side-by-side electrospinning technique, Chen *et al.* prepared spring fibers from flexible and rigid polymers [9]. Zhao *et al.* modified the spinneret by embedding two to five metallic capillaries and successfully produced tubular with two to five channels in the fibers [57]. In another report, Chen *et al.* developed a multifluidic coaxial electrospinning approach to produce core-shell fibers with a novel nanowire-in-microtube structures [58].

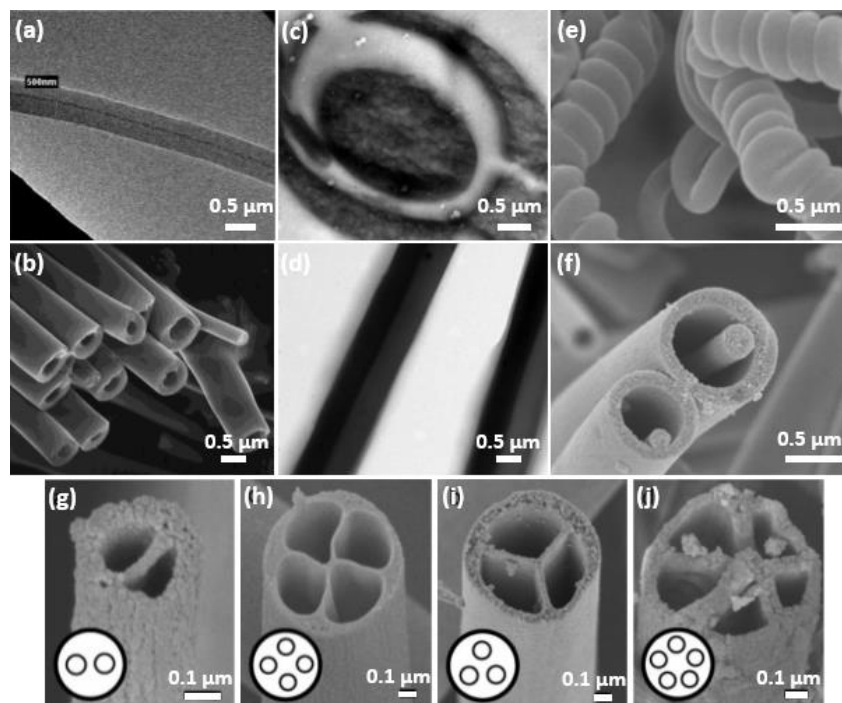


**Figure 1-3.** Core-shell (a) (Reprinted with permission from ref. [19]. Copyright 2003, John Wiley and Sons), hollow (b) (Reprinted with permission from ref. [55]. Copyright 2004, American Chemical Society), triaxial (c) (Reprinted with permission from ref. [28].

Copyright 2014, American Chemical Society), Janus (d) (Reprinted with permission from ref. [56]. Copyright 2014, John Wiley and Sons), spring (e) (Reprinted with permission from ref. [9]. Copyright 2009, John Wiley and Sons), nanowire-in-microtube (f) (Reprinted with permission from ref. [58]. Copyright 2010, American Chemical Society), and multi-channel tubular (g-j) (Reprinted with permission from ref. [57]) structures of electrospun fibers obtained by the modification of spinnerets.

#### 1.2.4 Short electrospun fibers

Traditional short microfibers have been broadly applied in composites as reinforcements due to their good distribution in matrix and good processing by industrial methods, for instance, extrusion. However, the studies on short electrospun fibers are countable. It is believed that short nanofibers prepared directly from electrospinning would greatly promote the development of electrospinning technology and electrospun nanofibers. Researchers tried many attempts to fabricate electrospun short fibers by optimizing electrospinning parameters (**Figure 1-4**). Luo *et al.* presented short microfibers with aspect ratio in the range of 10-200 directly by electrospinning [59]. However, the fibers are not smooth and uniform in diameter, which would limit their applications. Recently, Fathona and Yabuki successfully obtained cellulose acetate short electrospun fibers by carefully adjusting the concentration of the polymer solution [60]. They found the good concentration should be ranging from 13 to 15% and the length of short fibers increased by increasing the flow rate and decreasing the applied voltage. However, the concentration region was too small and the studies did not show the universality for other polymers. In another report from the same group [61], they incorporated TiO<sub>2</sub> nanoparticles into cellulose acetate solution to prepare short electrospun composite nanofibers and studied the effects of nanoparticle concentration and surface charge on the fiber length. The increased nanoparticle concentration led to the decrease of fiber length and the negatively charged nanoparticle in negatively charged polymers would lead to the elongation of the short fibers [61]. The most developed method to prepare short electrospun fibers are post-treatments on the obtained electrospun continuous long fibers. Stoiljkovic *et al.* developed an effective method to prepare short electrospun fibers by using a UV cutting method [62]. The short fibers were prepared by removing the non-cross-linked soluble part and the length of the short fibers can be controlled by changing the size of the employed mask [62]. Zhao *et al.* [63], Sawawi *et al.* [64], and Xu *et al.* [65] reported the short electrospun glass, PS and carbon fibers by ultra-

sonication. In those examples, the materials used for the preparation showed the common characteristic of brittleness and non-uniform fiber length. Our group developed a mechanical cutting method with a high speed mixer/blender to fabricate the short electrospun fibers and showed different applications for controlled movement [66], composites [67, 68], inhalation applications [69], and sponges [70]. Recently, a similar strategy to prepare short electrospun fiber dispersions with mechanical homogenization was adopted by Ding's group for the aerogel preparations [71, 72].

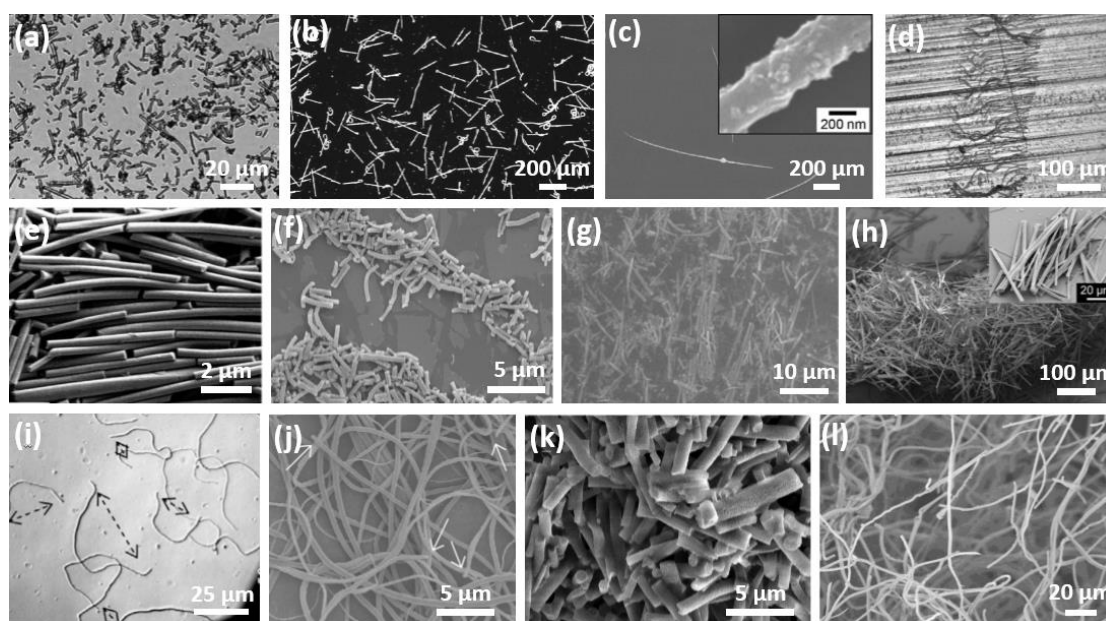


**Figure 1-4.** Short electrospun fibers. (a) Polymethylsilsesquioxane (PMSQ) (Reprinted with permission from ref. [59]. Copyright 2011, Springer), (b) cellulose acetate (Reprinted with permission from ref. [60]. Copyright 2014, Springer), (c) cellulose/TiO<sub>2</sub> (Reprinted with permission from ref. [61]. Copyright 2014, Elsevier), (d) UV cross-linked polymer (Reprinted with permission from ref. [62]. Copyright 2008, John Wiley and Sons), (e) glass (Reprinted with permission from ref. [63]. Copyright 2015, John Wiley and Sons), (f) PS (Reprinted with permission from ref. [64]. Copyright 2013, Elsevier), (g) carbon (Reprinted with permission from ref. [65]. Copyright 2015, Elsevier), (h) Co/P(MMA-c-VA) (Reprinted with permission from ref. [66]. Copyright 2007, John Wiley and Sons), (i) nylon-6 (Reprinted with permission from ref. [67]. Copyright 2013, Elsevier), (j) polyimide (PI) (Reprinted with permission from ref. [68]. Copyright 2013, Elsevier), (k) poly(lactide-co-ethylene oxide) (Reprinted with permission from ref. [69]. Copyright 2009, John Wiley and Sons), and (l) cross-linked poly(MA-MMA-MABP) ([70]. Open access, John Wiley and Sons).

### 1.2.5 Assembly of electrospun fibers

Single fiber prepared from electrospinning belongs to the group of one dimensional materials. However, their assembly from one dimensional to three dimensional have attracted broad interests including the physical properties and applications.

#### 1.2.5.1 One dimensional electrospun fiber

During the electrospinning, the charged jet is stretched thousands of times along the fiber axis to form ultrathin fibers. In this process, the macromolecules in the jet are drawn and oriented, which greatly enhances the mechanical properties of the single electrospun fiber. In most cases, it is difficult to isolate the single electrospun fiber for investigations. However, in order to get the mechanical properties of single electrospun fiber, researchers developed approaches to catch and handle the individual fiber. For example, Chen *et al.* proposed a simple procedure to get the individual electrospun fiber and make it easy to be handled for single fiber tensile test [73]. The procedure contains four steps: (1) using a rectangle steel frame to catch electrospun fibers; (2) using another pre-taped paper frame to pick up an individual fiber; (3) dropping super glue to fix tightly the single fiber and (4) covering a piece of paper on the paper frame to avoid the adhesive tape sticking to the clamps of the tensile tester [73]. With this method, the mechanical properties of single polyimide (PI) electrospun fiber was measured, which showed superior tensile strength of 1.7 GPa and E modulus of 76 GPa [73]. Recently, Papkov *et al.* found that a single electrospun fiber showed size effect on mechanical properties (**Figure 1-5**) [74]. They took a single PAN electrospun fiber for studies and demonstrated that toughness, elastic modulus and tensile strength dramatically increased, when the fiber diameter was reduced from 2.8  $\mu\text{m}$  to about 100 nm [74].

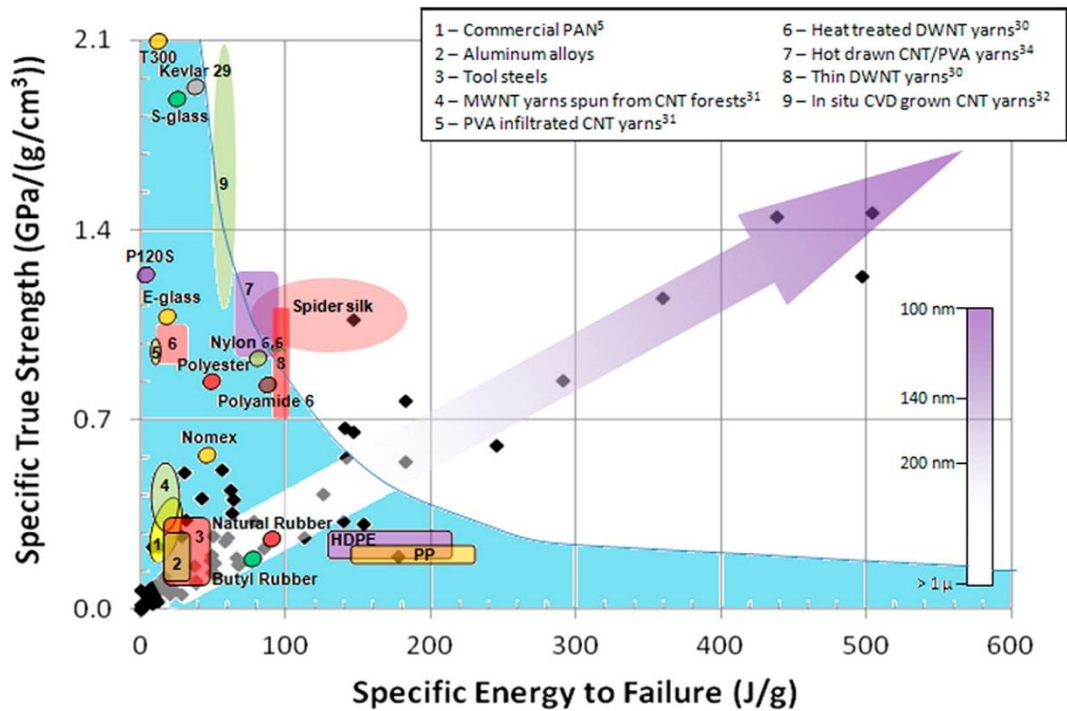


**Figure 1-5.** Comparison of specific strength and specific energy to failure of as-spun PAN nanofibers (diamonds) with typical values for commercial and developmental fibers and materials. The arrow density indicates approximate values of nanofiber diameters (see scale bar). The colored area represents the strength/toughness region occupied by traditional materials. (Reprinted with permission from ref. [74]. Copyright 2013, American Chemical Society).

In addition, 1D electrospun single fiber can be assembled into bigger 1D fiber bundles, yarns and ropes by modification the electrospinning setup [75, 76]. These 1D fiber bundles, yarns and ropes shows special mechanical properties and are promising materials for the textile-based applications.

### 1.2.5.2 Two dimensional electrospun fiber materials

The electrospun fibers can be collected in different 2D morphologies. Generally, electrospun fibers with random deposition can be collected by normal substrates, such as aluminum foil, stainless steel meshes, and drums with low speed rotation [5]. However, special modifications on the electrospinning set-up can lead to an assembly of the nanofibers as aligned and patterned nanofibers/nanofiber products (**Figure 1-6**). The highly aligned nanofibers can be prepared by some special designed collectors, such as high speed rotating discs [77], and aluminum plates with electric field assisted [78]. Uniaxially aligned nanofiber arrays can be fabricated by a device with two, four or six electrodes deposited on quartz wafers and collectors with magnetic field assisted

[79]. Fan-shaped nanofiber pattern with similar surface pattern of goose leaf can be collected by a speculate copper needle perpendicular to a rectilinear copper strip [80]. Other kinds of patterned nanofiber mats can be realized by controlling the pattern of the collectors, such as stainless mesh and electro-conductive templates [81].

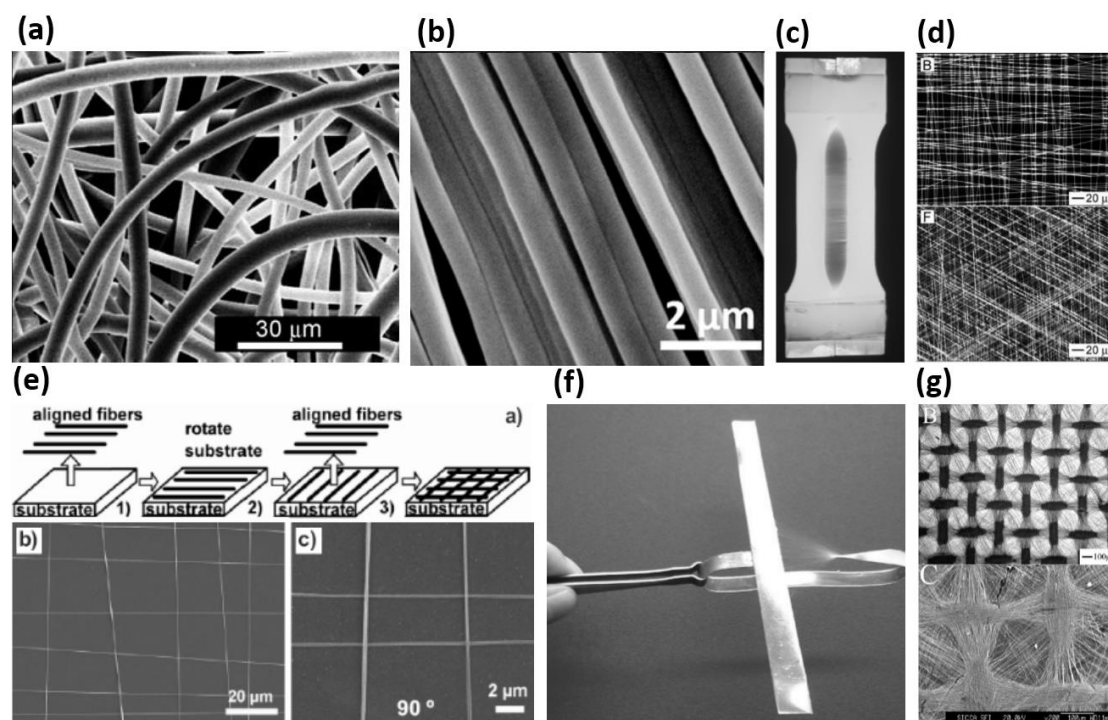


**Figure 1-6.** 2D electrospun fiber assembly. (a) Randomly (Reprinted with permission from ref. [5]. Copyright 2007, John Wiley and Sons), (b) (Reprinted with permission from ref. [77]. Copyright 2015, Royal Society of Chemistry) and (c) aligned (Reprinted with permission from ref. [78]. Copyright 2007, American Chemical Society), (d) (Reprinted with permission from ref. [82]. Copyright 2004, John Wiley and Sons) and (e) (Reprinted with permission from ref. [79]. Copyright 2007, John Wiley and Sons) weaved, (f) fan-shape (Reprinted with permission from ref. [80]. Copyright 2008, Royal Society of Chemistry) and (g) grid-patterned (Reprinted with permission from ref. [81]. Copyright 2007, John Wiley and Sons).

### 1.2.5.3 Three dimensional electrospun fiber materials

Three dimensional (3D) electrospun fiber materials assembling from 1D electrospun fibers possess highly porous structures and have attracted a lot of attention for applications in cellular infiltration [83], bone tissue regeneration [84], tissue engineering [85], electrodes in microbial fuel cells [86], and oil adsorption [87] (**Figure 1-7**). The straight-forward way to make 3D fiber scaffolds can be achieved by

deposition of electrospun fibers for a long time and therefore form the third dimension in “Z” direction. Cai *et al.* fabricated 3D electrospun fiber scaffold for cell culture based on the principle of electrostatic repulsion [88]. Compared with the 2D scaffold, the 3D structure led to an improvement of nearly 5 times in cell proliferation after 7 days of cell culture [88]. 3D shaped nanofiber materials could also be fabricated by depositing the nanofibers on 3D with/without interconnected tubular structures [89]. 3D fibrous tubes with different sizes, shapes, structures and patterns were prepared by using this method, and the tubes are expected to be used in biomedical and industrial applications [89]. Simonet *et al.* used ice crystals as a removable void template and successfully prepared 3D ultraporous polymer meshes, which showed four times higher porosity when compared to the conventional fiber electrospinning [90]. Salts (NaCl [91] and NaOH [92]) were also used as removable templates used in electrospinning for the preparation of 3D porous scaffolds. Chen *et al.* presented 3D porous electrospun carbon fiber nonwovens for microbial fuel cell applications, which was produced by a solution-blown assisted electrospinning technology [86]. Our group recently developed the self-assembly of the short electrospun fibers to form ultralight sponges, which show low density, high porosity and superior compression properties [70]. The obtained sponges exhibit various applications, such as uptake of hydrophobic liquids and cell culture [70]. Ding’s group developed 3D nanofibrous composite aerogels with cellular structures, highly compression strength and ultralow density [71, 72]. The obtained aerogels showed wide applications, such as thermal insulation, sound absorption, emulsion separation, electric conduction and oil/water separation [71, 72]. Recently, Xu *et al.* reported an electrospun PCL 3D nanofibrous scaffold with interconnected and hierarchically structured pores by self-agglomeration followed by freeze-drying and showed its application in bone tissue engineering [93].

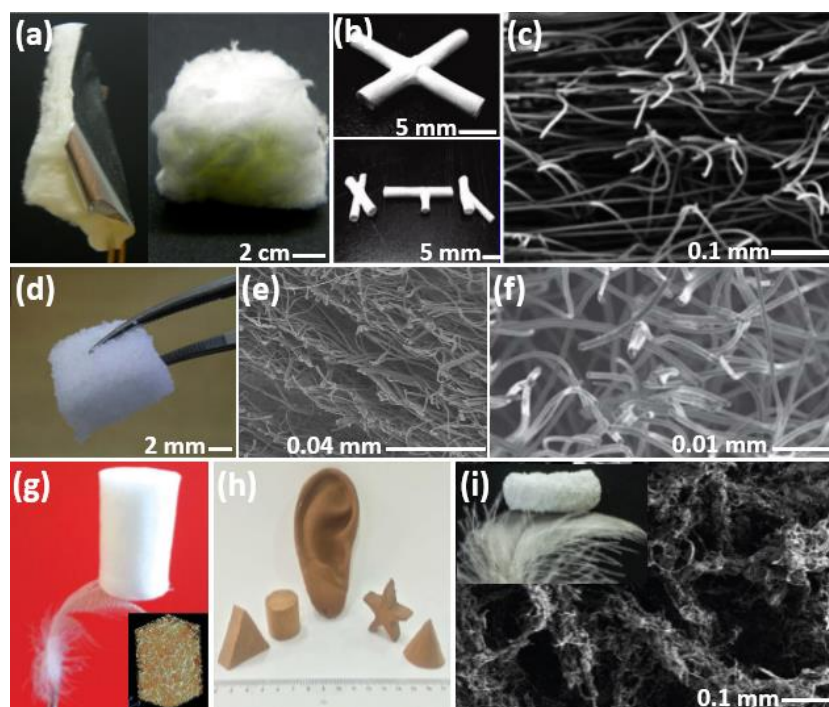


**Figure 1-7.** 3D electrospun fibrous porous materials. (a) zein electrospun scaffolds (Reprinted with permission from ref. [88]. Open access, American Chemical Society), (b) 3D fibrous tubes with different shapes (Reprinted with permission from ref. [89]. Copyright 2008, American Chemical Society), (c) poly(lactic acid-co-glycolic acid) (PLGA) (Reprinted with permission from ref. [90]. Copyright 2007, John Wiley and Sons), (d) hyaluronic acid/collagen/salt hybrid scaffold (Reprinted with permission from ref. [92]. Copyright 2008, Elsevier), (e) PLLA (Reprinted with permission from ref. [91]. Copyright 2011, Elsevier), (f) carbon (Reprinted with permission from ref. [86]. Copyright 2011, Royal Society of Chemistry), (g) cross-linked poly(MA-co-MMA-co-ABP) (Reprinted with permission from ref. [70]. Open access, John Wiley and Sons), (h) PAN/SiO<sub>2</sub> (Reprinted with permission from ref. [71]. Copyright 2014, Nature Publishing Group) and (i) PCL (Reprinted with permission from ref. [93]. Copyright 2015, John Wiley and Sons).

## 1.2.6 Applications of electrospun materials

### 1.2.6.1 Filtration and separation

Air pollution is one of the most serious problems in many cities, which trigger the fast development of filter media. In recently years, electrospun fibrous porous membranes have gained great interest as filter media due to their fascinating characteristics like high surface-area-to-volume ratio, high porosity, tunable pore structure and pore size, light weight, easy-tailored functionalization, and many others [94, 95]. Two main kinds

of electrospun materials have been reported as efficient air filter media for fine particle filtration. The first class is self-standing electrospun polymeric fibrous membranes. Polyamide (PA) [96-98], polyacrylonitrile (PAN) [99], polyurethane (PU) [100], polyethylene oxide (PEO) [101, 102], and polycarbonate (PC) [103], were successfully processed into electrospun fibrous membranes and served as air filter media. Kim *et al.* investigated the effect of electrospun fiber diameter in the ranges of 100-730 nm on the filtration efficiency and found that the filter with fiber mean diameter of 100 nm had a much lower pressure drop performance and the highest filtration efficiency of over 99.98% with tested particle size of 0.02-1.0  $\mu\text{m}$  (**Figure 1-8**) [98].

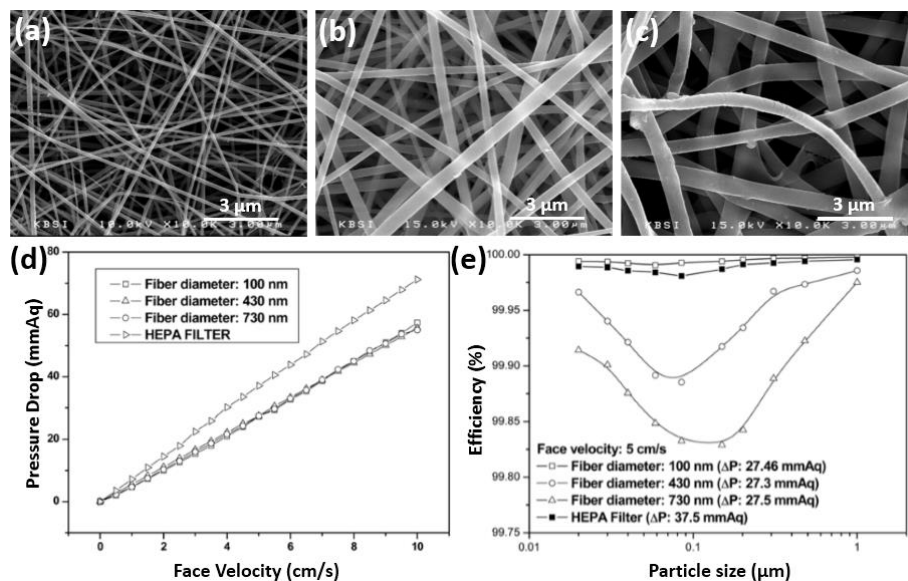


**Figure 1-8.** Electrospun PA6 nanofiber membranes with different mean fiber diameters of (a) 100 nm, (b) 430 nm and (c) 730 nm, and their pressure drop (d) and filtration efficiency (e) performance for filtration application (Reprinted with permission from ref. [98]. Copyright 2008, Springer).

The second class is the hybrid fibrous membrane. Zhang *et al.* found that multiple thin layered nanofiber membranes had a better filter quality factor than the single thick layer nanofiber membrane [104]. Wang *et al.* fabricated a multilevel structured fibrous composite mat of silica nanoparticles and electrospun PAN nanofibers [105]. The filtration efficiency could be tunable by changing the composition of the precursor solutions and the layer-by-layer stacking structure [105]. Another interesting work by the same group (Wang *et al.*) presented a two-tier composite structure with one nanofiber/net top layer and a conventional nonwoven microfibrinous support layer for high filtration efficiency with a low pressure drop [106]. Recently, Liu *et al.* reported

an impressive work for high efficiency PM<sub>2.5</sub> (Particulate matter with particle size below 2.5  $\mu\text{m}$ ) capture [107]. They fabricated transparent air filters by electrospinning one very thin layer of ultrafine polymeric nanofibers on fiber glass wire mesh and found that these transparent composite filters could achieve high air flow filtration with > 95.00% removal of PM<sub>2.5</sub> under extreme hazardous air-quality conditions [107].

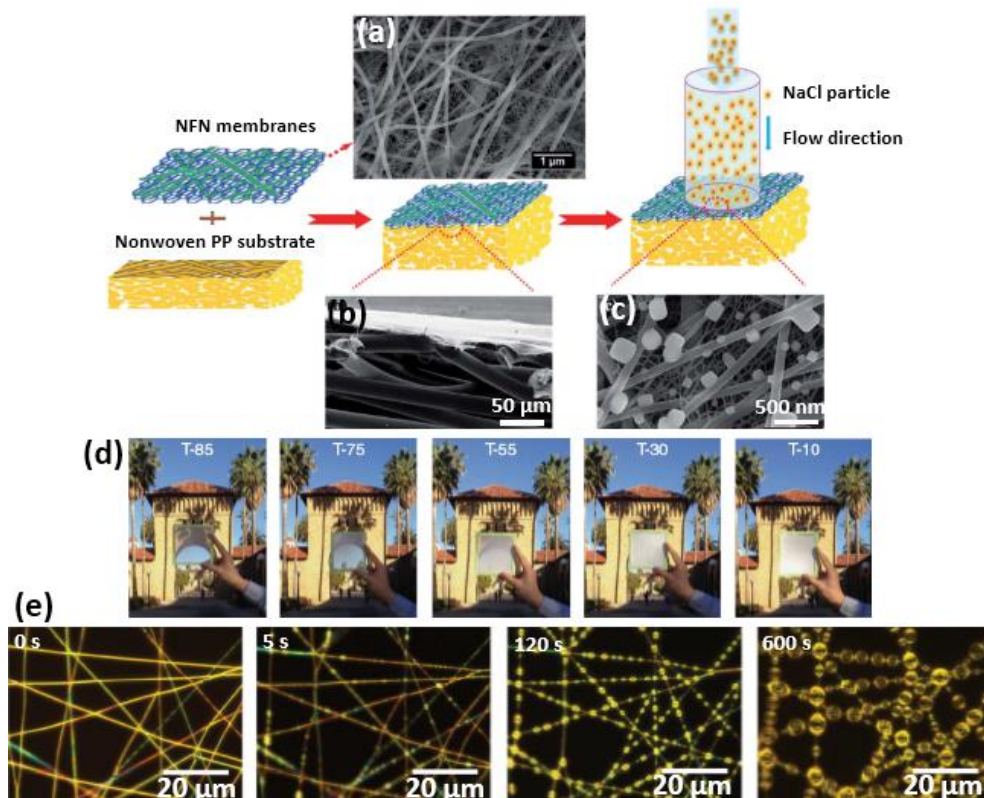


**Figure 1-9.** Schematics of preparation of 3D PA66 nanofiber/nets on nonwoven PP scaffold and their filtration process (a-c) (Reprinted with permission from ref. [106]. Copyright 2011, Royal Society of Chemistry), transparent polymeric nanofibers on fiber glass wire mesh with different optical transparency of 85, 75, 55, 30 and 10% (d) and optical microscopy images on *in-situ* study of PM capture at different time (e) (Reprinted with permission from ref. [107]. Copyright 2015, Nature Publishing Group).

Water pollution is another serious problem in the world. Many efforts have been devoted to develop the liquid filtration to remove the undesired suspended particles, ions, and bacteria. (**Figure 1-10**). Gopal *et al.* published a series of works regarding the particle filtration from water by electrospun fibrous membranes from different polymers, like PS [108], PSA [109], PVDF [108]. Wang *et al.* fabricated an electrospun PAN/polyethylene terephthalate (PET) composite filter, which showed excellent filtration for micro-particles [110]. Electrospun PA6 [111], carbon [112, 113] and PAN

[110, 114] nanofiber membranes were also reported for efficient particle filtration from water. Interesting application on *E. coli* bacteria filtration by electrospun fiber membranes was also reported [115]. Another pollutant source are the heavy metal ions in water. Electrospun fibrous membranes could be applied to absorb the metal ions in water. Haider and Park electrospun chitosan nanofiber mats for Cu(II) and Pb(II) adsorption [116]. Compared to the Cu(II) adsorption by chitosan microsphere and plain chitosan, electrospun chitosan nanofibers showed 6 and 11 times higher adsorption capacity. Similar removal of heavy metal ions, like Cu(II), Hg(II), Cd(II), and Ag(I), was also achieved by electrospun cellulose acetate, PCL and PA6 [117-119].

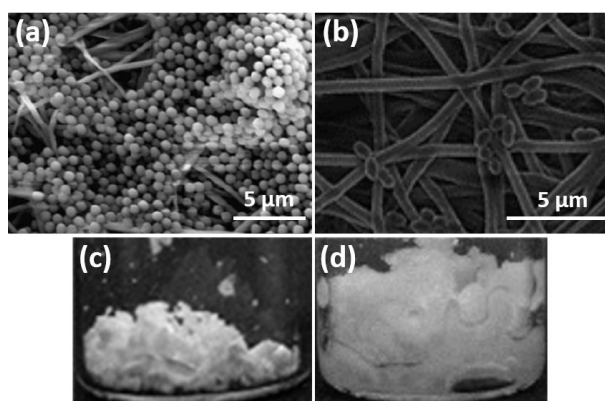


**Figure 1-10.** Electrospun PVDF fiber membrane for particle separation (a) (Reprinted with permission from ref. [108]. Copyright 2006, Elsevier), grain proteins/PEO composite fiber membrane for bacteria filtration (b) (Reprinted with permission from ref. [115]. Copyright 2016, Royal Society of Chemistry) and cellulose acetate electrospun fibers mat before (c) and after (d) Cu(II) adsorption (Reprinted with permission from ref. [118]. Copyright 2011, Elsevier).

Oil contamination is another pollution sources of water. In the last decades, separation oil from water has become a hot topic, which is important for recycling the oil and cleaning the water. Many groups paid their attentions to use electrospun fibrous membranes for oil/water separation. Shang *et al.* coated electrospun cellulose acetate nanofibers with a functionalized layer of SiO<sub>2</sub> nanoparticles to get a superhydrophobic-superoleophilic membrane [120]. The membranes showed opportunities to increase the oil/water separation efficiency. Lee *et al.* successfully fabricated superhydrophobic-superoleophilic membrane for oil/water separation by simply depositing electrospun PS nanofibers onto a stainless steel mesh (**Figure 1-11**) [121]. Tai *et al.* successfully applied electrospun carbon-silica nanofibrous membranes for ultrafast gravity-triggered oil/water separation [122]. In addition, many others

electrospun fibrous membranes, like polysulfone and polysulfone-amorphous SiO<sub>2</sub> nanoparticle composites [123, 124], PVDF [125], TPU [126], polyvinyl chloride/polystyrene [127], core-shell polystyrene/polyurethane [128], and poly(styrene-butyl acrylate) [129], have been reported as powerful oil/water separators.

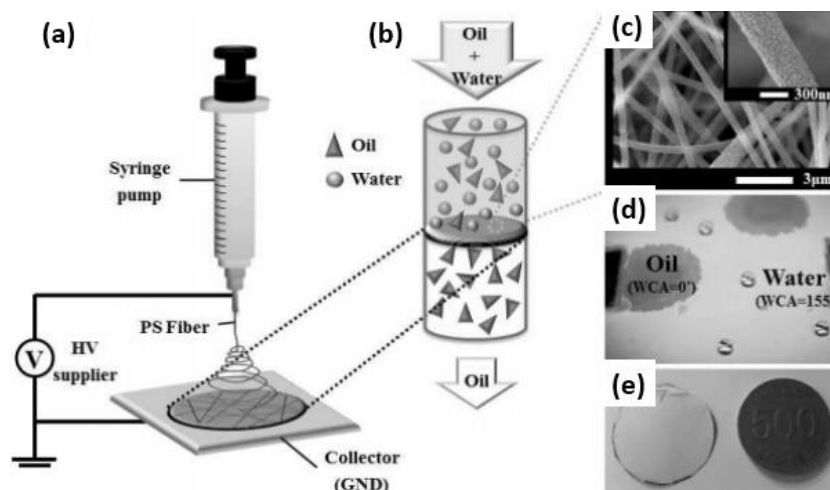


**Figure 1-11.** A schematic showing the electrospun membrane for oil/water separation. (a) Electrospinning process, (b) a schematic of separation process, (c) SEM images with high and low magnifications, (d) A photograph showing superoleophilic and superhydrophobic PS nanofiber membrane, and (e) The real scale as-prepared PS nanofiber membrane attached to the stainless mesh, whose size is compared with a coin (Reprinted with permission from ref. [121]. Copyright 2013, American Chemical Society).

Compared with the conventional nonwovens, electrospun fiber membranes showed smaller pore size, higher porosity and air permeability, which make them excellent candidates as battery separators [130]. Until now, many kinds of fiber materials processed by electrospinning, like polyimide [131], PAN [132], cellulose [133], PET [134], and PVDF [135], have been used for battery separators and showed outstanding battery performances, like high-rate capability, long cycle life and large capacity.

Besides the above mentioned filtrations and separations, electrospun fibrous membranes also show some other interesting separation applications. Strain *et al.* used recycled PET bottles for electrospinning and applied the tough fibrous PET membranes for smoke filtration [136]. The membranes with 0.4  $\mu\text{m}$  thick fibers showed the best smoke filtration efficiency (**Figure 1-12**). Recently, Sevam and Nallathambi applied electrospun silver nanoparticle (AgNP) incorporated PAN

nanofibrous membranes for bacterial filtration and anti-bacteria applications [137]. The novel filter showed 99% bacterial filtration efficiency and good anti-bacteria activity, which renders it a good candidate for protective mask applications. Similar research was done by Ma *et al.* [138]. They prepared surface functionalized PAN electrospun nanofibers as microfiltration membrane systems for effective removal of bacteria and viruses from contaminated water.

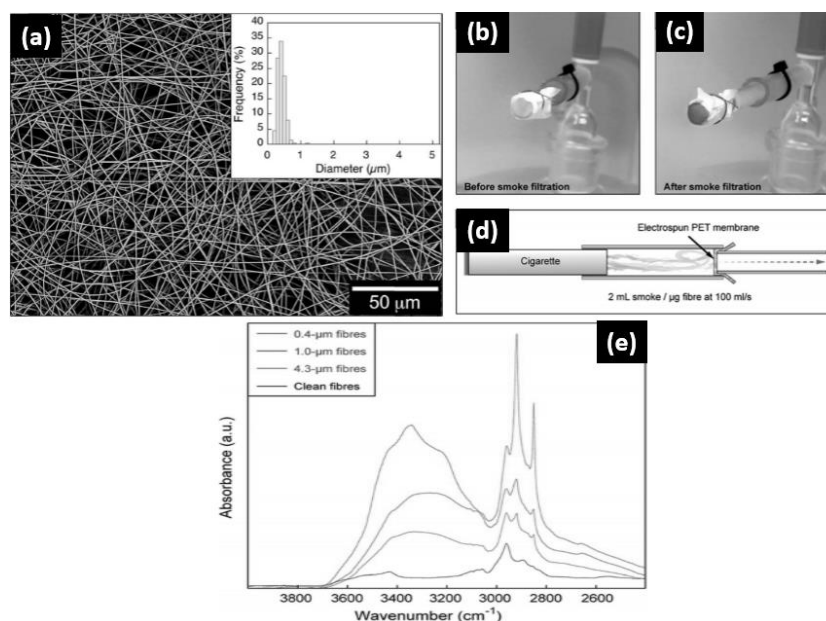


**Figure 1-12.** Electrospun PET nanofibers from recycled PET bottles (a), fiber mats before (b) and after (c) smoke filtration testing (1.0 mm diameter), IR-spectroscopy (e) of a clean fiber mat compared to that of smoke-exposed fiber mats with different fiber diameters (Reprinted with permission from ref. [136]. Open access, Royal Society of Chemistry).

### 1.2.6.2 Scaffolds for tissue engineering

Nanofiber scaffolds prepared by electrospinning consist of entangled polymer ultrathin fibers, which are packed into 3D materials. They have characteristics like high porosity, low density, suitable mechanical performance, and biodegradability, making them good candidates for tissue engineering application. Generally, the choice of materials, fiber diameters, fiber alignment, porosity and surface properties play a key role for the microscopic and macroscopic properties of electrospun fibrous scaffolds for tissue engineering. The most important characteristic is that the materials should be biocompatible. In previous reports, many biocompatible materials have been electrospun into fibrous scaffolds, such as PLLA [139, 140], silk [141, 142], PCL [143,

144], PLGA [145, 146], and collagen [147]. Fiber geometry including fiber diameter, fiber alignment, pore size and porosity can be controlled by electrospinning parameters. Many researchers studied the effect of fiber geometry on the cell proliferation [148-153]. Badami *et al.* prepared PLA fibrous substrates and found that the fiber diameter significantly influenced the spreading and proliferation of osteoblastic cells [152]. Lowery *et al.* found that the pore size of electrospun PCL scaffolds had effect on the growth of cells [148]. A faster cell growth rate was found when using the scaffolds with peak pore size larger than 6  $\mu\text{m}$  and the cells began to align to single fibers instead of multiple fibers when changing the peak pore diameter from 12 to 23  $\mu\text{m}$ . Recently, Zhong *et al.* found that aligned electrospun fibrous scaffolds could maintain cell shapes (**Figure 1-13 d-f**) but the random nanofibrous scaffolds could not during the cell culture process (**Figure 1-13 a-c**) [153].

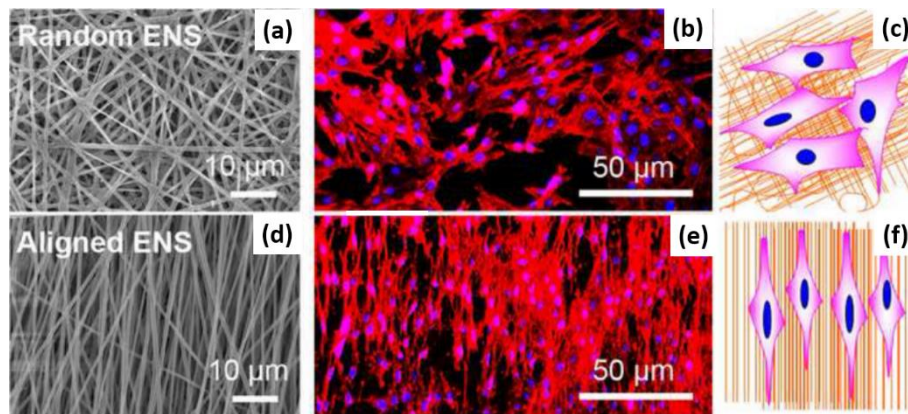


**Figure 1-13.** Effect of electrospun fiber alignment on the grow of cells (Reprinted with permission from ref. [153]. Copyright 2015, Elsevier).

Although many kinds of biocompatible polymers have been electrospun into fibrous scaffolds, there are still challenges for large-scale application in tissue engineering. One challenge is to develop the electrospun scaffolds with suitable mechanical properties. The possible strategies could either involve incorporating biocompatible reinforcements into the fibers, like cellulose nanocrystals [154, 155], montmorillonite [156], CNTs [157], and graphenes [158], or coating other kinds of polymers with better mechanical performance, such as poly(*p*-xylylene) (PPX). Another challenge is to prepare the fibrous scaffolds by green electrospinning. Until now, most of the scaffolds in the previous reports involved using organic solvents, which are harmful to the environment and toxic to human bodies. One of the solutions could be to develop water soluble polymers for electrospinning, which could be post-treated into water insoluble materials. Another solution could be to prepare the fibrous scaffolds by

emulsion electrospinning [159, 160]. The polymeric particles were embedded into a water soluble polymer matrix and later the matrix was removed by water treatment or a sintering process.

### 1.2.6.3 Catalyst

Electrospun ultrafine nanofibers have attracted a lot of attention in catalyst application as efficient catalysts or catalyst supports due to their high porosity and reusability. Generally, three main kinds of catalysts could be prepared by electrospinning. The first class is electrospun carbon nanofibers (ECNFs) without any additives, which are usually used as an electrocatalyst and low-cost alternative to platinum in batteries [161-163]. Chen *et al.* prepared 3D ECNFs as electrodes for bioelectrochemical systems such as microbial fuel cells or microbial electrolysis cells (**Figure 1-14a**) [162]. Similar research was also done by Ghasemi *et al.*, who successfully applied activated ECNFs as an alternative cathode catalyst to platinum in microbial fuel cells [163]. Joshi *et al.* used ECNFs as an alternative to platinum for triiodide reduction in dye-sensitized solar cells [161]. The obtained ECNFs counter electrodes showed a large capacitance and fast reaction rates for triiodide reduction. The second class are electrospun carbon nanofiber supported catalysts. In this case, the catalysts can be deposited on the surface of ECNFs, blended with ECNFs or located in-between ECNFs. Li *et al.* deposited platinum clusters on ECNFs by cyclic voltammetry (CV) method for catalyzing methanol oxidation and revealed that the special structure of fibrous carbon nanofiber mats could efficiently improve the catalyst performance (**Figure 1-14b**) [164]. Many kinds of metal catalyst precursor can be incorporated into the precursor of ECNFs and after annealing, the catalyst precursors are converted into catalysts supported in ECNFs. ECNFs supported silver [165], gold [166], CNTs [167], Co/CeO<sub>2</sub> [168], TiO<sub>2</sub> [169], and Pt [170], have been successfully prepared and applied as catalysts. The third class of catalysts is the nanofibers self-assembling from the metal particles by a sintering process. These catalyst fibers were prepared by electrospinning the blend of the precursor of catalyst and another sacrificial polymer like PEO, PVP, and PVA. Wang *et al.* fabricated Bi<sub>2</sub>O<sub>3</sub> nanofibers with diameter of 70-200 nm as photocatalysts by electrospinning the precursor blends of PAN and bismuth nitrate followed by calcination at 500-600 °C (**Figure 1-14c**) [171]. The similar strategy is also applied to prepare bimetallic nanofibers for catalisation, like PtRh/PtRu [172], Cu-doped cerium oxide [173], CeO<sub>2</sub>-ZnO [174], Erbium-TiO<sub>2</sub> [175], Fe-Pt [176], Pt-Co [177], Pt-Au [178], and many more.

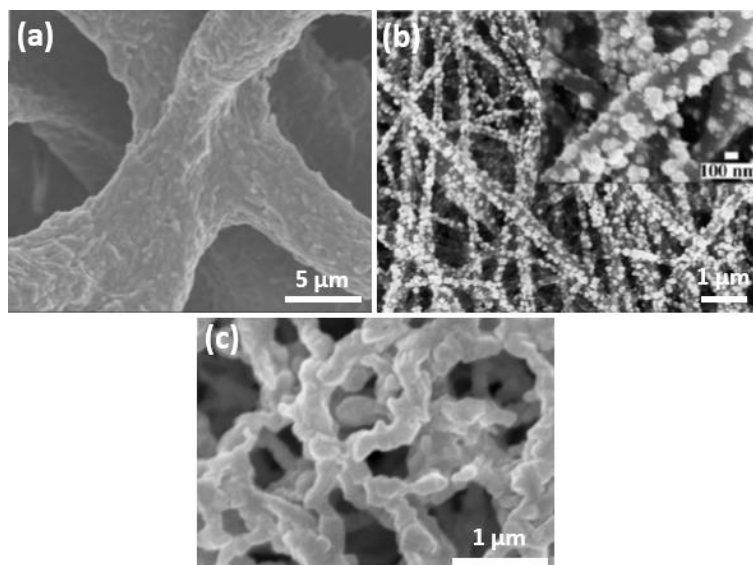


**Figure 1-14.** (a) ECNF supported electroactive biofilm for microbial fuel cells (Reprinted with permission from ref. [162]. Copyright 2011, Royal Society of Chemistry), (b) platinum clusters deposited on ECNFs for catalyzing methanol oxidation (Reprinted with permission from ref. [164]. Copyright 2008, Elsevier) and (c) electrospun  $\text{Bi}_2\text{O}_3$  fibers for photodegradation of the organic pollutant Rhodamine B (Reprinted with permission from ref. [171]. Copyright 2009, Elsevier).

#### 1.2.6.4 Drug delivery

Due to the high porosity, high specific surface area to volume ratio and highly tailored properties, electrospun nanofibers can act as drug carrier for drug delivery systems [179-181]. Numerous drugs such as anti-cancer drugs [182-184], anti-biotics [185, 186], proteins/enzymes [187-190], DNA/RNA [191-194] and anti-inflammatory agents [195-197], have been incorporated into electrospun polymeric nanofibers for drug delivery systems. As an efficient drug delivery system, the first important goal is to load the drugs into the electrospun fibers. Till now, there are several methods to load drugs into the fibers.

(1) Loading the drugs by adsorption. This is a straightforward method to produce drug-loaded fibrous systems, which provide versatile drug delivery platforms to release the drugs from the same fiber matrix and can avoid the exposure of drugs to the electrospinning process. However, this method possesses the disadvantage of burst release due to the open-porous system. Boelgen *et al.* successfully loaded the anti-biotic ornidazole to PCL electrospun nanofiber mats by adsorption, but the system showed burst release (80%) of the drugs in 3 h [198].

(2) Loading the drugs by electrospinning the blend of drugs and the polymer solutions. This method has been adopted by most of the researchers, as it provides more possibilities to control the drug release by controlling the properties of drugs and polymer matrix. The affinities among the drugs, polymer fiber matrix and the delivery environment play an important role on the drug delivery. For example, Zeng *et al.* studied the influence of the solubility and compatibility of anti-cancer drugs in the drug/polymers/solvents system on the loading of drugs in the PLLA electrospun fibers and the release behavior [199]. A burst release was observed when the dispersion of the acid-based drugs in PLLA was electrospun, which was attributed to the fast wash-off of the drugs from the surface of the fibers whereas for the base-based drugs in PLLA solutions were used for electrospinning, a modest burst release was observed [199]. In addition, the polymer degradation also plays an important role on the release of drugs from electrospun fibers. Ranganath and Wang compared the sustained drug release from electrospun PLGA copolymer fibers with 85:15 and 50:50 monomer ratios [200]. It took more than 80 days for the drug release from the fibers and a faster release rate from PLGA 50:50 was observed than from PLGA 85:15 fibers, which could be due to the faster degradation of polyesters with higher amount of glycolic acid component [200].

(3) Loading the drugs by coaxial electrospinning. This method can protect the drug during electrospinning, provide the possibility to load non-spinnable drugs as core encapsulated by the shell and avoid the initial burst release due to the barrier of the shell. For instance, Zhang *et al.* successfully decreased the initial burst of FITC-labeled BSA by coaxial electrospinning where the core solution of PCL was incorporated with FITC-labeled BSA and the shell solution of PEG, when comparing with the traditional electrospinning from the blends of PCL and PEG with addition of FITC-labeled BSA [201].

The above electrospun nanofiber delivery systems only show a temporary and spatial control of the drugs by controlling the fiber diameter, fiber porosity, drug dissolution and diffusion, and polymer degradation. In the future, efforts to develop smart drug release systems with activation and feedbacks from electrospun fibers to initiate the release of drugs over time are highly required. The successful smart drug delivery systems might be derived from smart electrospun nanofibers which could be stimulated by light, temperature, pH, electrical field or magnetic field [202].

Another important issue for drug release from electrospun fibers is their drug loading

capacity. Until now, due to the 2D characteristics of the mat, the drug loading capacity is not too high, which requests an advanced hierarchical structure of nanofibers as support for drug loading. This structures made of electrospun nanofibers with high drug loading capacity can be achieved by the nanofiber sponges with super high porosity. In our recently report, the sponges prepared from electrospun nanofibers shows a super high porosity of 99.6%, which would be a good candidate as drug loading support for drug release [70].

### **1.3 Ultralight porous 3D materials**

Recently ultralight porous 3D materials have attracted a lot of attention because of their 3D connected networks, high porosity, high flexibility and elasticity, and abundant material resources. These materials have been widely applied as electrode materials in the energy and sensor area, absorber materials including absorbing both gases and liquids, insulating materials (thermal, sound and electromagnetism), tissue engineering, oil/water separation, and many more [203-206]. In the published reports, three words, “sponge”, “aerogel” and “foam” are usually used to describe these ultralight porous 3D materials. Depending on the material sources, ultralight porous 3D materials can be divided into four main classifications, including carbon-based, polymer-based, inorganic, and hybrid ultralight porous materials. In the following sections, an introduction to these four classes of 3D material and their applications are briefly described.

#### **1.3.1 Carbon-based ultralight porous 3D materials**

Carbon materials are one class of the most attractive materials in last several decades. They includes carbon black, CNTs, graphenes and carbon fibers. Among them, CNTs, graphene and carbon fibers are famous high performance carbon materials with superior properties of electrical conductivity, thermal conductivity and excellent mechanical properties. In last few years, many researcher have devoted their efforts to develop CNT, graphene and CNT/graphene hybrid based ultralight porous 3D materials and have successfully applied them in adsorption (liquid, gas, heavy ions), capacitor, battery, catalyst, insulation, and many more, due to their high porosity (>95%), low density (<10 mg/cm<sup>3</sup>), high specific surface area and high electrical conductivity (**Figure 1-15**) [204, 205, 207-211]. Carbon fibers are also high performance carbon materials. However, there are countable reports regarding the

ultralight porous 3D materials of carbon fibers. Bi *et al.* prepared carbon fiber aerogels from raw cotton and used it as efficient and recyclable sorbent for oils and organic solvents [212]. The obtained carbon fiber aerogel possesses a relatively low density of  $12 \text{ mg/cm}^3$ , but high sorption capacity of 50-192 g/g. Compared to the ultralow density of CNT and graphene based aerogel/sponge, the relatively high density in Bi's report could be attributed to the large fiber diameter in the range of 15-20  $\mu\text{m}$  [212]. Another report on using carbon nanofiber to prepare carbon nanofiber aerogels was from Yu's group [213]. The carbon nanofiber aerogel by sol-gel process has a self-assembled, interconnected, 3D network structure with low density ( $10 \text{ mg/cm}^3$ ), high porosity (>99%), excellent mechanical stability, high hydrophobicity and superoleophilicity [213]. Electrospinning is an effective method to produce carbon nanofibers with diameters in the range of tens of nanometers to several micrometers [17, 162, 214, 215]. Electrospun carbon nanofibers could be promising candidates for the fabrication of ultralight porous materials in the future.

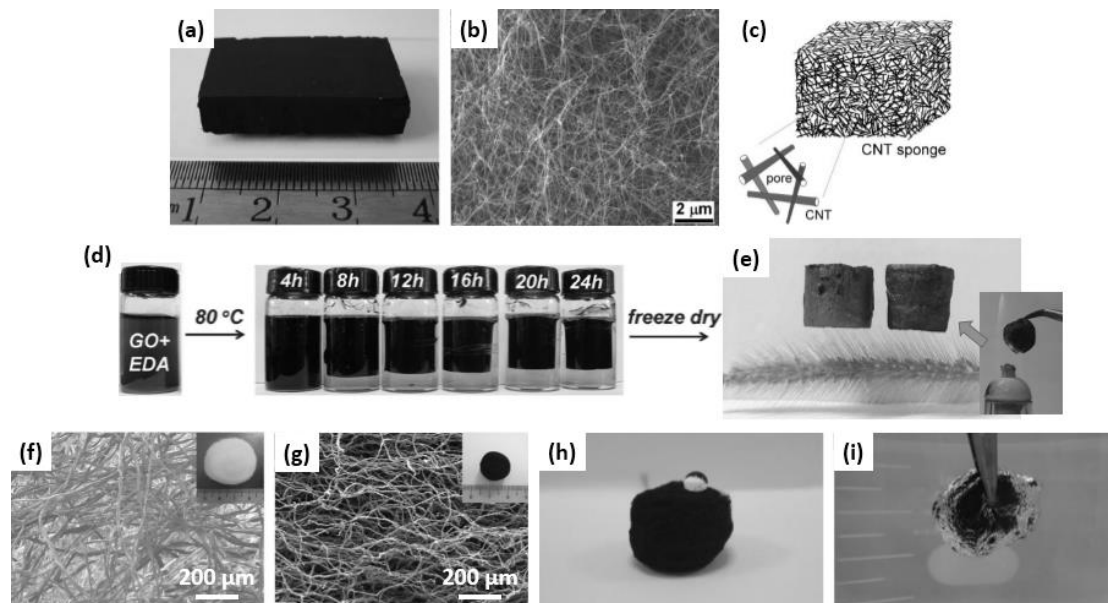


**Figure 1-15.** A monolithic CNT sponge with a bulk density of  $7.5 \text{ mg/cm}^3$  (a), cross-sectional SEM image of (a) showing a porous morphology and overlapped CNT (b), illustration of the sponge consisting of CNT piles (black lines) as the skeleton and open pores (c), images of the fabrication process of the graphene aerogel (d), an image of an original aerogel (left) and a flame treated aerogel (right) sitting on a green bristlegrass (e), SEM image of the cellulose fibers in raw cotton (f), SEM image of the carbon fibers in carbon fiber aerogel (g), photograph of a water droplet supported on a carbon fiber aerogel (h) and mirror-reflection can be observed when a carbon fiber aerogel was immersed into water, which is convincing evidence for the hydrophobicity

of the TCF aerogel (i). (a-c) (Reprinted with permission from ref. [207]. Copyright 2009, John Wiley and Sons), (d, e) (Reprinted with permission from ref. [211]. Copyright 2013, Royal Society of Chemistry) and (f-i) (Reprinted with permission from ref. [212]. Copyright 2013, John Wiley and Sons).

### 1.3.2 Polymer-based ultralight porous 3D materials

Polymers have their own special characteristic of low density with comparison to the inorganic materials. Therefore, they can be the natural option for preparing ultralight porous 3D materials. One main class of polymer materials for polymer-based ultralight 3D materials is cellulose [216-218]. Zhang *et al.* demonstrated a compressed cross-linked native cellulose nano/micro fibril cellulose aerogel with fast recovery properties (**Figure 1-16a**) [219]. Carlsson *et al.* presented an electroactive nanofibrillated cellulose aerogel composite, which showed tunable structure and electrochemical properties [220]. Liebner *et al.* showed an ultralight cellulose aerogel with density range from 0.05 to 0.26 g/cm<sup>3</sup> [221]. In Granstrom's report, water repellent cellulose aerogels were prepared from cellulose aerogel with a chemical esterification method [222]. Similar hydrophobic cellulose aerogel for oil absorption was also shown in many other reports [223-228].

Besides of cellulose, other polymers were also found to be used as materials for the preparation of ultralight porous 3D materials. Lorjai *et al.* made polybenzoxazine-based organic aerogel by thermal curing reaction of a benzoxazine monomer with xylene [229]. However, because of the high concentrations of benzoxazine in the solution (20 and 40 wt%), the resulting aerogels showed high densities of 260 and 590 mg/cm<sup>3</sup>, respectively. Gioia *et al.* reported a porous chitosan aerogel for catalyst application [230]. In another report, a polysaccharide-based aerogel was fabricated for oral drug delivery [231]. Song *et al.* presented a ultra-flyweight compressible hydrophobic poly(m-phenylenediamine) aerogel for selective absorption (**Figure 1-16b**) [232]. The aerogel exhibited ultralow density of 0.8 mg/cm<sup>3</sup>, large surface area of 338 m<sup>2</sup>/g, low thermal conductivity of 0.0125W/m/K and excellent mechanical properties [232]. Cardea *et al.* prepared PVDF aerogels as drug delivery systems [233]. A homogenous drug distribution in the aerogel, a quasi-constant release rate and no burst release effect were achieved by the aerogels (**Figure 1-16c**) [233]. Lee *et al.* reported a lightweight polydicyclopentadiene-based aerogels [234]. The aerogel with high porosity and low thermal conductivity showed promising applications for thermal and acoustic insulation [234].

Polymers are good candidates to be processed into nanofibers by electrospinning and the electrospun fibers recently are reported to be used for the preparation of 3D porous materials. Ding's group successfully fabricated ultralight electrospun nanofiber-assembled aerogels with superelasticity and showed multifunctionalities like ultralow density, rapid mechanical recovery, efficient energy absorption, thermal insulation, sound absorption and oil/water separation [71, 72]. Fong's group firstly reported electrospun PCL 3D nanofibrous scaffolds [93]. The scaffolds showed very high porosity of about 96.4% and were successfully applied in bone tissue engineering [93]. Our group also fabricated ultralight polymer sponges by freeze-drying dispersions of short electrospun fibers [70]. The sponges show extremely low density of smaller than  $3 \text{ mg/cm}^3$ , softness with reversible compression, hydrophobicity with excellent uptake for hydrophobic liquids, and successfully applied for cell culturing (**Figure 1-16d**) [70].

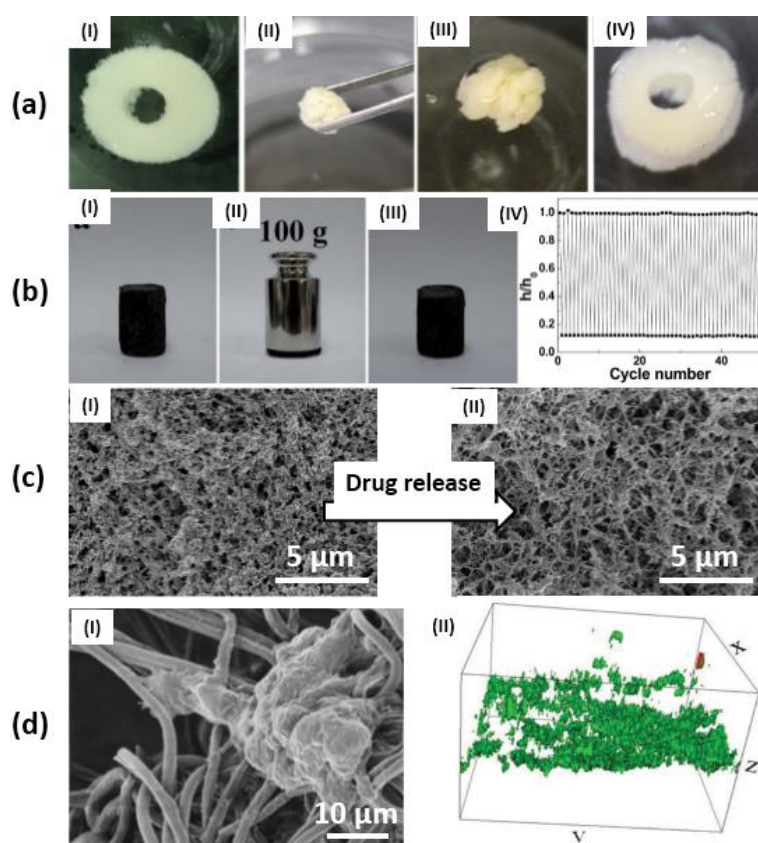


**Figure 1-16.** (a) Compressed cross-linked native cellulose nano/micro fibrillar cellulose aerogels with fast recovery properties in water (Reprinted with permission from ref. [219]. Copyright 2012, Royal Society of Chemistry), (b) ultra-flyweight hydrophobic poly(m-phenylenediamine) aerogel with compression recovery for 50 cycles (Reprinted with permission from ref. [232]. Copyright 2014, Royal Society of

Chemistry), (c) PVDF sponges loaded with amoxicillin for drug release (Reprinted with permission from ref. [233]. Copyright 2011, Elsevier), and (d) electrospun polymer nanofibers for cell culture (green: live cells; red: dead cells) (Reprinted with permission from ref. [70]. Open access, John Wiley and Sons).

### 1.3.3 Inorganic ultralight porous 3D materials

Compared to polymers, inorganic materials possess exceptional properties, such as superior thermal resistance, chemical resistance, ultralow permittivity dielectrics and high E modulus. Until now, a lot of inorganic materials have been processed into ultralight porous 3D materials. Among these materials, silica aerogels are the most studied ultralight porous 3D materials [203, 235-237]. They have highly abundant sources and are highly porous with a 3D silica connected skeleton. This characteristic make silica aerogels broadly applicable as absorption materials and encapsulation supporters. Cui *et al.* used silica aerogels to adsorb nitrobenzene from wastewater [238] while Simirnova *et al.* applied them for the adsorption and release of ketoprofen [239, 240].

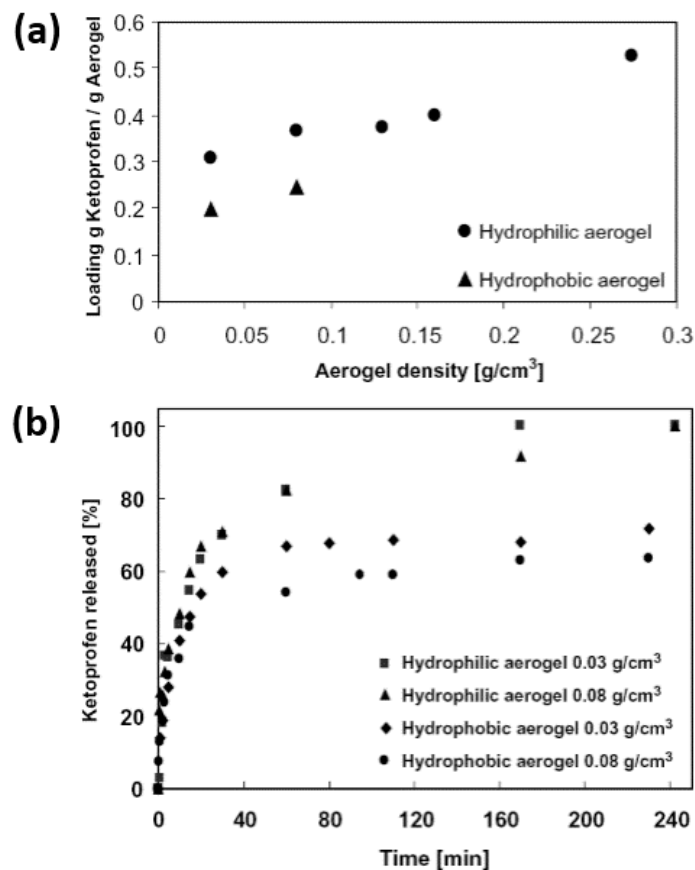


**Figure 1-17.** Loading (a) and release (b) profiles of ketoprofen from hydrophilic and hydrophobic silica aerogels of different densities in 0.1N HCl at 37 °C (Reprinted with

permission from ref. [240]. Copyright 2004, Elsevier).

Silica aerogels possess very low thermal conductivity, which is even much lower than that of air. Thus, they are considered as the best thermal insulating materials [241, 242]. Although silica aerogels are highly porous and tend to scatter the transmitted light, they can be optically transparent with high light transmittance, which make them good candidates for transparent thermal insulating components, such as windows [243, 244]. Recently, Tabata *et al.* presented hydrophobic transparent silica aerogel tiles with large area of  $18 \times 18 \times 2 \text{ cm}^3$  and high refractive index of about 1.05 for application as Cherenkov radiators (**Figure 18**) [245]. The high porosity, highly interconnected network and the full-filling of air make silica aerogels a good choice for applications as sound insulating materials [246, 247]. In silica aerogels, the propagation of sound is attenuated both in amplitude and velocity from the air inside the aerogels to the aerogel solid network [246, 247]. Another characteristic of silica aerogels is their low dielectric constant in the range of 1-2 [248-250]. Thus, silica aerogels can be used as electrical insulation materials [251, 252].

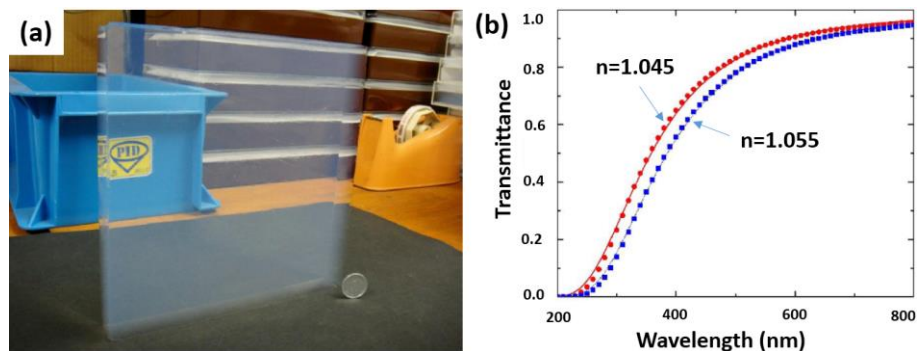


**Figure 1-1-18.** Silica aerogel sample with refractive index ( $n$ ) = 1.045 and size of  $18 \times 18 \times 2 \text{ cm}^3$  (a) and UV-Vis spectra of 20 mm thick aerogel tiles with  $n = 1.045$  and  $n = 1.055$ , respectively (b) (Reprinted with permission from ref. [245]. Copyright 2016, Elsevier).

Besides of the silica aerogels, there are also many kinds of other ultralight porous 3D inorganic materials. Yin *et al.* fabricated 3D porous boron nitride foams with density below  $10 \text{ mg/cm}^3$ , ultralow permittivity of 1.03 and excellent mechanical recovery (**Figure 19**) [253]. Jung *et al.* developed a facile method to produce inorganic nanowire aerogels in large scale and at low cost [254]. Depending on the used materials, the obtained aerogels can be used for catalyst or adsorption for heavy metal ions and toxic organic contents. Recently, Chabi *et al.* prepared ultralight and strong 3D SiC foams with low density ranging between 9 and  $17 \text{ mg/cm}^3$ , superior compression strength

and mechanical recovery [255]. Kim *et al.* reported a Ni-Al aerogel catalysts, which showed remarkably improved activity to convert CO<sub>2</sub> to CH<sub>4</sub> when comparing with the catalyst prepared by conventional impregnation method [256]. In Le's report, V<sub>2</sub>O<sub>5</sub> aerogels showed a high surface area up to 450 m<sup>2</sup>/g and a specific pore volume of 2.3 cm<sup>3</sup>/g, which were used as reversible and high capacity hosts for lithium ion intercalation [257]. Similar application as intercalation host for sodium ion battery from V<sub>2</sub>O<sub>5</sub> aerogels was also shown by Passerini's group [258]. Wei *et al.* made mesoporous cobalt oxide aerogels with high specific surface areas and high porosity for supercapacitor application [259]. The cobalt oxide aerogel-based supercapacitor exhibited more than 600 F/g capacitance, onset frequencies and excellent reversibility and cycle stability.

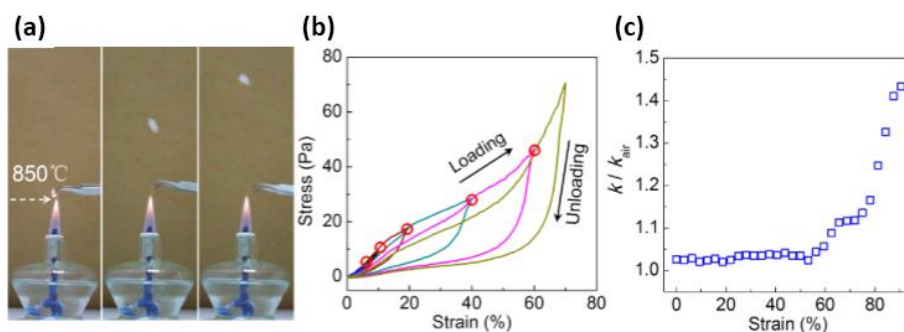


**Figure 1-19.** 3D porous boron nitride foam with thermal stability to 850 oC, mechanical recovery and low dielectric constant (Reprinted with permission from ref. [253]. Copyright 2013, American Chemical Society).

### 1.3.4 Hybrid-based ultralight porous 3D materials

Hybrids of different materials provide more choices for the preparation of ultralight porous 3D materials by different combinations. Hybrid-based ultralight porous 3D materials can be the combination of carbon-based, polymer-based and inorganic-based materials, and the combination of different functionalities. The most studied hybrid-based ultralight porous 3D materials are the combination of carbon-based materials with other materials. Carbon-based hybrid aerogels are usually applied in energy storage applications. Nickel cobaltite/carbon aerogel composites [260] by Chien *et al.*, cellulose nanofibers/multi-walled carbon nanotube nanohybrid aerogels [261] by Gao *et al.*, and graphene/polypyrrole nanotube hybrid aerogel [262] by Ye *et al.*, graphene/MnO<sub>2</sub> composite [263] by He *et al.*, were applied for the preparation of supercapacitors. Xiao *et al.* fabricated Fe<sub>2</sub>O<sub>3</sub>/graphene oxide aerogel for lithium storage application which showed excellent reversible capacity of 995 mA h/g after 50

cycles with the charge rate of 100 mA/g (**Figure 1-20**) [264]. Besides the energy storage application, aerogels based on MWCNTs/FeCo(Ni)/SiO<sub>2</sub> [265], graphene/carbon [266], TiO<sub>2</sub>/carbon [267], Pt/carbon [268, 269], and sulfur/carbon [270], were reported for catalyst application. Other composite aerogels with polymers and inorganics are also attracted a lot of attention for different applications. For example, Williams *et al.* developed a ZnO/TiO<sub>2</sub>/SiO<sub>2</sub> hybrid aerogel for fast electron transportation in dye-sensitized solar cells [271]. Casu *et al.* studied the magnetic properties and structure morphology of highly porous CoFe<sub>2</sub>O<sub>4</sub>/SiO<sub>2</sub> aerogels [272] while Kwon *et al.* applied silica aerogel doped with TiO<sub>2</sub> powder for thermal insulation application [273]. Ding's group prepared PAN/SiO<sub>2</sub> composite aerogels from a dispersion of the corresponding electrospun fibers followed by freeze-drying and sintering [71, 72]. The obtained composite aerogels showed ultralow density, rapid mechanical recovery and superhydrophobic-superoleophilic property, and presented various applications, like oil/water separation, thermal insulation, sound absorption, and many more [71, 72].

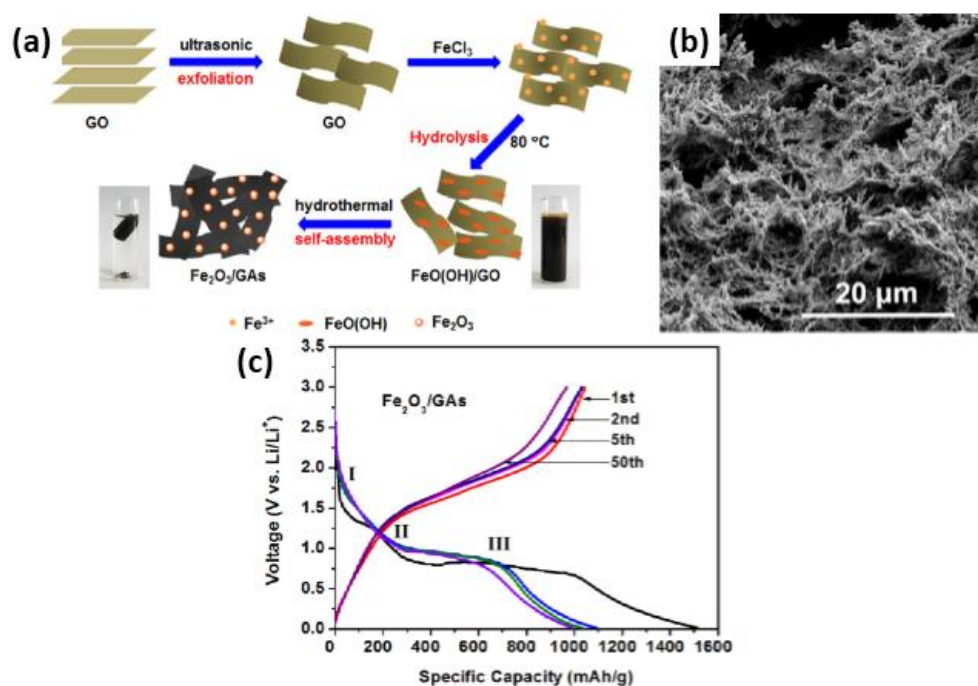


**Figure 1-20.** A schematic illustration of the preparation of 3D porous Fe<sub>2</sub>O<sub>3</sub>/graphene oxide hybrid aerogel (a), SEM image showing the 3D macroporous structure (b) and the discharge curves at the current density of 100 mA/g between 0.01 and 3.0 V in the first, second, fifth and 50<sup>th</sup> cycle (Reprinted with permission from ref. [264]. Copyright 2013, American Chemical Society).

### 1.3.5 Modifications on ultralight porous 3D materials

Ultralight porous 3D materials possess high porosity and hierarchical pore structures, which made them good candidates for further development to new materials. By filling apolar liquid in the pores of porous 3D materials, the newly formed 3D constructs could be considered as a spongy gel, which not only possesses the same features as a traditional gel (a liquid phase, a 3D network, and essentially no flow), but also shows its own advantages, such as the controlled structure of the 3D fibrous network, no shrinkage, no sensitivity to impurities on gel formation and provide a wide range of possibilities for functionalization. Unlike the traditional formation of organogels via bottom-up approach, this spongy gel is formed by a top-down approach, where a pre-formed 3D sponge was used to fill apolar liquid. Chemical vapor deposition (CVD) is another effective approach to functionalize the 3D materials. Yavari et al. modified nickel foams by CVD of methane for gas sensor application [274]. The modified sponge showed very high sensitivities to NH<sub>3</sub> and NO<sub>2</sub> and the response time was very short. In another report, Langner et al. modified electrical insulated melamine-formaldehyde foam with silver and copper nanoparticles by wet-chemical metallization and the resultant composite foams could achieve very high electrical conductivity [275]. In addition, due to the high porosity and the relatively large pore sizes, the ultralight porous 3D materials could also be used to seed cells and bacterial for further applications [70, 276, 277].

## 1.4 References

- [1] Dzenis Y. Spinning continuous fibers for nanotechnology. *Science*. 2004;304(5679):1917-1919.
- [2] Smith LA, Ma PX. Nano-fibrous scaffolds for tissue engineering. *Colloids Surf B Biointerfaces*. 2004;39(3):125-131.
- [3] Burger C, Hsiao BS, Chu B. Nanofibrous materials and their applications. *Annu Rev Mater Res*. 2006;36:333-368.
- [4] Agarwal S, Jiang S. Nanofibers and electrospinning. In: Kobayashi S, Müllen K, editors. *Encyclopedia of polymeric nanomaterials*: Springer Berlin Heidelberg; 2015. p. 1323–1337.
- [5] Greiner A, Wendorff JH. Electrospinning: a fascinating method for the preparation of ultrathin fibers. *Angew Chem Int Ed*. 2007;46(30):5670-5703.
- [6] Huang Z-M, Zhang YZ, Kotaki M, Ramakrishna S. A review on polymer nanofibers by electrospinning and their applications in nanocomposites. *Compos Sci Technol*. 2003;63(15):2223-2253.
- [7] He J-H, Liu Y, Xu L. Apparatus for preparing electrospun nanofibres: a comparative review. *Mater Sci Technol*. 2010;26(11):1275-1287.
- [8] Chen S, Hou H, Hu P, Wendorff JH, Greiner A, Agarwal S. Polymeric nanosprings by bicomponent electrospinning. *Macromol Mater Eng*. 2009;294(4):265-271.
- [9] Chen S, Hou H, Hu P, Wendorff JH, Greiner A, Agarwal S. Effect of different bicomponent

electrospinning techniques on the formation of polymeric nanosprings. *Macromol Mater Eng.* 2009;294(11):781-786.

[10] Kim C, Park S-H, Lee W-J, Yang K-S. Characteristics of supercapacitor electrodes of PBI-based carbon nanofiber web prepared by electrospinning. *Electrochim Acta.* 2004;50(2-3):877-881.

[11] Kim J-S, Reneker DH. Polybenzimidazole nanofiber produced by electrospinning. *Polym Eng Sci.* 1999;39(5):849-854.

[12] Son WK, Youk JH, Lee TS, Park WH. The effects of solution properties and polyelectrolyte on electrospinning of ultrafine poly(ethylene oxide) fibers. *Polymer.* 2004;45(9):2959-2966.

[13] Zhang C, Yuan X, Wu L, Han Y, Sheng J. Study on morphology of electrospun poly(vinyl alcohol) mats. *Eur Polym J.* 2005;41(3):423-432.

[14] Jiang S, Hou H, Greiner A, Agarwal S. Tough and transparent nylon-6 electrospun nanofiber reinforced melamine-formaldehyde composites. *ACS Appl Mat Interfaces.* 2012;4(5):2597-2603.

[15] Li Y, Huang Z, Lü Y. Electrospinning of nylon-6,6,1010 terpolymer. *Eur Polym J.* 2006;42(7):1696-1704.

[16] Fong H, Liu W, Wang C-S, Vaia RA. Generation of electrospun fibers of nylon 6 and nylon 6-montmorillonite nanocomposite. *Polymer.* 2002;43(3):775-780.

[17] Duan G, Zhang H, Jiang S, Xie M, Peng X, Chen S, Hanif M, Hou H. Modification of precursor polymer using co-polymerization: A good way to high performance electrospun carbon nanofiber bundles. *Mater Lett.* 2014;122:178-181.

[18] Peng L, Jiang S, Seuß M, Fery A, Lang G, Scheibel T, Agarwal S. Two-in-One composite fibers with side-by-side arrangement of silk fibroin and poly(L-lactide) by electrospinning. *Macromol Mater Eng.* 2015;doi: 10.1002/mame.201500217.

[19] Sun Z, Zussman E, Yarin AL, Wendorff JH, Greiner A. Compound core-shell polymer nanofibers by co-electrospinning. *Adv Mater.* 2003;15(22):1929-1932.

[20] Jiang H, Hu Y, Li Y, Zhao P, Zhu K, Chen W. A facile technique to prepare biodegradable coaxial electrospun nanofibers for controlled release of bioactive agents. *J Controlled Release.* 2005;108(2-3):237-243.

[21] Zhang YZ, Venugopal J, Huang ZM, Lim CT, Ramakrishna S. Characterization of the surface biocompatibility of the electrospun PCL-Collagen nanofibers using fibroblasts. *Biomacromolecules.* 2005;6(5):2583-2589.

[22] Zhang X, Baughman CB, Kaplan DL. In vitro evaluation of electrospun silk fibroin scaffolds for vascular cell growth. *Biomaterials.* 2008;29(14):2217-2227.

[23] Hu Q, Wu H, Zhang L, Fong H, Tian M. Rubber composite fibers containing silver nanoparticles prepared by electrospinning and in situ chemical crosslinking. *Express Polym Lett.* 2012;6:258-265.

[24] Liu H, Hsieh Y-L. Ultrafine fibrous cellulose membranes from electrospinning of cellulose acetate. *J Polym Sci, Part B: Polym Phys.* 2002;40(18):2119-2129.

[25] Kim C-W, Kim D-S, Kang S-Y, Marquez M, Joo YL. Structural studies of electrospun cellulose nanofibers. *Polymer.* 2006;47(14):5097-5107.

[26] He Y, Han D, Chen J, Ding Y, Jiang S, Hu C, Chen S, Hou H. Highly strong and highly tough electrospun polyimide/polyimide composite nanofibers from binary blend of polyamic acids. *RSC Adv.* 2014;4(104):59936-59942.

[27] Yao J, Pantano MF, Pugno NM, Bastiaansen CWM, Peijs T. High-performance electrospun copolyimide nanofibers. *Polymer.* 2015;76:105-112.

[28] Jiang S, Duan G, Zussman E, Greiner A, Agarwal S. Highly flexible and tough concentric triaxial

- polystyrene fibers. *ACS Appl Mat Interfaces*. 2014;6(8):5918-5923.
- [29] Welle A, Kröger M, Döring M, Niederer K, Pindel E, Chronakis IS. Electrospun aliphatic polycarbonates as tailored tissue scaffold materials. *Biomaterials*. 2007;28(13):2211-2219.
- [30] Krishnappa RVN, Desai K, Sung C. Morphological study of electrospun polycarbonates as a function of the solvent and processing voltage. *Journal of Materials Science*. 2003;38(11):2357-2365.
- [31] Shawon J, Sung C. Electrospinning of polycarbonate nanofibers with solvent mixtures THF and DMF. *Journal of Materials Science*. 2004;39(14):4605-4613.
- [32] Wang P, Zhang D, Ma F, Ou Y, Chen QN, Xie S, Li J. Mesoporous carbon nanofibers with a high surface area electrospun from thermoplastic polyvinylpyrrolidone. *Nanoscale*. 2012;4(22):7199-7204.
- [33] Varabhas JS, Chase GG, Reneker DH. Electrospun nanofibers from a porous hollow tube. *Polymer*. 2008;49(19):4226-4229.
- [34] Liu J, Kumar S. Microscopic polymer cups by electrospinning. *Polymer*. 2005;46(10):3211-3214.
- [35] Qian Y-F, Su Y, Li X-Q, Wang H-S, He C-L. Electrospinning of polymethyl methacrylate nanofibres in different solvents. *Iran Polym J*. 2010;19(2):123.
- [36] Baker SC, Atkin N, Gunning PA, Granville N, Wilson K, Wilson D, Southgate J. Characterisation of electrospun polystyrene scaffolds for three-dimensional in vitro biological studies. *Biomaterials*. 2006;27(16):3136-3146.
- [37] Shen Y, Chen L, Jiang S, Ding Y, Xu W, Hou H. Electrospun nanofiber reinforced all-organic PVDF/PI tough composites and their dielectric permittivity. *Mater Lett*. 2015;160:515-517.
- [38] Choi S-S, Lee YS, Joo CW, Lee SG, Park JK, Han K-S. Electrospun PVDF nanofiber web as polymer electrolyte or separator. *Electrochim Acta*. 2004;50(2-3):339-343.
- [39] Li D, McCann JT, Xia Y, Marquez M. Electrospinning: a simple and versatile technique for producing ceramic nanofibers and nanotubes. *J Am Ceram Soc*. 2006;89(6):1861-1869.
- [40] Sigmund W, Yuh J, Park H, Maneeratana V, Pyrgiotakis G, Daga A, Taylor J, Nino JC. Processing and structure relationships in electrospinning of ceramic fiber systems. *J Am Ceram Soc*. 2006;89(2):395-407.
- [41] Ramaseshan R, Sundarrajan S, Jose R, Ramakrishna S. Nanostructured ceramics by electrospinning. *J Appl Phys*. 2007;102(11):111101.
- [42] Wu H, Hu L, Rowell MW, Kong D, Cha JJ, McDonough JR, Zhu J, Yang Y, McGehee MD, Cui Y. Electrospun metal nanofiber webs as high-performance transparent electrode. *Nano Lett*. 2010;10(10):4242-4248.
- [43] Wu H, Zhang R, Liu X, Lin D, Pan W. Electrospinning of Fe, Co, and Ni nanofibers: synthesis, assembly, and magnetic properties. *Chem Mater*. 2007;19(14):3506-3511.
- [44] Gensheimer M, Becker M, Brandis-Heep A, Wendorff JH, Thauer RK, Greiner A. Novel biohybrid materials by electrospinning: nanofibers of poly(ethylene oxide) and living bacteria. *Adv Mater*. 2007;19(18):2480-2482.
- [45] Lee S-W, Belcher AM. Virus-based fabrication of micro- and nanofibers using electrospinning. *Nano Lett*. 2004;4(3):387-390.
- [46] Ner Y, Grote JG, Stuart JA, Sotzing GA. White luminescence from multiple-dye-doped electrospun DNA nanofibers by fluorescence resonance energy transfer. *Angew Chem Int Ed*. 2009;48(28):5134-5138.
- [47] Wang Z-G, Wan L-S, Liu Z-M, Huang X-J, Xu Z-K. Enzyme immobilization on electrospun polymer nanofibers: An overview. *J Mol Catal B: Enzym*. 2009;56(4):189-195.
- [48] Park J-Y, Lee I-H. Controlled release of ketoprofen from electrospun porous polylactic acid (PLA)

- nanofibers. *J Polym Res*. 2011;18(6):1287-1291.
- [49] Casper CL, Stephens JS, Tassi NG, Chase DB, Rabolt JF. Controlling surface morphology of electrospun polystyrene fibers: effect of humidity and molecular weight in the electrospinning process. *Macromolecules*. 2004;37(2):573-578.
- [50] Jin Y, Yang D, Kang D, Jiang X. Fabrication of necklace-like structures via electrospinning. *Langmuir*. 2010;26(2):1186-1190.
- [51] Chang Z. "Firecracker-shaped" ZnO/polyimide hybrid nanofibers via electrospinning and hydrothermal process. *Chem Commun*. 2011;47(15):4427-4429.
- [52] Shengyuan Y, Peining Z, Nair AS, Ramakrishna S. Rice grain-shaped TiO<sub>2</sub> mesostructures—synthesis, characterization and applications in dye-sensitized solar cells and photocatalysis. *J Mater Chem*. 2011;21(18):6541-6548.
- [53] Koombhongse S, Liu W, Reneker DH. Flat polymer ribbons and other shapes by electrospinning. *J Polym Sci, Part B: Polym Phys*. 2001;39(21):2598-2606.
- [54] Holzmeister A, Greiner A, Wendorff JH. "Barbed nanowires" from polymers via electrospinning. *Polym Eng Sci*. 2009;49(1):148-153.
- [55] Li D, Xia Y. Direct fabrication of composite and ceramic hollow nanofibers by electrospinning. *Nano Lett*. 2004;4(5):933-938.
- [56] Jiang S, Jin Q, Agarwal S. Template assisted change in morphology from particles to nanofibers by side-by-side electrospinning of block copolymers. *Macromol Mater Eng*. 2014;299(11):1298-1305.
- [57] Zhao Y, Cao X, Jiang L. Bio-mimic multichannel microtubes by a facile method. *J Am Chem Soc*. 2007;129(4):764-765.
- [58] Chen H, Wang N, Di J, Zhao Y, Song Y, Jiang L. Nanowire-in-microtube structured core/shell fibers via multilfluidic coaxial electrospinning. *Langmuir*. 2010;26(13):11291-11296.
- [59] Luo CJ, Stride E, Stoyanov S, Pelan E, Edirisinghe M. Electrospinning short polymer micro-fibres with average aspect ratios in the range of 10–200. *J Polym Res*. 2011;18(6):2515-2522.
- [60] Fathona I, Yabuki A. A simple one-step fabrication of short polymer nanofibers via electrospinning. *J Mater Sci*. 2014;49(9):3519-3528.
- [61] Fathona IW, Yabuki A. Short electrospun composite nanofibers: Effects of nanoparticle concentration and surface charge on fiber length. *Curr Appl Phys*. 2014;14(5):761-767.
- [62] Stoilkovic A, Agarwal S. Short electrospun fibers by UV cutting method. *Macromol Mater Eng*. 2008;293(11):895-899.
- [63] Zhao Y, Xu T, Ma X, Xi M, Salem DR, Fong H. Hybrid multi-scale epoxy composites containing conventional glass microfibers and electrospun glass nanofibers with improved mechanical properties. *J Appl Polym Sci*. 2015;132(44): 42731.
- [64] Sawawi M, Wang TY, Nisbet DR, Simon GP. Scission of electrospun polymer fibres by ultrasonication. *Polymer*. 2013;54(16):4237-4252.
- [65] Xu W, Feng Y, Ding Y, Jiang S, Fang H, Hou H. Short electrospun carbon nanofiber reinforced polyimide composite with high dielectric permittivity. *Mater Lett*. 2015;161:431-434.
- [66] Kriha O, Becker M, Lehmann M, Kriha D, Kriegelstein J, Yosef M, Schlecht S, Wehrspohn RB, Wendorff JH, Greiner A. Connection of hippocampal neurons by magnetically controlled movement of short electrospun polymer fibers—a route to magnetic micromanipulators. *Adv Mater*. 2007;19(18):2483-2485.
- [67] Jiang S, Greiner A, Agarwal S. Short nylon-6 nanofiber reinforced transparent and high modulus thermoplastic polymeric composites. *Compos Sci Technol*. 2013;87:164-169.

- [68] Jiang S, Duan G, Schöbel J, Agarwal S, Greiner A. Short electrospun polymeric nanofibers reinforced polyimide nanocomposites. *Compos Sci Technol*. 2013;88:57-61.
- [69] Thieme M, Agarwal S, Wendorff JH, Greiner A. Electrospinning and cutting of ultrafine bioerodible poly(lactide-co-ethylene oxide) tri- and multiblock copolymer fibers for inhalation applications. *Polym Adv Technol*. 2011;22(9):1335-1344.
- [70] Duan G, Jiang S, Jérôme V, Wendorff JH, Fathi A, Uhm J, Altstädt V, Herling M, Breu J, Freitag R, Agarwal S, Greiner A. Ultralight, soft polymer sponges by self-assembly of short electrospun fibers in colloidal dispersions. *Adv Funct Mater*. 2015;25(19):2850-2856.
- [71] Si Y, Yu J, Tang X, Ge J, Ding B. Ultralight nanofibre-assembled cellular aerogels with superelasticity and multifunctionality. *Nat Commun*. 2014;5:5802.
- [72] Si Y, Fu Q, Wang X, Zhu J, Yu J, Sun G, Ding B. Superelastic and superhydrophobic nanofiber-assembled cellular aerogels for effective separation of oil/water emulsions. *ACS Nano*. 2015;9(4):3791-3799.
- [73] Chen F, Peng X, Li T, Chen S, Wu XF, Reneker DH, Hou H. Mechanical characterization of single high-strength electrospun polyimide nanofibres. *J Phys D: Appl Phys*. 2008;41:025308.
- [74] Papkov D, Zou Y, Andalib MN, Goponenko A, Cheng SZD, Dzenis YA. Simultaneously strong and tough ultrafine continuous nanofibers. *ACS Nano*. 2013;7(4):3324-3331.
- [75] Abbasipour M, Khajavi R. Nanofiber bundles and yarns production by electrospinning: a review. *Adv Polym Tech*. 2013;32(3):21363.
- [76] Teo WE, Ramakrishna S. A review on electrospinning design and nanofibre assemblies. *Nanotechnology*. 2006;17(14):R89.
- [77] Chen L, Jiang S, Chen J, Chen F, He Y, Zhu Y, Hou H. Single electrospun nanofiber and aligned nanofiber belts from copolyimide containing pyrimidine units. *New J Chem*. 2015;39(11):8956-8963.
- [78] Kakade MV, Givens S, Gardner K, Lee KH, Chase DB, Rabolt JF. Electric field induced orientation of polymer chains in macroscopically aligned electrospun polymer nanofibers. *J Am Chem Soc*. 2007;129(10):2777-2782.
- [79] Yang D, Lu B, Zhao Y, Jiang X. Fabrication of aligned fibrous arrays by magnetic electrospinning. *Adv Mater*. 2007;19(21):3702-3706.
- [80] Wu H, Zhang R, Sun Y, Lin D, Sun Z, Pan W, Downs P. Biomimetic nanofiber patterns with controlled wettability. *Soft Matter*. 2008;4(12):2429-2433.
- [81] Zhang D, Chang J. Patterning of electrospun fibers using electroconductive templates. *Adv Mater*. 2007;19(21):3664-3667.
- [82] Li D, Wang Y, Xia Y. Electrospinning nanofibers as uniaxially aligned arrays and layer-by-layer stacked films. *Adv Mater*. 2004;16(4):361-366.
- [83] Zhong S, Zhang Y, Lim CT. Fabrication of large pores in electrospun nanofibrous scaffolds for cellular infiltration: a review. *Tissue Eng, Part B*. 2011;18(2):77-87.
- [84] Shin S-H, Purevdorj O, Castano O, Planell JA, Kim H-W. A short review: Recent advances in electrospinning for bone tissue regeneration. *J Tissue Eng*. 2012;3(1).
- [85] Holzwarth JM, Ma PX. 3D nanofibrous scaffolds for tissue engineering. *J Mater Chem*. 2011;21(28):10243-10251.
- [86] Chen S, Hou H, Harnisch F, Patil SA, Carmona-Martinez AA, Agarwal S, Zhang Y, Sinha-Ray S, Yarin AL, Greiner A. Electrospun and solution blown three-dimensional carbon fiber nonwovens for application as electrodes in microbial fuel cells. *Energy Environ Sci*. 2011;4(4):1417-1421.
- [87] Wu J, Wang N, Wang L, Dong H, Zhao Y, Jiang L. Electrospun porous structure fibrous film with high

- oil adsorption capacity. *ACS Appl Mat Interfaces*. 2012;4(6):3207-3212.
- [88] Cai S, Xu H, Jiang Q, Yang Y. Novel 3D electrospun scaffolds with fibers oriented randomly and evenly in three dimensions to closely mimic the unique architectures of extracellular matrices in soft tissues: fabrication and mechanism study. *Langmuir*. 2013;29(7):2311-2318.
- [89] Zhang D, Chang J. Electrospinning of three-dimensional nanofibrous tubes with controllable architectures. *Nano Lett*. 2008;8(10):3283-3287.
- [90] Simonet M, Schneider OD, Neuenschwander P, Stark WJ. Ultraporous 3D polymer meshes by low-temperature electrospinning: Use of ice crystals as a removable void template. *Polym Eng Sci*. 2007;47(12):2020-2026.
- [91] Wright LD, Andric T, Freeman JW. Utilizing NaCl to increase the porosity of electrospun materials. *Mater Sci Eng, C*. 2011;31(1):30-36.
- [92] Kim TG, Chung HJ, Park TG. Macroporous and nanofibrous hyaluronic acid/collagen hybrid scaffold fabricated by concurrent electrospinning and deposition/leaching of salt particles. *Acta Biomater*. 2008;4(6):1611-1619.
- [93] Xu T, Miszuk JM, Zhao Y, Sun H, Fong H. Electrospun polycaprolactone 3D nanofibrous scaffold with interconnected and hierarchically structured pores for bone tissue engineering. *Adv Healthcare Mater*. 2015;4(15):2238-2246.
- [94] Sundarrajan S, Tan KL, Lim SH, Ramakrishna S. Electrospun nanofibers for air filtration applications. *Procedia Eng*. 2014;75:159-163.
- [95] Wang N, Mao X, Zhang S, Yu J, Ding B. Electrospun nanofibers for air filtration. In: Ding B, Yu J, editors. *Electrospun nanofibers for energy and environmental applications*: Springer Berlin Heidelberg; 2014. p. 299-323.
- [96] Matulevicius J, Kliucininkas L, Martuzevicius D, Krugly E, Tichonovas M, Baltrusaitis J. Design and characterization of electrospun polyamide nanofiber media for air filtration applications. *J Nanomater*. 2014;2014:13.
- [97] Heikkilä P, Taipale A, Lehtimäki M, Harlin A. Electrospinning of polyamides with different chain compositions for filtration application. *Polym Eng Sci*. 2008;48(6):1168-1176.
- [98] Kim G, Ahn Y, Lee J. Characteristics of Nylon 6 nanofilter for removing ultra fine particles. *Korean J Chem Eng*. 2008;25(2):368-372.
- [99] Mei Y, Wang Z, Li X. Improving filtration performance of electrospun nanofiber mats by a bimodal method. *J Appl Polym Sci*. 2013;128(2):1089-1094.
- [100] Sambaer W, Zatloukal M, Kimmer D. 3D modeling of filtration process via polyurethane nanofiber based nonwoven filters prepared by electrospinning process. *Chem Eng Sci*. 2011;66(4):613-623.
- [101] Patanaik A, Jacobs V, Anandjiwala RD. Performance evaluation of electrospun nanofibrous membrane. *J Membr Sci*. 2010;352(1-2):136-142.
- [102] Dotti F, Varesano A, Montarsolo A, Aluigi A, Tonin C, Mazzuchetti G. Electrospun porous mats for high efficiency filtration. *J Ind Text*. 2007;37(2):151-162.
- [103] Hsiao H-Y, Huang C-M, Liu Y-Y, Kuo Y-C, Chen H. Effect of air blowing on the morphology and nanofiber properties of blowing-assisted electrospun polycarbonates. *J Appl Polym Sci*. 2012;124(6):4904-4914.
- [104] Zhang Q, Welch J, Park H, Wu C-Y, Sigmund W, Marijnissen JCM. Improvement in nanofiber filtration by multiple thin layers of nanofiber mats. *J Aerosol Sci*. 2010;41(2):230-236.
- [105] Wang N, Si Y, Wang N, Sun G, El-Newehy M, Al-Deyab SS, Ding B. Multilevel structured polyacrylonitrile/silica nanofibrous membranes for high-performance air filtration. *Sep Purif Technol*.

2014;126:44-51.

[106] Wang N, Wang X, Ding B, Yu J, Sun G. Tunable fabrication of three-dimensional polyamide-66 nano-fiber/nets for high efficiency fine particulate filtration. *J Mater Chem*. 2012;22(4):1445-1452.

[107] Liu C, Hsu P-C, Lee H-W, Ye M, Zheng G, Liu N, Li W, Cui Y. Transparent air filter for high-efficiency PM2.5 capture. *Nat Commun*. 2015;6:6205.

[108] Gopal R, Kaur S, Ma Z, Chan C, Ramakrishna S, Matsuura T. Electrospun nanofibrous filtration membrane. *J Membr Sci*. 2006;281(1-2):581-586.

[109] Gopal R, Kaur S, Feng CY, Chan C, Ramakrishna S, Tabe S, Matsuura T. Electrospun nanofibrous polysulfone membranes as pre-filters: Particulate removal. *J Membr Sci*. 2007;289(1-2):210-219.

[110] Wang R, Liu Y, Li B, Hsiao BS, Chu B. Electrospun nanofibrous membranes for high flux microfiltration. *J Membr Sci*. 2012;392-393:167-174.

[111] Aussawasathien D, Teerawattananon C, Vongachariya A. Separation of micron to sub-micron particles from water: Electrospun nylon-6 nanofibrous membranes as pre-filters. *J Membr Sci*. 2008;315(1-2):11-19.

[112] Faccini M, Borja G, Boerrigter M, Mart M, Crespiera S, Vazquez-Campos S, Aubouy L, Amantia D. Electrospun carbon nanofiber membranes for filtration of nanoparticles from water. *J Nanomater*. 2015;2015:9.

[113] Liang H-W, Wang L, Chen P-Y, Lin H-T, Chen L-F, He D, Yu S-H. Carbonaceous nanofiber membranes for selective filtration and separation of nanoparticles. *Adv Mater*. 2010;22(42):4691-4695.

[114] Makaremi M, De Silva RT, Pasbakhsh P. Electrospun nanofibrous membranes of polyacrylonitrile/aalloysite with superior water filtration ability. *J Phys Chem C*. 2015;119(14):7949-7958.

[115] Makaremi M, Lim CX, Pasbakhsh P, Lee SM, Goh KL, Chang H, Chan ES. Electrospun functionalized polyacrylonitrile-chitosan Bi-layer membranes for water filtration applications. *RSC Adv*. 2016;6(59):53882-53893.

[116] Haider S, Park S-Y. Preparation of the electrospun chitosan nanofibers and their applications to the adsorption of Cu(II) and Pb(II) ions from an aqueous solution. *J Membr Sci*. 2009;328(1-2):90-96.

[117] Hota G, Kumar BR, Ng WJ, Ramakrishna S. Fabrication and characterization of a boehmite nanoparticle impregnated electrospun fiber membrane for removal of metal ions. *Journal of Materials Science*. 2008;43(1):212-217.

[118] Tian Y, Wu M, Liu R, Li Y, Wang D, Tan J, Wu R, Huang Y. Electrospun membrane of cellulose acetate for heavy metal ion adsorption in water treatment. *Carbohydr Polym*. 2011;83(2):743-748.

[119] Sang Y, Gu Q, Sun T, Li F, Liang C. Filtration by a novel nanofiber membrane and alumina adsorption to remove copper(II) from groundwater. *J Hazard Mater*. 2008;153(1-2):860-866.

[120] Shang Y, Si Y, Raza A, Yang L, Mao X, Ding B, Yu J. An in situ polymerization approach for the synthesis of superhydrophobic and superoleophilic nanofibrous membranes for oil-water separation. *Nanoscale*. 2012;4(24):7847-7854.

[121] Lee MW, An S, Latthe SS, Lee C, Hong S, Yoon SS. Electrospun polystyrene nanofiber membrane with superhydrophobicity and superoleophilicity for selective separation of water and low viscous oil. *ACS Appl Mat Interfaces*. 2013;5(21):10597-10604.

[122] Tai MH, Gao P, Tan BYL, Sun DD, Leckie JO. Highly efficient and flexible electrospun carbon-silica nanofibrous membrane for ultrafast gravity-driven oil-water separation. *ACS Appl Mat Interfaces*. 2014;6(12):9393-9401.

[123] Obaid M, Tolba GMK, Motlak M, Fadali OA, Khalil KA, Almajid AA, Kim B, Barakat NAM. Effective

polysulfone-amorphous SiO<sub>2</sub> NPs electrospun nanofiber membrane for high flux oil/water separation. *Chem Eng J.* 2015;279:631-638.

[124] Obaid M, Barakat NAM, Fadali OA, Motlak M, Almajid AA, Khalil KA. Effective and reusable oil/water separation membranes based on modified polysulfone electrospun nanofiber mats. *Chem Eng J.* 2015;259:449-456.

[125] Zhou Z, Wu X-F. Electrospinning superhydrophobic–superoleophilic fibrous PVDF membranes for high-efficiency water–oil separation. *Mater Lett.* 2015;160:423-427.

[126] Wang L, Yang S, Wang J, Wang C, Chen L. Fabrication of superhydrophobic TPU film for oil–water separation based on electrospinning route. *Mater Lett.* 2011;65(5):869-872.

[127] Zhu H, Qiu S, Jiang W, Wu D, Zhang C. Evaluation of electrospun polyvinyl chloride/polystyrene fibers as sorbent materials for oil spill cleanup. *Environ Sci Technol.* 2011;45(10):4527-4531.

[128] Lin J, Tian F, Shang Y, Wang F, Ding B, Yu J, Guo Z. Co-axial electrospun polystyrene/polyurethane fibres for oil collection from water surface. *Nanoscale.* 2013;5(7):2745-2755.

[129] Ning LQ, Xu NK, Wang R, Liu Y. Fibrous membranes electrospun from the suspension polymerization product of styrene and butyl acrylate for oil-water separation. *RSC Adv.* 2015;5(70):57101-57113.

[130] Zhang X, Ji L, Toprakci O, Liang Y, Alcoutlabi M. Electrospun nanofiber-based anodes, cathodes, and separators for advanced lithium-ion batteries. *Polym Rev.* 2011;51(3):239-264.

[131] Miao Y-E, Zhu G-N, Hou H, Xia Y-Y, Liu T. Electrospun polyimide nanofiber-based nonwoven separators for lithium-ion batteries. *J Power Sources.* 2013;226:82-86.

[132] Cho T-H, Tanaka M, Onishi H, Kondo Y, Nakamura T, Yamazaki H, Tanase S, Sakai T. Battery performances and thermal stability of polyacrylonitrile nano-fiber-based nonwoven separators for Li-ion battery. *J Power Sources.* 2008;181(1):155-160.

[133] Zhang J, Liu Z, Kong Q, Zhang C, Pang S, Yue L, Wang X, Yao J, Cui G. Renewable and superior thermal-resistant cellulose-based composite nonwoven as lithium-ion battery separator. *ACS Appl Mat Interfaces.* 2012;5(1):128-134.

[134] Hao J, Lei G, Li Z, Wu L, Xiao Q, Wang L. A novel polyethylene terephthalate nonwoven separator based on electrospinning technique for lithium ion battery. *J Membr Sci.* 2013;428:11-16.

[135] Gao K, Hu X, Dai C, Yi T. Crystal structures of electrospun PVDF membranes and its separator application for rechargeable lithium metal cells. *Mater Sci Eng B.* 2006;131(1):100-105.

[136] Strain IN, Wu Q, Pourrahimi AM, Hedenqvist MS, Olsson RT, Andersson RL. Electrospinning of recycled PET to generate tough mesomorphic fibre membranes for smoke filtration. *J Mater Chem A.* 2015;3(4):1632-1640.

[137] Selvam A, Nallathambi G. Polyacrylonitrile/silver nanoparticle electrospun nanocomposite matrix for bacterial filtration. *Fibers Polym.* 2015;16(6):1327-1335.

[138] Ma H, Hsiao BS, Chu B. Functionalized electrospun nanofibrous microfiltration membranes for removal of bacteria and viruses. *J Membr Sci.* 2014;452:446-452.

[139] Ru C, Wang F, Pang M, Sun L, Chen R, Sun Y. Suspended, Shrinkage-Free, Electrospun PLGA Nanofibrous Scaffold for Skin Tissue Engineering. *ACS Appl Mat Interfaces.* 2015;7(20):10872-10877.

[140] Yang F, Murugan R, Wang S, Ramakrishna S. Electrospinning of nano/micro scale poly(l-lactic acid) aligned fibers and their potential in neural tissue engineering. *Biomaterials.* 2005;26(15):2603-2610.

[141] Li C, Vepari C, Jin H-J, Kim HJ, Kaplan DL. Electrospun silk-BMP-2 scaffolds for bone tissue engineering. *Biomaterials.* 2006;27(16):3115-3124.

[142] Sung Yeun Y, Tae Heon H, Lihua C, Jin Soo O, Yoon H, WonHyoun R. Membrane-reinforced three-

dimensional electrospun silk fibroin scaffolds for bone tissue engineering. *Biomed Mater.* 2015;10(3):035011.

[143] Yoshimoto H, Shin YM, Terai H, Vacanti JP. A biodegradable nanofiber scaffold by electrospinning and its potential for bone tissue engineering. *Biomaterials.* 2003;24(12):2077-2082.

[144] Ghasemi-Mobarakeh L, Prabhakaran MP, Morshed M, Nasr-Esfahani M-H, Ramakrishna S. Electrospun poly( $\epsilon$ -caprolactone)/gelatin nanofibrous scaffolds for nerve tissue engineering. *Biomaterials.* 2008;29(34):4532-4539.

[145] Meng ZX, Wang YS, Ma C, Zheng W, Li L, Zheng YF. Electrospinning of PLGA/gelatin randomly-oriented and aligned nanofibers as potential scaffold in tissue engineering. *Mater Sci Eng, C.* 2010;30(8):1204-1210.

[146] Jose MV, Thomas V, Johnson KT, Dean DR, Nyairo E. Aligned PLGA/HA nanofibrous nanocomposite scaffolds for bone tissue engineering. *Acta Biomater.* 2009;5(1):305-315.

[147] Matthews JA, Wnek GE, Simpson DG, Bowlin GL. Electrospinning of collagen nanofibers. *Biomacromolecules.* 2002;3(2):232-238.

[148] Lowery JL, Datta N, Rutledge GC. Effect of fiber diameter, pore size and seeding method on growth of human dermal fibroblasts in electrospun poly( $\epsilon$ -caprolactone) fibrous mats. *Biomaterials.* 2010;31(3):491-504.

[149] Moroni L, Licht R, de Boer J, de Wijn JR, van Blitterswijk CA. Fiber diameter and texture of electrospun PEOT/PBT scaffolds influence human mesenchymal stem cell proliferation and morphology, and the release of incorporated compounds. *Biomaterials.* 2006;27(28):4911-4922.

[150] Bashur CA, Dahlgren LA, Goldstein AS. Effect of fiber diameter and orientation on fibroblast morphology and proliferation on electrospun poly(D,L-lactic-co-glycolic acid) meshes. *Biomaterials.* 2006;27(33):5681-5688.

[151] Christopherson GT, Song H, Mao H-Q. The influence of fiber diameter of electrospun substrates on neural stem cell differentiation and proliferation. *Biomaterials.* 2009;30(4):556-564.

[152] Badami AS, Kreke MR, Thompson MS, Riffle JS, Goldstein AS. Effect of fiber diameter on spreading, proliferation, and differentiation of osteoblastic cells on electrospun poly(lactic acid) substrates. *Biomaterials.* 2006;27(4):596-606.

[153] Zhong J, Zhang H, Yan J, Gong X. Effect of nanofiber orientation of electrospun nanofibrous scaffolds on cell growth and elastin expression of muscle cells. *Colloids Surf B Biointerfaces.* 2015;136:772-778.

[154] Zoppe JO, Peresin MS, Habibi Y, Venditti RA, Rojas OJ. Reinforcing poly( $\epsilon$ -caprolactone) nanofibers with cellulose nanocrystals. *ACS Appl Mat Interfaces.* 2009;1(9):1996-2004.

[155] Zhou C, Shi Q, Guo W, Terrell L, Qureshi AT, Hayes DJ, Wu Q. Electrospun bio-nanocomposite scaffolds for bone tissue engineering by cellulose nanocrystals reinforcing maleic anhydride grafted PLA. *ACS Appl Mat Interfaces.* 2013;5(9):3847-3854.

[156] Lee YH, Lee JH, An I-G, Kim C, Lee DS, Lee YK, Nam J-D. Electrospun dual-porosity structure and biodegradation morphology of Montmorillonite reinforced PLLA nanocomposite scaffolds. *Biomaterials.* 2005;26(16):3165-3172.

[157] Liao H, Qi R, Shen M, Cao X, Guo R, Zhang Y, Shi X. Improved cellular response on multiwalled carbon nanotube-incorporated electrospun polyvinyl alcohol/chitosan nanofibrous scaffolds. *Colloids Surf B Biointerfaces.* 2011;84(2):528-535.

[158] Chaoying W, Biqiong C. Poly( $\epsilon$ -caprolactone)/graphene oxide biocomposites: mechanical properties and bioactivity. *Biomed Mater.* 2011;6(5):055010.

- [159] Agarwal S, Greiner A. On the way to clean and safe electrospinning—green electrospinning: emulsion and suspension electrospinning. *Polym Adv Technol*. 2011;22(3):372-378.
- [160] Yarin AL. Coaxial electrospinning and emulsion electrospinning of core-shell fibers. *Polym Adv Technol*. 2011;22(3):310-317.
- [161] Joshi P, Zhang L, Chen Q, Galipeau D, Fong H, Qiao Q. Electrospun carbon nanofibers as low-cost counter electrode for dye-sensitized solar cells. *ACS Appl Mat Interfaces*. 2010;2(12):3572-3577.
- [162] Chen S, Hou H, Harnisch F, Patil SA, Carmona-Martinez AA, Agarwal S, Zhang Y, Sinha-Ray S, Yarin AL, Greiner A, Schroder U. Electrospun and solution blown three-dimensional carbon fiber nonwovens for application as electrodes in microbial fuel cells. *Energy Environ Sci*. 2011;4(4):1417-1421.
- [163] Ghasemi M, Shahgaldi S, Ismail M, Kim BH, Yaakob Z, Wan Daud WR. Activated carbon nanofibers as an alternative cathode catalyst to platinum in a two-chamber microbial fuel cell. *Int J Hydrogen Energy*. 2011;36(21):13746-13752.
- [164] Li M, Han G, Yang B. Fabrication of the catalytic electrodes for methanol oxidation on electrospinning-derived carbon fibrous mats. *Electrochem Commun*. 2008;10(6):880-883.
- [165] Zhang P, Shao C, Zhang Z, Zhang M, Mu J, Guo Z, Liu Y. In situ assembly of well-dispersed Ag nanoparticles (AgNPs) on electrospun carbon nanofibers (CNFs) for catalytic reduction of 4-nitrophenol. *Nanoscale*. 2011;3(8):3357-3363.
- [166] Both Engel A, Bechelany M, Fontaine O, Cherifi A, Cornu D, Tingry S. One-pot route to gold nanoparticles embedded in electrospun carbon fibers as efficient catalyst material for hybrid alkaline glucose biofuel cell. *ChemElectroChem*. 2015; 3(4):629-637.
- [167] Guo Q, Zhao D, Liu S, Chen S, Hanif M, Hou H. Free-standing nitrogen-doped carbon nanotubes at electrospun carbon nanofibers composite as an efficient electrocatalyst for oxygen reduction. *Electrochim Acta*. 2014;138:318-324.
- [168] Ghouri ZK, Barakat NAM, Obaid M, Lee JH, Kim HY. Co/CeO<sub>2</sub>-decorated carbon nanofibers as effective non-precious electro-catalyst for fuel cells application in alkaline medium. *Ceram Int*. 2015;41(2, Part A):2271-2278.
- [169] Zhang P, Shao C, Zhang Z, Zhang M, Mu J, Guo Z, Liu Y. TiO<sub>2</sub>@carbon core/shell nanofibers: Controllable preparation and enhanced visible photocatalytic properties. *Nanoscale*. 2011;3(7):2943-2949.
- [170] Peng X, Ye W, Ding Y, Jiang S, Hanif M, Liao X, Hou H. Facile synthesis, characterization and application of highly active palladium nano-network structures supported on electrospun carbon nanofibers. *RSC Adv*. 2014;4(80):42732-42736.
- [171] Wang C, Shao C, Wang L, Zhang L, Li X, Liu Y. Electrospinning preparation, characterization and photocatalytic properties of Bi<sub>2</sub>O<sub>3</sub> nanofibers. *J Colloid Interface Sci*. 2009;333(1):242-248.
- [172] Kim YS, Nam SH, Shim H-S, Ahn H-J, Anand M, Kim WB. Electrospun bimetallic nanowires of PtRh and PtRu with compositional variation for methanol electrooxidation. *Electrochem Commun*. 2008;10(7):1016-1019.
- [173] Xu S, Sun D, Liu H, Wang X, Yan X. Fabrication of Cu-doped cerium oxide nanofibers via electrospinning for preferential CO oxidation. *Catal Commun*. 2011;12(6):514-518.
- [174] Li C, Chen R, Zhang X, Shu S, Xiong J, Zheng Y, Dong W. Electrospinning of CeO<sub>2</sub>-ZnO composite nanofibers and their photocatalytic property. *Mater Lett*. 2011;65(9):1327-1330.
- [175] Yang Y, Zhang C, Xu Y, Wang H, Li X, Wang C. Electrospun Er:TiO<sub>2</sub> nanofibrous films as efficient photocatalysts under solar simulated light. *Mater Lett*. 2010;64(2):147-150.
- [176] Lee J, Yoo JM, Ye Y, Mun Y, Lee S, Kim O-H, Rhee H-W, Lee HI, Sung Y-E, Lee J. Development of

highly stable and mass transfer-enhanced cathode catalysts: support-free electrospun intermetallic FePt nanotubes for polymer electrolyte membrane fuel cells. *Adv Energy Mater.* 2015;5(11):1402093.

[177] Higgins DC, Wang R, Hoque MA, Zamani P, Abureden S, Chen Z. Morphology and composition controlled platinum–cobalt alloy nanowires prepared by electrospinning as oxygen reduction catalyst. *Nano Energy.* 2014;10:135-143.

[178] Huang J, Hou H, You T. Highly efficient electrocatalytic oxidation of formic acid by electrospun carbon nanofiber-supported Pt<sub>x</sub>Au<sub>100-x</sub> bimetallic electrocatalyst. *Electrochem Commun.* 2009;11(6):1281-1284.

[179] Chou S-F, Carson D, Woodrow KA. Current strategies for sustaining drug release from electrospun nanofibers. *J Controlled Release.* 2015;220, Part B:584-591.

[180] Meinel AJ, Germershaus O, Luhmann T, Merkle HP, Meinel L. Electrospun matrices for localized drug delivery: Current technologies and selected biomedical applications. *Eur J Pharm Biopharm.* 2012;81(1):1-13.

[181] Hu X, Liu S, Zhou G, Huang Y, Xie Z, Jing X. Electrospinning of polymeric nanofibers for drug delivery applications. *J Controlled Release.* 2014;185:12-21.

[182] Xu X, Chen X, Ma Pa, Wang X, Jing X. The release behavior of doxorubicin hydrochloride from medicated fibers prepared by emulsion-electrospinning. *Eur J Pharm Biopharm.* 2008;70(1):165-170.

[183] Yohe ST, Herrera VLM, Colson YL, Grinstaff MW. 3D superhydrophobic electrospun meshes as reinforcement materials for sustained local drug delivery against colorectal cancer cells. *J Controlled Release.* 2012;162(1):92-101.

[184] Chen P, Wu Q-S, Ding Y-P, Chu M, Huang Z-M, Hu W. A controlled release system of titanocene dichloride by electrospun fiber and its antitumor activity in vitro. *Eur J Pharm Biopharm.* 2010;76(3):413-420.

[185] Kim K, Luu YK, Chang C, Fang D, Hsiao BS, Chu B, Hadjiargyrou M. Incorporation and controlled release of a hydrophilic antibiotic using poly(lactide-co-glycolide)-based electrospun nanofibrous scaffolds. *J Controlled Release.* 2004;98(1):47-56.

[186] Thakur RA, Florek CA, Kohn J, Michniak BB. Electrospun nanofibrous polymeric scaffold with targeted drug release profiles for potential application as wound dressing. *Int J Pharm.* 2008;364(1):87-93.

[187] Jiang H, Hu Y, Zhao P, Li Y, Zhu K. Modulation of protein release from biodegradable core–shell structured fibers prepared by coaxial electrospinning. *J Biomed Mater Res Part B.* 2006;79B(1):50-57.

[188] Chew SY, Wen J, Yim EKF, Leong KW. Sustained Release of Proteins from Electrospun Biodegradable Fibers. *Biomacromolecules.* 2005;6(4):2017-2024.

[189] Kim TG, Lee DS, Park TG. Controlled protein release from electrospun biodegradable fiber mesh composed of poly( $\epsilon$ -caprolactone) and poly(ethylene oxide). *Int J Pharm.* 2007;338(1–2):276-283.

[190] Zeng J, Aigner A, Czubayko F, Kissel T, Wendorff JH, Greiner A. Poly(vinyl alcohol) nanofibers by electrospinning as a protein delivery system and the retardation of enzyme release by additional polymer coatings. *Biomacromolecules.* 2005;6(3):1484-1488.

[191] Luu YK, Kim K, Hsiao BS, Chu B, Hadjiargyrou M. Development of a nanostructured DNA delivery scaffold via electrospinning of PLGA and PLA–PEG block copolymers. *J Controlled Release.* 2003;89(2):341-353.

[192] Nie H, Wang C-H. Fabrication and characterization of PLGA/HAp composite scaffolds for delivery of BMP-2 plasmid DNA. *J Controlled Release.* 2007;120(1–2):111-121.

[193] Cao H, Jiang X, Chai C, Chew SY. RNA interference by nanofiber-based siRNA delivery system. *J*

- Controlled Release. 2010;144(2):203-212.
- [194] Rujitanaroj P-o, Wang Y-C, Wang J, Chew SY. Nanofiber-mediated controlled release of siRNA complexes for long term gene-silencing applications. *Biomaterials*. 2011;32(25):5915-5923.
- [195] Tungprapa S, Jangchud I, Supaphol P. Release characteristics of four model drugs from drug-loaded electrospun cellulose acetate fiber mats. *Polymer*. 2007;48(17):5030-5041.
- [196] Kenawy E-R, Abdel-Hay FI, El-Newehy MH, Wnek GE. Controlled release of ketoprofen from electrospun poly(vinyl alcohol) nanofibers. *Mater Sci Eng, A*. 2007;459(1-2):390-396.
- [197] Pattama T, Uracha R, Pitt S. Drug-loaded electrospun mats of poly(vinyl alcohol) fibres and their release characteristics of four model drugs. *Nanotechnology*. 2006;17(9):2317.
- [198] Bölgen N, Vargel İ, Korkusuz P, Menceloğlu YZ, Pişkin E. In vivo performance of antibiotic embedded electrospun PCL membranes for prevention of abdominal adhesions. *J Biomed Mater Res, Part B*. 2007;81B(2):530-543.
- [199] Zeng J, Yang L, Liang Q, Zhang X, Guan H, Xu X, Chen X, Jing X. Influence of the drug compatibility with polymer solution on the release kinetics of electrospun fiber formulation. *J Controlled Release*. 2005;105(1-2):43-51.
- [200] Ranganath SH, Wang C-H. Biodegradable microfiber implants delivering paclitaxel for post-surgical chemotherapy against malignant glioma. *Biomaterials*. 2008;29(20):2996-3003.
- [201] Zhang YZ, Wang X, Feng Y, Li J, Lim CT, Ramakrishna S. Coaxial electrospinning of (fluorescein isothiocyanate-conjugated bovine serum albumin)-encapsulated poly( $\epsilon$ -caprolactone) nanofibers for sustained release. *Biomacromolecules*. 2006;7(4):1049-1057.
- [202] Weng L, Xie J. Smart Electrospun nanofibers for controlled drug release: recent advances and new perspectives. *Curr Pharm Des*. 2015;21(15):1944-1959.
- [203] Akimov YK. Fields of application of aerogels (review). *Instrum Exp Tech*. 2003;46(3):287-299.
- [204] Chabot V, Higgins D, Yu A, Xiao X, Chen Z, Zhang J. A review of graphene and graphene oxide sponge: material synthesis and applications to energy and the environment. *Energy Environ Sci*. 2014;7(5):1564-1596.
- [205] Nardecchia S, Carriazo D, Ferrer ML, Gutierrez MC, del Monte F. Three dimensional macroporous architectures and aerogels built of carbon nanotubes and/or graphene: synthesis and applications. *Chem Soc Rev*. 2013;42(2):794-830.
- [206] Thapliyal PC, Singh K. Aerogels as promising thermal insulating materials: an overview. *J Mater*. 2014;2014:10.
- [207] Gui X, Wei J, Wang K, Cao A, Zhu H, Jia Y, Shu Q, Wu D. Carbon nanotube sponges. *Adv Mater*. 2010;22(5):617-621.
- [208] Song W-L, Guan X-T, Fan L-Z, Cao W-Q, Wang C-Y, Cao M-S. Tuning three-dimensional textures with graphene aerogels for ultra-light flexible graphene/texture composites of effective electromagnetic shielding. *Carbon*. 2015;93:151-160.
- [209] Wu X-L, Wen T, Guo H-L, Yang S, Wang X, Xu A-W. Biomass-derived sponge-like carbonaceous hydrogels and aerogels for supercapacitors. *ACS Nano*. 2013;7(4):3589-3597.
- [210] Moreno-Castilla C, Maldonado-Hódar FJ. Carbon aerogels for catalysis applications: An overview. *Carbon*. 2005;43(3):455-465.
- [211] Li J, Li J, Meng H, Xie S, Zhang B, Li L, Ma H, Zhang J, Yu M. Ultra-light, compressible and fire-resistant graphene aerogel as a highly efficient and recyclable absorbent for organic liquids. *J Mater Chem A*. 2014;2(9):2934-2941.
- [212] Bi H, Yin Z, Cao X, Xie X, Tan C, Huang X, Chen B, Chen F, Yang Q, Bu X, Lu X, Sun L, Zhang H. Carbon

fiber aerogel made from raw cotton: a novel, efficient and recyclable sorbent for oils and organic solvents. *Adv Mater.* 2013;25(41):5916-5921.

[213] Wu Z-Y, Li C, Liang H-W, Zhang Y-N, Wang X, Chen J-F, Yu S-H. Carbon nanofiber aerogels for emergent cleanup of oil spillage and chemical leakage under harsh conditions. *Sci Rep.* 2014;4:4079.

[214] Inagaki M, Yang Y, Kang F. Carbon nanofibers prepared via electrospinning. *Adv Mater.* 2012;24(19):2547-2566.

[215] Zhang L, Aboagye A, Kelkar A, Lai C, Fong H. A review: carbon nanofibers from electrospun polyacrylonitrile and their applications. *J Mater Sci.* 2014;49(2):463-480.

[216] Innerlohinger J, Weber HK, Kraft G. Aerocellulose: aerogels and aerogel-like materials made from cellulose. *Macromol Symp.* 2006;244(1):126-135.

[217] Fischer F, Rigacci A, Pirard R, Berthon-Fabry S, Achard P. Cellulose-based aerogels. *Polymer.* 2006;47(22):7636-7645.

[218] Jin H, Nishiyama Y, Wada M, Kuga S. Nanofibrillar cellulose aerogels. *Colloids Surf Physicochem Eng Aspects.* 2004;240(1-3):63-67.

[219] Zhang W, Zhang Y, Lu C, Deng Y. Aerogels from crosslinked cellulose nano/micro-fibrils and their fast shape recovery property in water. *J Mater Chem.* 2012;22(23):11642-11650.

[220] Carlsson DO, Nystrom G, Zhou Q, Berglund LA, Nyholm L, Stromme M. Electroactive nanofibrillated cellulose aerogel composites with tunable structural and electrochemical properties. *J Mater Chem.* 2012;22(36):19014-19024.

[221] Liebner F, Potthast A, Rosenau T, Haimer E, Wendland M. Ultralight-weight cellulose aerogels from NBnMO-stabilized lyocell dopes. *Res Lett Mater Sci.* 2007;2007:4.

[222] Granstrom M, nee Paakko MK, Jin H, Kolehmainen E, Kilpelainen I, Ikkala O. Highly water repellent aerogels based on cellulose stearyl esters. *Polym Chem.* 2011;2(8):1789-1796.

[223] Chin SF, Binti Romainor AN, Pang SC. Fabrication of hydrophobic and magnetic cellulose aerogel with high oil absorption capacity. *Mater Lett.* 2014;115:241-243.

[224] Nguyen ST, Feng J, Le NT, Le ATT, Hoang N, Tan VBC, Duong HM. Cellulose aerogel from paper waste for crude oil spill cleaning. *Ind Eng Chem Res.* 2013;52(51):18386-18391.

[225] Aulin C, Netrval J, Wagberg L, Lindstrom T. Aerogels from nanofibrillated cellulose with tunable oleophobicity. *Soft Matter.* 2010;6(14):3298-3305.

[226] Nguyen ST, Feng J, Ng SK, Wong JPW, Tan VBC, Duong HM. Advanced thermal insulation and absorption properties of recycled cellulose aerogels. *Colloids Surf Physicochem Eng Aspects.* 2014;445:128-134.

[227] Jin H, Kettunen M, Laiho A, Pynnönen H, Paltakari J, Marmur A, Ikkala O, Ras RHA. Superhydrophobic and superoleophobic nanocellulose aerogel membranes as bioinspired cargo carriers on water and oil. *Langmuir.* 2011;27(5):1930-1934.

[228] Cervin N, Aulin C, Larsson P, Wågberg L. Ultra porous nanocellulose aerogels as separation medium for mixtures of oil/water liquids. *Cellulose.* 2012;19(2):401-410.

[229] Lorjai P, Chaisuwan T, Wongkasemjit S. Porous structure of polybenzoxazine-based organic aerogel prepared by sol-gel process and their carbon aerogels. *J Sol-Gel Sci Technol.* 2009;52(1):56-64.

[230] Gioia C, Ricci A, Bernardi L, Bourahla K, Tanchoux N, Robitzer M, Quignard F. Chitosan aerogel beads as a heterogeneous organocatalyst for the asymmetric aldol reaction in the presence of water: an assessment of the effect of additives. *Eur J Org Chem.* 2013;2013(3):588-594.

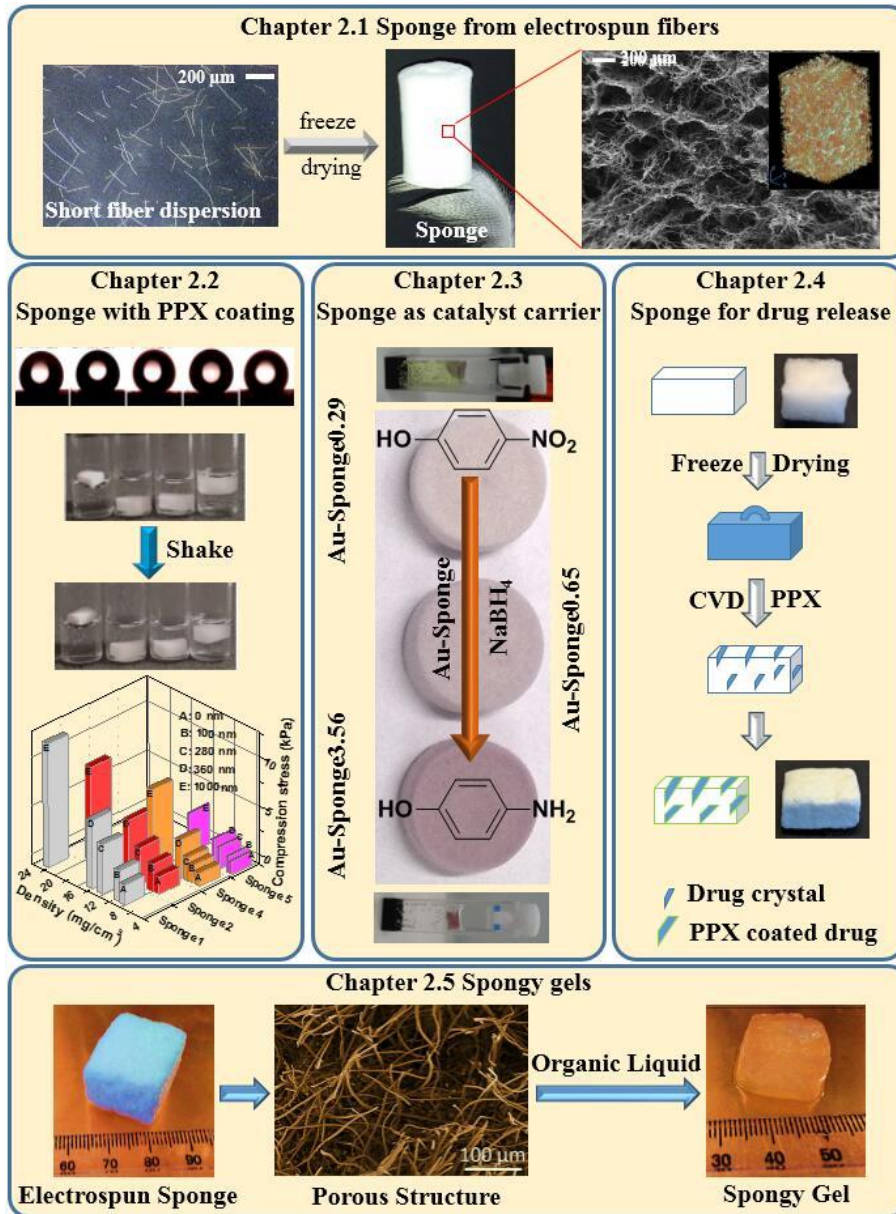
[231] García-González CA, Jin M, Gerth J, Alvarez-Lorenzo C, Smirnova I. Polysaccharide-based aerogel microspheres for oral drug delivery. *Carbohydr Polym.* 2015;117:797-806.

- [232] Song X, Yang S, He L, Yan S, Liao F. Ultra-flyweight hydrophobic poly(m-phenylenediamine) aerogel with micro-spherical shell structures as a high-performance selective adsorbent for oil contamination. *RSC Adv.* 2014;4(90):49000-49005.
- [233] Cardea S, Sessa M, Reverchon E. Supercritical CO<sub>2</sub> assisted formation of poly(vinylidene fluoride) aerogels containing amoxicillin, used as controlled release device. *J Supercrit Fluids.* 2011;59:149-156.
- [234] Lee J, Gould G. Polycyclopentadiene based aerogel: a new insulation material. *J Sol-Gel Sci Technol.* 2007;44(1):29-40.
- [235] Pierre A, Rigacci A. SiO<sub>2</sub> aerogels. In: Aegerter MA, Leventis N, Koebel MM, editors. *Aerogels Handbook*: Springer New York; 2011. p. 21-45.
- [236] Yokogawa H. Hydrophobic silica aerogel. *Handbook of sol-gel science and technology.* 2005;3:73-84.
- [237] Patel RP, Purohit NS, Suthar AM. An overview of silica aerogels. *Int J ChemTech Res.* 2009;1(4):1052-1057.
- [238] Cui S, Liu X, Liu Y, Shen X, Lin B, Han G, Wu Z. Adsorption properties of nitrobenzene in wastewater with silica aerogels. *Sci China: Technol Sci.* 2010;53(9):2367-2371.
- [239] Smirnova I, Mamic J, Arlt W. Adsorption of drugs on silica aerogels. *Langmuir.* 2003;19(20):8521-8525.
- [240] Smirnova I, Suttirungwong S, Arlt W. Feasibility study of hydrophilic and hydrophobic silica aerogels as drug delivery systems. *J Non-Cryst Solids.* 2004;350:54-60.
- [241] Baetens R, Jelle BP, Gustavsen A. Aerogel insulation for building applications: A state-of-the-art review. *Energ Buildings.* 2011;43(4):761-769.
- [242] Yoldas BE, Annen MJ, Bostaph J. Chemical engineering of aerogel morphology formed under nonsupercritical conditions for thermal insulation. *Chem Mater.* 2000;12(8):2475-2484.
- [243] Tillotson TM, Hrubesh LW. Transparent ultralow-density silica aerogels prepared by a two-step sol-gel process. *J Non-Cryst Solids.* 1992;145:44-50.
- [244] Rubin M, Lampert CM. Transparent silica aerogels for window insulation. *Sol Energy Mater.* 1983;7(4):393-400.
- [245] Tabata M, Adachi I, Hatakeyama Y, Kawai H, Morita T, Sumiyoshi T. Large-area silica aerogel for use as Cherenkov radiators with high refractive index, developed by supercritical carbon dioxide drying. *J Supercrit Fluids.* 2016; 110:183-192.
- [246] Gronauer M, Kadur A, Fricke J. Mechanical and Acoustic Properties of Silica Aerogel. In: Fricke J, editor. *Aerogels*, vol. 6: Springer Berlin Heidelberg; 1986. p. 167-173.
- [247] Gross J, Fricke J. Ultrasonic velocity measurements in silica, carbon and organic aerogels. *J Non-Cryst Solids.* 1992;145:217-222.
- [248] Nobuyuki K, Yoshito F, Takashi K, Kohei S, Ken-ichi I. Preparation of highly porous silica aerogel thin film by supercritical drying. *Jpn J Appl Phys.* 2000;39(3A):L182.
- [249] Hyun SH, Kim JJ, Park HH. Synthesis and characterization of low-dielectric silica aerogel films. *J Am Ceram Soc.* 2000;83(3):533-540.
- [250] Kim GS, Hyun SH, Park HH. Synthesis of low-dielectric silica aerogel films by ambient drying. *J Am Ceram Soc.* 2001;84(2):453-455.
- [251] Brüesch P, Stucki F, Baumann T, Kluge-Weiss P, Brühl B, Niemeyer L, Strümpfer R, Ziegler B, Mielke M. Electrical and infrared dielectrical properties of silica aerogels and of silica-aerogel-based composites. *Appl Phys A.* 1993;57(4):329-337.
- [252] Cao Y, Zhongfu X, Qing L, Jun S, Linyan C, Bing Z. Study of porous dielectrics as electret materials.

- IEEE Trans Dielectr Electr Insul. 1998;5(1):58-62.
- [253] Yin J, Li X, Zhou J, Guo W. Ultralight three-dimensional boron nitride foam with ultralow permittivity and superelasticity. *Nano Lett.* 2013;13(7):3232-3236.
- [254] Jung SM, Jung HY, Fang W, Dresselhaus MS, Kong J. A facile methodology for the production of in situ inorganic nanowire hydrogels/aerogels. *Nano Lett.* 2014;14(4):1810-1817.
- [255] Chabi S, Rocha VG, Garcia-Tunton E, Ferraro C, Saiz E, Xia Y, Zhu Y. Ultralight, strong, three-dimensional SiC structures. *ACS Nano.* 2016; 10 (2):1871-1876.
- [256] Kim J-H, Suh DJ, Park T-J, Kim K-L. Effect of metal particle size on coking during CO<sub>2</sub> reforming of CH<sub>4</sub> over Ni–alumina aerogel catalysts. *Appl Catal, A.* 2000;197(2):191-200.
- [257] Le DB, Passerini S, Guo J, Ressler J, Owens BB, Smyrl WH. High surface area V<sub>2</sub>O<sub>5</sub> aerogel intercalation electrodes. *J Electrochem Soc.* 1996;143(7):2099-2104.
- [258] Moretti A, Secchiaroli M, Buchholz D, Giuli G, Marassi R, Passerini S. Exploring the Low Voltage Behavior of V<sub>2</sub>O<sub>5</sub> Aerogel as Intercalation Host for Sodium Ion Battery. *J Electrochem Soc.* 2015;162(14):A2723-A2728.
- [259] Wei T-Y, Chen C-H, Chang K-H, Lu S-Y, Hu C-C. Cobalt oxide aerogels of ideal supercapacitive properties prepared with an epoxide synthetic route. *Chem Mater.* 2009;21(14):3228-3233.
- [260] Chien H-C, Cheng W-Y, Wang Y-H, Lu S-Y. Ultrahigh specific capacitances for supercapacitors achieved by nickel cobaltite/carbon aerogel composites. *Adv Funct Mater.* 2012;22(23):5038-5043.
- [261] Gao K, Shao Z, Wang X, Zhang Y, Wang W, Wang F. Cellulose nanofibers/multi-walled carbon nanotube nanohybrid aerogel for all-solid-state flexible supercapacitors. *RSC Adv.* 2013;3(35):15058-15064.
- [262] Ye S, Feng J. Self-assembled three-dimensional hierarchical graphene/polypyrrole nanotube hybrid aerogel and its application for supercapacitors. *ACS Appl Mat Interfaces.* 2014;6(12):9671-9679.
- [263] He Y, Chen W, Li X, Zhang Z, Fu J, Zhao C, Xie E. Freestanding three-dimensional graphene/MnO<sub>2</sub> composite networks as ultralight and flexible supercapacitor electrodes. *ACS Nano.* 2013;7(1):174-182.
- [264] Xiao L, Wu D, Han S, Huang Y, Li S, He M, Zhang F, Feng X. Self-assembled Fe<sub>2</sub>O<sub>3</sub>/Graphene aerogel with high lithium storage performance. *ACS Appl Mat Interfaces.* 2013;5(9):3764-3769.
- [265] Vanyorek L, Loche D, Katona H, Casula MF, Corrias A, Kónya Z, Kukovec Á, Kiricsi I. Optimization of the catalytic chemical vapor deposition synthesis of multiwall carbon nanotubes on FeCo(Ni)/SiO<sub>2</sub> aerogel catalysts by statistical design of experiments. *J Phys Chem C.* 2011;115(13):5894-5902.
- [266] Meng F, Zhang X, Xu B, Yue S, Guo H, Luo Y. Alkali-treated graphene oxide as a solid base catalyst: synthesis and electrochemical capacitance of graphene/carbon composite aerogels. *J Mater Chem.* 2011;21(46):18537-18539.
- [267] Maldonado-Hódar FJ, Moreno-Castilla C, Rivera-Utrilla J. Synthesis, pore texture and surface acid–base character of TiO<sub>2</sub>/carbon composite xerogels and aerogels and their carbonized derivatives. *Appl Catal, A.* 2000;203(1):151-159.
- [268] Wei S, Wu D, Shang X, Fu R. Studies on the structure and electrochemical performance of Pt/carbon aerogel catalyst for direct methanol fuel cells. *Energy Fuels.* 2009;23(2):908-911.
- [269] King JS, Wittstock A, Biener J, Kucheyev SO, Wang YM, Baumann TF, Giri SK, Hamza AV, Baeumer M, Bent SF. Ultralow loading Pt nanocatalysts prepared by atomic layer deposition on carbon aerogels. *Nano Lett.* 2008;8(8):2405-2409.
- [270] Baker WS, Long JW, Stroud RM, Rolison DR. Sulfur-functionalized carbon aerogels: a new approach for loading high-surface-area electrode nanoarchitectures with precious metal catalysts. *J Non-Cryst Solids.* 2004;350:80-87.

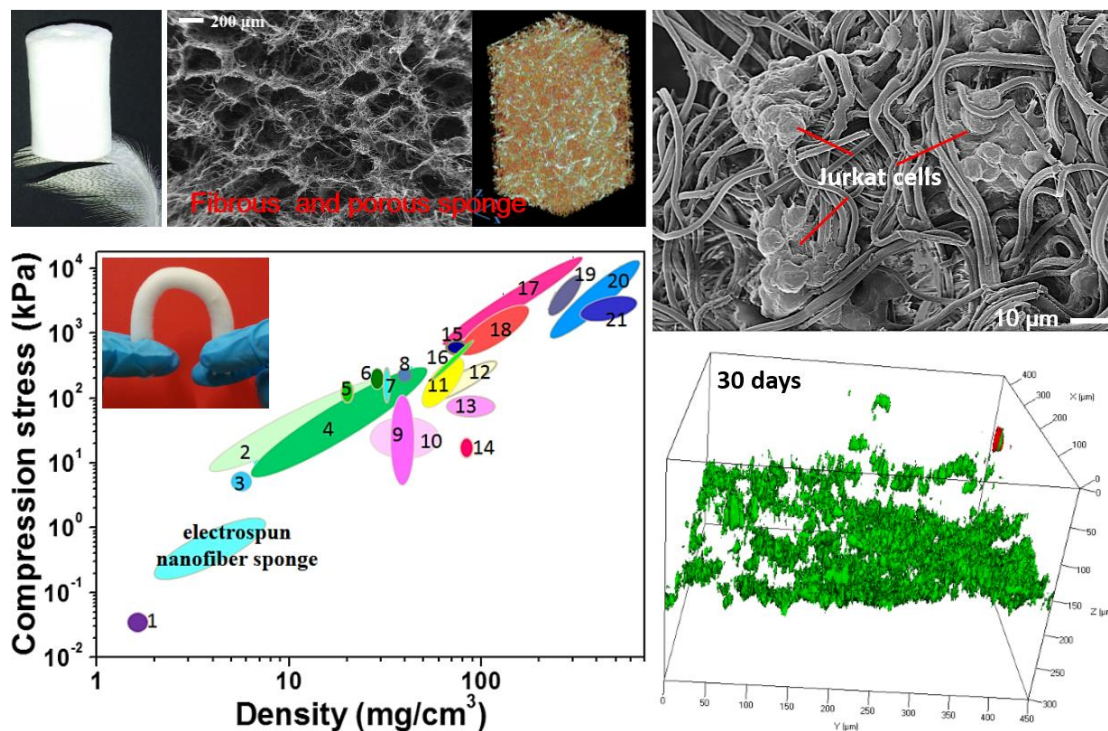
- [271] Williams VO, Jeong NC, Prasittichai C, Farha OK, Pellin MJ, Hupp JT. Fast Transporting ZnO–TiO<sub>2</sub> coaxial photoanodes for dye-sensitized solar cells based on ALD-Modified SiO<sub>2</sub> aerogel frameworks. *ACS Nano*. 2012;6(7):6185-6196.
- [272] Casu A, Casula MF, Corrias A, Falqui A, Loche D, Marras S. Magnetic and structural investigation of highly porous CoFe<sub>2</sub>O<sub>4</sub>–SiO<sub>2</sub> nanocomposite aerogels. *J Phys Chem C*. 2007;111(2):916-922.
- [273] Kwon Y-G, Choi S-Y, Kang E-S, Baek S-S. Ambient-dried silica aerogel doped with TiO<sub>2</sub> powder for thermal insulation. *J Mater Sci*. 2000;35(24):6075-6079.
- [274] Yavari F, Chen Z, Thomas AV, Ren W, Cheng H-M, Koratkar N. High sensitivity gas detection using a macroscopic three-dimensional graphene foam network. *Sci Rep*. 2011;1:166.
- [275] Langner M, Agarwal S, Baudler A, Schröder U, Greiner A. Large multipurpose exceptionally conductive polymer sponges obtained by efficient wet-chemical metallization. *Adv Funct Mater*. 2015;25(39):6182-6188.
- [276] Yao Q, Cosme JG, Xu T, Miszuk JM, Picciani PH, Fong H, Sun H. Three dimensional electrospun PCL/PLA blend nanofibrous scaffolds with significantly improved stem cells osteogenic differentiation and cranial bone formation. *Biomaterials*. 2017;115:115-127.
- [277] Li D, Chen W, Sun B, Li H, Wu T, Ke Q, Huang C, Hany E-H, Al-Deyab SS, Mo X. A comparison of nanoscale and multiscale PCL/gelatin scaffolds prepared by disc-electrospinning. *Colloids Surf B Biointerfaces*. 2016;146:632-641.

## 2 Cumulative part of dissertation



This thesis contains four publications and one manuscript in **Section 2.1** to **2.5**. The main contents involve the preparation, properties and applications of fibrous porous three dimensional (3D) sponges, which are summarized in the following sections. In **Section 2.1**, initial investigations of 3D sponges from electrospun fibers on the fabrication, structures, mechanical properties and applications including liquid uptake and cell growth are performed. **Section 2.2** aims at the disadvantages (poor mechanical properties and instability in solvents) of the sponges prepared in **Section 2.1**, proposing a useful strategy by coating another polymers on the whole surface of the sponges to form stable junctions between the fibers to improve the compression properties and solvent resistance. **Section 2.3** applies functionalized 3D fibrous sponges with immobilized Au nanoparticles (Au-sponge) as efficient catalyst support. The Au-sponge possesses low density and carried small amount of AuNPs, but the Au-sponges exhibit superior high normalized rate constant versus the amount of immobilized AuNPs due to the large pore volume of the sponge. **Section 2.4** uses the porous sponges as drug carrier for drug release. Due to the large pore volume of the sponge, the drug loading capacity by the sponge can be up to 2639 mg/g. The drug release from the sponge can be controlled by adjusting the thickness of an additional polymer coating. The last section (**Section 2.5**) aims the development of new spongy gel based on the 3D sponges from electrospun fibers. The spongy gels exhibited not only the same features as traditional organogels, but also possessed advantages such as no shrinkage, no sensitivity to impurities on gel formation, good control over the 3D network, and a wide range of possibilities for functionalization due to the abundant resources of electrospun fibers. Detailed coverage of the experimental parts, results and discussions can be found in **Chapter 3**.

## 2.1 Ultralight, soft polymer sponges by self-assembly of short electrospun fibers in colloidal dispersions



This work has already been published in:

**Gaigai Duan**, Shaohua Jiang, Valérie Jérôme, Joachim H Wendorff, Amir Fathi, Jaqueline Uhm, Volker Altstädt, Markus Herling, Josef Brey, Ruth Freitag, Seema Agarwal, Andreas Greiner. Ultralight, Soft Polymer Sponges by Self-Assembly of Short Electrospun Fibers in Colloidal Dispersions. *Adv. Funct. Mater.* **2015**; 25(19):2850-2856.

### Specific contributions by authors:

Gaigai Duan was involved in the whole work on the experimental part and wrote the manuscript. Dr. Shaohua Jiang have done all the SEM measurement and gave many suggestion and discussion on the project and manuscript. Dr. Valérie Jérôme and Prof. Ruth Freitag carried out the application of cell growth and wrote the corresponding

part of the manuscript. Amir Fathi, Jaqueline Uhm and Prof. Volker Altstädt contributed to the work by the performance of micro-CT analysis. Markus Herling and Prof. Josef Breu carried out the BET measurement on the specific surface area of the sponges. Prof. Seema Agarwal gave many valuable suggestions and discussion for this project. Prof. Andreas Greiner was in charge for the whole project.

Three dimensional (3D) sponges with interconnected networks possess excellent properties, such as large porosity, hierarchical pore structure, low density, and reversible compressibility. However, it is difficult to fabricate such mechanical stable 3D sponges straightforwardly from electrospinning. In this work, we developed a novel procedure to prepare 3D sponges from electrospun fibers (**Figure 2-1**). By changing the concentrations of short electrospun fibers from 2.42 to 8.76 mg/mL in the dispersion, the sponges exhibits ultralow density in the range of 2.72-9.12 mg/cm<sup>3</sup>. A highly porous structure with porosity >99% is found in the fibrous sponge and the sponge contains hierarchical order of the pores and interconnection of the fibers, where big pores of 300-430  $\mu\text{m}$  and small pores of 10-30  $\mu\text{m}$  are observed (**Figure 2-1**).

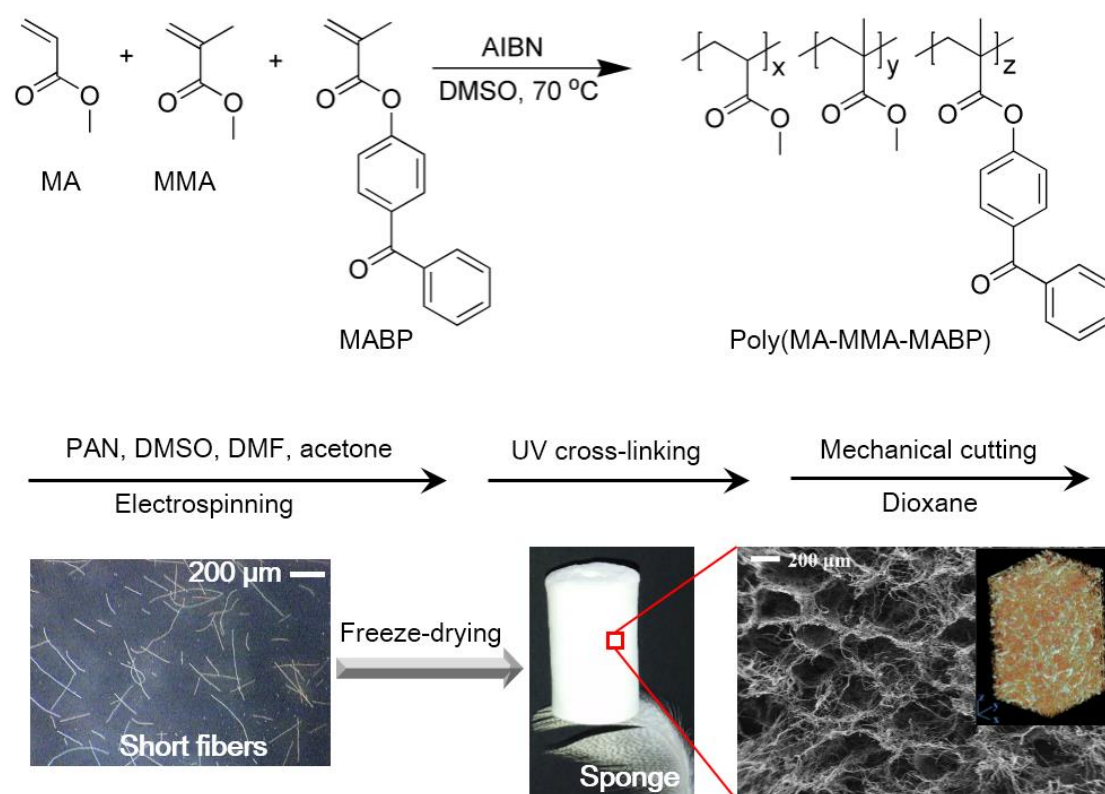


**Figure 2-1.** Preparation of fibrous and porous sponge from short electrospun fibers and the porous structure of the sponge.

The sponge exhibits reversible compressibility and bendability without any fracture and tunable compression properties (**Figure 2-2**). As the density increased from 2.72 to 5.05 mg/cm<sup>3</sup>, the compression strength at 50% compression strain increases from 0.3 to 1 kPa. Although the density of the sponge is low, the fibrous sponge can cover an important area in the Ashby plot of the compression stress vs density with comparison to other porous materials and is also close to the natural sponge (spongia

officinalis).

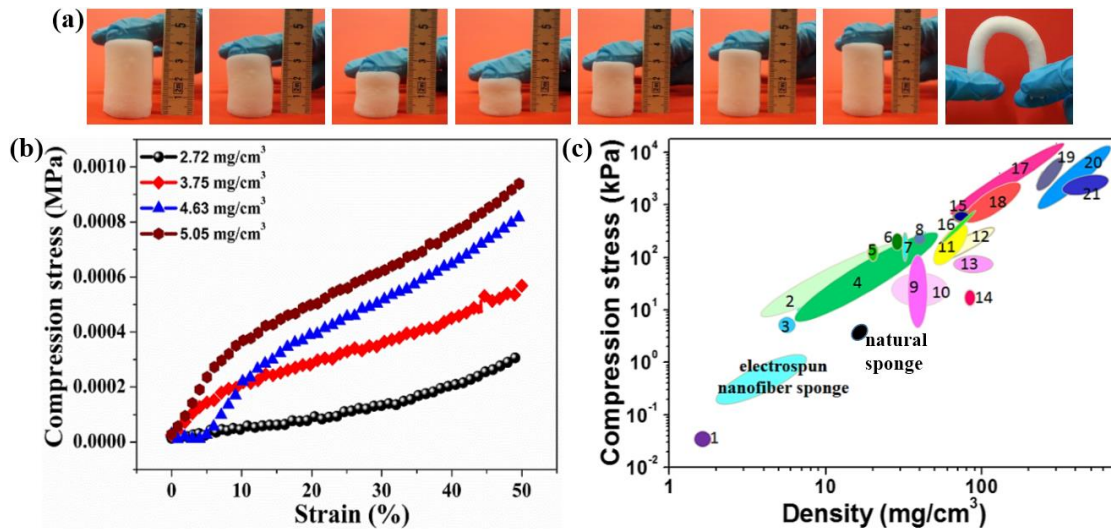


**Figure 2-2.** Digital photos of the reversibly compressible and bendable sponge (a), compression stress-strain curves of the sponges with different densities (b), and Ashby plot of the compression stress vs density with comparison to other porous materials. (1) boron nitride, (2) carbon nanotube, (3) carbon aerogel, (4) cellulose fiber, (5) cross-linked polystyrene, (6) polyolefin (closed cell), (7) polyethylene (closed cell), (8) polyimide, (9) polyethylene (50% strain), (10) silk fibroin, (11) melamine-formaldehyde (rigid), (12) tannin-based (rigid), (13) PDLLA/Bioglass composite, (14) latex rubber, (15) PAN-microspheres and fibers, (16) rigid polyurethane, (17) PVC (cross-linked), (18) epoxy-boroxine, (19) bio-based macroporous polymers, (20) silicon oxycarbide ceramic, (21) aluminum foams.

Due to the highly porous structure, the fibrous sponges are successfully applied for high capacity oil adsorption and cell tissue engineering (**Figure 2-3**). Unlike other surface wetting behavior for liquid adsorption, the porous sponges exhibit a pore filling mechanism for the oil adsorption so that large oil adsorption and reversible sorption and desorption from the sponge can be achieved (**Figure 2-3a, b**). 3D porous structure is also highly required for the growth of cells. The Jurkat cells can be survived in the sponge and formed cell clusters (**Figure 2-3c**). Further incubation of Jurkat cells indicates that the sponge is suitable for the cell growth into tissue even after 30 days' incubation (**Figure 2-3d**).

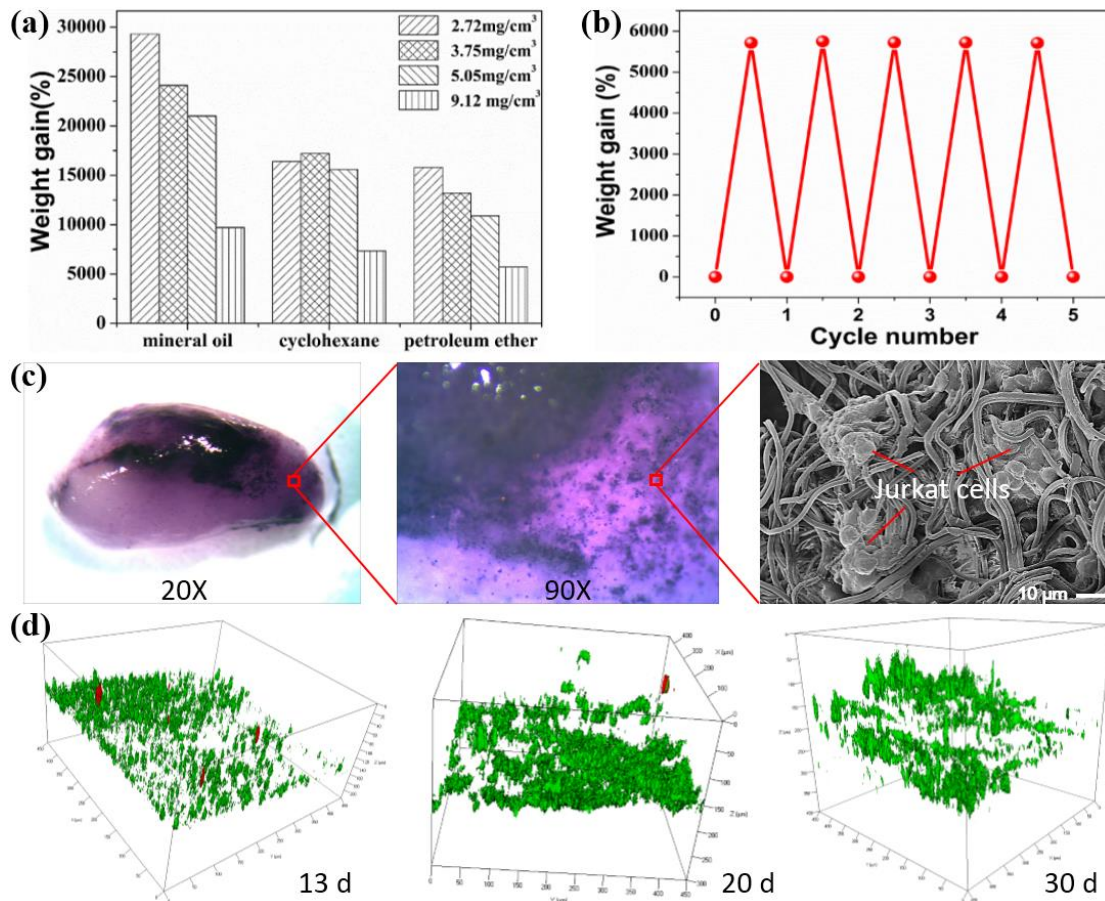
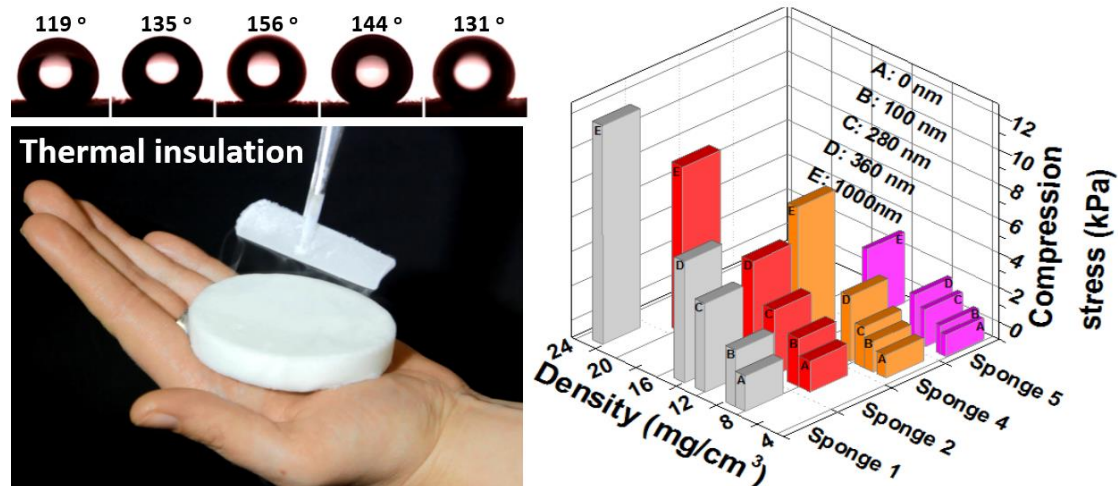


**Figure 2-3.** Weight gain of liquids (mineral oil, cyclohexane and petroleum ether) (a) and reversible sorption and desorption of cyclohexane (b) from the porous sponge; Jurkat cells colonized on a sponge (c); and 3D confocal images of Jurkat cells incubation for 13, 20 and 30 days in the sponges (d), where green and red color indicated the live and dead cells.

In conclusion, fibrous 3D sponges with ultralow density, low specific surface area and high pore volume are successfully prepared from dispersions of short electrospun fibers. The sponges have excellent mechanical compression properties and liquid absorption and are successfully applied for cell growth. This technique for the fabrication of fibrous porous sponges opens a wide door to prepare the sponges from various electrospun fibers and to functionalize the sponge with various functions for different applications.

## 2.2 Ultralight open cell polymer sponges with advanced properties by PPX CVD coating



This work has already been published in:

**Gaigai Duan**, Shaohua Jiang, Tobias Moss, Seema Agarwal, Andreas Greiner. Ultralight open cell polymer sponges with advanced properties by PPX CVD coating. *Polym. Chem.* **2016**; 7(15):2759-2764.

### Specific contributions by authors:

Gaigai Duan performed the whole work on the experimental part and wrote the manuscript. Dr. Shaohua Jiang has done all the SEM measurements and corrected the first version of the manuscript. Tobias Moss carried out the experiment of PPX coating and wrote the corresponding part of the manuscript. Prof. Seema Agarwal gave many valuable suggestions and discussion for this project. Prof. Andreas Greiner was responsible for the guidance and supervision of the whole project.

In **Section 2.1**, we showed ultralight 3D fibrous sponges made from short electrospun fibers which possesses low density, large porosity and compressibility, and can be applied for oil absorption and cell tissue engineering. However, the relatively low compressive strength (<1 kPa) and the poor resistance of the sponges to the solvents greatly limited their applications in harsh environment. In this work, an additional polymer coating of poly(*p*-xylylene) (PPX), which has good adhesion to other surfaces, excellent chemical resistance, mechanical properties and thermal stability, is coated on the surface of the fibrous sponges (**Figure 2-4a**). Depending on the density of the un-coated original sponges and the coating thickness of PPX, the PPX coated sponges possesses tunable densities, compression properties, water contact angle and enhanced solvent resistance.

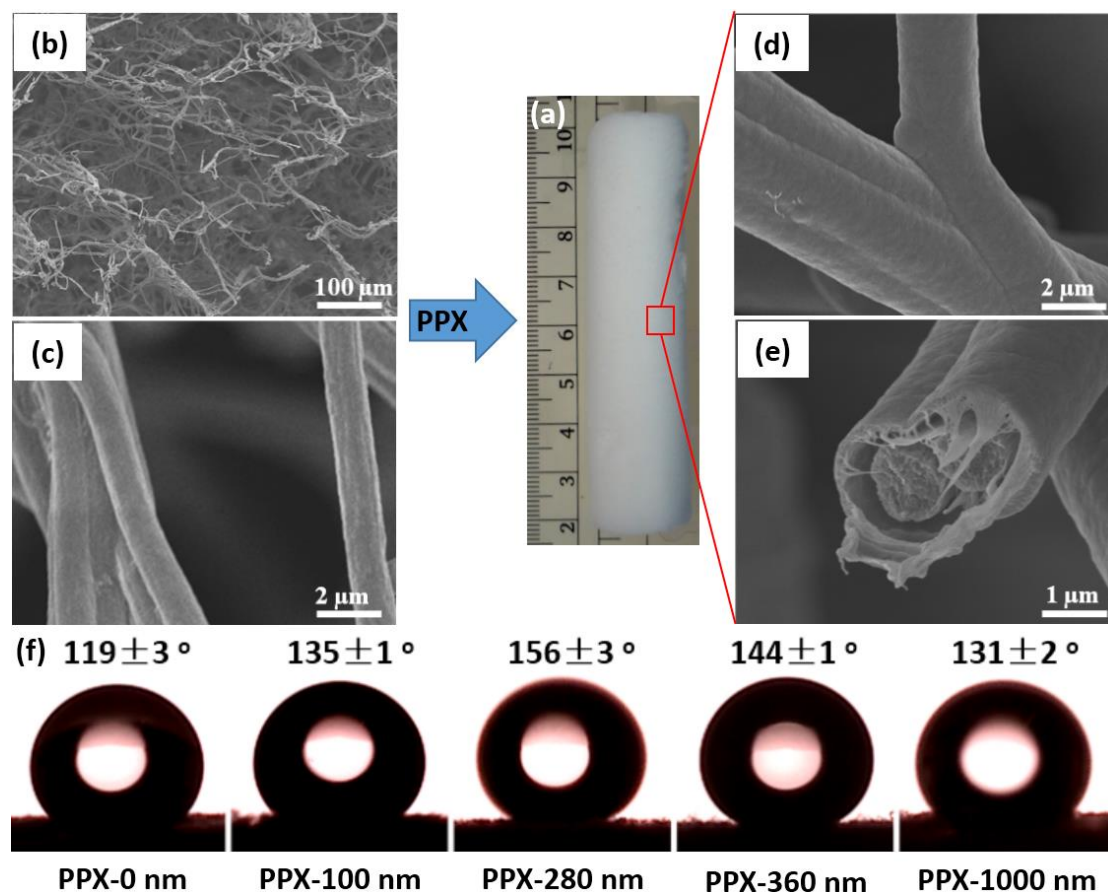


**Figure 2-4.** Digital photo of PPX-coated sponge (a); SEM images of original sponge (b, c) with density of  $5.16 \text{ mg/cm}^3$ , and the corresponding sponge after PPX coating with 1000 nm (d, e); Typical water contact angle of sponges with different PPX coating thicknesses (f).

The original sponges shows fibrous porous structures (**Figure 2-4b**) and have densities in the range of 4.34-8.42 mg/cm<sup>3</sup>. After coating by a uniform layer of PPX with different coating thicknesses, the density increases in the range of 4.83-22.59 mg/cm<sup>3</sup> and the fibers show core-shell structures as shown in **Figure 2-4c, d, e**.

The PPX coating on the sponges leads to a significant improvement on water contact angle (**Figure 2-4f**). The PPX coated sponge shows superhydrophobicity with water contact angle of 156° in comparison to the 119° of the original sponges. In addition, depending on the sponge densities and the coating densities, the water contact angle can be varied in the range of 114-156°.

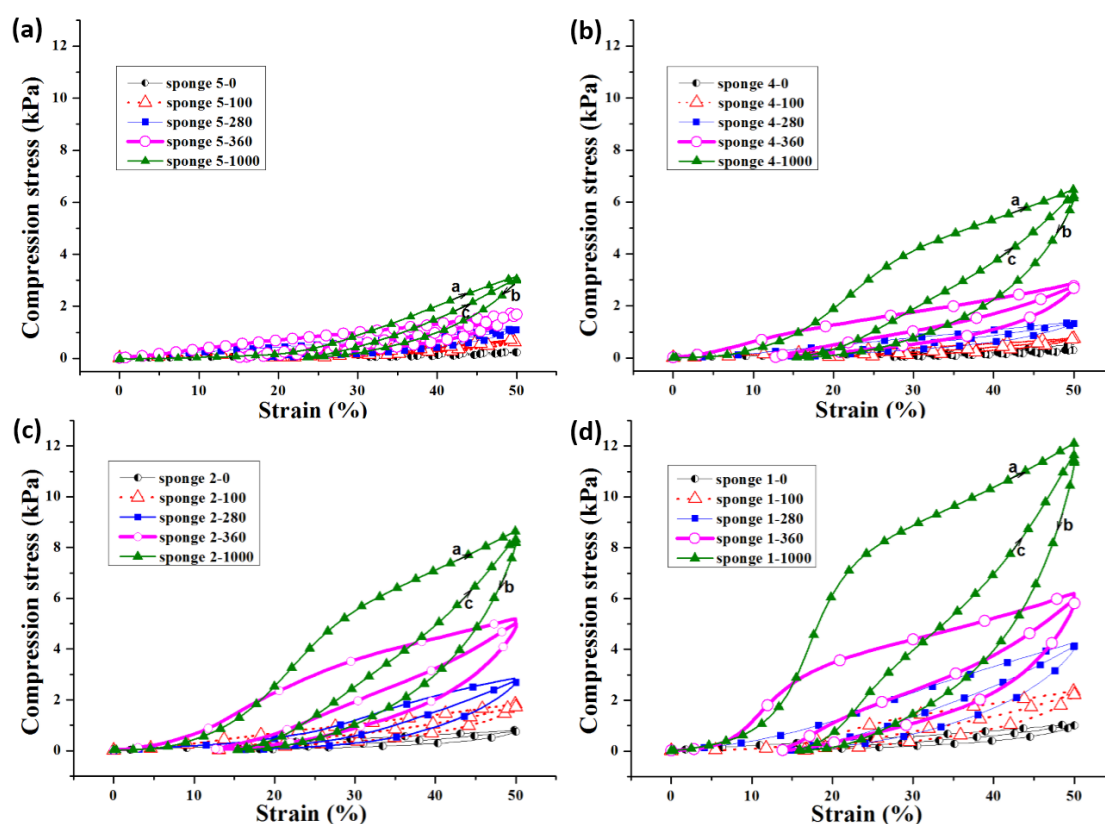


**Figure 2-5.** Compression stress-strain curves of the sponges with different densities and different PPX coating thicknesses. The densities for the sponges without PPX coating of (a), (b), (c) and (d) are 4.34, 5.16, 7.43 and 8.42 mg/cm<sup>3</sup>, respectively.

The PPX coating on the fibrous sponges leads to an obvious improvement on compression properties (**Figure 2-5**). As expected, the sponges with smaller density show lower compression strength at 50% compression strain. After coating with PPX with increased thickness, the compression strength of the sponge also increases. Compared to the bare sponges, the sponge coating with 100 nm and 1000 nm PPX shows more than 2 times and 10 times compression strength, which greatly improve

the mechanical stability of the sponges. The cyclic compression measurements show that the PPX coated sponge exhibits the same compression strength after one cycle of compressing and releasing.

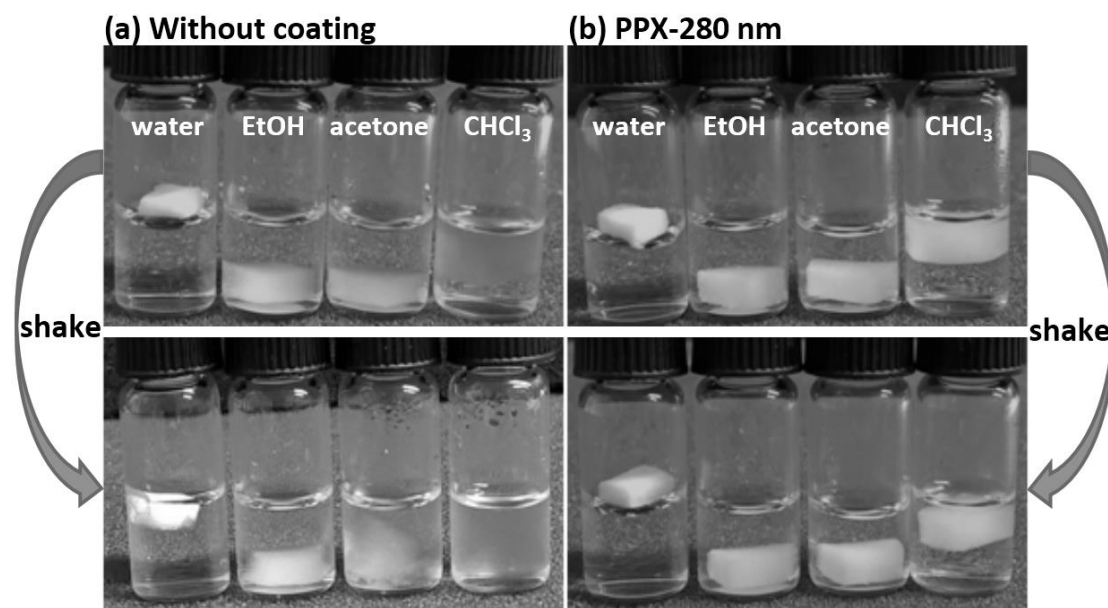
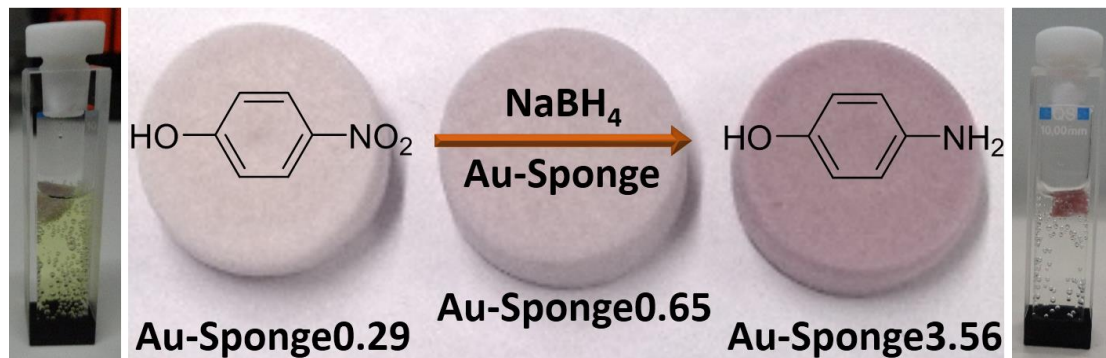


**Figure 2-6.** Solvent resistance of the sponges without (a) and with (b) 280 nm PPX coating.

Due to the excellent solvent resistance of PPX and the stable junctions formed in-between the fibers as cross-linking network, the sponges coated with PPX also show improved solvent resistance (**Figure 2-6**), which provides many more chances for different kinds of applications. The sponge without PPX coating would be disintegrated in the solvents after shaking. As comparison, the sponges coated with 280 nm PPX show excellent solvent resistance so that higher shape stability is observed even if the sponges are strongly shaken in the solvents.

In conclusion, CVD method is successfully applied to modify the fibrous sponges with improved mechanical properties, tunable wetting properties and enhanced solvent resistance. This improvement on mechanical stability and solvent resistance of the sponges provides the opportunity to apply the sponges in harsher environment. The superhydrophobicity of the composite sponges would attract particular interest for application in oil/water separation.

## 2.3 Highly efficient reusable sponge-type catalyst carriers based on short electrospun fibers



This work has already been published in:

**Gaigai Duan**, Melissa Koehn-Serrano, Andreas Greiner. Highly Efficient Reusable Sponge-Type Catalyst Carriers Based on Short Electrospun Fibers. *Macromol. Rapid Comm.* **2017**; *38*: 1600511.

### Specific contributions by authors:

Gaigai Duan performed the whole work on the experimental part and wrote the manuscript. Dr. Melissa Koehn-Serrano prepared the gold nanoparticles. Prof. Andreas Greiner was responsible for the guidance and supervision of the whole project.

Carriers for catalysts with highly efficiency often require large specific surface area and large amount of catalyst. In this work, a novel catalyst carrier with low specific surface area but large pore volume presents highly efficient mass transfer of educts and products, and can reduce the blockage of the active catalyst carrier surface by product adhesion. The spongy carrier is made from functionalized electrospun fibers with immobilized Au nanoparticles (AuNPs). Following with the same preparation procedure as described in **section 2.1** and **section 2.2**, the sponges with different amount of AuNPs (0.29 wt%, 0.65 wt% and 3.56 wt%, Au-sponge) are prepared (**Figure 2-7**).

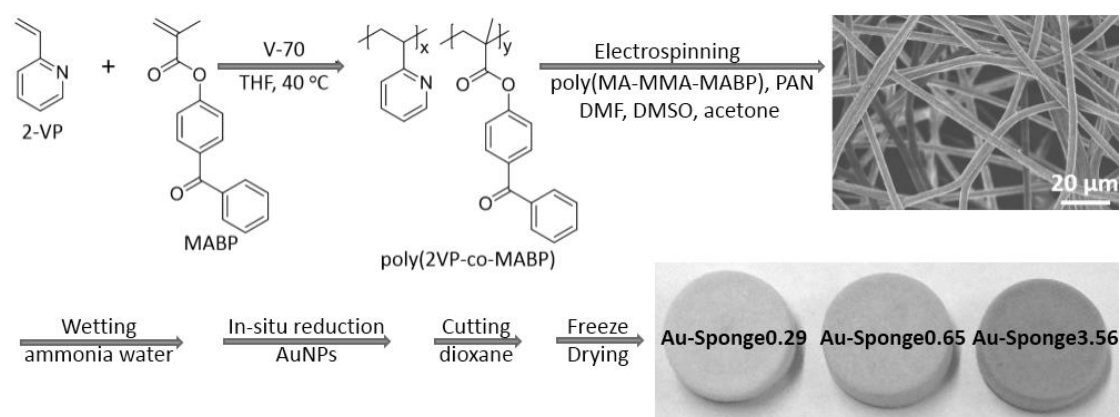


**Figure 2-7.** Procedure of the preparation of Au-sponges.

As expected, the Au-sponge possesses hierarchical porous structure that the pore size can be as large as 400 μm (**Figure 2-8a**). The immobilization of AuNPs with average particle size of  $5.7 \pm 0.8$  nm was confirmed by EDX spectra (**Figure 2-8b**) and TEM images (**Figure 2-8c**). In addition, the Au-sponge also shows excellent mechanical stability (**Figure 2-8d**). The Au-sponge3.56 shows a compression strength of 0.55 kPa at 50% compression. The cyclic compression test indicated that the sponge possesses the same compression strength after one cycle compression and release. This mechanical stability provides the possibility of the reuse of the Au-sponge for catalysis.

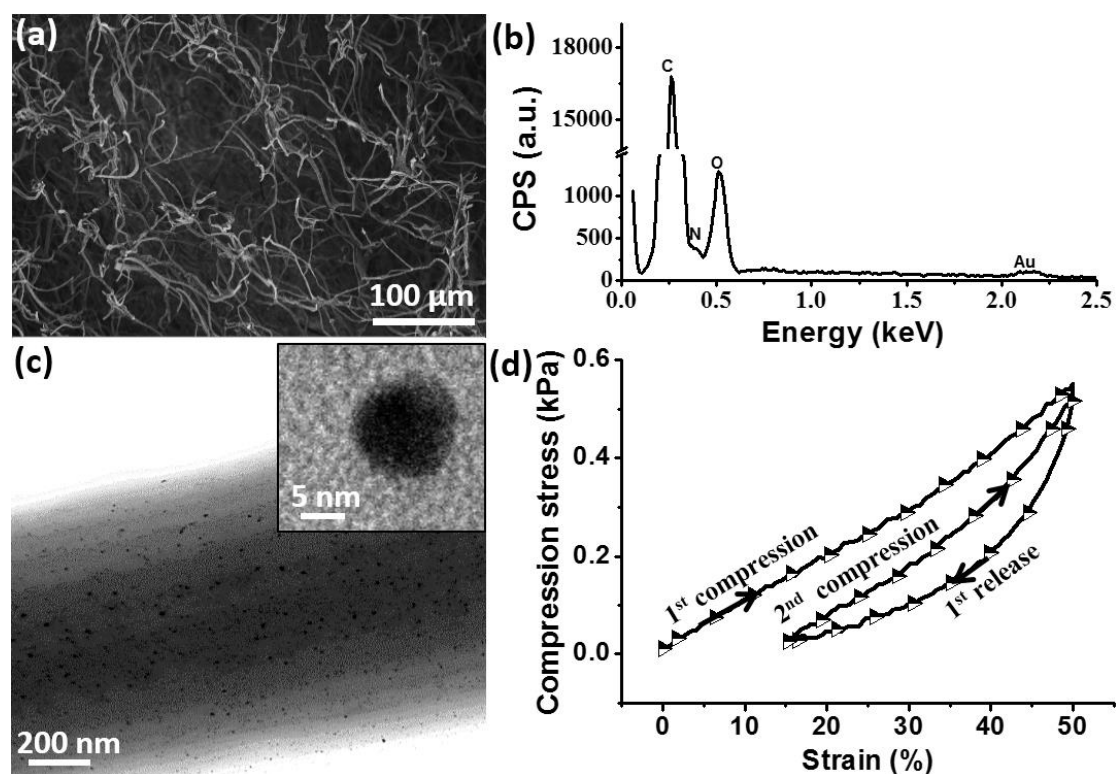


**Figure 2-8.** SEM image of Au-sponge3.56 (a), EDX spectra of AuNP-immobilized fibers (b), TEM images of AuNPs on the sponge (c), and cyclic compression measurement of Au-sponge3.56 (d).

The catalytic performance indicates that the amount of AuNPs in the sponge plays an important role on the catalyst efficiency (**Figure 2-9a, b**). With the same reaction time of 32 min, Au-sponge3.56 shows a higher efficiency than Au-sponge0.29 for the reduction of 4-nitrophenol. The intensity of the absorption peak at 400 nm decreases to 0.06 and 0.22 and the color of the product become colorless and still light yellow, respectively. Further investigation on the normalized reaction rate constant ( $K_{nor}$ ) indicates that the Au-sponge possessed very high value of  $K_{nor}$  of 10 / (min g), which can be achieved by very small amount of AuNPs (0.0029 mg). This value is 100% more efficient than that achieves by other carrier system with immobilized AuNPs. Other dispersed AuNPs also show comparable  $K_{nor}$  to the Au-sponge system, but these systems are hardly achieving the reusability of the catalyst. In this work, the sponge catalyst (Au-sponge3.56) shows feasible reuse for catalysis so that after 5 cycles of reuse, the rate constant decreases slightly from 0.090/min to 0.072/min.

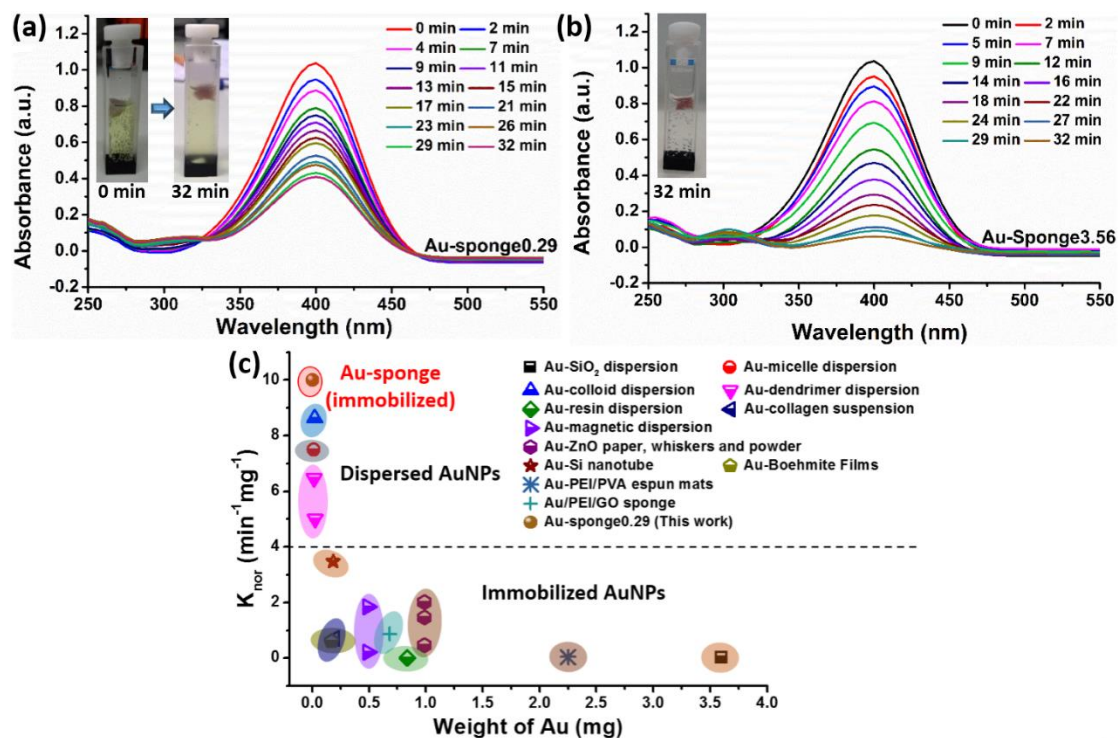
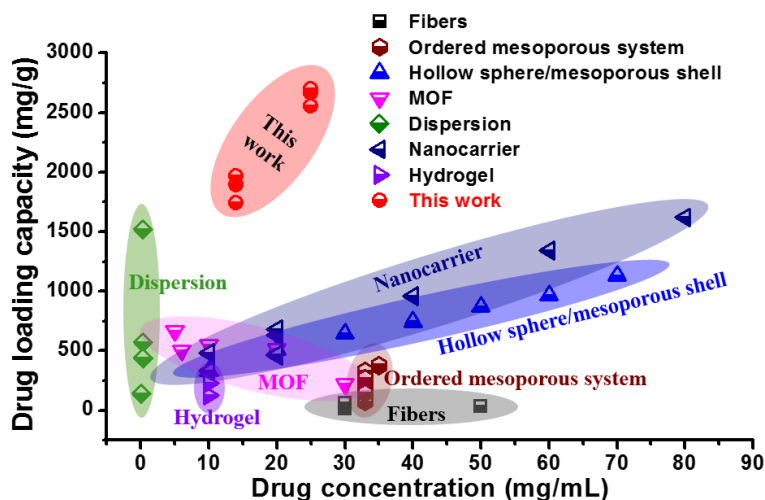


**Figure 2-9.** UV-Vis spectra to monitor the reduction of 4-nitrophenol using Au-sponge0.29 (a) and Au-sponge3.56 (b) as catalysts, and Ashby plot of the comparison of normalized rate constant ( $K_{nor}$ ) versus the amount of AuNPs on the different kinds of supports.

In conclusion, the Au-sponge system with very small amount of AuNPs and low specific surface areas possesses surprisingly high catalytic rate constants, which are in the range of the top values with comparison to other AuNP carrier systems with high specific surface area. The large pore volume of the Au-sponge can effectively improve the mass transfer of the educts and products in the reaction solution. It is obvious that the mass transfer in the reaction system also plays a very important role in catalyst efficiency. This Au-sponge system also opens a new direction for design of new catalyst carrier system with large pore volume but small specific surface area.

## 2.4 Exploration of Macroporous Polymeric Sponges As Drug Carriers



This work has already been published in:

**Gaigai Duan**, Amir Reza Bagheri, Shaohua Jiang, Jacob Golenser, Seema Agarwal, Andreas Greiner. Exploration of Macroporous Polymeric Sponges As Drug Carriers. *Biomacromolecules*. **2017**; DOI: [10.1021/acs.biomac.7b00852](https://doi.org/10.1021/acs.biomac.7b00852).

### Specific contributions by authors:

Gaigai Duan performed the whole work on the experimental part and wrote the manuscript. Amir Reza Bagheri helped with the drug release. Dr. Shaohua Jiang gave suggestions on the experiment and wrote the manuscript. Prof. Seema Agarwal and Prof. Jacob Golenser gave many valuable suggestions and discussion for this project. Prof. Andreas Greiner was responsible for the guidance and supervision of the whole project.

How to achieve a high drug loading capacity and a controlled drug release is the challenges for the current drug release system. In this work, a novel drug carrier of fibrous porous sponges is developed to solve the above problems. Due to the large pore volume (up to  $285 \text{ cm}^3/\text{g}$ ), the sponges can load superior high drug amounts of up to  $2693 \text{ mg/g}$  by freeze-drying (**Figure 2-10**), which is achieved by only using 1 vol% of the total pore volume of the sponges. Additional PPX coating around the whole drug loaded sponges (**Figure 2-10**) is used to realize the controllable drug release.

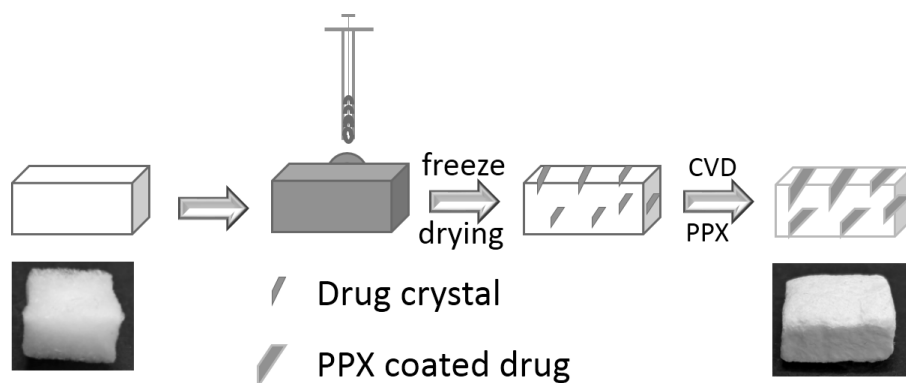


**Figure 2-10.** Procedure of the preparation of drug-loaded sponge.

The as-prepared sponges with density of  $3.5 \text{ mg/cm}^3$  (SG3.5) exhibits hierarchical porous structures (**Figure 2-11a**) and high specific pore volume, which are useful to load large amounts of drug. After loading with the drug, Artemisone in this work, the drug is distributed in-between the fibers (**Figure 2-11b, c**). After the coating, the whole sponges including the fibers and the drugs are completely covered by the PPX coating (**Figure 2-11d, e**). The EDX spectra by sulfur element mapping (**Figure 2-11f**) indicates the homogeneous distribution of the drug (Artemisone) in the sponge.

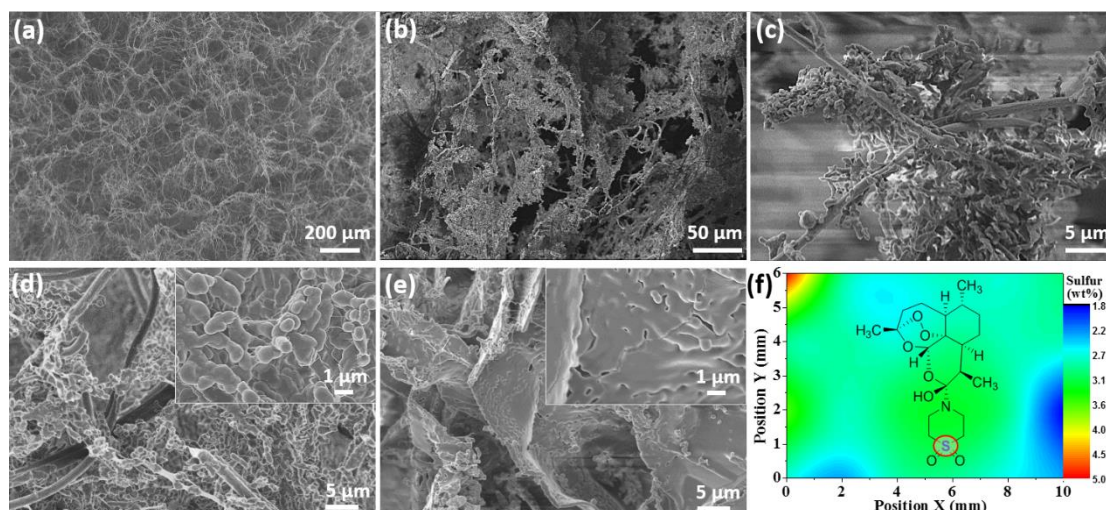


**Figure 2-11.** SEM images of as-prepared sponge ( $3.5 \text{ mg/cm}^3$ , SG3.5) (a), sponge ( $6 \text{ mg/cm}^3$ , SG6) loading with drug Artemisone (b, c), drug-loaded SG6 after coating with PPX thickness of 150 nm (d) and 423 nm (e), and the corresponding EDX mapping of Artemisone distribution in the sponges by monitoring the sulfur element (f).

Previous reports indicated that the specific drug loading capacity increased as increasing the initial feeding drug concentrations (**Figure 2-12**). However, most of previous reported drug carrier systems, such as dispersion, mesoporous materials, metal organic frameworks (MOF), nanocarrier and hydrogel, possessed specific drug loading capacity below  $1000 \text{ mg/g}$  even with very high drug concentrations. In comparison, the porous sponges used in this work exhibits superior specific drug loading capacity of  $1870$  and  $2639 \text{ mg/g}$ , when applying the initial feeding drug concentration of  $14$  and  $25 \text{ mg/mL}$ , respectively. If considering the volume of the loaded drugs, only  $1 \text{ vol\%}$  of the pore volume of the sponges is used, which suggests a larger potential increment in the drug loading capacity by the fibrous porous sponges.

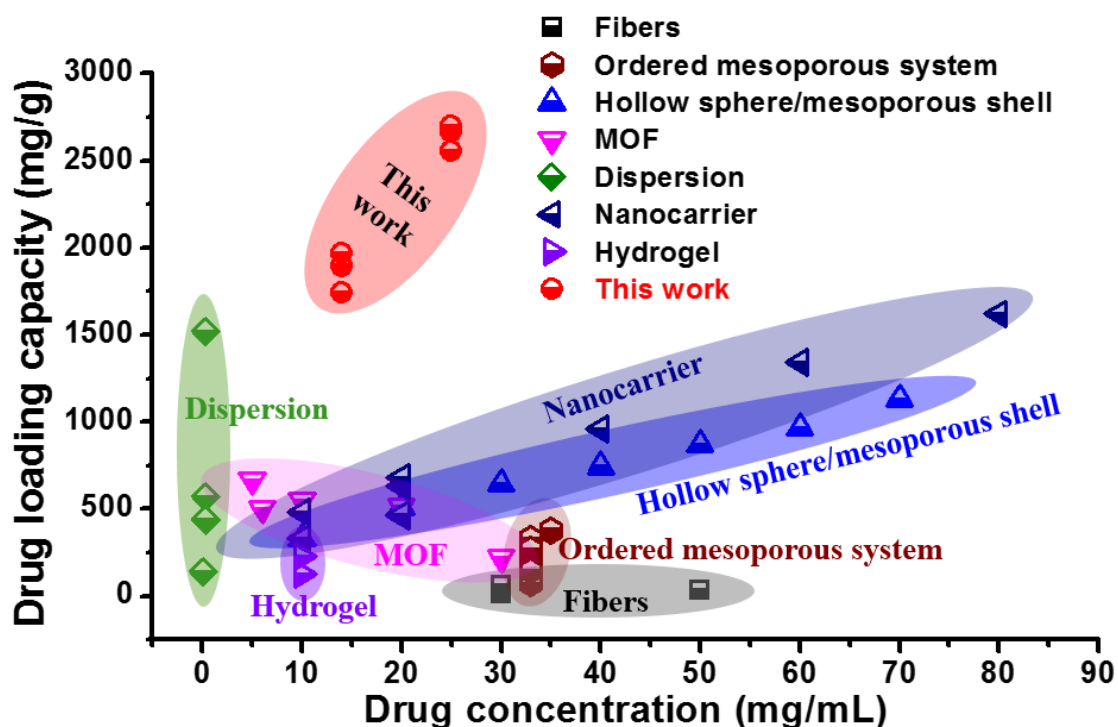
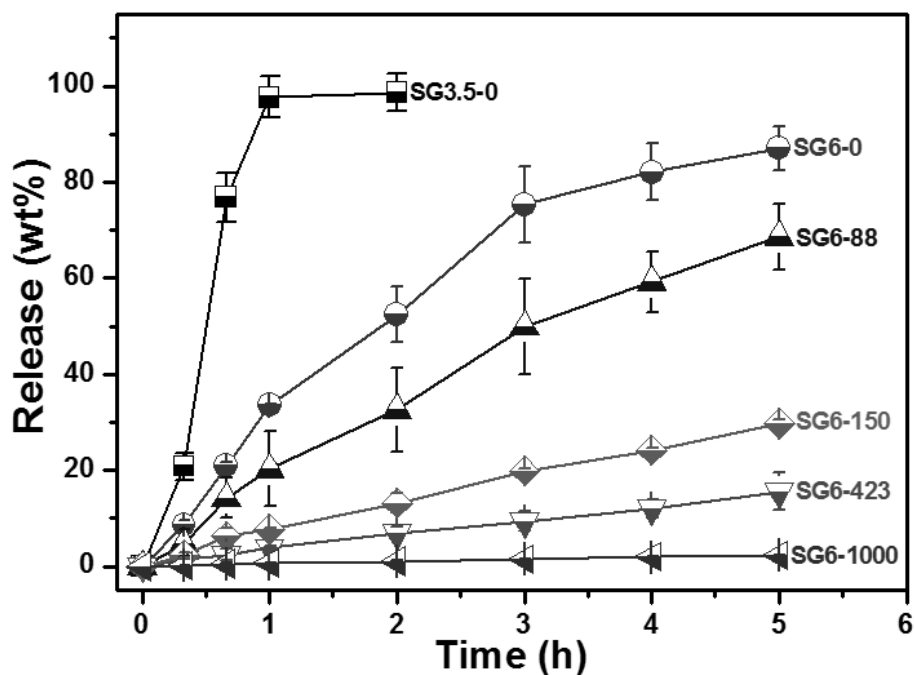


Figure 2-12. Drug loading capacity of sponges with comparison to other supporters.

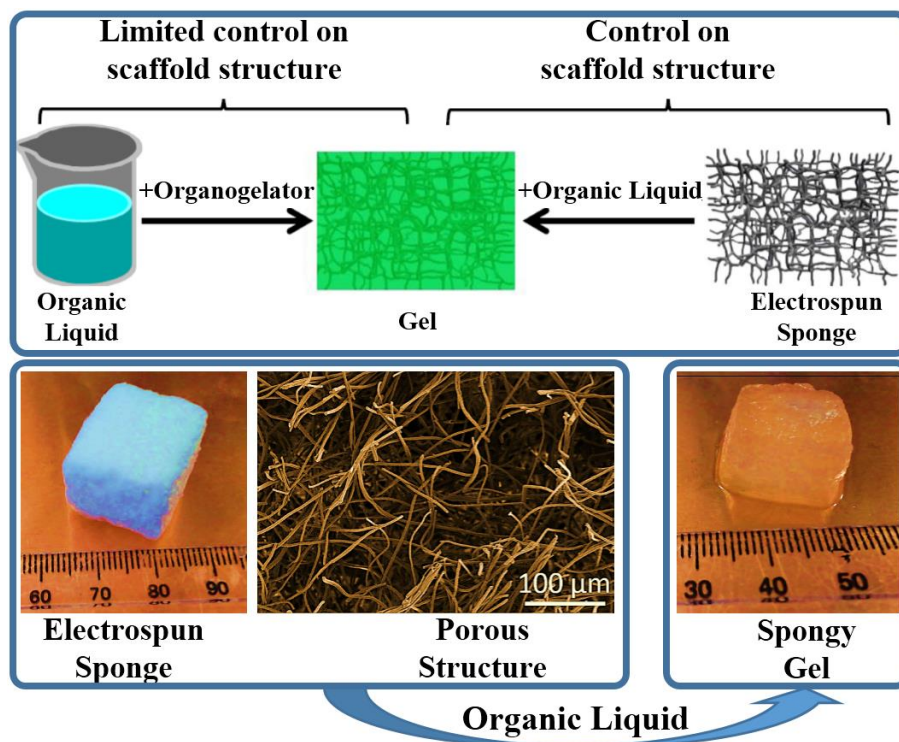
The drug release from the sponge carrier is highly influenced by the density of the sponge and the coating thickness of the sponges (Figure 2-13). The sponges without PPX coating and with lower density (SG3.5) show burst drug release in the first 1 h with comparison to SG6, which can be due to the quicker mass transfer between the drug and the liquid medium. After increasing the thickness of the PPX layer, the drug release rate become slower and slower so that the sponges with 88, 150, 423 and 1000 nm PPX coating thickness release 33 wt%, 13 wt%, 7 wt%, and 1 wt% of the drug after 2 h, and 67 wt%, 30 wt%, 16 wt% and 2 wt% after 5 h. On the one hand, the additional PPX coating layer acts as an effective diffusion barrier for the drug release from inside to outside. On the other hand, the PPX coating increases the hydrophobicity of the sponges and postpones the contact between the sponge and the liquid medium.



**Figure 2-13.** Drug release profile of drug-loaded sponges with densities of 3.5 and 6  $\text{mg}/\text{cm}^3$  and PPX coating thicknesses of 0, 88, 150, 423 and 1000 nm.

In conclusion, fibrous sponges with high pore volume up to  $285 \text{ cm}^3/\text{g}$  are successfully applied as drug carrier with high drug loading capacity in the range of 1870-2639  $\text{mg}/\text{g}$ . Only 1 vol% of the pore volume of the sponges is needed for drug loading, suggesting the promising improvement on the drug loading capacity from the sponges. Controllable drug release can be realized by an additional coating of PPX.

## 2.5 Spongy gels by a top-down approach from polymer fibrous sponges



This work has been accepted by **Angewandte Chemie**.

Shaohua Jiang, **Gaigai Duan**, Ute Kuhn, Michaela Mörl, Volker Altstädt, Alexander L. Yarin, Andreas Greiner. Spongy gels by a top-down approach from polymer fibrous sponges. *Angew. Chem.* **2017**; DOI: 10.1002/ange.201611787.

### Specific contributions by authors:

Gaigai Duan and Shaohua Jiang contributed equally in this work. Shaohua Jiang and Gaigai Duan carried out the experiments and wrote the manuscript. Ute Kuhn and Michaela Mörl carried out the rheological measurements and wrote the manuscript. Alexander L. Yarin applied the theory. Alexander L. Yarin, Volker Altstädt and Andreas Greiner directed the project and wrote the manuscript.

Organogels compose of a liquid organic phase within a three-dimensional, cross-linked network, which are formed from the self-assembly of low- or high-molecular weight molecules via a bottom-up approach. However, these organogels have disadvantages of high cost and sensitivity to impurities in conjunction with the gelation process, which greatly hamper their technical applications. In this work, a novel spongy gel was produced based on polymer fibrous sponges via a top-down approach. This spongy gels not only possess the same characteristics as an organogel, but also exhibit their own advantages, such as no shrinkage, no sensitivity to impurities on gel formation, good control over the 3D network, and a wide range of possibilities for functionalization due to the abundant resources of electrospun fibers.

The spongy gel can be formed by filling apolar liquid into the 3D fibrous sponges made from electrospun fibers (**Figure 2-14**). It possesses the same features as an organogel, such as a liquid phase, a 3D network, and essentially no flow.

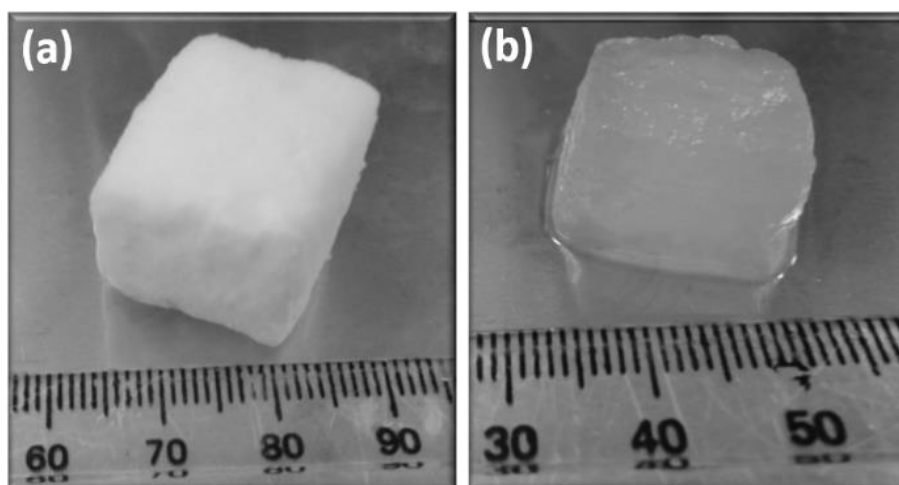


**Figure 2-14.** Sponge made from electrospun fibers (a) and the spongy gel after uptake of mineral oil.

Organogels show no flow but their storage modulus should larger than loss modulus. In this work, the spongy gels also exhibited the same rheological behavior as the organogels. As shown in **Figure 2-15**, all the curves showed the larger storage modulus than loss modulus in the entire measuring range. This behavior suggests a highly elasticity of the material, which is typical for an organogel. The frequency-dependent measurements at 25 and 50 °C indicate that the storage modulus is almost constant over the entire frequency range, which is another feature for gel behavior.

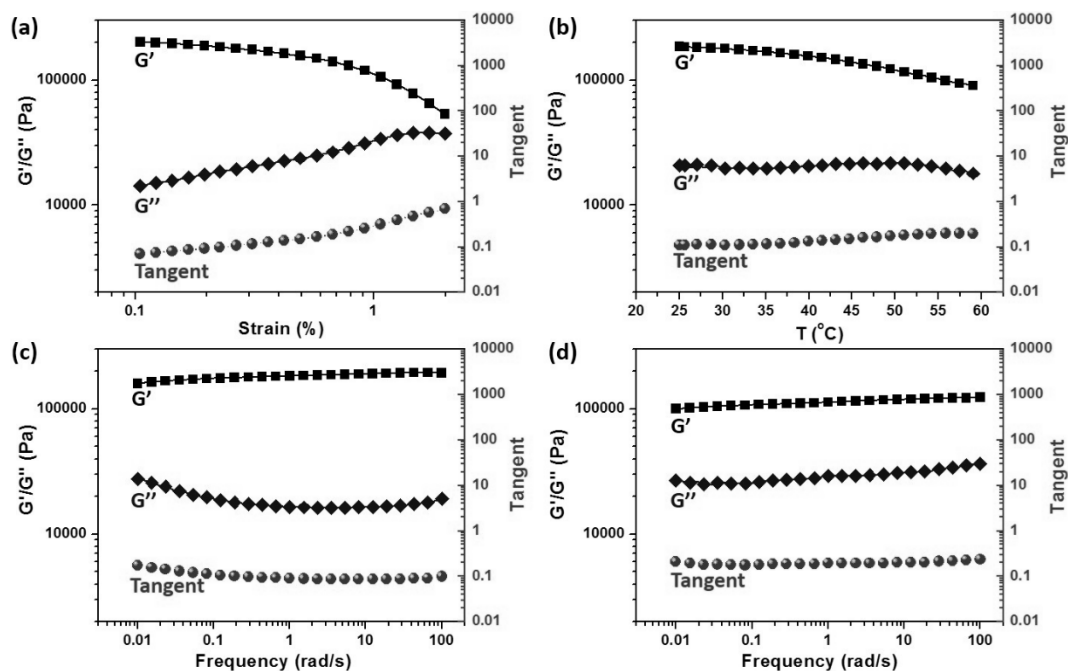


**Figure 2-15.** Dynamic oscillatory shear rheological properties of spongy gel loaded with ethylene glycol as functions of strain (a), temperature (b), and frequency at 25 (c) and 50 °C (d).

For practical applications, the evaporation of the liquid from the spongy gel could be a serious issue. Therefore, the evaporation behavior of wetting (ethanol) and non-wetting (water) liquids, the sponges with different densities (P-SG1: 16.2 mg/cm<sup>3</sup>; P-SG2: 30.6 mg/cm<sup>3</sup>), and the methods of liquid delivery are investigated (**Figure 2-16**). The evaporation of water and ethanol from the sponges is similar and independent of the sponge density, but the evaporation rate greatly differed for the wetting and non-wetting liquid. This behavior could not only be due to the different vapor pressures of water and ethanol. Therefore, a modified d<sup>2</sup>-law for droplet evaporation was developed to describe the evaporation of ethanol and water from spongy gels. In all of the cases, the modified d<sup>2</sup>-law fit the experimental data accurately, which ascertains that the liquid evaporation from the sponge could be considered as a shrinking-in-time blob.

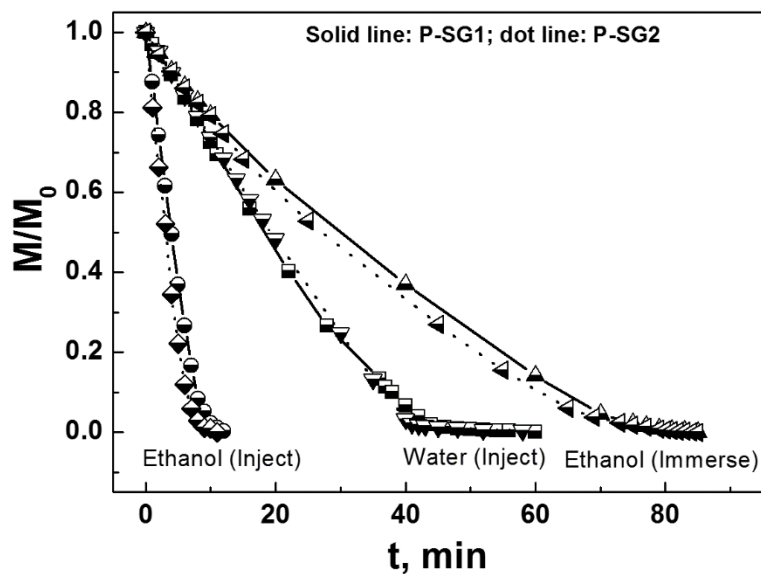


**Figure 2-16.** Evaporation of water and ethanol from sponges of P-SG1 and P-SG2.

In conclusion, highly porous sponges made from electrospun fibers have been successfully applied to load organic solvents to form spongy gels. These spongy gels possess similar features as organic gels including a liquid phase, a 3D network, no flow, mechanical stability, and similar rheological behavior. The modified  $d^2$ -law can be successfully used to describe the evaporation behavior of ethanol and water from the spongy gels and the evaporation of both solvents could be considered as shrinking-in-time blobs. These spongy gels could be found many applications in the future.

## 3 Publications

### 3.1 Ultralight, soft polymer sponges by self-assembly of short electrospun fibers in colloidal dispersions

**Gaigai Duan**, Shaohua Jiang, Valérie Jérôme, Joachim H Wendorff, Amir Fathi, Jaqueline Uhm, Volker Altstädt, Markus Herling, Josef Brey, Ruth Freitag, Seema Agarwal, Andreas Greiner. Ultralight, Soft Polymer Sponges by Self-Assembly of Short Electrospun Fibers in Colloidal Dispersions. *Adv. Funct. Mater.* **2015**; 25(19):2850-2856.

This is an open access article under the terms of the Creative Commons Attribution-NonCommercial-NoDerivs License, which permits use and distribution in any medium, provided the original work is properly cited, the use is non-commercial and no modifications or adaptations are made.

# Ultralight, Soft Polymer Sponges by Self-Assembly of Short Electrospun Fibers in Colloidal Dispersions

Gaigai Duan, Shaohua Jiang, Valérie Jérôme, Joachim H. Wendorff, Amir Fathi, Jaqueline Uhm, Volker Altstädt, Markus Herling, Josef Breu, Ruth Freitag, Seema Agarwal, and Andreas Greiner\*

Ultralight polymer sponges are prepared by freeze-drying of dispersions of short electrospun fibers. In contrast to many other highly porous materials, these sponges show extremely low densities ( $<3 \text{ mg cm}^{-3}$ ) in combination with low specific surface areas. The resulting hierarchical pore structure of the sponges gives basis for soft and reversibly compressible materials and to hydrophobic behavior in combination with excellent uptake for hydrophobic liquids. Owing to their large porosity, cell culturing is successful after hydrophilic modification of the sponges.

reported on the formation of sponge skeletons shown to feature great bending strength and on the role of silicatein- $\alpha$  in the biomineralization of silicates in sponges, which accounts for the high reversible compressibility of sponges in spite of low densities.<sup>[3]</sup> Aizenberg et al. pointed out on the example of the so-called glass sponges (*Euplectella*) the important role of the hierarchical design from the nanometer to macroscopic length scale for structural materials.<sup>[4]</sup> The

## 1. Introduction

Natural sponges (*porifera*) are multicellular animals (*metazoa*) with large diversity and highly attractive properties not yet met by man-made substances.<sup>[1]</sup> For instances, natural sponges are light-weight materials with a density of  $15 \text{ mg cm}^{-3}$  (dried sponge) displaying excellent reversible compressibility. They can take-up large amounts of liquids and are excellent filters. Sponges with a volume of  $1000 \text{ cm}^3$  can process up to  $3000 \text{ L water h}^{-1}$ . Furthermore, they can conduct light as discovered recently by Brümmer et al.<sup>[2]</sup> In addition, Natalio et al.

structural base of sponges are multiarmed spicules of silicate or calcium carbonate, which form highly porous structures of several hierarchical layers as shown in Figure 1A,B. This leads to highly porous ultralight 3D materials (ultralight is defined when the density of material is  $<10 \text{ mg cm}^{-3}$ ).<sup>[5]</sup> In recent literature, a variety of highly porous ultralight 3D materials were reported based on carbon, ceramics, and cellulose, which were characterized by porosities  $>99\%$  and relatively high compressive strength.<sup>[6–10]</sup> Carbon and cellulose based sponges show ultralow densities and excellent mechanical properties but soft sponges with similar mechanical integrity are missing.

Since spicules of natural sponges conspicuously resemble polymer fibers, formation of such fibrous structures by electrospinning<sup>[11]</sup> could be a promising concept for the preparation of polymer-based biomimetic analogous of natural sponges and would open the huge potential of electrospun materials for 3D sponge-type structures. Indeed, 3D porous structures were prepared by electrospinning which was nicely summarized in comprehensive review in recent literature.<sup>[7]</sup> However, previous efforts of making 3D highly porous electrospun materials, for example, via ultrasonic treatment, resulted in higher densities and correspondingly lower porosities of  $<99\%$ ,<sup>[12]</sup> as well as relatively poor mechanical performance. Remarkably, Eichhorn et al. claimed that theoretically ultrahigh porosities of electrospun nonwovens  $>99\%$  could not be achieved.<sup>[13]</sup> In contrast to these reports, we present here the formation of ultralight weight highly porous 3D electrospun polymer fiber-based spongy structures with densities as low as  $2.7 \text{ mg cm}^{-3}$  corresponding to a porosity of 99.6%. They were prepared by electrospinning of a photo cross-linkable polymer followed by UV cross-linking, mechanical cutting, suspending cut fibers in liquid dispersion, and freeze-drying. These polymer sponges showed in analogy to natural sponges very good reversible soft compressibility and bendability without structural disintegration. Applications of

G. Duan, Dr. S. Jiang, Prof. S. Agarwal,  
Prof. A. Greiner  
Macromolecular Chemistry II and Bayreuth  
Center for Colloids and Interfaces  
University of Bayreuth  
Universitätsstrasse 30, 95440 Bayreuth, Germany  
E-mail: greiner@uni-bayreuth.de



Dr. V. Jérôme, Prof. R. Freitag  
Process Biotechnology  
University of Bayreuth  
Universitätsstrasse 30, 95440 Bayreuth, Germany

Prof. J. H. Wendorff  
Department of Chemistry  
Philipps-Universität Marburg Hans-Meerwein-Strasse  
35032 Marburg, Germany

Dr. A. Fathi, J. Uhm, Prof. V. Altstädt  
Polymer Engineering  
University of Bayreuth  
Universitätsstrasse 30, 95440 Bayreuth, Germany  
M. Herling, Prof. J. Breu  
Inorganic Chemistry  
University of Bayreuth  
Universitätsstrasse 30, 95440 Bayreuth, Germany

DOI: 10.1002/adfm.201500001

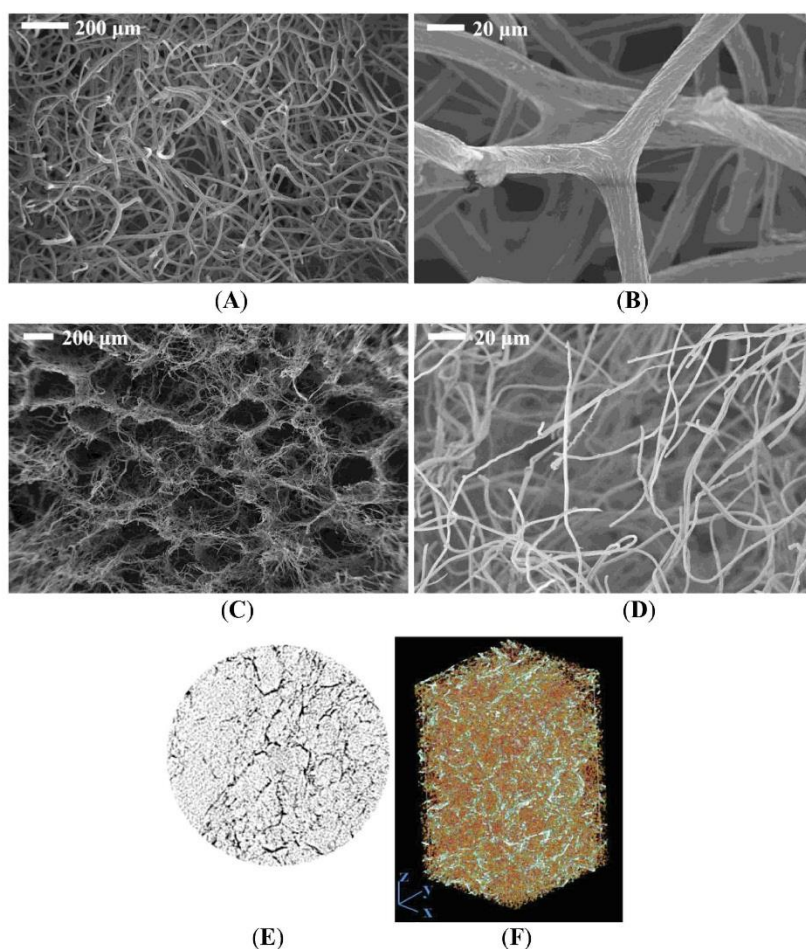


**Figure 1.** SEM images of A,B) a skeleton of a dried natural sponge (*spongia officinalis*) and of C,D) a polymer sponge prepared by freeze-drying of short electrospun fiber dispersion of cross-linked poly(MA-MMA-MABP).  $\mu$ -CT analysis (sample no. 2) with top view, magnification: E) 60 $\times$  and F) 3D side view, magnification: 90 $\times$ .

these materials can be envisioned in a broad spectrum ranging from efficient filters and separation materials, functional construction materials (electrical, sound, or heat–cold insulation), scaffolds for tissue engineering, shape responsive materials, and confined catalysts.

## 2. Results and Discussion

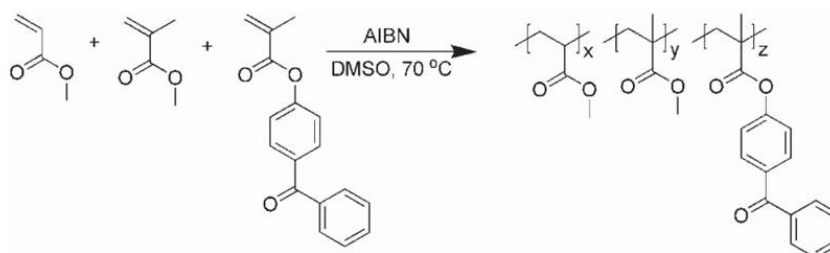
### 2.1. Preparation of Polymer Sponges

An acrylate copolymer with photo cross-linkable units (poly(methylacrylate(MA)-*co*-methyl methacrylate(MMA)-*co*-4-methacryloyloxybenzophenone(MABP))

(poly(MA-*co*-MMA-*co*-MABP)), **Scheme 1**, details are given in Supporting Information) was synthesized and electrospun together with polyacrylonitrile (PAN) from pure DMF or a mixture of DMF, DMSO. As a result, fibers of different average diameters were obtained. Subsequently, dispersions of short electrospun fibers were prepared by cutting of the electrospun nonwovens of poly(MA-*co*-MMA-*co*-MABP) in dioxane in different concentrations. Sponges of different densities were prepared from these dispersions by freeze drying.

### 2.2. Structure and Mechanical Properties of Sponges

Based on the finding that dispersions of short electrospun fibers with high aspect ratio could form—under certain



Scheme 1. Preparation of poly(MA-MMA-MABP) from MA, MMA, and MABP by free radical copolymerization.

conditions—sponge-like structures combined with knowledge about the structure of natural sponges, we anticipate that percolation in combination with self-assembly played a significant role in the formation of man-made polymer sponge structure. Important for the formation of stable spongy structures after freeze drying was the use of short electrospun fibers with aspect ratio of 120–150 dispersed in dioxane. Obviously, porosity and density should correspond to the one defined by percolation threshold of fibers of a fibrillary structure with given length and radius. According to Berhan and Sastry,<sup>[14]</sup> the threshold can be represented for fibers with large aspect ratios by Equation (1)

$$\phi_c = \frac{V}{V_{ex}} \quad (1)$$

where  $\phi_c$  is the volume fraction of the fibers. Here, the fibers are represented as capped cylinders. The volume  $V$  and excluded volume  $V_{ex}$  of such a fiber with length  $L$  and radius  $r$  is given by Equations (2) and (3)

$$V = \frac{4\pi r^3}{3} + r^2 \pi L \quad (2)$$

$$V_{ex} = \frac{32\pi r^3}{3} + 8\pi L r^2 + \pi L^2 r \quad (3)$$

For typical values of the system under consideration with  $L = 100 \mu\text{m}$ ,  $r = 250 \text{ nm}$ , we find  $\phi_c = 0.00245$  and a porosity  $\varepsilon = (1 - \phi_c) = 0.9975$ , which is close to the observed one of  $\varepsilon = 0.9981$ . In terms of predictions going from a radius of 250 nm to one of 25 nm, we estimate  $\phi_c = 0.000249$  and  $\varepsilon = 0.99975$  ( $\rho = 0.27 \text{ mg cm}^{-3}$ ) which are highly interesting values since these porosities and densities are close to the ones reported for record aerogels.<sup>[15]</sup> These calculations strongly support the experimental findings reported here for the sponge porosity. Analysis of the present polymer sponges by scanning electron microscopy (SEM) showed hierarchical order of the pores and interconnection of the fibers (fiber diameters in the range of 0.5–0.8  $\mu\text{m}$ ). Large pores of about 300–430  $\mu\text{m}$  in diameter (Figure 1C) contained smaller pores of 10–30  $\mu\text{m}$  (Figure 1D). The large pores could be attributed to the formation of crystals of frozen solvent formed in the freeze-drying process. The specific densities of the sponge were readily controlled by the concentration of the fibers in dispersion and by the average fiber diameter (Table S1, Supporting Information). The sponge density varied from 2.72 to 9.12  $\text{mg cm}^{-3}$  on changing the short

fiber dispersion concentration from 2.42 to 8.76  $\text{mg mL}^{-1}$  for fibers with average diameter between 400 and 500 nm.

BET-surfaces of the present sponges generally were very low. For example, we measured a specific surface of 2.66  $\text{m}^2 \text{g}^{-1}$  (determined with argon gas) for a sponge with a density of 3.75  $\text{mg cm}^{-3}$ . According to micro-computer tomography ( $\mu\text{-CT}$ ), the fibers were homogeneously distributed in the sponge (Figure 1E,F) which attributed to the integral stability of the sponge.

### 2.3. Properties of Sponges

Although the density of the sponge was extremely low, they could be handled manually without disintegration (Figure 2A–C). The compressive strength correlated with decreasing density of the sponge (Figure 2D). The Ashby plot of the compressive strength versus material density clearly revealed that electrospun polymer fiber sponges cover an important gap in this plot in comparison to other porous materials and are close to natural sponge (Figure 2E).

The high porosity of the sponge evidently has also significant effects on a variety of macroscopic properties. An illustrative example of macroscopic properties was the uptake of mineral oil from water. In these experiments, we found that the oil was taken up selectively from water in less than a minute as soon as the present sponge came in contact with the liquid phase (Figure 3A). After complete uptake of oil it was still shape persistent (inset in Figure 3B). Interestingly, with sponge sample no. 1 of lowest density (2.72  $\text{mg cm}^{-3}$ , Table S1, Supporting Information), the weight of mineral oil in the sponge closely corresponded to the density of the mineral oil itself and, thereby, close to 30 000% of the weight of the pure sponge. This indicates the role of a fiber network in the sponge-like material for the stabilization of the liquids which compares to the role of collagen nanofiber networks in natural tissues. Interestingly, the as prepared sponges were hydrophobic (Figure 3B), which makes them of interest for membrane applications.

The liquid absorption capacity of the electrospun freeze dried sponges was inversely proportional to their densities (Figure 3C), which indicates pore filling as mechanism for oil uptake rather than surface wetting. Similar behaviour for selective uptake of other hydrophobic organic liquids from water was observed (Figure 3C). For instances, reversible sorption and desorption of cyclohexane was found (Figure 3D). Importantly,

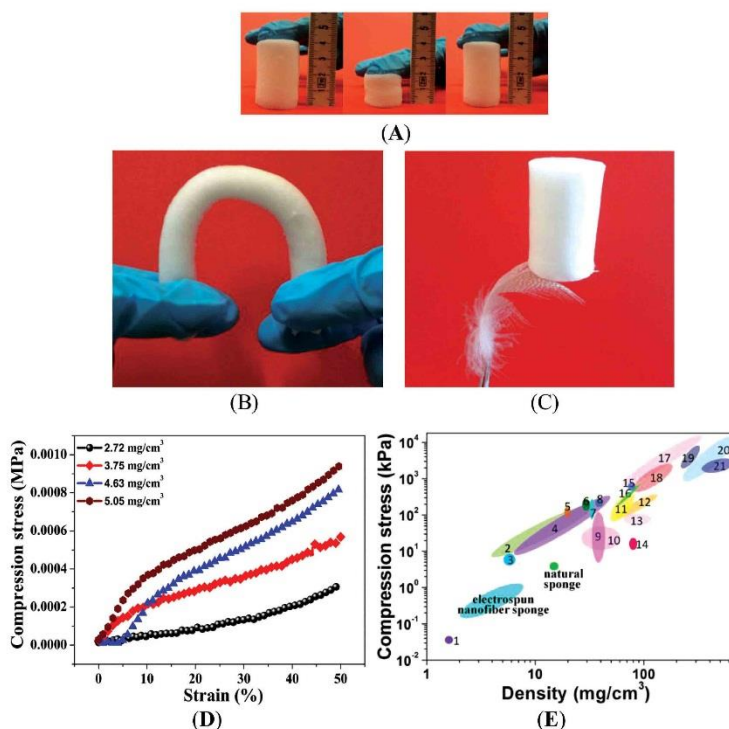


**Figure 2.** A) Reversible manual compression, B) bending test, C) demonstration of ultralight weight of a present electrospun/freeze dried sponge (sample no. 3), D) compression test of sponges of different densities, and E) Ashby plot of sponge compressive strength versus density for different materials. 1) Boron nitride,<sup>[9]</sup> 2) carbon nanotube,<sup>[6]</sup> 3) carbon aerogel,<sup>[15]</sup> 4) cellulose fiber,<sup>[16]</sup> 5) cross-linked polystyrene,<sup>[17]</sup> 6) polyolefin (closed cell),<sup>[18]</sup> 7) polyethylene (closed cell),<sup>[19]</sup> 8) polyimide,<sup>[20]</sup> 9) polyethylene (50% strain),<sup>[19]</sup> 10) silk fibroin,<sup>[21]</sup> 11) melamine-formaldehyde (rigid),<sup>[22]</sup> 12) tannin-based (rigid),<sup>[23]</sup> 13) PDLA/Bioglass composite,<sup>[24]</sup> 14) latex rubber,<sup>[19]</sup> 15) PAN-microspheres and fibers,<sup>[25]</sup> 16) rigid polyurethane,<sup>[26]</sup> 17) PVC (cross-linked),<sup>[27]</sup> 18) epoxy-boroxine,<sup>[28]</sup> 19) bio-based macroporous polymers,<sup>[29]</sup> 20) silicon oxycarbide ceramic,<sup>[30]</sup> and<sup>[21]</sup> aluminum foams.<sup>[31]</sup>

when the procedure was repeated several times, no loss in efficiency was observed. It should not remain unmentioned here that similar liquid uptakes were reported for other ultralight 3D structures,<sup>[6,10]</sup> however observed with other materials than man-made polymers.

#### 2.4. Application of Electrospun Sponges

3D nanostructured materials are also of interest for other applications such as for filtration, mechanical damping, catalysis, and cell–material biointerface design.<sup>[32]</sup> High porosities are required for the successful growth of cells in materials. In contrast to known ultralight high porosity materials, the mechanical softness of the present polymer sponges and its potential for chemical and biological functionalization is of major interest for cell tissue formation. In order to explore whether cells could grow in the present polymer sponges, Jurkat cells, which were used previously in cell

electrospinning, were brought into contact with the sponge. Before contact the sponges were coated with poly(vinyl alcohol) in order to provide sufficient hydrophilicity for contact with cell culture media. After 2 d of incubation, the cells have formed cell clusters with the sponge (**Figure 4A**). SEM revealed that clusters of cells grew on to the fibers of the sponge and cells adhered to the fibers (**Figure 4B**). Viable cells were found inside the sponge by confocal microscopy after 13, 20, and 30 d of culture, indicating significant cell growth (**Figure 4C–E**). 1929 cells gave similar results but are not reported here in detail.

### 3. Conclusion

In conclusion, ultralight highly porous 3D polymer sponges of extremely low density and low specific surface area were obtained from dispersions of short electrospun fibers in an attempt to mimic the design principle of natural sponges.

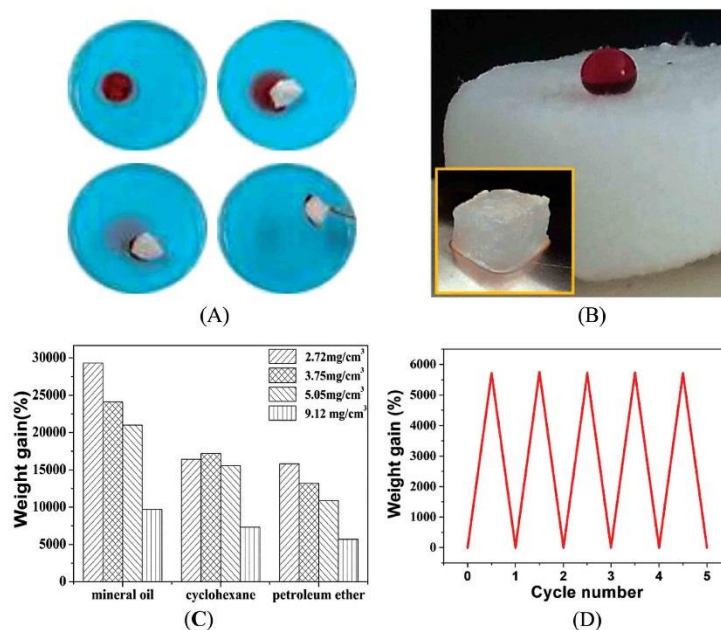


**Figure 3.** Liquid uptake by polymer fiber sponges. Photographs of A) mineral oil (dyed by Sudan red) uptake from water, B) one drop of rhodamine B dyed water on the top of sponge sample 7 (inset shows shape persistent sponge completely soaked with mineral oil (1.2 cm × 0.9 cm × 0.85 cm)). C) Uptake of hydrophobic liquids from water in wt% as a function of sponge density. D) Reversibility of cyclohexane uptake (sample 4,  $\rho = 9.12 \text{ mg cm}^{-3}$ ), after uptake cyclohexane was evaporated for deloading the sponge.

The porosity of the polymer sponges obtained from the dispersions of short electrospun fibers produced by subsequent freeze drying could be understood by the classical percolation theory. Remarkably, the pore morphologies of the sponge featured hierarchical order for reasons currently not yet understood, but which could account to the surprisingly good reversible compressibility and bendability, given their low densities, which was also confirmed by the recent contribution of Ding et al.<sup>[33]</sup> The mechanical properties of the novel polymer sponges close an important gap in an Ashby plot of compressibility versus density. It should not remain unmentioned that the compressive strength of the sponge could be tailored with negligible loss in porosity by several coating techniques which are presently under investigation in our lab. In contrast to many other highly porous materials, the present sponges prepared by electrospinning/freeze-drying gain functionality pore filling rather than surface wetting, which opens completely new perspectives for functional materials. Given the wide variety of polymers that can and have been electrospun into filaments combined with the formation process presented here, such sponge materials will enable the design of many new functional materials ranging from ultralight materials to membranes, filters, insulators, electrodes, and scaffolds for biomedical applications.

#### 4. Experimental Section

All experimental details regarding polymer synthesis, characterization, UV cross-linking, sponge densities, cell studies are provided in Supporting Information.

**Electrospinning of Fibers:** Solutions for electrospinning were prepared by dissolving 8.0 g of poly(MA-co-MMA-co-MABP) and 1.0 g of PAN in a mixture of solvents (31.0 g of DMSO, 6.5 g of DMF and 1.8 g of acetone; total polymer concentration = 18.6 wt%). Another solution for electrospinning with polymer concentration of 20 wt% was prepared by dissolving poly(MA-co-MMA-co-MABP) (8 g) and PAN (1 g) in pure DMF (36 g). The conditions used for electrospinning were: electric potential 12 kV, flow rate 1.8 mL h<sup>-1</sup>, and a distance between the electrodes of 13.0 cm. The electrospun fibers were collected in the form of a nonwoven on a grounded rotating drum (diameter 20 cm) with a rotating speed of 20 rotations per minute.

**Preparation of Electrospun Fiber Dispersion:** The electrospun fiber nonwoven was first dried in vacuum oven at room temperature for 3 d and then irradiated under UV light (UV lamp 250 GS) with a distance of 15 cm for 5 h. Afterward the cross-linked nonwoven was cut into short fibers in dioxane with a mixer at a rotation speed of about 5000 rpm for 45 s. Short fiber dispersions with different concentrations (Table S1, Supporting Information) were prepared by controlling the weight ratio of fiber nonwoven in the dispersion and the volume of the dispersion solvent, here dioxane.

**Preparation of Polymer Sponges:** The above short fiber dispersions were freeze-dried in cylindrical glass vials for 48 h to yield sponges with different densities (Table S1, Supporting Information).

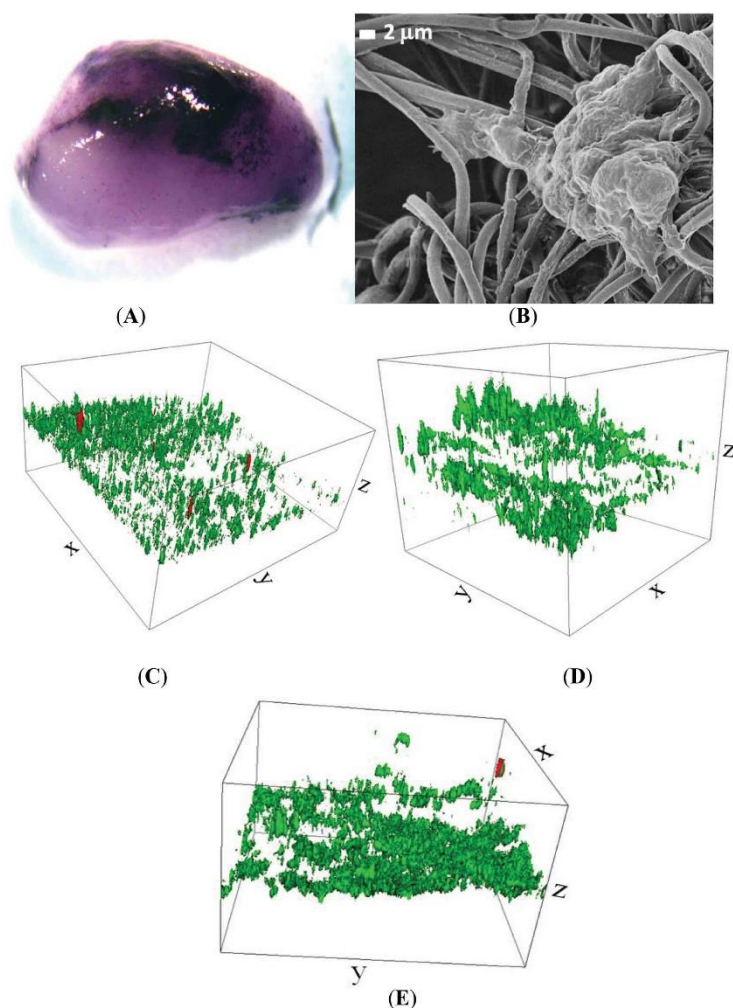


**Figure 4.** Cell growth in electrospun/freeze dried polymer fiber sponges. A) Image (MTT staining, long axis of the sponge is about 5 mm) and B) SEM photo of Jurkat cells colonized on a sponge (sample no. 2) after 2 d of colonization. 3D confocal microscopy of live (green) and dead (red) Jurkat cells in sponge (sample no. 2 after 13 d (C) ( $x \times y \times z = 450 \times 450 \times 250 \mu\text{m}$ ), 20 d (D) ( $x \times y \times z = 450 \times 450 \times 400 \mu\text{m}$ ), and 30 d (E) ( $x \times y \times z = 450 \times 450 \times 300 \mu\text{m}$ ) of cells incubation.

### Supporting Information

Supporting Information is available from the Wiley Online Library or from the author.

MP1206 is kindly acknowledged. Part of this work was presented at the ACS National Spring Meeting in New Orleans, March 18, 2014.

Received: January 1, 2015

Revised: March 4, 2015

Published online: March 30, 2015

### Acknowledgements

The authors are indebted to Prof. Paul Smith for many helpful discussions. Financial support by DFG (SFB840) and COST Action

[1] S. P. Leys, A. Hill, *Adv. Mar. Biol.* **2012**, *62*, 1.

[2] F. Brümmer, M. Pfannkuchen, A. Baltz, T. Hauser, V. Thiel, *J. Exper. Mar. Biology Ecology* **2008**, *367*, 61.

- [3] F. Natalio, T. P. Corrales, M. Panthöfer, D. Schollmeyer, I. Lieberwirth, W. E. G. Müller, M. Kappl, H.-J. Butt, W. Tremel, *Science* **2013**, 339, 1298.
- [4] J. Aizenberg, J. C. Weaver, M. S. Thanawala, V. C. Sundar, D. E. Morse, P. Fratzl, *Science* **2005**, 309, 275.
- [5] T. A. Schaedler, A. J. Jacobsen, A. Torrents, A. E. Sorensen, J. Lian, J. R. Greer, L. Valdevit, W. B. Carter, *Science* **2011**, 334, 962.
- [6] X. Gui, J. Wei, K. Wang, A. Cao, H. Zhu, Y. Jia, Q. Shu, D. Wu, *Adv. Mater.* **2010**, 22, 617.
- [7] B. Sun, Y. Z. Long, H. D. Zhang, M. M. Li, J. L. Duvail, X. Y. Jiang, H. L. Yin, *Prog. Polym. Sci.* **2014**, 39, 862.
- [8] D. Jang, L. R. Meza, F. Greer, J. R. Greer, *Nat. Mater.* **2013**, 12, 893.
- [9] J. Yin, X. Li, J. Zhou, W. Guo, *Nano Lett.* **2013**, 13, 3232.
- [10] F. Jiang, Y.-L. Hsieh, *J. Mater. Chem. A* **2014**, 2, 6337.
- [11] S. Agarwal, A. Greiner, J. H. Wendorff, *Prog. Polym. Sci.* **2013**, 38, 963.
- [12] J. B. Lee, S. I. Jeong, M. S. Bae, D. H. Yang, D. N. Heo, C. H. Kim, E. Alsberg, K. Kwon, *Tissue Eng.* **2011**, 17, 2695.
- [13] S. J. Eichhorn, W. W. Sampson, *J. R. Soc. Interface.* **2005**, 2, 309.
- [14] L. Berhan, A. M. Sastry, *Phys. Rev. E* **2007**, 75, 041120.
- [15] H. Sun, Z. Xu, C. Gao, *Adv. Mater.* **2013**, 25, 2554.
- [16] H. Sehaqui, M. Salajkova, Q. Zhou, L. A. Berglund, *Soft Matter* **2010**, 6, 1824.
- [17] J. M. Williams, D. A. Wroblewski, *Langmuir* **1988**, 4, 656.
- [18] M. A. Rodríguez-Pérez, J. I. Velasco, D. Arencón, O. Almanza, J. A. De Saja, *J. Appl. Polym. Sci.* **2000**, 75, 156.
- [19] R. E. Skochdopole, L. C. Rubens, *J. Cell. Plast.* **1965**, 1, 91.
- [20] M. K. Williams, E. S. Weiser, J. E. Fesmire, B. W. Grimsley, T. M. Smith, J. R. Brenner, G. L. Nelson, *Polym. Adv. Technol.* **2005**, 16, 167.
- [21] R. Nazarov, H. J. Jin, D. L. Kaplan, *Biomacromolecules* **2004**, 5, 718.
- [22] V. Nemanič, B. Zajec, M. Žumer, N. Figar, M. Kavšek, I. Mihelič, *Appl. Energy* **2014**, 114, 320.
- [23] A. Celzard, W. Zhao, A. Pizzi, V. Fierro, *Mater. Sci. Eng. A* **2010**, 527, 4438.
- [24] J. J. Blaker, V. Maquet, R. Jérôme, A. R. Boccaccini, S. N. Nazhat, *Acta Biomater.* **2005**, 1, 643.
- [25] L. Vaikhanski, S. R. Nutt, *Composites Part A* **2003**, 34, 755.
- [26] W. J. Seo, H. C. Jung, J. C. Hyun, W. N. Kim, Y. B. Lee, K. H. Choe, S. B. Kim, *J. Appl. Polym. Sci.* **2003**, 90, 12.
- [27] M. C. Saha, H. Mahfuz, U. K. Chakravarty, M. Uddin, M. E. Kabir, S. Jeelani, *Mater. Sci. Eng. A* **2005**, 406, 328.
- [28] H. H. Chen, A. C. Nixon, *Polym. Eng. Sci.* **1965**, 5, 90.
- [29] T. H. M. Lau, L. L. C. Wong, K. Y. Lee, A. Bismarck, *Green Chem.* **2014**, 16, 1931.
- [30] P. Colombo, J. R. Hellmann, D. L. Shelleman, *J. Am. Ceram. Soc.* **2001**, 84, 2245.
- [31] E. Andrews, W. Sanders, L. J. Gibson, *Mater. Sci. Eng. A* **1999**, 270, 113.
- [32] X. Liu, S. Wang, *Chem. Soc. Rev.* **2014**, 43, 2385.
- [33] Y. Si, J. Yu, X. Tang, J. Ge, B. Ding, *Nat Commun.* **2014**, 5, 5802.

Copyright WILEY-VCH Verlag GmbH & Co. KGaA, 69469 Weinheim, Germany, 2015.

# ADVANCED FUNCTIONAL MATERIALS

## Supporting Information

for *Adv. Funct. Mater.*, DOI: 10.1002/adfm.201500001

Ultralight, Soft Polymer Sponges by Self-Assembly of Short  
Electrospun Fibers in Colloidal Dispersions

*Gaigai Duan, Shaohua Jiang, Valérie Jérôme, Joachim  
H. Wendorff, Amir Fathi, Jaqueline Uhm, Volker Altstädt,  
Markus Herling, Josef Breu, Ruth Freitag, Seema Agarwal,  
and Andreas Greiner\**

## Materials and methods for the synthesis of poly(MA-MMA-MABP)

### Materials

Methyl acrylate (MA, Aldrich, 99%) and methyl methacrylate (MMA, Aldrich, 99%) were purified by distillation at reduced pressure. 2, 2'-Azobis (isobutyronitrile) (AIBN, Fluka, 98%) was recrystallized from methanol before use. Polyacrylonitrile (Mw 150,000, polyscience Inc.), dimethyl sulfoxide (DMSO, Fisher Chemical, 99.99%), dimethyl formamide (DMF, Fisher Chemical, 99.99%), methanol (Aldrich, 99.8%), dioxane (technical grade), and acetone (technical grade) were used without further purification. 4-Methacryloyloxybenzophenone (MABP) was synthesized according to the previous work in our group<sup>1</sup>.

### Synthesis of poly(MA-MMA-MABP)

Poly (MA-MMA-MABP) was prepared by free radical copolymerization of MA, MMA and MABP using AIBN as an initiator at 70 °C under nitrogen atmosphere. 8.66 ml of MA (96 mmol), 6.78 ml of MMA (64 mmol), 2.3408 g of MABP (8.8 mmol), 0.1466 g of AIBN (0.89 mmol) and 20 ml of DMSO were added to a three-necked flask. The mixture was reacted for 6 h. The poly (MA-MMA-MABP) was precipitated by methanol and dried at 50 °C in vacuum oven for 24 h. The yield was 88 % and molar mass (Mn) as determined by gel permeation chromatography using THF as eluting solvent was  $2.43 \times 10^5$  g/mol.

### Characterization of poly(MA-MMA-MABP)

The <sup>1</sup>HNMR spectra of poly (MA-MMA-MABP) was shown in **Figure S1**. The assignment of protons was indicated in the chemical structure and the spectra respectively. Both the structure and the spectra were in good agreement.

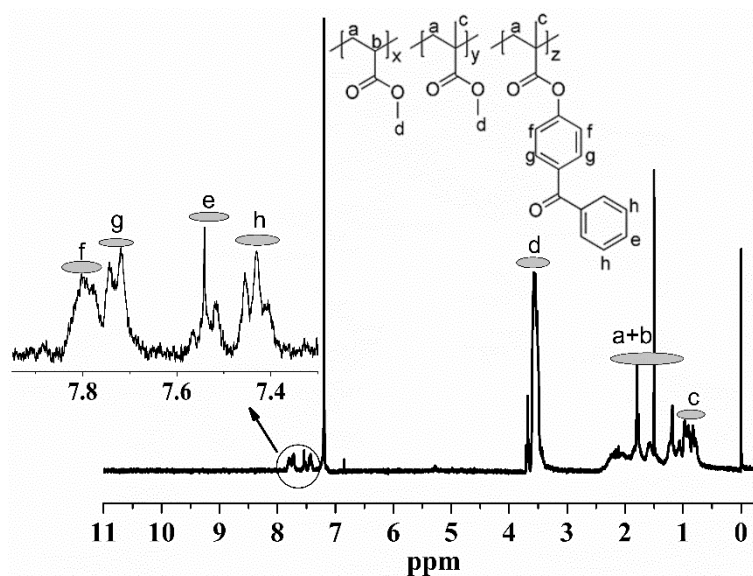


**Figure S1.**  $^1\text{H NMR}$  spectra of poly (MA-MMA-MABP). (Mol ratio = 6:4:0.06 calculated by NMR).

The thermal properties were characterized by thermogravimetric analysis (TGA) (**Figure S2**). Thermal properties of the composites were evaluated on Mettler Toledo TGA/SDTA 851e at a heating rate of  $10\text{ }^\circ\text{C}/\text{min}$  in  $\text{N}_2$  from 25 to  $800\text{ }^\circ\text{C}$ . The poly (MA-MMA-MABP) had good thermal stability with the starting decomposition temperature, 5% and 10% weight loss temperature at about 250, 333 and  $345\text{ }^\circ\text{C}$  respectively.

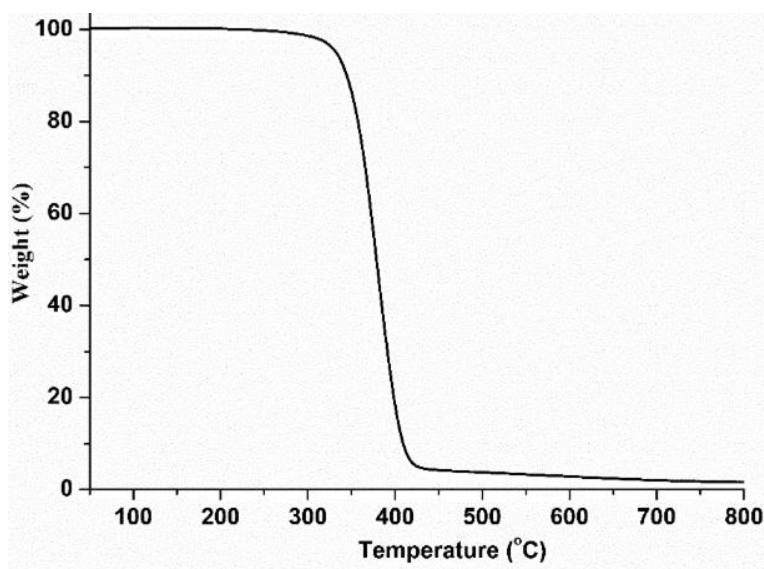


**Figure S2.** TGA curves of poly (MA-MMA-MABP).

#### UV crosslinking of poly (MA-MMA-MABP)

The cross-linking led to insolubility of fibers in organic solvents. Moreover, the cross-linking of poly(MA-MMA-MABP) could also be confirmed by ATR-IR measurement according to the literature (**Figure S3**)<sup>2-5</sup> as MABP is a well-known photo cross-linkable monomer. After treating with UV light, two characteristic peaks of MABP at  $1659\text{ cm}^{-1}$  ( $\text{-C(O)-}$  stretching vibrations) and  $1597\text{ cm}^{-1}$  ( $\text{-C=C-}$  stretching vibrations of benzene ring in conjugation with  $\text{-C(O)-}$ ) nearly disappeared. The UV-exposure generates radicals at carbonyl carbon which initiate cross-linking reaction leading to a network structure which was followed by disappearance of vibrations originating from carbonyl ( $\text{-C=O}$ ) and conjugated double bonds of benzene rings ( $\text{-C=C-C(O)-}$ ) in ATR-IR.

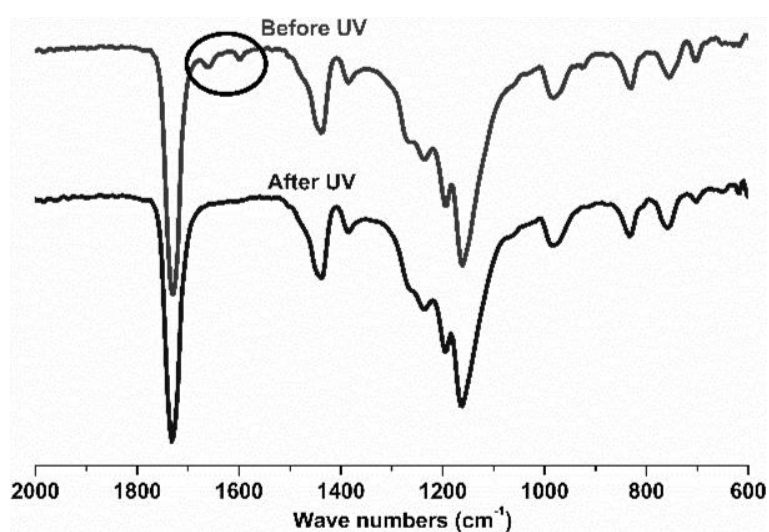


**Figure S3.** ATR-IR spectra of poly(MA-MMA-MABP) before and after cross-linking by UV light.

**Table S1.** Densities of sponges composed of short nanofibers with different diameters and concentrations in dispersions.

Sample No.	Average fiber diameter (nm)	Concentration of nanofibers in dispersion (mg/mL)	Density of sponges ( $\text{mg/cm}^3$ )
1 <sup>a)</sup>	400-500	2.42	$2.72 \pm 0.02$
2 <sup>b)</sup>	800-1000	2.57	$3.65 \pm 0.23$

3 <sup>a)</sup>	400-500	3.00	3.75 ± 0.04
4 <sup>b)</sup>	800-1000	3.58	4.41 ± 0.19
5 <sup>a)</sup>	400-500	3.74	4.63 ± 0.06
6 <sup>b)</sup>	800-1000	4.24	5.05 ± 0.13
7 <sup>a)</sup>	400-500	8.76	9.12 ± 0.17

a) DMF was used as solvent for electrospinning; b) A mixture of DMSO, DMF and acetone was used for electrospinning.

### Materials and Methods for cell incubation

#### Materials for cell incubation

Plastic materials and standard chemicals were from established suppliers and used as received. High quality water (MilliQ) was produced by a Millipore unit. Culture media (RPMI 1640 with and without phenol red) and solutions (Trypsin, L-Glutamine, Dulbecco's PBS1X (D-PBS)) were from PAA Laboratories GmbH, Austria. Minimum Essential Medium (MEM) cell culture media (with and without phenol red) and fetal calf serum (FCS) were from BioChrom, Germany. 3-(4, 5-dimethyl-2-thiazolyl)-2, 5-diphenyl-2H-tetrazolium bromide (MTT) and glutardialdehyde solution (grade I, 25%) was from Sigma-Aldrich, Germany. Agarose was from Bionline, Germany.

#### Cells and cell culture

Jurkat cells (DMSZ number: ACC 282) were maintained in RPMI1640 culture medium, supplemented with 10% fetal calf serum (FCS), 2 mM L-glutamine, 100 units/mL penicillin and 100 µg/mL streptomycin. Cells were cultivated at 37°C in a humidified 5% CO<sub>2</sub> atmosphere. Jurkat cells were collected by centrifugation (200 g, 5 min) and then use for the described experiments. Experiments were performed in 6-well plates coated with agarose to immobilize the nanofiber sponges.

#### Cell seeding technique

One small piece of sterilized (UV-254nm, 5 h) ultra-light sponge was placed and

immobilized per well into 6-well plates coated with agarose. The sponge was wetted with culture medium followed by coating with FCS.  $1 \times 10^6$  cells were resuspended in 40  $\mu$ L of culture medium. The cell suspension was carefully dispersed evenly on the top surface of the sponge. The seeded sponge was transferred into the 37°C/5% CO<sub>2</sub> incubator for 30 min to let the cells enter the sponge. Five hundred microliters of medium were then added to each well. After a further two hours of incubation, enough medium was slowly and carefully added along the side of the well to completely cover the sponge. Well plates were placed back into the 37°C/5% CO<sub>2</sub> incubator and the cells cultured for the indicate time. Throughout the cultivation, the medium was exchanged daily to supply the cells with nutrients and remove metabolites.

### **MTT staining**

At the indicate time, the cultivated sponges were rinsed with D-PBS, placed in fresh 6-well plates and incubated at 37°C for 2 h with 0.5 mg/mL MTT in the respective culture medium without phenol red to assess the spatial distribution of cells. MTT is converted by the mitochondria of metabolically active cells into an insoluble purple formazan salt and therefore allows a qualitative assessment of the cellular location within the sponge. For analysis, the MTT-stained sponges were vertically cross-sectioned at the middle of the sponge and observed with a stereo-microscope (HUND WERZLAR FLQ150).

### **Cell viability**

Viability of the cells within the sponges was determined with the Live/Dead® reduced biohazard viability/cytotoxicity kit (Invitrogen, Germany) that stains living cells green with the highly permeable-permanent nucleic acid dye SYTO 10 and dead cells red with the cell-impermeant dye DEAD Red™. At the indicated time, the cultivated sponges were rinsed with D-PBS, placed in new 6-well plates and stained according to the manufacturer's instruction. For analysis, images were acquired using a confocal microscope (LSM 710, Carl Zeiss, Germany) at 20x ZEN 2008 software.

### **Sample for SEM**

Cells spreading in the sponges was investigated through scanning electron microscopy (SEM). For this, the sponges were rinsed twice with D-PBS and the ingrown cells fixed

with 2.5% glutardialdehyde in D-PBS for 60 minutes. After washing with MilliQ water, dehydration was performed by slow water replacement using series of ethanol solutions (35%, 50%, 75%, and 95%) for 15 minutes with final dehydration in absolute ethanol for 15 minutes.

### Characterization of the sponges

The densities ( $\rho$ ) of the cylinder-shaped sponges were calculated by the following equation based on the weight ( $m$ ) and the volume ( $V$ ) of the sponges:

$$\rho = \frac{m}{V} = \frac{4m}{\pi d^2 h}$$

where  $d$  and  $h$  are the diameter and the height of the sponges, measured by the Vernier caliper.

The morphologies of the sponges and cells on the sponges were characterized by SEM (Zeiss LEO 1530, EHT = 3 kV). Prior to scanning, the samples were sputter-coated with platinum of 3.0 nm thickness.

Compression tests were carried out by a universal Zwick/Roell Z 2.5 with a 20 N load sensor at a compressing speed of 3 mm/min at room temperature. Cylinder-shaped sponge with height of 32 mm and diameter of 27 mm were used for the tests.

Micro CT photos and three-dimensional (3D) images were scanned with Skyscan 1072 Micro-CT (Bruker, Artselaar, Belgium). The images with 90x and 60x magnifications were taken by the conditions of a linear resolution of 3.11 and 4.67  $\mu\text{m}$ , an accelerating voltage of 63 and 31kV, and tube current of 162 and 178  $\mu\text{A}$ , respectively. Projection images were acquired over 180° at angular increments of 0.23° with an exposure time of 1.0 seconds per frame averaged over four frames. 3D images were reconstructed using the reconstruction software provided by the manufacturer (NRecon Version 1.6.4.1).

The specific surface area of the sponges was performed on Quantachrome Autosorb 1. Prior to measurement, the samples were dried 24 h at 100 °C in high vacuum. Physisorption of Argon measurements were done at 87.35 K. The software of ASiQ V3.00 was used for analysis and to obtain the data of specific surface area.

**References**

1. Giebel E, Greiner A. Water-Stable Nonwovens Composed of Electrospun Fibers from Aqueous Dispersions by Photo-Cross-Linking. *Macromol. Mater. Eng.* **297**, 532-539 (2012).
2. Bunte C, Rhe J. Photochemical Generation of Ferrocene-Based Redox-Polymer Networks. *Macromol. Rapid. Commun.* **30**, 1817-1822 (2009).
3. Bunte C, Prucker O, Knig T, Rhe Jr. Enzyme Containing Redox Polymer Networks for Biosensors or Biofuel Cells: A Photochemical Approach. *Langmuir* **26**, 6019-6027 (2009).
4. Toomey R, Freidank D, Rhe J. Swelling Behavior of Thin, Surface-Attached Polymer Networks. *Macromolecules* **37**, 882-887 (2004).
5. Kajtna J, Krajnc M. UV Crosslinkable Microsphere Pressure Sensitive Adhesivesinfluence on Adhesive Properties. *International Journal of Adhesion & Adhesives* **31**, 29-35 (2011).

### 3.2 Ultralight open cell polymer sponges with advanced properties by PPX CVD coating

**Gaigai Duan**, Shaohua Jiang, Tobias Moss, Seema Agarwal, Andreas Greiner. Ultralight open cell polymer sponges with advanced properties by PPX CVD coating. *Polym. Chem.* **2016**; 7(15):2759-2764.

This article is licensed under a Creative Commons Attribution-NonCommercial 3.0 Unported Licence. Material from this article can be used in other publications provided that the correct acknowledgement is given with the reproduced material and it is not used for commercial purposes.



Cite this: *Polym. Chem.*, 2016, **7**, 2759

Received 24th February 2016,  
Accepted 21st March 2016

DOI: 10.1039/c6py00339g

www.rsc.org/polymers

## Ultralight open cell polymer sponges with advanced properties by PPX CVD coating†

Gaigai Duan, Shaohua Jiang, Tobias Moss, Seema Agarwal and Andreas Greiner\*

Ultralight polyacrylate sponges were prepared from dispersions of short electrospun polymer fibres by freeze drying and coated with poly(p-xylylene) (PPX) by chemical vapour deposition (CVD). The PPX coating of the sponges increased the compression strength, the water contact angle, and the solvent resistance significantly without significant alteration of the sponge morphology.

### Introduction

Ultraporous, ultralight, three-dimensional (3D) materials are very attractive due to their high porosity and elasticity that makes them suitable for various fields, including energy applications, absorber materials, insulating materials, and tissue engineering.<sup>1–4</sup> Among these materials, 3D ultralight polymer scaffolds assembled from electrospun fibres recently experienced a fast development in applications for tissue engineering,<sup>5–7</sup> microbial fuel cells,<sup>8</sup> oil adsorption,<sup>9</sup> and oil/water separation.<sup>10</sup> Recently, our group developed novel ultralight 3D sponges from the dispersion of short electrospun fibres, which possessed ultralow density (2.7–9.1 mg cm<sup>-3</sup>) and high porosity (99.6%).<sup>11</sup> These sponges are highly breathable open cell solids. The sponges showed applications in cell culture and high uptake of hydrophobic liquids.<sup>11</sup> In another recent report, Xu *et al.* adopted a similar strategy and prepared a 3D nanofibrous polycaprolactone (PCL) scaffold for bone tissue engineering.<sup>12</sup> However, due to the highly porous structures, these 3D fibrous sponges/scaffolds showed poor mechanical properties, which would greatly limit their practical applications. A solution for the disadvantage of such sponges could be additional coatings on the surface of the fibres, in particular at the junction points. Poly(p-xylylene) (PPX) prepared by chemical vapour deposition (CVD) could be an ideal coating material due to its homogeneous and conformal surfaces, good adhesion to other materials, chemical resistance, excellent biocompatibility, and thermal stability.<sup>13–15</sup> It can be used for hydrophobic coating for moisture barriers,<sup>16,17</sup> reinforcement of microstructures,<sup>18</sup> and protection materials for plastic, rubber, and metals from a harsh environment.<sup>19,20</sup>

In this work, PPX was coated onto the ultralight polymer fibre sponges. By varying the coating thickness, PPX reinforced composite sponges exhibited tuneable properties including densities, mechanical properties, water contact angle, and solvent resistance.

### Experimental

#### Materials

Methyl acrylate (MA, Aldrich, 99%) and methyl methacrylate (MMA, Aldrich, 99%) were purified by passing through a neutral aluminium oxide column. 2,2'-Azobis(isobutyronitrile) (AIBN, Fluka, 98%) was recrystallised from methanol (Aldrich, 99.8%). Parylene N (Specialty Coating Systems), polyacrylonitrile ( $M_w = 150\,000$ , polyscience Inc.), dimethyl sulfoxide (DMSO, Fisher Chemical, 99.99%), dimethyl formamide (DMF, Fisher Chemical, 99.99%), dioxane (technical grade), and acetone (technical grade) were used as received. 4-Methacryloyloxybenzophenone (MABP) was synthesised according to a previous report.<sup>21</sup>

#### Preparation of sponges

The polymer fibre sponges were prepared according to our previous report.<sup>11</sup> In brief, copolymer poly(MA-co-MMA-MABP) was prepared by radical copolymerisation of MMA (13.5 ml), MA (17.3 ml), and MABP (4.681 g) using AIBN (0.293 g) as initiator in DMSO at 70 °C for 5 hours. The copolymer was precipitated in methanol and dried in a vacuum oven at 40 °C for 2 days. The obtained poly(MA-co-MMA-MABP) had a molar mass ( $M_n$ ) of  $2.43 \times 10^5$  as determined by gel permeation chromatography using THF as the eluting solvent against poly(methyl methacrylate) standards.

6.17 g of poly(MA-co-MMA-MABP) were dissolved in DMSO with a concentration of 20 wt%. A 13.2 wt% PAN solution was prepared by dissolving PAN in DMF.

Macromolecular Chemistry II and Bayreuth Center for Colloid and Interfaces,  
Universität Bayreuth, Universitätsstraße 30, 95440 Bayreuth, Germany.  
E-mail: greiner@uni-bayreuth.de; Fax: +49-921-553393

† Electronic supplementary information (ESI) available. See DOI: 10.1039/c6py00339g



**Table 1** Detailed information about short electrospun fibre dispersions and densities of the sponges

Sponge	Volume of short fibre dispersion (ml)	Volume of dioxane (ml)	Density (mg cm <sup>-3</sup> )
1	65	0	8.42
2	60	5	7.43
3	50	15	6.61
4	40	25	5.16
5	30	35	4.34

The solution (17.8 wt%) for electrospinning was prepared by mixing 26.2 g of poly(MA-co-MMA-MABP) solution in DMSO (20 wt%), 2 g of PAN solution in DMF (13.2 wt%) and 2.68 g of acetone. Electrospinning was performed by applying a voltage of 9 kV and a flow rate of 1.5 ml h<sup>-1</sup> in 55% humidity. The electrospun fibres were collected on aluminium foil and dried in a vacuum oven at 40 °C for 24 h.

1.17 g of the above electrospun fibres were cross-linked using UV light (UV lamp 250GS) with a distance of 15 cm for 5 h. Then the cross-linked nanofibres were cut into short fibres with a length of 150 ± 30 μm in 350 ml of dioxane with a razor blade at a rotation of 5000 rpm for 45 s. Different short fibre dispersions were prepared by controlling the volume of the above short fibre dispersion and dioxane (Table 1). Sponges with different densities of 8.42, 7.43, 6.61, 5.16, and 4.34 mg cm<sup>-3</sup> were prepared by freeze-drying the above short fibre dispersions in cylindrical glass tubes at 0.03 mbar for 48 h.

#### PPX coating on sponge fibres

The above sponges were put in the deposition chamber of a CVD coater. For CVD coating, 170 mg of [2.2]paracyclophane were sublimed at 150 °C followed by pyrolysis at 650 °C in a pyrolysis oven of the coater under reduced pressure. The pyrolysed monomer gas was deposited on the fibres of the sponges at 20 °C under 52 mtorr in the deposition chamber and formed a PPX film with 100 nm thickness. Different samples with varied coating thickness of PPX (100, 280, 360, and 1000 nm) were made by changing the amount of the precursor.

#### Characterisation

The morphology of sponges was characterised by scanning electron microscopy (SEM, Zeiss Leo 1530) and all the samples were sputtered with 3 nm thick platinum before measurements. A compression test was done using a Z 2.5 machine with a 20 N sensor at a speed of 10 mm min<sup>-1</sup>. The samples for the compression test were cut into cylindrical shape with a diameter of 20 mm and a height of 8 mm. Each of these samples was compressed once, released, and compressed again for measurement. The water contact angle was measured by using a G10 contact angle analysis system (Krüss, Hamburg, Germany) using an 8 μl water droplet. The PPX coating thickness was measured using a Veeco Dektak 150 profilometer. An indirect method was used for thickness determi-

nation. A glass slide was coated simultaneously to the sponge. The PPX coated layer on the glass slide was cut at three different positions and the thickness of the layer was determined by analysing the step height with the profilometer. The average height at the three positions was used as the coating thickness.

## Results and discussion

Electrospun nanofibres were fabricated from a blended solution of poly(MA-co-MMA-MABP) and PAN. The fibres have a smooth surface without any beads and the diameter of the fibre was 1000 ± 100 nm (Fig. 1). The polymer sponge prepared from short electrospun nanofibre dispersion was free-standing with a 3D cylindrical-shape with a diameter of 20 ± 2 mm (Fig. 1, inset).

The pore size could be tuned by controlling the density of the sponge. As shown in Fig. 2, the pore size of the sponge became larger as the density decreased from 8.42 to 5.16 mg cm<sup>-3</sup>.

The average fibre diameter of the sponge was about 1000 ± 100 nm (Fig. 2D), which is similar to the starting nanofibres before cutting and freeze-drying. The fibre diameter increased after PPX coating depending upon the coating thickness (Fig. 2E). The increasing PPX thickness led to the film formation around the entanglement position of the fibres (Fig. 2E), which could contribute to the increase in compression strength observed for the coated sponges (see below). Fig. 2F shows the cross-sectional morphology of the PPX coated fibres, where a core (original sponge fibre)-shell (PPX) morphology was clearly obvious. CVD (gas phase polymerisation) of PPX has the advantage that it provides uniform coating without film deposition on the surface. PPX coating also provides an additional way of tuning the density of sponges. The sponge density increased with an increase in PPX thickness (Table 2). For uncoated sponges, the density is controlled by the amount of short fibres in the dispersion for

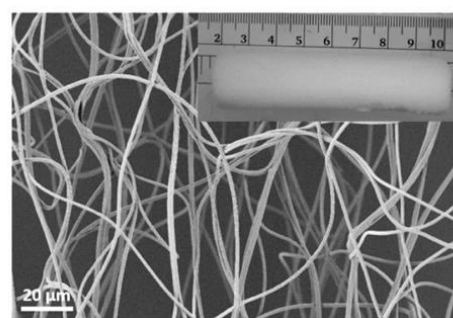


**Fig. 1** SEM image of an electrospun nanofibre mat and the digital photo of sponge made after cutting and drying (inset).



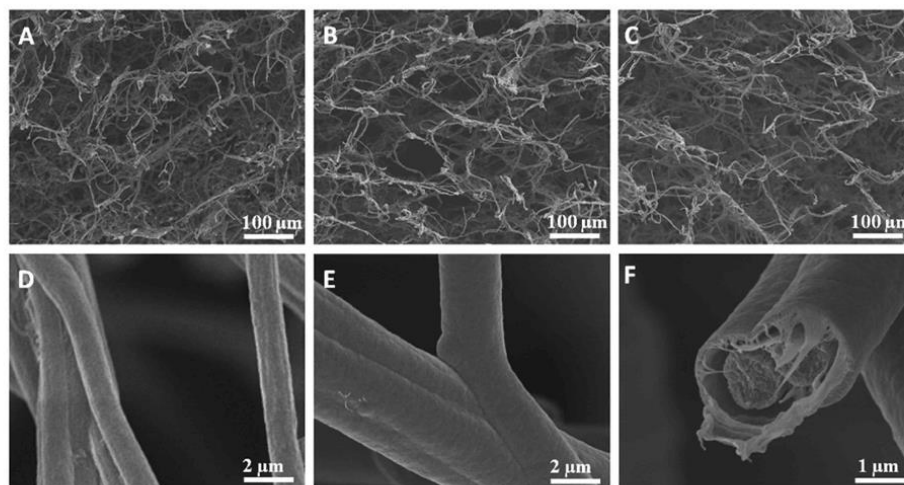


Fig. 2 SEM images of original sponge 1 (A,  $8.42 \text{ mg cm}^{-3}$ ), sponge 2 (B,  $7.43 \text{ mg cm}^{-3}$ ), sponge 4 (C,  $5.16 \text{ mg cm}^{-3}$ ), higher magnification of sponge 4 (D), sponge 4 coated with 1000 nm PPX (E, sponge 4–1000), and the corresponding cross section of sponge 4–1000.

Table 2 Densities of sponges before and after PPX coating

PPX thickness (nm)	Density ( $\text{mg cm}^{-3}$ )			
	Sponge 1	Sponge 2	Sponge 4	Sponge 5
0	8.42	7.43	5.16	4.34
100	9.41	8.55	6.40	4.83
280	12.45	10.99	7.30	6.41
360	14.48	13.05	8.66	7.42
1000	22.59	20.06	13.93	12.15

freeze-drying. The original electrospun fibre sponges exhibited densities in the range of  $4.34\text{--}8.42 \text{ mg cm}^{-3}$ . Upon coating with different thicknesses of PPX, the composite sponges showed a considerable density variation from  $4.83$  to  $22.59 \text{ mg cm}^{-3}$  without a major change in the pore structure of the sponges. This diversity in density would greatly promote the sponges in different applications.

The compression properties of sponges with different densities and PPX coating thicknesses were investigated. The compression stress–strain curves are shown in Fig. 3 and the corresponding data are summarized in Table 3. As expected, a higher sponge density led to higher compression strength. When compressed at 50% strain, sponge 5 (density =  $4.34 \text{ mg cm}^{-3}$ ), sponge 4 (density =  $5.16 \text{ mg cm}^{-3}$ ), sponge 2 (density =  $7.43 \text{ mg cm}^{-3}$ ), and sponge 1 (density =  $8.43 \text{ mg cm}^{-3}$ ) possessed a compression strength of  $0.26$ ,  $0.47$ ,  $0.76$ , and  $0.92 \text{ kPa}$ , respectively. After coating with PPX, the composite sponges showed significant enhancement in compression stress. The composite sponges with a coating of  $100 \text{ nm}$  thick PPX exhibited compression strength more than

two times compared to that of the bare sponges. When  $1000 \text{ nm}$  of PPX were coated on the sponges, the compression strength increased more than 10 times the original sponges. One cyclic compression test was also performed to assess the mechanical performance of the sponges before and after PPX coating. As shown in Fig. 3, it is obvious that the second compression curves (c) are always under the first compression curves (a) and there are blank areas in between curves a and c. These areas could be used to access the energy loss during the cyclic compression test. The sponges with higher density showed higher compression strength, but they also showed much more energy loss during the cyclic test. Although there was energy loss, the ultimate compression strength of the second compression could return to the same values as the first test showed. Fig. 4 shows the relationship between the compression strength and the densities of the sponges. It was obvious that the thicker PPX coating led to a higher density and the sponges with higher densities possessed higher compression strength. Furthermore, a coated sponge (density was  $5.0 \pm 0.1 \text{ mg cm}^{-3}$ , before coating) with  $100 \text{ nm}$  PPX can support a piece of dry ice on the top without compression deformation, whereas an uncoated sponge is not able to bear such a force. These sponges have low thermal conductivity of about  $0.05 \text{ W (K m)}^{-1}$ . A sponge could protect human skin from dry ice ( $\text{CO}_2$ ,  $-78 \text{ }^\circ\text{C}$ ) as shown in a real time video in the ESI.†

Previous research by Boduroglu *et al.* reported that the structured PPX films showed superhydrophobicity with a water contact angle (WCA) of about  $152^\circ$ .<sup>16</sup> A PPX coating on sponge fibres could also lead to a significant increase of the hydrophobicity of the sponges, which was indeed the case but not as



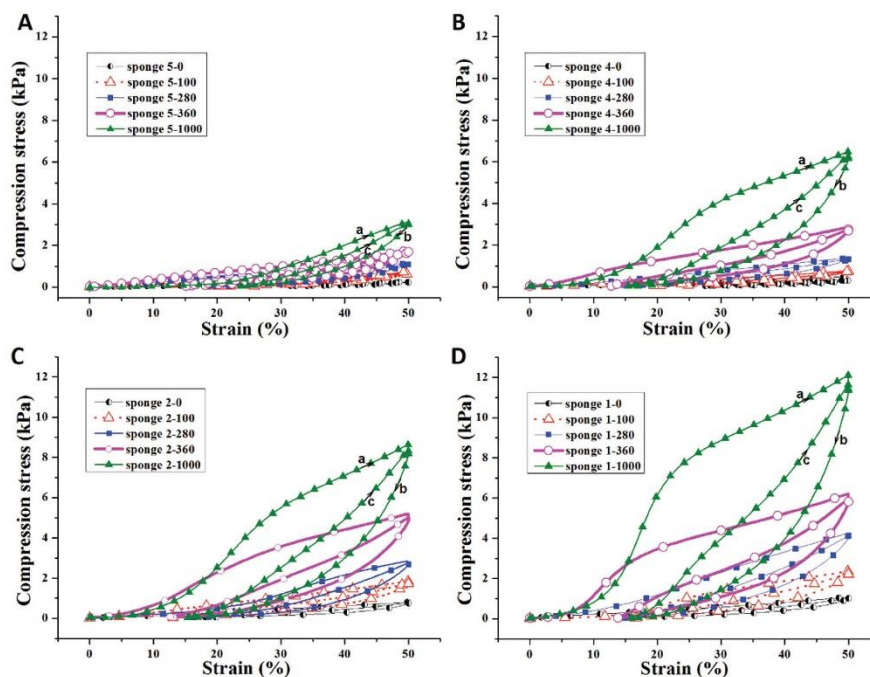


Fig. 3 Cyclic compression test of sponges with 0, 100, 280, 360, and 1000 nm thick PPX coating. The upper curve (a): first compression cycle; the middle curve (b): release; the bottom curve (c): the second compression cycle.



Table 3 Compression stress of sponges before and after PPX coating

PPX thickness (nm)	Compression stress (kPa)			
	Sponge 1	Sponge 2	Sponge 4	Sponge 5
0	0.92	0.76	0.47	0.26
100	2.31	1.93	0.97	0.81
280	4.13	2.74	1.40	1.20
360	6.21	5.19	2.89	1.72
1000	12.13	8.67	6.52	3.08

expected. Fig. 5A presents the typical WCA of sponge 2 with varying PPX coating thickness. The as-prepared sponge 2 had a WCA of  $119^\circ$ . When the PPX thickness increased to 280 nm, the composite sponge (sponge 2-280) became superhydrophobic with a WCA of  $156^\circ$ . A further increase of the PPX coating thickness led to a decrease of WCA, but the WCA ( $144$  and  $131^\circ$ ) was still much higher than that of the as-prepared sponge ( $119^\circ$ ). Fig. 5B reveals the relationship between the WCA and the PPX thickness. Generally, the WCA on PPX coated sponges showed a trend of an increase in contact angle with thickness up to a certain value and then decreased on a

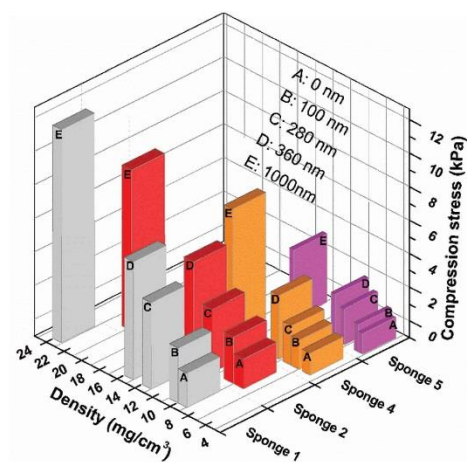


Fig. 4 Compression stress of sponges before and after PPX coating as a function of density.

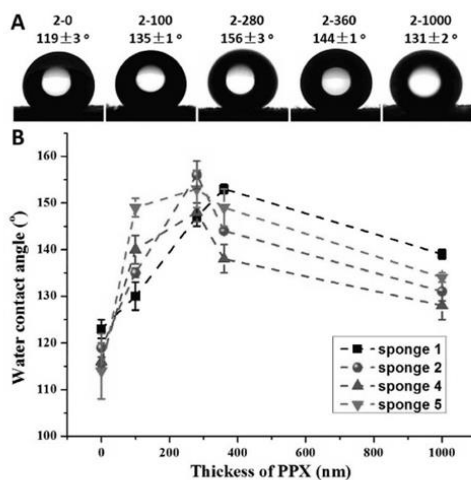


Fig. 5 Typical water contact angle of sponge 2 with different PPX coating thicknesses (A) and water contact angles as a function of the PPX coating thickness of sponges 1, 2, 4, and 5 (B).

further increase in PPX coating thickness. The optimum PPX thickness providing the highest contact angles was about 280 nm. An analogous trend of the hydrophobicity as a function of PPX thickness was found for electrospun mats (see the ESI Fig. S1†).

Surface structures play an important role on the WCA. In this study, the surfaces of the sponge fibres were observed by SEM. The as-prepared sponge fibre showed many nanopores (Fig. 6A), which could be attributed to the phase separation during the preparation of the sponge. These pores led to a

rough surface and this may be the reason for the hydrophobicity of the as-prepared electrospun polymer sponge. The coating of PPX greatly changed the surface morphology of the composite sponge fibres. When coated with 100 nm PPX, the fibre surface became smooth but some salient features were observed (Fig. 2B), which could be due to the occupation of the nanopores of the as-prepared fibres. The composite sponge fibres exhibited bigger salient features and much smoother surface when the sponges were coated with 280 and 1000 nm PPX, respectively (Fig. 6C and D). This explains the lower WCA at higher PPX coating thicknesses. Quite obviously, the hydrophobicity of fibrous materials as a function of PPX coating thickness is a combined effect of inherent hydrophobicity and surface roughness which becomes smaller when thicker PPX layers flatten fibrous substrates.

PPX has excellent solvent resistance. Therefore, we expected improved solvent resistance of the sponges by PPX coating, which would open up many new chances for advanced applications. The solvent resistance of the sponges with and without PPX coating was investigated in water, ethanol, acetone, and chloroform. As shown in Fig. 7, the sponges with the size of 3 mm × 5 mm × 7 mm were put in a 1.5 mL vial with 0.8 mL solvents. Both uncoated and coated sponge floated on the surface of water but they were totally soaked in organic solvents (Fig. 7A and B). Interestingly, the sponges sank to the bottom of the vial in ethanol and acetone, but floated in chloroform due to the density difference between the sponge polymer and solvents: the polymer density of the sponges was larger than those of ethanol and acetone, but smaller than the density of chloroform. It is necessary to point out that the stability of non-coated sponges in organic solvents depends upon the type of the solvent used. The sponges kept their original shapes in ethanol even for a very long time but swelled a little in acetone and chloroform. Coated sponges had higher shape stability even after intense shaking (Fig. 7D).

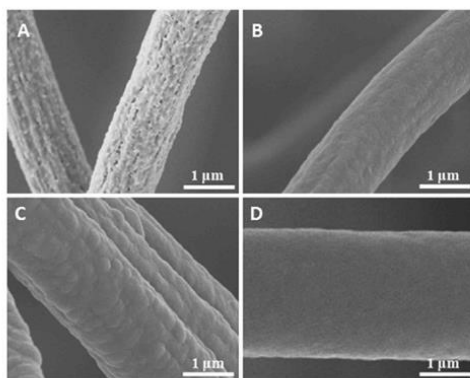


Fig. 6 SEM images of sponge (sponge 2) fibres with the PPX thicknesses of 0 (A), 100 (B), 280 (C), and 1000 nm (D).

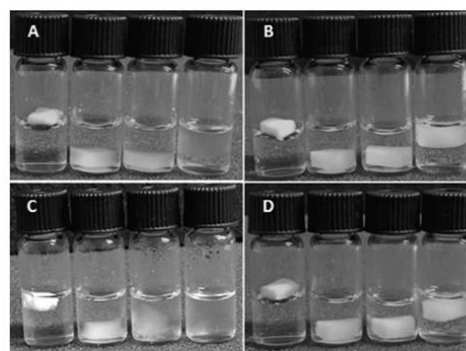


Fig. 7 Sponges in different solvents (from left to right: water, ethanol, acetone, chloroform). (A) before coating, (B) PPX coating thickness of 280 nm, (C) and (D) after intense shaking of (A) and (B) respectively.



However, uncoated sponges lost their structure in acetone and chloroform during shaking by hand (Fig. 7C), which forces the formation of short fibres and these short fibres can be reused for the preparation of new sponges in dioxane.

## Conclusions

Ultralight composite sponges were achieved by CVD coating with different coating thicknesses of PPX on the as-prepared short electrospun polymer sponges under ambient conditions. The density, compression strength, and the water contact angle of the composite sponges could be well tuned by adjusting the thickness of the PPX coating layer. However, with higher PPX layer thickness the hydrophobicity of the sponges decreased, which could be explained by planarization of the fractal structure on the fibre surfaces. In addition, the PPX coating could significantly improve the solvent resistance of the sponges and retain their shape in various solvents. The PPX coating removes the inherent disadvantage of lower chemical and mechanical stability of polymeric sponges made from short electrospun fibres without destroying their porous structure. This is a big step forward in the direction of future use of 3D porous fibrous scaffolds under harsh conditions. With this the PPX coated sponges have become of particular interest for separation applications. Due to the low thermal conductivity and the improvement of the mechanical properties of sponges after PPX coating, these coated sponges can be applied in the heat insulation field as a new kind of light weight material.

## Acknowledgements

The authors are indebted to DFG for financial support (SFB840) and to Specialty Coating Systems for the donation of paracyclophane. We are thankful to Mrs Bianca Uch for taking the video with dry ice on sponge.

## Notes and references

1 Y. K. Akimov, *Instrum. Exp. Tech.*, 2003, **46**, 287–299.

- 2 V. Chabot, D. Higgins, A. Yu, X. Xiao, Z. Chen and J. Zhang, *Energy Environ. Sci.*, 2014, **7**, 1564–1596.
- 3 S. Nardecchia, D. Carriazo, M. L. Ferrer, M. C. Gutierrez and F. del Monte, *Chem. Soc. Rev.*, 2013, **42**, 794–830.
- 4 P. C. Thapliyal and K. Singh, *J. Mater.*, 2014, **2014**, 10.
- 5 S. Zhong, Y. Zhang and C. T. Lim, *Tissue Eng., Part B*, 2011, **18**, 77–87.
- 6 S.-H. Shin, O. Purevdorj, O. Castano, J. A. Planell and H.-W. Kim, *J. Tissue Eng.*, 2012, **3**.
- 7 J. M. Holzwarth and P. X. Ma, *J. Mater. Chem.*, 2011, **21**, 10243–10251.
- 8 S. Chen, H. Hou, F. Harnisch, S. A. Patil, A. A. Carmona-Martinez, S. Agarwal, Y. Zhang, S. Sinha-Ray, A. L. Yarin and A. Greiner, *Energy Environ. Sci.*, 2011, **4**, 1417–1421.
- 9 J. Wu, N. Wang, L. Wang, H. Dong, Y. Zhao and L. Jiang, *ACS Appl. Mater. Interfaces*, 2012, **4**, 3207–3212.
- 10 Y. Si, J. Yu, X. Tang, J. Ge and B. Ding, *Nat. Commun.*, 2014, DOI: 10.1038/ncomms6802; Y. Si, Q. Fu, X. Wang, J. Zhu, J. Yu, G. Sun and B. Ding, *ACS Nano*, 2015, **9**, 3791–3799.
- 11 G. Duan, S. Jiang, V. Jérôme, J. H. Wendorff, A. Fathi, J. Uhm, V. Altstädt, M. Herling, J. Breu, R. Freitag, S. Agarwal and A. Greiner, *Adv. Funct. Mater.*, 2015, **25**, 2850–2856.
- 12 T. Xu, J. M. Miszuk, Y. Zhao, H. Sun and H. Fong, *Adv. Healthcare Mater.*, 2015, **4**, 2238–2246.
- 13 H. Hou, Z. Jun, A. Reuning, A. Schaper, J. H. Wendorff and A. Greiner, *Macromolecules*, 2002, **35**, 2429–2431.
- 14 P. Simon, S. Mang, A. Hasenhindl, W. Gronski and A. Greiner, *Macromolecules*, 1998, **31**, 8775–8780.
- 15 A. Greiner, S. Mang, O. Schäfer and P. Simon, *Acta Polym.*, 1997, **48**, 1–15.
- 16 S. Boduroglu, M. Cetinkaya, W. Dressick, A. Singh and M. Demirel, *Langmuir*, 2007, **23**, 11391–11395.
- 17 H. Shao, X. Hu, K. Xu, C. Tang, Y. Zhou, M. Shuai, J. Mei, Y. Zhu and W.-m. Lau, *RSC Adv.*, 2015, **5**, 55713–55719.
- 18 K. Y. Suh, R. Langer and J. Lahann, *Appl. Phys. Lett.*, 2003, **83**, 4250–4252.
- 19 C. Hassler, R. P. von Metzzen, P. Ruther and T. Stieglitz, *J. Biomed. Mater. Res., Part B*, 2010, **93**, 266–274.
- 20 K. Yamashita, T. Mori and T. Mizutani, *J. Phys. D: Appl. Phys.*, 2001, **34**, 740.
- 21 I. Yilgor, S. Bilgin, M. Isik and E. Yilgor, *Polymer*, 2012, **53**, 1180–1188.



**Supplementary Information**

**Fig. S1** showed the water contact angle of fiber mat before PPX coating was no more than  $110^\circ$ , and it has nearly  $140^\circ$  when coated with 280 nm PPX then water contact angle decreased if PPX layer become thicker. This trend was consistent with water contact angle of sponge before and after coating. It was easy to find that PPX is one kind of hydrophobic materials, and different thickness PPX coating changed the surface roughness of fiber.

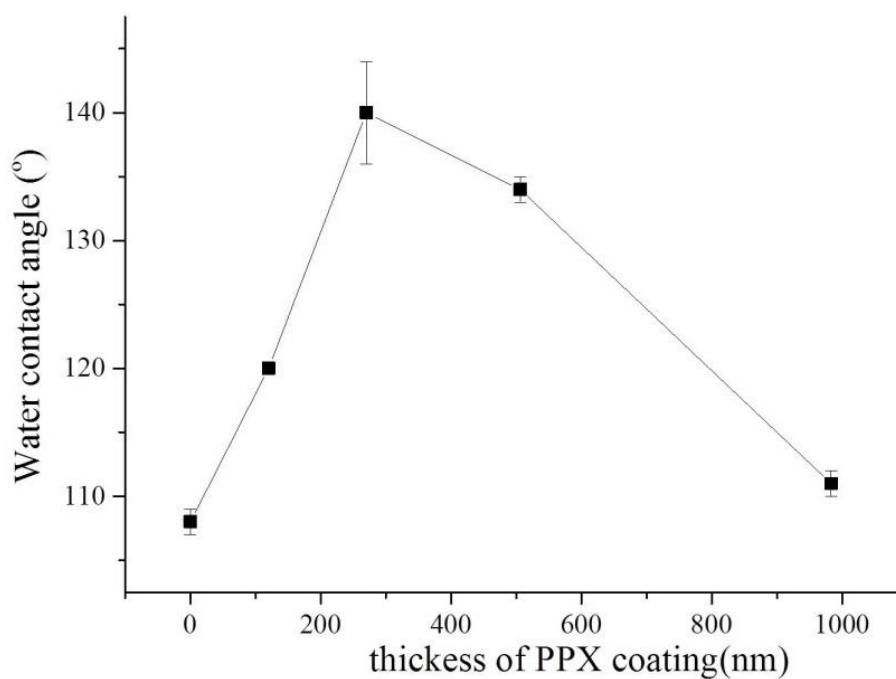


**Figure S1.** Water contact angle of fiber mat as a function of different thickness of PPX coating.

### **3.3 Highly efficient reusable sponge-type catalyst carriers based on short electrospun fibers**

**Gaigai Duan**, Mellisa Koehn-Serrano, Andreas Greiner. Highly Efficient Reusable Sponge-Type Catalyst Carriers Based on Short Electrospun Fibers. *Macromol. Rapid Comm.* **2017**; 38: 1600511.

2016/12/1

RightsLink - Your Account

## JOHN WILEY AND SONS LICENSE TERMS AND CONDITIONS

Dec 01, 2016

This Agreement between University of Bayreuth -- Gaigai Duan ("You") and John Wiley and Sons ("John Wiley and Sons") consists of your license details and the terms and conditions provided by John Wiley and Sons and Copyright Clearance Center.

License Number	4000051151174
License date	Dec 01, 2016
Licensed Content Publisher	John Wiley and Sons
Licensed Content Publication	Macromolecular Rapid Communications
Licensed Content Title	Highly Efficient Reusable Sponge - Type Catalyst Carriers Based on Short Electrospun Fibers
Licensed Content Author	Gaigai Duan, Melissa Koehn - Serrano, Andreas Greiner
Licensed Content Date	Nov 23, 2016
Licensed Content Pages	1
Type of Use	Dissertation/Thesis
Requestor type	Author of this Wiley article
Format	Print and electronic
Portion	Full article
Will you be translating?	No
Title of your thesis / dissertation	3D porous sponges from electrospun polymer fibers and their applications
Expected completion date	Dec 2017
Expected size (number of pages)	160
Requestor Location	University of Bayreuth Universitätsstrasse 30  Bayreuth, 95440 Germany Attn: Gaigai Duan
Publisher Tax ID	EU826007151
Billing Type	Invoice
Billing Address	University of Bayreuth Universitätsstrasse 30  Bayreuth, Germany 95440 Attn: Gaigai Duan
Total	<b>0.00 EUR</b>
Terms and Conditions	

### TERMS AND CONDITIONS

This copyrighted material is owned by or exclusively licensed to John Wiley & Sons, Inc. or one of its group companies (each a "Wiley Company") or handled on behalf of a society with which a Wiley Company has exclusive publishing rights in relation to a particular work (collectively "WILEY"). By clicking "accept" in connection with completing this licensing transaction, you agree that the following terms and conditions apply to this transaction (along with the billing and payment terms and conditions established by the Copyright Clearance Center Inc., ("CCC's Billing and Payment terms and conditions"), at the time that you opened your RightsLink account (these are available at any time at <http://myaccount.copyright.com>).

#### Terms and Conditions

- The materials you have requested permission to reproduce or reuse (the "Wiley Materials") are protected by copyright.

2016/12/1

RightsLink - Your Account

- You are hereby granted a personal, non-exclusive, non-sub licensable (on a stand-alone basis), non-transferable, worldwide, limited license to reproduce the Wiley Materials for the purpose specified in the licensing process. This license, and any **CONTENT (PDF or image file) purchased as part of your order**, is for a one-time use only and limited to any maximum distribution number specified in the license. The first instance of republication or reuse granted by this license must be completed within two years of the date of the grant of this license (although copies prepared before the end date may be distributed thereafter). The Wiley Materials shall not be used in any other manner or for any other purpose, beyond what is granted in the license. Permission is granted subject to an appropriate acknowledgement given to the author, title of the material/book/journal and the publisher. You shall also duplicate the copyright notice that appears in the Wiley publication in your use of the Wiley Material. Permission is also granted on the understanding that nowhere in the text is a previously published source acknowledged for all or part of this Wiley Material. Any third party content is expressly excluded from this permission.
- With respect to the Wiley Materials, all rights are reserved. Except as expressly granted by the terms of the license, no part of the Wiley Materials may be copied, modified, adapted (except for minor reformatting required by the new Publication), translated, reproduced, transferred or distributed, in any form or by any means, and no derivative works may be made based on the Wiley Materials without the prior permission of the respective copyright owner. **For STM Signatory Publishers clearing permission under the terms of the STM Permissions Guidelines only, the terms of the license are extended to include subsequent editions and for editions in other languages, provided such editions are for the work as a whole in situ and does not involve the separate exploitation of the permitted figures or extracts**. You may not alter, remove or suppress in any manner any copyright, trademark or other notices displayed by the Wiley Materials. You may not license, rent, sell, loan, lease, pledge, offer as security, transfer or assign the Wiley Materials on a stand-alone basis, or any of the rights granted to you hereunder to any other person.
- The Wiley Materials and all of the intellectual property rights therein shall at all times remain the exclusive property of John Wiley & Sons Inc, the Wiley Companies, or their respective licensors, and your interest therein is only that of having possession of and the right to reproduce the Wiley Materials pursuant to Section 2 herein during the continuance of this Agreement. You agree that you own no right, title or interest in or to the Wiley Materials or any of the intellectual property rights therein. You shall have no rights hereunder other than the license as provided for above in Section 2. No right, license or interest to any trademark, trade name, service mark or other branding ("Marks") of WILEY or its licensors is granted hereunder, and you agree that you shall not assert any such right, license or interest with respect thereto
- NEITHER WILEY NOR ITS LICENSORS MAKES ANY WARRANTY OR REPRESENTATION OF ANY KIND TO YOU OR ANY THIRD PARTY, EXPRESS, IMPLIED OR STATUTORY, WITH RESPECT TO THE MATERIALS OR THE ACCURACY OF ANY INFORMATION CONTAINED IN THE MATERIALS, INCLUDING, WITHOUT LIMITATION, ANY IMPLIED WARRANTY OF MERCHANTABILITY, ACCURACY, SATISFACTORY QUALITY, FITNESS FOR A PARTICULAR PURPOSE, USABILITY, INTEGRATION OR NON-INFRINGEMENT AND ALL SUCH WARRANTIES ARE HEREBY EXCLUDED BY WILEY AND ITS LICENSORS AND WAIVED BY YOU.
- WILEY shall have the right to terminate this Agreement immediately upon breach of this Agreement by you.
- You shall indemnify, defend and hold harmless WILEY, its Licensors and their respective directors, officers, agents and employees, from and against any actual or threatened claims, demands, causes of action or proceedings arising from any breach of this Agreement by you.
- IN NO EVENT SHALL WILEY OR ITS LICENSORS BE LIABLE TO YOU OR ANY OTHER PARTY OR ANY OTHER PERSON OR ENTITY FOR ANY SPECIAL, CONSEQUENTIAL, INCIDENTAL, INDIRECT, EXEMPLARY OR PUNITIVE DAMAGES, HOWEVER CAUSED, ARISING OUT OF OR IN CONNECTION WITH THE DOWNLOADING, PROVISIONING, VIEWING OR USE OF THE MATERIALS REGARDLESS OF THE FORM OF ACTION, WHETHER FOR BREACH OF CONTRACT, BREACH OF WARRANTY, TORT, NEGLIGENCE, INFRINGEMENT OR OTHERWISE (INCLUDING, WITHOUT LIMITATION, DAMAGES BASED ON LOSS OF PROFITS, DATA, FILES, USE, BUSINESS OPPORTUNITY OR CLAIMS OF THIRD PARTIES), AND WHETHER OR NOT THE PARTY HAS BEEN ADVISED OF THE POSSIBILITY OF SUCH DAMAGES. THIS LIMITATION SHALL APPLY NOTWITHSTANDING ANY FAILURE OF ESSENTIAL PURPOSE OF ANY LIMITED REMEDY PROVIDED HEREIN.
- Should any provision of this Agreement be held by a court of competent jurisdiction to be illegal, invalid, or unenforceable, that provision shall be deemed amended to achieve as nearly as possible the same economic effect as the original provision, and the legality, validity and enforceability of the remaining provisions of this Agreement shall not be affected or impaired thereby.
- The failure of either party to enforce any term or condition of this Agreement shall not constitute a waiver of either party's right to enforce each and every term and condition of this Agreement. No breach under this agreement shall be deemed waived or excused by either party unless such waiver or consent is in writing signed by the party granting such waiver or consent. The waiver by or consent of a party to a breach of any provision of this Agreement shall not operate or be construed as a waiver of or consent to any other or subsequent breach by such other party.

<https://s100.copyright.com/MyAccount/web/jsp/viewprintablelicensefrommyorders.jsp?ref=352abae3-079b-48a2-a2f8-9cddc83f81d0&email=>

2/3

2016/12/1

RightsLink - Your Account

- This Agreement may not be assigned (including by operation of law or otherwise) by you without WILEY's prior written consent.
- Any fee required for this permission shall be non-refundable after thirty (30) days from receipt by the CCC.
- These terms and conditions together with CCC's Billing and Payment terms and conditions (which are incorporated herein) form the entire agreement between you and WILEY concerning this licensing transaction and (in the absence of fraud) supersedes all prior agreements and representations of the parties, oral or written. This Agreement may not be amended except in writing signed by both parties. This Agreement shall be binding upon and inure to the benefit of the parties' successors, legal representatives, and authorized assigns.
- In the event of any conflict between your obligations established by these terms and conditions and those established by CCC's Billing and Payment terms and conditions, these terms and conditions shall prevail.
- WILEY expressly reserves all rights not specifically granted in the combination of (i) the license details provided by you and accepted in the course of this licensing transaction, (ii) these terms and conditions and (iii) CCC's Billing and Payment terms and conditions.
- This Agreement will be void if the Type of Use, Format, Circulation, or Requestor Type was misrepresented during the licensing process.
- This Agreement shall be governed by and construed in accordance with the laws of the State of New York, USA, without regards to such state's conflict of law rules. Any legal action, suit or proceeding arising out of or relating to these Terms and Conditions or the breach thereof shall be instituted in a court of competent jurisdiction in New York County in the State of New York in the United States of America and each party hereby consents and submits to the personal jurisdiction of such court, waives any objection to venue in such court and consents to service of process by registered or certified mail, return receipt requested, at the last known address of such party.

#### WILEY OPEN ACCESS TERMS AND CONDITIONS

Wiley Publishes Open Access Articles in fully Open Access Journals and in Subscription journals offering Online Open. Although most of the fully Open Access journals publish open access articles under the terms of the Creative Commons Attribution (CC BY) License only, the subscription journals and a few of the Open Access Journals offer a choice of Creative Commons Licenses. The license type is clearly identified on the article.

##### The Creative Commons Attribution License

The [Creative Commons Attribution License \(CC-BY\)](#) allows users to copy, distribute and transmit an article, adapt the article and make commercial use of the article. The CC-BY license permits commercial and non-

##### Creative Commons Attribution Non-Commercial License

The [Creative Commons Attribution Non-Commercial \(CC-BY-NC\) License](#) permits use, distribution and reproduction in any medium, provided the original work is properly cited and is not used for commercial purposes.(see below)

##### Creative Commons Attribution-Non-Commercial-NoDerivs License

The [Creative Commons Attribution Non-Commercial-NoDerivs License \(CC-BY-NC-ND\)](#) permits use, distribution and reproduction in any medium, provided the original work is properly cited, is not used for commercial purposes and no modifications or adaptations are made. (see below)

##### Use by commercial "for-profit" organizations

Use of Wiley Open Access articles for commercial, promotional, or marketing purposes requires further explicit permission from Wiley and will be subject to a fee.

Further details can be found on Wiley Online Library <http://olabout.wiley.com/WileyCDA/Section/id-410895.html>

#### Other Terms and Conditions:

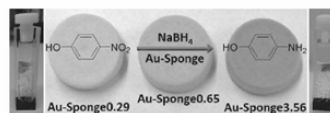
v1.10 Last updated September 2015

Questions? [customercare@copyright.com](mailto:customercare@copyright.com) or +1-855-239-3415 (toll free in the US) or +1-978-646-2777.

# Highly Efficient Reusable Sponge-Type Catalyst Carriers Based on Short Electrospun Fibers

Gaigai Duan, Melissa Koehn-Serrano, Andreas Greiner\*

This study reports on gold nanoparticles (AuNPs) immobilized in a sponge made of short electrospun fibers (Au-sponge), which show surprisingly high reaction rates at extremely low gold amount. Au-sponges are made by freeze-drying of dispersions of short electrospun fibers with preimmobilization of AuNPs. The resulting Au-sponges show very low densities around  $7 \text{ mg cm}^{-3}$  corresponding to a pore volume of about  $150 \text{ mL g}^{-1}$ , but low surface area and very low amount of AuNPs in the range of 0.29–3.56 wt%. In general, catalysts with immobilized AuNPs show much low reaction rates compared to systems with dispersed AuNPs. By contrast, the Au-sponge catalyst with immobilized AuNPs is discerned here as an extremely efficient catalyst even superior to other systems with dispersed AuNPs. The fidelity of the Au-sponges after reactions is good enough for manifold use and thereby provides a sustainable catalyst design as well.



## 1. Introduction

Supported catalysts are most topical as they offer unique chances for the design of novel highly efficient catalytic systems.<sup>[1]</sup> Gold nanoparticles (AuNPs) play an important role as catalysts in the investigation of novel catalyst concepts including CO oxidation,<sup>[2]</sup> hydrogenation,<sup>[3]</sup> carbon–carbon coupling,<sup>[4]</sup> and degradation of organic molecules.<sup>[5]</sup> In many cases, AuNPs are immobilized on supports, such as micelles,<sup>[6]</sup> dendrimers,<sup>[7]</sup> colloid particles,<sup>[8]</sup> and nanorods.<sup>[9]</sup> These kinds of Au catalysts showed good catalytic performance, but they also exhibited disadvantages in efficiency and manifold use. Efforts have been made to develop reusable AuNP catalysts by immobilization of AuNPs on 2D fibrous porous membranes. Examples are carbon nanotubes,<sup>[10]</sup> polyethylenimine-modified polyacrylonitrile,<sup>[11]</sup> polyphenol-grafted collagen fibers,<sup>[12]</sup> and boron nitride nanosheets.<sup>[13]</sup> Our group developed

a “tea-bag-like” AuNP catalyst for repeated use with AuNP-loaded polymer nanotubes as catalyst.<sup>[14]</sup> The catalyst showed significantly increased catalytic activity and excellent reusability due to the large amount of immobilized AuNPs and the protective shell of the polymer tube.<sup>[14]</sup> Recently, 2D electrospun fibrous membranes were reported as support of AuNPs for catalyst application.<sup>[15]</sup> 3D porous materials received growing attention as catalyst support due to their special 3D-connected networks, ultrahigh porosity, and tunable mechanical properties. 3D carbon materials, like graphene aerogel and foam,<sup>[16]</sup> graphite foam,<sup>[17]</sup> carbon aerogel,<sup>[18]</sup> carbon nanotube aerogel/sponge,<sup>[19]</sup> and carbon nanofiber aerogel,<sup>[20]</sup> are the most studied supports for catalytic applications.

A novel class of 3D sponge-type materials made from electrospun fibers was reported recently by several groups.<sup>[21]</sup> These fibrous sponges display very low densities at low surface to volume ratio ( $\approx 2 \text{ m}^2 \text{ g}^{-1}$ ) and high mechanical integrity, with applications in separation of water from organic liquids<sup>[21a-c]</sup> and cell culturing.<sup>[21b,d]</sup> The mechanical properties of these fibrous sponges were further increased by additional coating of poly(p-xylylene) (PPX) from the vapor phase.<sup>[21e]</sup> These PPX-coated sponges showed additional features of superhydrophobicity, excellent solvent resistance, and very

G. Duan, M. Koehn-Serrano, Prof. A. Greiner  
Macromolecular Chemistry  
Bavarian Polymer Institute  
University of Bayreuth  
Universitätsstrasse 30, 95440 Bayreuth, Germany  
E-mail: greiner@uni-bayreuth.de

good thermal insulation. Surface-functionalized sponges made of electrospun fibers are not known. A promising polymer for the surface functionalization of sponges could be poly(vinyl pyridine), including poly(2-vinyl pyridine) (P2VP) and poly(4-vinyl pyridine) (P4VP), which can efficiently immobilize various metal nanoparticles.<sup>[15d,22]</sup>

The combination of the novel 3D sponge made from short electrospun fibers and P2VP could be an excellent carrier for AuNPs and a promising novel catalyst carrier. Highly efficient known catalyst carriers display large surface to volume ratio and require often large amount of catalysts, which is in strong contrast to spongy catalysts described in this contribution. The expectation from the spongy catalyst is that the large pore volume and combination with low surface area will allow highly efficient mass transfer of educts and products and reduce blockage of the active catalyst carrier surface by product adhesion. In order to verify this hypothesis, we have investigated spongy catalysts. The spongy catalyst made of ultraporos sponges from short electrospun fibers loaded with different amount of AuNPs was assigned here as Au-sponge. The AuNPs were immobilized in the scaffold of the sponge while the positioning of AuNPs in the sponge mimics a dispersion-like distribution. In order to challenge the new system by a sound quantitative comparison of this new system with other known catalysts systems we employed the well-documented AuNP-catalyzed reduction of *p*-nitrophenol. Surprisingly, the Au-sponge showed the highest catalytic rates in comparison to immobilized and dispersed systems at the lowest gold amount. As an additional feature the Au-sponges were reusable many times. With these features, the Au-sponges represent a novel type of catalyst paradigm combining the advantages of dispersed systems and immobilized systems.

## 2. Results & Discussion

Au-sponges with different amount of AuNPs were prepared by the following protocol:

1. Synthesis of poly(2VP-co-MABP) according to Scheme S1 (Supporting Information).
2. Fiber nonwoven preparation by electrospinning of a mixture of poly(2VP-co-MABP) and polyacrylonitrile (PAN) in dimethyl formamide (DMF).
3. Photo cross-linking of the nonwovens.
4. Hydrophilization of the nonwovens by treatment with ammonia water.
5. Loading of the nonwovens by wetting with auric acid solution of different concentrations.
6. Reduction of Au<sup>3+</sup> by treatment with sodium borohydride.
7. Purification of the nonwovens by washing with water.
8. Preparation of short fibers by cutting of the AuNP-loaded nonwovens.
9. Sponge preparation by freeze-drying of short nanofiber dispersions.

Details of the experimental procedure are available in the Supporting Information.

The electrospun fibers were uniform with an average diameter of 3.04  $\mu\text{m}$  and showed a fractal surface (Figure 1a,b). The structured surface of the fibers could be due to phase separation during electrospinning and fast evaporation of solvents as previously reported for MMA/P4VP24 and other blends in relevant publications.<sup>[23]</sup> The sponges showed typical hierarchical pore structures with big pores (50–400  $\mu\text{m}$ ) due to the drying of solvent crystals during freeze-drying and small pores (tens micrometers) between the short fibers (Figure 1c). All the sponges possessed high porosity of >99%, which was agreed with the porosity value of the sponges from the same preparation method.<sup>[21a,b]</sup> Figure 1d shows the sponges with different amounts of AuNPs. The sponges used for the catalysis reactions had a diameter of 1.6 cm, a thickness of 0.5 cm, and a density of 7  $\text{mg cm}^{-3}$ . As expected, the color of the sponges became darker with increasing amount of AuNPs. The presence of AuNPs on the fibers was further confirmed by energy dispersive X-ray spectroscopy (EDX), as shown in Figure 1e. One cyclic compression test was performed to show the mechanical stability of the Au-sponge. As shown in Figure 1f, the Au-sponge3.56 exhibited a compression strength of 0.55 kPa at 50% compression rate and there was blank area between the first and second compression curves. This area could be attributed to the energy loss during the cyclic test. Although the energy loss existed, the compression strength could come back to the same value as the first compression, which indicated the mechanical stability and compressive reversibility of the sponges. These excellent mechanical properties provided the possibility of the reuse of the sponges in further catalyst application.

Transmission electron microscope (TEM) images were used to characterize the morphology of AuNPs and the distribution of AuNPs on the fibers. Nonaggregated AuNPs were observed on the surface as proved by Figure 2a–d. The diameter of AuNPs was in the range of 1–13 nm with an average particle size of  $5.7 \pm 0.8$  nm (Figure 2e). The overall amount of Au in the sponges was analyzed by thermal gravity analyzer (TGA). The sponges with different amount of Au were assigned according to the amount of gold found in the sponge.

The catalytic performance of Au-sponges was investigated by reduction of 4-nitrophenol to 4-aminophenol with NaBH<sub>4</sub>. The reaction progress was monitored by time-dependent UV–vis spectrometry. The characteristic peak of 4-nitrophenol was at  $\approx 400$  nm, which could be assigned to the 4-nitrophenolate ions.<sup>[12]</sup> The reaction mixture without catalyst exhibited no color change even after few days. In comparison, the addition of the catalyst Au-sponge0.29 to the solution caused color fading from

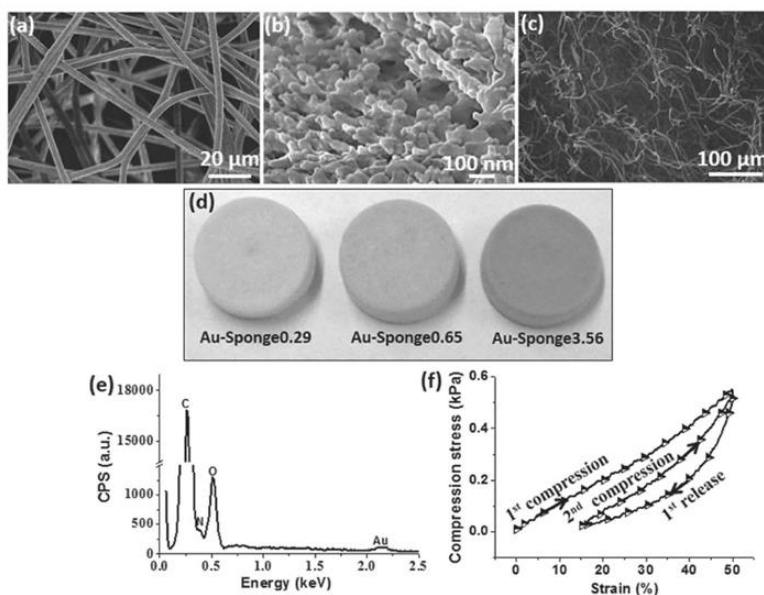


**Figure 1.** a,b) Scanning electron microscope (SEM) images of as-spun fibers; c) SEM images of the pore structure of the Au-sponge3.56 with AuNPs on the fibers; d) photograph of the sponges with different amount of AuNPs; e) EDX spectra of AuNP-immobilized fibers; and f) cyclic compression test of Au-sponge3.56.

yellow to faint yellow (inset of Figure 3a) in combination with a decrease of the intensity of the absorption peak at 400 nm to 0.43 after 32 min (Figure 3a). When the amount of AuNPs was increased to 0.65 wt%, the intensity of the absorption peak at 400 nm decreased to 0.22 in the same

time (32 min) (Figure 3b). This result indicates that more 4-nitrophenol has been reduced to 4-aminophenol by the catalyst Au-sponge0.65 than by Au-sponge0.29.

When Au-sponge3.56 was applied, after the same reaction time of 32 min, the solution became colorless (inset

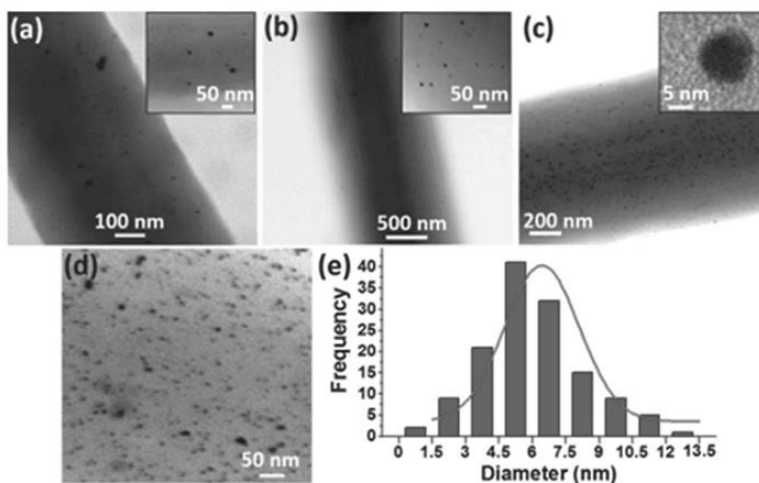


**Figure 2.** TEM images of different amounts of AuNPs immobilized on nanofibers of the sponges a) 0.29 wt%, b) 0.65 wt%, and c) 3.56 wt%. The insets of (a), (b), and (c) indicate the individual AuNP. Higher magnification of TEM image of (c) and d,e) diameter distribution of AuNPs.

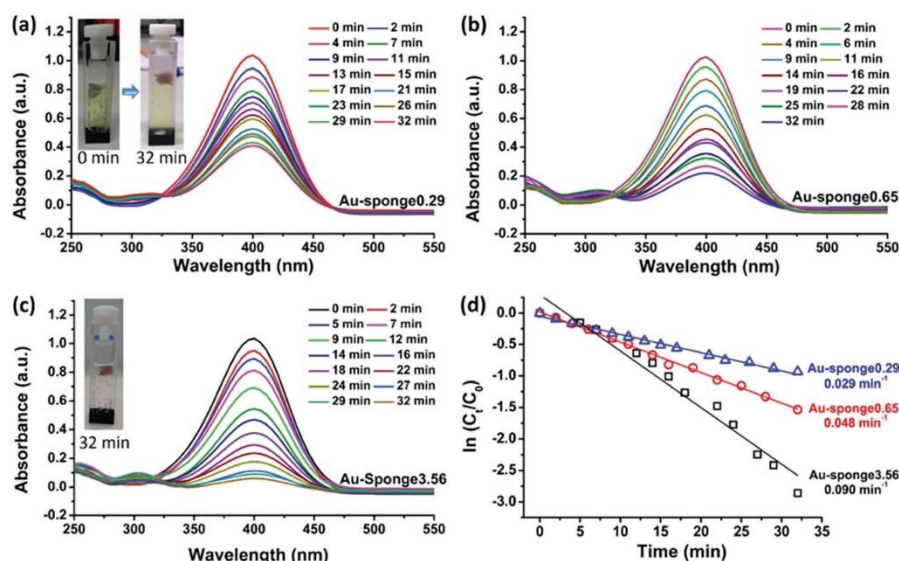


**Figure 3.** Time-dependent UV-vis absorption spectra for the reduction of 4-nitrophenol using a) Au-sponge0.29, b) Au-sponge0.65, and c) Au-sponge3.56 as catalysts, and pseudo-first-order plot of  $\ln(C_t/C_0)$  versus time and the corresponding rate constant values for the reduction of 4-nitrophenol by d) Au-sponges. The insets of (a) and (c) show the color change depending on the time and the catalysts.

of Figure 3c) and the intensity of the absorption peak at 400 nm decreased to 0.06 (Figure 3), suggesting that most of the 4-nitrophenol has been reduced to 4-aminophenol. During the experiment, the concentration of  $\text{NaBH}_4$  was much larger than the concentration of 4-nitrophenol, thus the reduction rate could be considered independent of the concentration of  $\text{NaBH}_4$ . Therefore, the evaluation of the catalytic rate of the reduction of 4-nitrophenol by Au-sponges could be applied by a pseudo-first-order with regard to the concentration of 4-nitrophenol and the reaction kinetics can be described by equation<sup>[12,24]</sup>

$$-\ln \frac{C_t}{C_0} = -\ln \frac{A_t}{A_0} = Kt \quad (1)$$

where  $K$  is the reaction rate constant,  $t$  is the reaction time,  $C_t$  and  $C_0$  are the concentration of 4-nitrophenol at time  $t$  and at the initial time 0 min, respectively, and  $A_t$  and  $A_0$  are the intensity of the absorption peak at 400 nm at time  $t$  and at the initial time 0 min, respectively. Figure 3d presents the plot of  $\ln(C_t/C_0)$  versus time. As expected, the  $\ln(C_t/C_0)$  showed a linear correlation to the reaction time  $t$  and the rate constant  $K$  could be obtained from the absolute value of the slope. As the amount of the AuNPs in the sponges increased, the kinetic rate constant  $K$  increased. The  $K$  values were 0.029, 0.048, and 0.090 min<sup>-1</sup> for the reduction catalyzed by Au-sponge0.29, Au-sponge0.65, and Au-sponge3.56, respectively. The amount of AuNPs has a significant effect on the rate constant for the

reduction of 4-nitrophenol.<sup>[24a]</sup> The excellent catalytic performance of the Au-sponges related to immobilized and dispersed systems is shown in the Ashby plot of the normalized rate constant ( $K_{\text{nor}}$ , min<sup>-1</sup> mg<sup>-1</sup>) versus the amount of AuNPs (Figure 4). In general, systems reported in the literature with dispersed AuNPs showed significantly higher reaction rates compared to systems with immobilized AuNPs. In contrast, Au-sponge with immobilized AuNPs showed even higher rate constant compared to systems with dispersed AuNPs and more than 100% more efficiency than any system with immobilized AuNPs. Recently, Zhang et al. reported an Au/PEI/GO composite sponge with AuNPs immobilized on graphene oxide (GO) for catalyzing 4-nitrophenol.<sup>[25]</sup> The Au/PEI/GO composite sponge showed a very high  $K$  value of  $9.87 \times 10^{-3} \text{ s}^{-1}$  ( $= 0.5922 \text{ min}^{-1}$ ), which was achieved on the base of high amount (0.68 mg, 13.6 wt%) of AuNPs in the sponges.<sup>[25]</sup> If considering the effect of the amount of AuNPs on the  $K$  value, then the  $K_{\text{nor}}$  was 0.871 min<sup>-1</sup> mg<sup>-1</sup>, which was much smaller than our Au-sponge catalysts. The possible reason could be the much more gold atoms on the surface of the AuNPs in this work than in Zhang's report due to the particle size effect.

The immobilization of the AuNPs in the sponge as carrier allowed their reusability, which is hard to achieve with dispersed AuNPs. The reusability of the Au-sponges was validated by removal from the reaction system, rinsing with distilled water, and drying. The cleaned

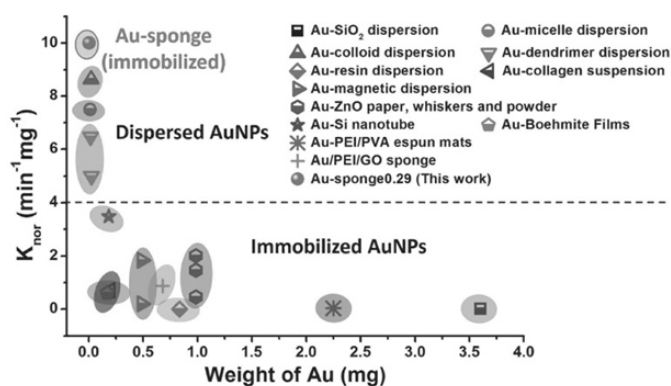


Figure 4. Ashby plot of the normalized rate constant ( $K_{\text{norm}}$ ) versus amount (mg) of Au on the supports. Au- $\text{SiO}_2$  dispersion,<sup>[24b]</sup> Au-micelle dispersion,<sup>[6a]</sup> Au-colloid dispersion,<sup>[24c]</sup> Au-dendrimer dispersion,<sup>[7,26]</sup> Au-resin dispersion,<sup>[24a]</sup> Au-collagen suspension,<sup>[12]</sup> Au-magnetic dispersion,<sup>[26]</sup> Au-ZnO paper, whiskers and powder,<sup>[27]</sup> Au-Si nanotube,<sup>[28]</sup> Au-boehmite films,<sup>[29]</sup> Au-PEI/PVA mats,<sup>[35c]</sup> and Au-PEI/GO.<sup>[35]</sup>

Au-sponges were reused up to five cycles for new reductions. The experiments with Au-sponge3.56 as catalyst showed that the rate constant decreased only slightly from  $0.090 \text{ min}^{-1}$  to  $0.072 \text{ min}^{-1}$ , after five-time use (Figure S1, Supporting Information). The slightly decrease of the rate constant might be due to the leakage of AuNPs from the sponges.

### 3. Conclusion

In conclusion, AuNPs immobilized in fibrous sponges, named here Au-sponge, represent a new class of catalyst carrier systems which display surprisingly high efficiencies with immobilized AuNPs. The rate constants are in the top range of catalyst systems with dispersed AuNPs. We believe that the excellent efficiency of Au-sponge is due to the quasi-dispersion-like immobilization of AuNPs in sponges in combination with very high pore volumes of about  $150 \text{ mL g}^{-1}$ . This large pore volume allows effective mass transfer of the reaction solution to the catalytic sites (AuNPs) and thereby accounts for the high rate constants. The novelty of this catalyst paradigm is the exploitation of the large pore volume while other catalyst systems make use of large surface area. Quite obviously the mass transfer of reagents plays a much larger role in catalysts efficiency than expected, which could balance easily humble amount of available catalysts at smaller surface area. As additional feature the Au-sponge catalysts could be reused manifold times. The preparation of the Au-sponges is highly versatile and straightforward and could therefore be transferred into many other nanoparticle-based catalyst systems with better catalyst

efficiency. Therefore, the paradigm of immobilization of catalytically active nanoparticles in fibrous sponges with large pore volumes represents a novel and general concept for a novel family of sustainable catalysts. This new finding will open completely new directions for novel catalyst carrier systems which could exploit the huge potential of electrospinning in combination with the superior efficiency of this new fibrous sponge-type system.

### Supporting Information

Supporting Information is available from the Wiley Online Library or from the author.

Acknowledgements: The authors acknowledge financial support from the Deutsche Forschungsgemeinschaft (DFG, SFB 840).

Received: August 18, 2016; Revised: September 11, 2016; Published online: November 23, 2016; DOI: 10.1002/marc.201600511

Keywords: catalysis; electrospinning; fibrous sponge; gold nanoparticle; reaction rate

- a) J. A. Lopez-Sanchez, N. Dimitratos, C. Hammond, G. L. Brett, L. Kesavan, S. White, P. Miedziak, R. Tiruvalam, R. L. Jenkins, A. F. Carley, D. Knight, C. J. Kiely, G. J. Hutchings, *Nat. Chem.* **2011**, *3*, 551; b) J.-W. Lee, T. Mayer-Gall, K. Opwis, C. E. Song, J. S. Gutmann, B. List, *Science* **2013**, *341*, 1225.
- a) N. Lopez, T. V. W. Janssens, B. S. Clausen, Y. Xu, M. Mavrikakis, T. Bligaard, J. K. Nørskov, *J. Catal.* **2004**, *223*, 232; b) A. Abad, A. Corma, H. Garcia, *Chem.—Eur. J.* **2008**, *14*, 212.
- a) S. Schimpf, M. Lucas, C. Mohr, U. Rodemerck, A. Brückner, J. Radnik, H. Hofmeister, P. Claus, *Catal. Today* **2002**, *72*, 63; b) P. Claus, A. Brückner, C. Mohr, H. Hofmeister, *J. Am. Chem. Soc.* **2000**, *122*, 11430.
- a) A. Primo, F. Quignard, *Chem. Commun.* **2010**, *46*, 5593; b) J. Han, Y. Liu, R. Guo, *J. Am. Chem. Soc.* **2009**, *131*, 2060.
- P. Sangpour, F. Hashemi, A. Z. Moshfegh, *J. Phys. Chem. C* **2010**, *114*, 13955.
- a) Y. Wang, G. Wei, W. Zhang, X. Jiang, P. Zheng, L. Shi, A. Dong, *J. Mol. Catal. A: Chem.* **2007**, *266*, 233; b) T. F. Jaramillo, S. H. Baeck, B. R. Cuenya, E. W. McFarland, *J. Am. Chem. Soc.* **2003**, *125*, 7148.
- K. Hayakawa, T. Yoshimura, K. Esumi, *Langmuir* **2003**, *19*, 5517.
- H. Tsunoyama, H. Sakurai, N. Ichikuni, Y. Negishi, T. Tsukuda, *Langmuir* **2004**, *20*, 11293.
- a) P. X. Huang, F. Wu, B. L. Zhu, X. P. Gao, H. Y. Zhu, T. Y. Yan, W. P. Huang, S. H. Wu, D. Y. Song, *J. Phys. Chem. B* **2005**, *109*, 19169; b) X. Liu, M.-H. Liu, Y.-C. Luo, C.-Y. Mou, S. D. Lin,

- H. Cheng, J.-M. Chen, J.-F. Lee, T.-S. Lin, *J. Am. Chem. Soc.* **2012**, *134*, 10251.
- [10] H. Wang, Z. Dong, C. Na, *ACS Sustainable Chem. Eng.* **2013**, *1*, 746.
- [11] M.-L. Wang, T.-T. Jiang, Y. Lu, H.-J. Liu, Y. Chen, *J. Mater. Chem. A* **2013**, *1*, 5923.
- [12] H. Wu, X. Huang, M. Gao, X. Liao, B. Shi, *Green Chem.* **2011**, *13*, 651.
- [13] R. Arup Kumer, P. Sung Young, I. Insik, *Nanotechnology* **2015**, *26*, 105601.
- [14] F. Mitschang, H. Schmalz, S. Agarwal, A. Greiner, *Angew. Chem. Int. Ed.* **2014**, *53*, 4972.
- [15] a) X. Liu, M. Li, G. Han, J. Dong, *Electrochim. Acta* **2010**, *55*, 2983; b) D. Hu, Y. Huang, H. Liu, H. Wang, S. Wang, M. Shen, M. Zhu, X. Shi, *J. Mater. Chem. A* **2014**, *2*, 2323; c) B. Guo, S. Zhao, G. Han, L. Zhang, *Electrochim. Acta* **2008**, *53*, 5174; d) H. Dong, E. Fey, A. Gandelman, W. E. Jones, *Chem. Mater.* **2006**, *18*, 2008; e) X. Fang, H. Ma, S. Xiao, M. Shen, R. Guo, X. Cao, X. Shi, *J. Mater. Chem.* **2011**, *21*, 4493.
- [16] a) Z.-S. Wu, S. Yang, Y. Sun, K. Parvez, X. Feng, K. Müllen, *J. Am. Chem. Soc.* **2012**, *134*, 9082; b) Y. Xue, D. Yu, L. Dai, R. Wang, D. Li, A. Roy, F. Lu, H. Chen, Y. Liu, J. Qu, *Phys. Chem. Chem. Phys.* **2013**, *15*, 12220.
- [17] H. Ji, L. Zhang, M. T. Pettes, H. Li, S. Chen, L. Shi, R. Piner, R. S. Ruoff, *Nano Lett.* **2012**, *12*, 2446.
- [18] N. Brun, S. A. Wohlgemuth, P. Osiceanu, M. M. Titirici, *Green Chem.* **2013**, *15*, 2514.
- [19] a) R. Du, N. Zhang, J. Zhu, Y. Wang, C. Xu, Y. Hu, N. Mao, H. Xu, W. Duan, L. Zhuang, L. Qu, Y. Hou, J. Zhang, *Small* **2015**, *11*, 3903; b) G. Yang, W. Choi, X. Pu, C. Yu, *Energy Environ. Sci.* **2015**, *8*, 1799.
- [20] H.-W. Liang, Z.-Y. Wu, L.-F. Chen, C. Li, S.-H. Yu, *Nano Energy* **2015**, *11*, 366.
- [21] a) Y. Si, J. Yu, X. Tang, J. Ge, B. Ding, *Nat. Commun.* **2014**, *5*, 5802; b) G. Duan, S. Jiang, V. Jérôme, J. H. Wendorff, A. Fathi, J. Uhm, V. Altstadt, M. Herling, J. Breu, R. Freitag, S. Agarwal, A. Greiner, *Adv. Funct. Mater.* **2015**, *25*, 2850; c) Y. Si, Q. Fu, X. Wang, J. Zhu, J. Yu, G. Sun, B. Ding, *ACS Nano* **2015**, *9*, 3791; d) T. Xu, J. M. Miszuk, Y. Zhao, H. Sun, H. Fong, *Adv. Healthcare Mater.* **2015**, *4*, 2238; e) G. Duan, S. Jiang, T. Moss, S. Agarwal, A. Greiner, *Polym. Chem.* **2016**, *7*, 2759.
- [22] S. Malynych, I. Luzinov, G. Chumanov, *J. Phys. Chem. B* **2002**, *106*, 1280.
- [23] a) M. Bognitzki, W. Czado, T. Frese, A. Schaper, M. Hellwig, M. Steinhart, A. Greiner, J. H. Wendorff, *Adv. Mater.* **2001**, *13*, 70; b) M. Bognitzki, T. Frese, M. Steinhart, A. Greiner, J. H. Wendorff, A. Schaper, M. Hellwig, *Polym. Eng. Sci.* **2001**, *41*, 982.
- [24] a) S. Panigrahi, S. Basu, S. Praharaj, S. Pande, S. Jana, A. Pal, S. K. Ghosh, T. Pal, *J. Phys. Chem. C* **2007**, *111*, 4596; b) Y. Peng, W. Leng, B. Dong, R. Ge, H. Duan, Y. a. Gao, *Chin. J. Catal.* **2015**, *36*, 1117; c) N. Pradhan, A. Pal, T. Pal, *Colloids Surf., A* **2002**, *196*, 247.
- [25] M. Zhang, X. Lu, H.-Y. Wang, X. Liu, Y. Qin, P. Zhang, Z. Guo, *RSC Adv.* **2016**, *6*, 35945.
- [26] Y.-C. Chang, D.-H. Chen, *J. Hazard. Mater.* **2009**, *165*, 664.
- [27] H. Koga, T. Kitaoka, *Chem. Eng. J.* **2011**, *168*, 420.
- [28] Z. Zhang, C. Shao, P. Zou, P. Zhang, M. Zhang, J. Mu, Z. Guo, X. Li, C. Wang, Y. Liu, *Chem. Commun.* **2011**, *47*, 3906.
- [29] D. Jana, A. Dandapat, G. De, *Langmuir* **2010**, *26*, 12177.

Copyright WILEY-VCH Verlag GmbH & Co. KGaA, 69469 Weinheim, Germany, 2016.



## Supporting Information

for *Macromol. Rapid Commun.*, DOI: 10.1002/marc.201600511

Highly Efficient Reusable Sponge-Type Catalyst Carriers  
Based on Short Electrospun Fibers

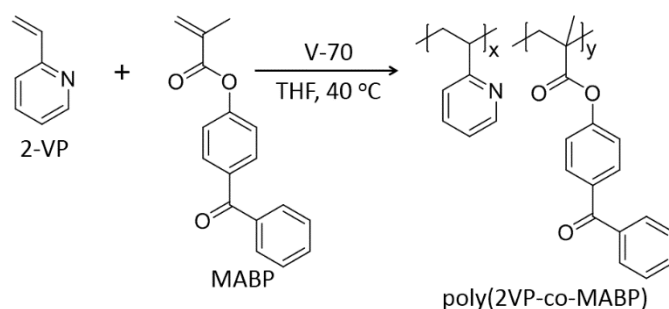
Gaigai Duan, Melissa Koehn-Serrano, Andreas Greiner\*

## Materials

2-vinyl pyridine (2-VP, 97%, Aldrich) was distilled under reduced pressure prior to use. Polyacrylonitrile (PAN,  $M_w=150,000$ , Polyscience Inc), 4-nitrophenol ( $\geq 99.5\%$ , Aldrich), 2, 2'-azobis(4-methoxy-2,4-dimethyl valeronitrile) (V-70, Wako), and 4-nitrophenol ( $\geq 99\%$ , Aldrich) were used as received. Auric acid (1 mM) and sodium borohydride (0.15 M and 0.10 M) were prepared from tetrachloroaurate trihydrate ( $\text{HAuCl}_4 \cdot 3\text{H}_2\text{O}$ , 50% Au basis, (Aldrich) and sodium borohydride ( $\geq 99\%$ , FLUKA). Poly (methylacrylate-co-methylmethacrylate-co-4methacryloyloxybenzophenone) (poly (MA-MMA-MABP)) and 4-methacryloyloxybenzo-phenone (MABP) was synthesized according to our previous report.<sup>[1]</sup>

## Polymer synthesis and electrospinning

Poly(2VP-co-MABP) was synthesized by free radical polymerization of 2-VP (15 ml) and MABP (1.84 g) in tetrahydrofuran (THF, 45 ml) with an initiator (V-70) (0.12g) at 39°C for 18 h in argon (**Scheme 1**). The resulting polymer solution was precipitated in cyclohexane. After filtration, the light yellow powder was dried at room temperature for 48 h. The yield was 73%. The molecular weight  $M_w$  and  $M_n$  was 5800 and 4600, respectively, and the amount of MABP was 9 mol% in poly(2VP-co-MABP) as determined by  $^1\text{H}$  NMR.



**Scheme S1.** Synthesis of poly (2VP-co-MABP).

The electrospinning solution was prepared by dissolution of 0.42 g of poly(2VP-co-MABP), 1.27 g of poly (MA-MMA-MABP), and 0.21 g of PAN in a solvent mixture of 1.83 g of DMF, 2.00 g of DMSO, and 0.56 g of acetone. The electrospinning was performed by applying high voltage of 20 kV, flow rate of

0.4 mL/h, and collecting distance of 13 cm between the two electrodes. The electrospun nanofiber nonwovens were collected on an aluminum foil and cross-linked under UV light (UV lamp 250 GS) for 5 h.

### Sponge supported AuNPs

Nanofiber nonwovens with different amount of Au were prepared by controlling the mass of nanofiber nonwovens and the volume of auric acid (1 mM) (**Table S1**). The nanofiber nonwovens were first wetted by ammonia water (25 wt%) to increase the hydrophilicity of the nanofibers. Then different amounts of auric acid (1 mM) were added to the nonwovens and reduced by 2 mL of sodium borohydride (0.15 M) for 3 min. After the reduction, the mats supported with AuNPs were washed with water for several times in order to remove the residual sodium borohydride. The nanofiber nonwovens with AuNPs were cut into short fibers in dioxane by a mixer rotating at 5000 rpm for 35 s and then dried by freeze-drying. 7 mg of the above short fibers with an average length of  $650 \pm 218 \mu\text{m}$  were re-dispersed in 1.40 mL of dioxane. The dispersions were frozen at  $-20^\circ\text{C}$  and then freeze-dried to yield the sponges with different amounts of AuNPs as determined by thermogravimetric (TGA) analysis. The sponges were designated as Au-sponge0.29, Au-sponge0.65, and Au-sponge3.56, respectively with 0.29, 0.65, and 3.56 wt% AuNPs.

**Table S1.** Summary of the composition of sponges.

Sponge	Fiber mat (mg)	Auric acid (1 mM) (mL)	Au (wt%)
A	16.8	0.33	0.29
B	14.0	0.56	0.65
C	11.0	2.20	3.56

### Catalysis

The performance of sponge-based nanoparticle catalyst was characterized by a typical reduction reaction of 4-nitrophenol. 2 ml of sodium borohydride (0.1 M) and 300  $\mu\text{l}$  of 4-nitrophenol (3.4 mg/50 ml) were put in a 10 mm quartz cuvette which has a magnetic stirrer at the bottom for UV-vis measurement. The stirring

speed was 300 rpm. 1.0 mg of the above sponges with different AuNP loadings were put in the holder for the sponges. At different time intervals, the reaction progress was monitored by UV-vis spectroscopy.

### Characterization

The molecular weight of poly (2VP-MABP) was measured by gel permeation chromatography (GPC) using THF as eluent and the amounts of MABP in the polymer were calculated from  $^1\text{H}$  NMR (Bruker 300 MHz NMR) with deuterated chloroform as solvent. A scanning electron microscope (SEM, Zeiss Leo 1530), equipped with an EDX detector, and a transmission electron microscope (TEM, Zeiss LEO 922 OMEGA) were used to observe the morphology of sponge and AuNPs. Thermogravimetric analysis (TGA) was performed on a Netzsch TG 209 F1Libra under  $\text{N}_2$  with a heating rate of  $10^\circ\text{C} / \text{min}$  from 25 to  $800^\circ\text{C}$ . The weight of the samples was measured by OHAUS Discovery balance with a readability of 0.01 mg. Time-dependent reduction of 4-nitrophenol was performed on a UV-vis spectrometer (V-630, JASCO) with a scanning range of 550-250 nm.

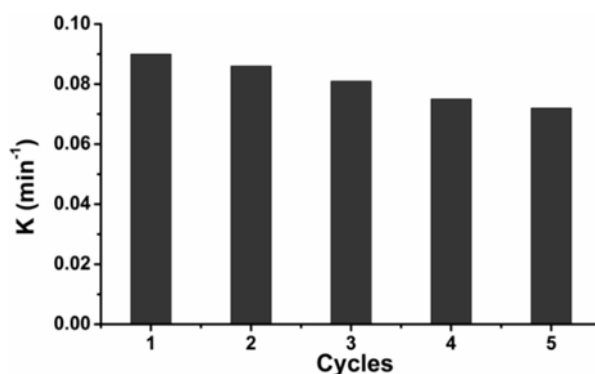


**Figure S1.** Rate constant values ( $k$ ) of the reduction in five cycles using Au-sponge3.56 as catalyst.

### References

1. G. Duan, S. Jiang, V. Jérôme, J. H. Wendorff, A. Fathi, J. Uhm, V. Altstädt, M. Herling, J. Brey, R. Freitag, S. Agarwal, A. Greiner, *Adv. Funct. Mater.* **2015**, *25*, 2850-2856.

### 3.4 Exploration of Macroporous Polymeric Sponges As Drug Carriers

**Gaigai Duan**, Amir Reza Bagheri, Shaohua Jiang, Jacob Golenser, Seema Agarwal, Andreas Greiner. Exploration of Macroporous Polymeric Sponges As Drug Carriers. *Biomacromolecules*. **2017**; DOI: 10.1021/acs.biomac.7b00852.



RightsLink®

Home

Create Account

Help



ACS Publications  
Most Trusted. Most Cited. Most Read.

**Title:** Exploration of macroporous polymeric sponges as drug carriers

**Author:** Gaigai Duan, Amir R Reza Bagheri, Shaohua Jiang, et al

**Publication:** Biomacromolecules

**Publisher:** American Chemical Society

**Date:** Aug 1, 2017

Copyright © 2017, American Chemical Society

LOGIN

If you're a [copyright.com](#) user, you can login to RightsLink using your copyright.com credentials. Already a [RightsLink](#) user or want to [learn more?](#)

#### PERMISSION/LICENSE IS GRANTED FOR YOUR ORDER AT NO CHARGE

This type of permission/license, instead of the standard Terms & Conditions, is sent to you because no fee is being charged for your order. Please note the following:

- Permission is granted for your request in both print and electronic formats, and translations.
- If figures and/or tables were requested, they may be adapted or used in part.
- Please print this page for your records and send a copy of it to your publisher/graduate school.
- Appropriate credit for the requested material should be given as follows: "Reprinted (adapted) with permission from (COMPLETE REFERENCE CITATION). Copyright (YEAR) American Chemical Society." Insert appropriate information in place of the capitalized words.
- One-time permission is granted only for the use specified in your request. No additional uses are granted (such as derivative works or other editions). For any other uses, please submit a new request.

## Exploration of Macroporous Polymeric Sponges As Drug Carriers

Gaigai Duan,<sup>†</sup> Amir Reza Bagheri,<sup>†</sup> Shaohua Jiang,<sup>†,‡</sup> Jacob Golenser,<sup>§</sup> Seema Agarwal,<sup>†</sup> and Andreas Greiner<sup>\*,†</sup>

<sup>†</sup>Macromolecular Chemistry, Bavarian Polymer Institute, University of Bayreuth, Universitätsstrasse 30, 95440 Bayreuth, Germany

<sup>§</sup>Department of Microbiology and Molecular Genetics, The Kuvim Centre for the Study of Infectious and Tropical Diseases, The Hebrew University of Jerusalem, Jerusalem, Israel

**ABSTRACT:** Achieving high drug loading capacity and controlling drug delivery are two main challenges related to drug carriers. In this study, polymeric macroporous sponges with very high pore volume and large porosity are introduced as a new-type of drug carrier. Due to the high pore volume (285 and 166 cm<sup>3</sup>/g for the sponges with densities of 3.5 and 6.0 mg/cm<sup>3</sup>, respectively), the sponges exhibit very high drug loading capacities with average values of 1870 ± 114 and 2697 ± 73 mg/g in the present study, which is much higher than the meso and microporous drug carriers (<1500 mg/g). In order to control the release profiles, an additional poly(*p*-xylylene) (PPX) coating was deposited by chemical vapor deposition on the drug loaded sponge. Consequently, Artemisone (ART) release in the aqueous medium could be retarded, depending on the density of the sponge and the thickness of the coating. In future, the new 3D polymeric sponges would be highly beneficial as drug carriers for the programmed release of drugs for treatment of chronic diseases.



### INTRODUCTION

Porous materials have attracted a great deal of attention due to their low density, high surface area, and large porosity and have been widely applied for tissue engineering, catalyst carrier, oil/water separation, gas storage/separation, sensor, and drug release.<sup>1–6</sup> Numerous research interests are focused on using meso and microporous materials as drug carriers.<sup>7–9</sup> The incorporation of the drug in such carriers is mainly carried out by soaking a concentrated drug solution, followed by drying. Therefore, the ordered accessible pore structure, the high surface area, and the high porosity are essential for optimum loading and controlled release. Mesoporous silica (functionalized and nonfunctionalized) and metal–organic frameworks are the most common porous drug carriers. The large surface area leads to the high drug adsorption, which can be stored and released from meso and micropores on the surface or in bulk. The drug loading capacity of mesoporous silica is less than 50 wt %, which can be increased to some extent by functionalization.<sup>10</sup> The metal–organic frameworks show relatively higher drug-loading capacity (as high as 150 wt %) due to the large surface area.<sup>11</sup> The drug loading capacity is of major importance for highly efficient drug-carrier systems next to the controlled and targeted release. In the past decade, two-dimensional electrospun polymeric porous nonwovens have emerged as another option of porous drug carrier.<sup>12–15</sup> Controllable drug release could be achieved by electrospun nonwovens; however, the drug-loading capacity was relatively low.

Recently, a novel class of polymeric three-dimensional (3D) sponges made from short electrospun fibers have attracted growing interest. These fibrous sponges have potential

applications in cell culturing, liquid separation, catalytic reactions, sound absorbing, and electromagnetism insulating/shielding due to their excellent properties like very low density (<10 mg/cm<sup>3</sup>), large pore volume (150 cm<sup>3</sup>/g), mechanical stability, and very high porosity (>99%).<sup>16–19</sup> The capacity of these sponges for the uptake of liquids was found to be as high as 100× the mass of the sponge itself.<sup>20</sup> The sponges have a hierarchical order of the macropores with a bimodal distribution of big pores (300–430 μm) formed by the sublimation of solvent crystals and smaller pores (10–30 μm) formed by the interconnection of the short fibers. Such sponges could be an ideal macroporous carrier for drugs, with high loading and intrinsic mechanical compressibility and multiple potential uses.<sup>17</sup> This would allow implantation of the drug-loaded sponge.

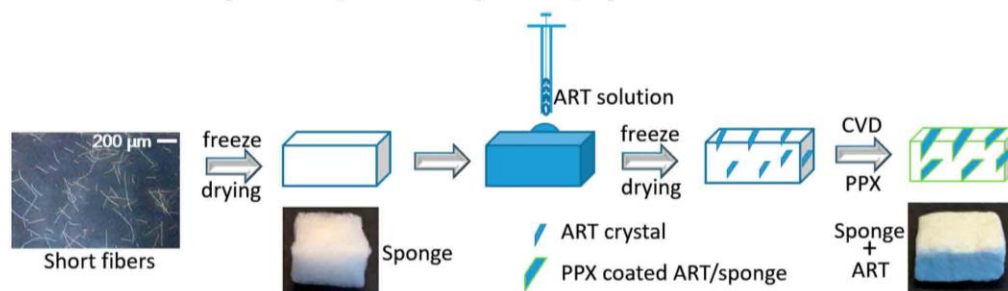
Here, we explored whether such 3D-polymeric macroporous sponges could serve as a novel drug carrier with very high drug-loading capacity, despite very low surface area (1 m<sup>2</sup>/g) due to the extremely large pore volume (>150 cm<sup>3</sup>/g). For comparison, the pore volume of mesostructured conventional drug carrier is only about 2 cm<sup>3</sup>/g. Most of the existing drug delivery structures (DDS) have low drug-loading content, causing extra toxicity and burden on patients due to the need to excrete carrier materials. With this in mind, emergence and fabrication of high drug-loading carriers may not provide the ultimate answer, but present a promising alternative approach

Received: June 16, 2017

Revised: August 15, 2017

Published: August 18, 2017

Scheme 1. Schematic Drawing for the Preparation of Drug Loaded Sponges



to solve these problems, because of the reduced use of carrier materials.

In order to probe potential applications, we used Artemisone (ART) as an artemisinin model drug due to its high relevance for antimalarial therapy.<sup>21,22</sup> Artemisinins are considered as the first line drugs against malaria. ART is an attractive drug because, in comparison to current artemisinins, it is not neurotoxic.<sup>23,24</sup> This is essential for the treatment of cerebral malaria, the most profound symptom of malaria. ART has an improved pharmacokinetics in comparison with other artemisinins.<sup>23,24</sup> ART was found to be highly effective in culture against *Plasmodium falciparum*, the causative agent of CM,<sup>21</sup> and in vivo against murine CM induced by *P. berghei* ANKA<sup>25</sup> and against *P. falciparum* in monkeys.<sup>26</sup> Also, ART can cure *Toxoplasma gondii*,<sup>27</sup> *Neospora caninum*,<sup>28</sup> and *Schistosoma mansoni*<sup>29</sup> in animal models. ART also had an anticancer effect.<sup>30</sup> However, being a hydrophobic compound, it is difficult to use it unless dissolved in DMSO, and for these chronic diseases there is a need to apply the drug in repeated injections during several days.<sup>25–28,31</sup> In order to improve the treatment, ART release rate from the sponges was tailored by an extra coating of biocompatible poly(*p*-xylylene) (PPX) through conformal chemical vapor deposition (CVD). The advantage of the CVD coating of the sponges by PPX is that it hardly reduces the porosity of the sponges. Drug combinations of artemisinins and other antimalarials have been suggested to reduce side effects (by reducing individual drug concentrations) and prevent induction of resistance.<sup>31</sup> Thus, controlled release of drug combinations using our new system will be investigated at a later stage.

## EXPERIMENTAL SECTION

**Sponge Preparation.** The macroporous sponges were prepared as reported previously.<sup>19,32</sup> In brief, poly(MA-co-MMA-MABP) was made in dimethyl sulfoxide (DMSO, Fisher Chemical, 99.99%) at 70 °C for 5 h from methyl methacrylate (13.5 mL, MMA, Aldrich, 99%), methyl acrylate (17.3 mL, MA, Aldrich, 99%), and 4-methacryloyloxybenzophenone (4.6810 g, MABP) using 2'-Azobis (isobutyronitrile) (0.2930 g, AIBN, Fluka, 98%, purified by recrystallization from methanol) as radical initiator. Then 26.20 g of poly(MA-co-MMA-MABP) solution (20 wt %) in DMSO, 2 g of polyacrylonitrile (PAN,  $M_w = 150000$ , Sigma-Aldrich) solution (13.2 wt %) in dimethylformamide (DMF, Fisher Chemical, 99.99%), and 2.68 g of acetone were mixed for electrospinning by use of a voltage of 9 kV, a flow rate of 1.5 mL/h, and a humidity of 40–60%. The obtained fibers were dried (40 °C, 24 h, a vacuum oven), cross-linked by UV light (UV lamp 250GS, 5 h), and processed into short fiber dispersions in dioxane (3.1 and 5.5 mg/mL) using a mixer (5000 rpm, 45 s). The short fibers in the dispersion possessed an average fiber diameter of  $1.1 \pm 0.2 \mu\text{m}$  and an average length of  $320 \pm 105 \mu\text{m}$ . The

dispersions were transferred in cylindrical glass tubes and freeze-dried (0.03 mbar, 48 h). The resultant sponges from 3.1 and 5.4 mg/mL dispersions possessed densities of 3.5 and 6.0 mg/cm<sup>3</sup> and were denoted as SG3.5 and SG6, respectively.

**Drug Loading.** ART (CIPLA, India) was dissolved in *tert*-butanol in concentrations of 14 and 25 mg/mL. Then, 1 mL of drug solution was filled in a syringe and slowly dropped onto the pre-cut SG3.5 and SG6 (10 × 10 × 5 mm) at room temperature ( $22 \pm 1 \text{ }^\circ\text{C}$ ) until the whole sponge was wetted by the solution. Drug-wetted sponges were put in liquid nitrogen for freezing and drying in vacuum for 24 h by a freeze-dryer. The amount of ART in the sponge was determined by a high precision analytical balance with a readability of 0.01 mg.

**PPX Coating.** The ART-loaded sponges were coated with PPX by CVD, as reported previously.<sup>19</sup> By controlling the amount of the monomer ([2.2] paracyclophane), the sponge SG6 with different PPX coating thicknesses of 88, 150, 423, and 1000 nm were prepared, and the corresponding sponges were marked as SG6-88, SG6-150, SG6-423, and SG6-1000. For a comparison, the sponges loaded with the drug but without PPX coating were also prepared and marked as SG3.5-0 and SG6-0, respectively. A schematic drawing for the drug loading was shown in Scheme 1.

**In Vitro Drug Release.** Pieces of the ART loaded sponges were immersed in the glass vessels containing 10 mL of an aqueous medium as the drug release medium. The aqueous medium consists of 1% w/v sodium lauryl sulfate (SLS) in distilled water. The solubility of ART could be clearly increased by addition of SLS, so that we could check the drug release pattern of ART from carriers until approximately 100% drug release. Without SLS addition, complete release was not easily achievable because of the hydrophobic nature of ART. Furthermore, it is obvious that the presence of SLS could support the sink condition because of its role in reduction of surface tension in aqueous medium.<sup>15</sup> The pH of the medium was adjusted at  $7.4 \pm 0.1$  by the addition of a very little amount of sodium bicarbonate. The vessel was sealed and placed in a thermostatic incubator at  $37 \pm 0.5 \text{ }^\circ\text{C}$  and shaken at 50 rpm. After prefixed time intervals, 400  $\mu\text{L}$  of the medium was taken out, and 400  $\mu\text{L}$  fresh medium was added to the vessel. The concentration of the drug inside was determined by high-pressure liquid chromatography (HPLC) technique. The amounts of released ART from sponges were determined by comparison to standard solutions of ART. HPLC instrument was equipped with an Eclipse XDB-C18, 4.6 × 150 mm, 5  $\mu\text{m}$  column. The mixture of acetonitrile (50 v/v %), H<sub>2</sub>O (30 v/v %), and methanol (20 v/v %) was used as the mobile phase, and UV detector was adjusted at  $\lambda$ : 260 nm. The temperature of the column was adjusted to 35 °C, the flow rate of the mobile phase was 0.8 mL/min, and the injection volume was 20  $\mu\text{L}$ . All release experiments have been repeated at least three times, and the results are reported as mean data  $\pm$  standard deviation (SD).

**Characterizations.** The morphology and the distribution of sulfur element in the sponge were measured by a scanning electron microscope (SEM) equipped with Oxford 6901 EDX detector. Before measurement, the samples for the SEM were coated with 3 nm of platinum by a sputter coater 208 HR from Cressington. Sulfur element mapping to determine the ART distribution was performed by EDX.

B

DOI: 10.1021/acs.biomac.7b00852  
Biomacromolecules XXXX, XXX, XXX–XXX

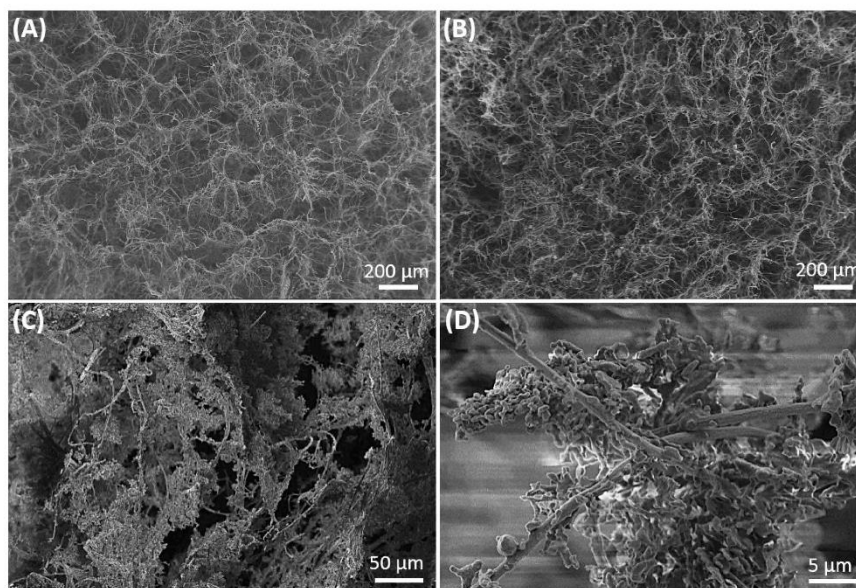


Figure 1. Cross-sectional SEM images of as-prepared sponges SG3.5 (A) and SG6 (B), and SG6 after loading with ART (C, D).

Table 1. Change of ART Loading Capacity of SG6 by Using *tert*-Butanol Solutions of ART with Concentrations of 14 and 25 mg/mL

	mass SG6 (mg)	mass SG6+drug (mg)	mass ART (mg)	ART loading capacity (mg ART/g sponge)/ART loading ratio (mass ART/mass sponge)
14 mg/mL	2.47	6.78	4.31	1745/1.75
	2.56	7.32	4.76	1896/1.90
	2.51	7.45	4.94	1968/1.97
	2.51 ± 0.05	7.18 ± 0.36	4.67 ± 0.32	1870 ± 114/1.87 ± 0.11
25 mg/mL	2.38	8.71	6.34	2664/2.66
	2.62	9.31	6.70	2557/2.56
	2.54	9.39	6.85	2697/2.70
	2.51 ± 0.12	9.14 ± 0.37	6.63 ± 0.26	2639 ± 73/2.64 ± 0.07

## RESULTS AND DISCUSSION

We report the utilization of macroporous sponges with densities of 3.5 and 6 mg/cm<sup>3</sup> (SG3.5 and SG6) as a drug carrier. The sponges displayed a bimodal pore-size distribution, including pores with a size of about 100 μm and pores of a few micrometers, between the fiber interconnections (Figure 1A,B). The porosity ( $P$ ) and specific pore volume (SPV) of the sponges could greatly influence the drug loading capacity and the drug release process<sup>10,33</sup> and can be calculated from the following equations:

$$P = \left(1 - \frac{\rho_{\text{SG}}}{\rho_{\text{bulk}}}\right) \times 100\% \quad (1)$$

$$\text{SPV} = \frac{P}{\rho_{\text{SG}} \times 10^{-3}} \quad (2)$$

where  $\rho_{\text{SG}}$  is the density of the sponge and  $\rho_{\text{bulk}} = 1.2 \text{ g/cm}^3$  is the density of the polymer in the bulk state. Both the SG3.5 and SG6 possessed high  $P$  of 99.7% and 99.5%, respectively. In comparison with the literature known microporous and mesoporous inorganic materials, the fibrous SG3.5 and SG6

in this work exhibited much higher SPV of 285 and 166 cm<sup>3</sup>/g. High ART loading was accomplished successfully with sponge SG6, which is visualized in Figure 1C,D. In contrast, the mechanical integrity of sponge SG3.5 due to its very low density was too low for the applied loading procedure. Owing to the much better mechanical stability of SG6, most of the following experiments were focused on the SG6.

In parallel with the increased concentration of the ART solution from 14 to 25 mg/mL, the ART loading amount of SG6 (2.51 mg) was changed from 4.67 to 6.63 mg, meaning that the loading capacity was increased from 1870 to 2639 mg/g (ART loading ratio increasing from 1.87 to 2.64) (Table 1). The free remaining pore volume after the ART loading is still about 99% of the original sponge volume. Although only 1% of the total volume was occupied by the drug, the drug loading capacities were still higher than the values obtained from functionalized mesoporous SiO<sub>2</sub>-based materials.<sup>10</sup>

Figure 2 shows an Ashby plot for the comparison of the ART loading capacity by our macroporous sponge, with a capacity of up to 2697 [mg ART]/[g sponge] and other drug carrier systems with different drugs. Most of the carriers using a mesoporous system showed a drug loading capacity below 1000

C

DOI: 10.1021/acs.biomac.7b00852  
Biomacromolecules XXXX, XXX, XXX–XXX

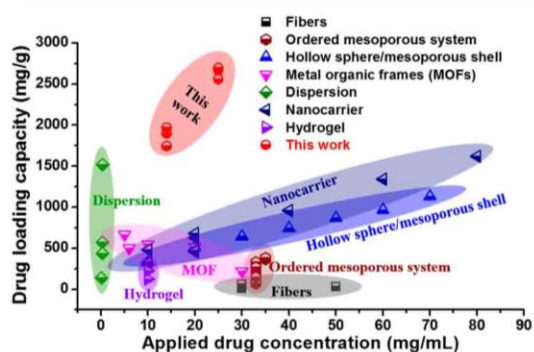


**Figure 2.** Comparison of drug loading capacity by sponges and other supports. Fibers ( $\text{TiO}_2$ ,<sup>44</sup>  $\text{SiO}_2\text{-AgNPs}$ <sup>45</sup>), ordered mesoporous system ( $\text{SiO}_2$ ,<sup>34,35</sup>  $\text{TiO}_2\text{-SiO}_2$ ,<sup>36</sup>  $\text{SiO}_2\text{-Al}_2\text{O}_3$ <sup>37</sup>), hollow sphere/mesoporous shell ( $\text{SiO}_2$ <sup>38</sup>), metal organic frames (MOF; Cr-based,<sup>39,40</sup> Zn-based,<sup>41</sup> Zr-BPYDC,<sup>42</sup> Zn-TATAT<sup>43</sup>), dispersion (nanotubes,<sup>47</sup> functionalized C-MPG1<sup>48</sup>), nanocarrier (calcium phosphate-AC and calcium phosphate-ibuprofen<sup>49</sup>), and hydrogel (alginate-g-polyAA/kaolin<sup>46</sup>).

mg/g, even when very high drug concentration was applied.<sup>34–38</sup> Another broadly used carrier system is metal organic frames (MOFs).<sup>39–43</sup> These materials yielded a drug loading capacity below 750 mg/g and the applied drug concentration below 30 mg/mL. Fibers and hydrogels were also reported as drug carriers, but their drug loading capacity was even lower, smaller than 500 mg/g.<sup>44–46</sup> Nanotubes in dispersion, serving as drug carriers, exhibited high drug loading capacity.<sup>47–49</sup> These preparations possessed a drug loading

capacity of up to 1500 mg/g when applying very low drug concentration (10–80 mg/mL). However, in comparison, our fibrous sponge carrier exhibited superior drug loading capacity.

Overall, the macroporous sponge possessed high pore volume and very high ART loading capacity. However, ART was loosely placed on the surface of the fibrous network of the sponges or just settled in the pores, which would lead to losses induced by mechanical stress and to burst release of ART during the initial release process. To improve the fixation of ART in the sponge and retard its release in a controlled fashion, we applied CVD coating of PPX with different thicknesses in the form of a conformal coating (Figure 3). The shapes of the ART crystals (Figure 3A) were still recognizable, with a PPX coating thickness of 150 nm, whereas with a PPX thickness of 423 nm, the ART crystals were hardly visible anymore (Figure 3B). These results of PPX coating lead to the retention of the high pore volume of the sponges (Figure 3A,B), which would facilitate the mass transfer of the drugs through the sponges during the release process. The EDX spectra by sulfur element scanning showed a homogeneous distribution of ART in the sponge (Figure 3C).

The porous structures of the sponge and the PPX coating play a major role in the drug release. For comparison, the drug release profile from the ART powder was also examined (Figure 4). The neat ART powder exhibited a burst release in the initial 20 min followed by a retarded release, which could be attributed to the broad size distribution (several micrometers to hundreds of micrometers) of ART crystals in the powders.<sup>15</sup> Previous reports showed that smaller particles of drugs exhibit faster dissolution than bigger ones, resulting in a quicker release.<sup>50,51</sup> Similarly, the small crystals of ART in the powder could be dissolved in the first stages of the release process. This

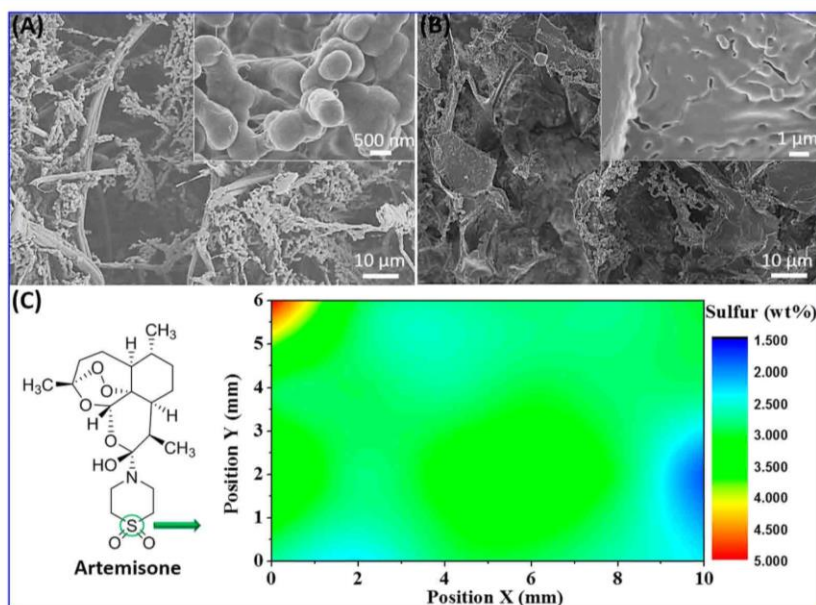


**Figure 3.** Morphology of the ART-loaded sponges (SG6) after coating with different PPX thicknesses of 150 (A) and 423 nm (B), and the corresponding EDX spectra of ART distribution in the sponges (SG6-150) by sulfur element scanning. Insets of (A) and (B) are the corresponding images with higher magnifications.

D

DOI: 10.1021/acs.biomac.7b00852  
Biomacromolecules XXXX, XXX, XXX–XXX

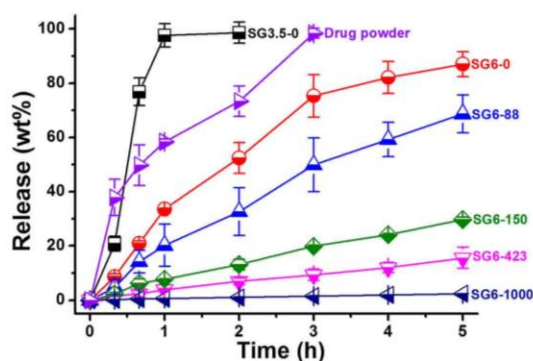


Figure 4. In vitro ART release from the ART powder and from sponges with different densities ( $3.5$  and  $6 \text{ mg/cm}^3$ ) and PPX coating thickness (0, 88, 150, 423, and 1000 nm).

behavior caused a burst release, seen in the initial 20 min. After that, the bigger particles of ART crystals gradually dissolve, initiating the retarded release. By loading the drug in the fibrous sponge with small density ( $3.5 \text{ mg/cm}^3$ , SG3.5-0) without PPX coating, 100% of the drug was released within the first hour. The ART loaded sponges were treated by freeze-drying that caused ART recrystallization into small crystals with a size of several micrometers, which led to the fast dissolution in the liquid medium and the fast burst release. In comparison, when the sponge with higher density ( $6 \text{ mg/cm}^3$ , SG6-0) was used, a retarded release was observed: about 50 and 87 wt % of ART was released in 2 and 5 h, respectively. The different drug release profiles from the sponges without PPX coating (SG3.5-0 and SG6-0) could be attributed to the much higher specific pore volume (SPV) of SG3.5 compared to SG6 ( $285$  vs  $166 \text{ cm}^3/\text{g}$ ), which facilitated the mass transfer of ART to the liquid medium. The coating of PPX on the surface of loaded sponges delays ART release; after 2 and 5 h, a very thin layer of PPX (88 nm) led to ART releases of 33 and 67 wt % from SG6-88, which were 17 and 20 wt % lower than SG6-0, respectively. Increasing the coating thickness of PPX was in correlation with the retardation of ART release, as shown in Table 2. Obviously, coating with the 1000 nm PPX is not useful because it completely prevents ART release.

Table 2. Amount of ART Release from Sponges with Different PPX Coating Thicknesses after 2 and 5 h

PPX thickness (nm)	0	88	150	423	1000
ART release after 2 h (wt %)	49	33	13	7	1
ART release after 5 h (wt %)	87	67	30	16	2

The retarded release of ART from the PPX coated sponges could be attributed to core-shell structure and triggered wettability. Additional shell on the surface of drug-loaded core perform as an efficient diffusion barrier that slows drug release<sup>52–55</sup> and the liquid slowly permeates through the PPX layer.<sup>56–58</sup> Our recent work also clearly showed that PPX coating on the surface of electrospun fibers led to a core-shell structure.<sup>19</sup> In this work, the additional PPX coating covered the drug-loaded fibers and also could form core-shell structure on the surface of ART crystals (Figure 3). Therefore, probably the liquid permeability of PPX coating on the drug loaded fibers would change the drug diffusion and consequently delay

the release. In addition, our previous results also showed that PPX coating would increase water contact angle, in correlation with PPX thickness.<sup>19</sup> Improved hydrophobicity of the sponge would then weaken the contact of the drug with the water-based liquid medium and therefore also contribute to the retarded time-dependent drug release.

## CONCLUSIONS

Polymeric fibrous sponges have been successfully prepared and used as a carrier system for the programmed release of the antimalarial drug ART. The extremely high pore volume of the sponges enables very high loading capacity of ART. The stable fixation of ART in the pores of the sponges and the programmed release of ART from the sponges under sink conditions was achieved by CVD coating of PPX. The release rate of ART was programmed by the control of the layer thickness of PPX coating which covered the ART crystals conformal in the sponges as well as the fiber scaffold of the sponges. The superhydrophobicity of the PPX coated sponges might contribute to the mass transport. Surely, drug loaded sponges like those shown here could be used as drug reservoir either for implantation or infusion systems. It could be further utilized for other drugs as well, and it could be even adapted to biodegradable sponges and multicompartiment drug release sponges. It is obvious that sponges based on short electrospun fibers offer numerous advantages over other nonpolymer systems. However, a particular not yet exploited the advantage of polymer based sponges could be the versatile chemical reactivity of polymers which enables further programming of drug-release rates and even more complex multidrug systems. Various administration methods of this device should be now examined for the specific diseases, e.g. subcutaneous insertion, infusion bags, stents and topical implants.

The PPX has been known as a coating material with robust adhesion and high biocompatibility. Likewise, it has been used for coating implantable medical devices,<sup>59,60</sup> and so are the sponges.<sup>61,62</sup> Our results suggest that the coated polymeric fibrous sponges are appropriate candidates for drug delivery of ART, for treating diseases that are caused by ART sensitive parasites and tumors.

## AUTHOR INFORMATION

### Corresponding Author

\*Tel.: +49-921-553399. Fax: +49-921-553393. E-mail: greiner@uni-bayreuth.de.

### Present Address

#College of Materials Science and Engineering, Nanjing Forestry University, 210037 Nanjing, China.

### Author Contributions

The manuscript was written through contributions of all authors. All authors have given approval to the final version of the manuscript.

### Notes

The authors declare no competing financial interest.

## ACKNOWLEDGMENTS

The support of Markus Langner in experimental work is kindly acknowledged. The authors are indebted to DFG (GIP project) for financial support, to CIPLA, India, for the kind donation of Artemisone, and to Speciality Coating systems for the donation of [2.2] paracyclopentane.

E

DOI: 10.1021/acs.biomac.7b00852  
Biomacromolecules XXXX, XXX, XXX–XXX

## REFERENCES

- (1) Davis, M. E. Ordered porous materials for emerging applications. *Nature* **2002**, *417* (6891), 813–821.
- (2) Nugent, P.; Belmabkhout, Y.; Burd, S. D.; Cairns, A. J.; Luebke, R.; Forrest, K.; Pham, T.; Ma, S.; Space, B.; Wojtas, L.; Eddaoudi, M.; Zaworotko, M. J. Porous materials with optimal adsorption thermodynamics and kinetics for CO<sub>2</sub> separation. *Nature* **2013**, *495* (7439), 80–84.
- (3) Ishizaki, K.; Komarneni, S.; Nanko, M. *Porous Materials: Process Technology and Applications*; Springer Science and Business Media, 2013; Vol. 4.
- (4) Parlett, C. M. A.; Wilson, K.; Lee, A. F. Hierarchical porous materials: catalytic applications. *Chem. Soc. Rev.* **2013**, *42* (9), 3876–3893.
- (5) Perego, C.; Millini, R. Porous materials in catalysis: challenges for mesoporous materials. *Chem. Soc. Rev.* **2013**, *42* (9), 3956–3976.
- (6) Li, Y.; Fu, Z.-Y.; Su, B.-L. Hierarchically Structured Porous Materials for Energy Conversion and Storage. *Adv. Funct. Mater.* **2012**, *22* (22), 4634–4667.
- (7) Yang, P.; Gai, S.; Lin, J. Functionalized mesoporous silica materials for controlled drug delivery. *Chem. Soc. Rev.* **2012**, *41* (9), 3679–3698.
- (8) Arruebo, M. Drug delivery from structured porous inorganic materials. *Wiley Interdiscip. Rev.: Nanomed. Nanobiotechnol.* **2012**, *4* (1), 16–30.
- (9) Horcajada, P.; Gref, R.; Baati, T.; Allan, P. K.; Maurin, G.; Couvreur, P.; Férey, G.; Morris, R. E.; Serre, C. Metal–Organic Frameworks in Biomedicine. *Chem. Rev.* **2012**, *112* (2), 1232–1268.
- (10) Vallet-Regí, M.; Balas, F.; Arcos, D. Mesoporous Materials for Drug Delivery. *Angew. Chem., Int. Ed.* **2007**, *46* (40), 7548–7558.
- (11) Horcajada, P.; Serre, C.; Vallet-Regí, M.; Sebban, M.; Taulelle, F.; Férey, G. Metal–Organic Frameworks as Efficient Materials for Drug Delivery. *Angew. Chem., Int. Ed.* **2006**, *45* (36), 5974–5978.
- (12) Sill, T. J.; von Recum, H. A. Electrospinning: Applications in drug delivery and tissue engineering. *Biomaterials* **2008**, *29* (13), 1989–2006.
- (13) Yoo, H. S.; Kim, T. G.; Park, T. G. Surface-functionalized electrospun nanofibers for tissue engineering and drug delivery. *Adv. Drug Delivery Rev.* **2009**, *61* (12), 1033–1042.
- (14) Hu, X.; Liu, S.; Zhou, G.; Huang, Y.; Xie, Z.; Jing, X. Electrospinning of polymeric nanofibers for drug delivery applications. *J. Controlled Release* **2014**, *185*, 12–21.
- (15) Bagheri, A. R.; Agarwal, S.; Greiner, J.; Greiner, A. Unlocking Nanocarriers for the Programmed Release of Antimalarial Drugs. *Global Challenges* **2017**, *1* (2), 1600011.
- (16) Si, Y.; Yu, J.; Tang, X.; Ge, J.; Ding, B. Ultralight nanofibre-assembled cellular aerogels with superelasticity and multifunctionality. *Nat. Commun.* **2014**, *5*, 5802.
- (17) Duan, G.; Jiang, S.; Jérôme, V.; Wendorff, J. H.; Fathi, A.; Uhm, J.; Altstadt, V.; Herling, M.; Breu, J.; Freitag, R.; Agarwal, S.; Greiner, A. Ultralight, Soft Polymer Sponges by Self-Assembly of Short Electrospun Fibers in Colloidal Dispersions. *Adv. Funct. Mater.* **2015**, *25* (19), 2850–2856.
- (18) Xu, T.; Miszuk, J. M.; Zhao, Y.; Sun, H.; Fong, H. Electrospun Polycaprolactone 3D Nanofibrous Scaffold with Interconnected and Hierarchically Structured Pores for Bone Tissue Engineering. *Adv. Healthcare Mater.* **2015**, *4* (15), 2238–2246.
- (19) Duan, G.; Jiang, S.; Moss, T.; Agarwal, S.; Greiner, A. Ultralight open cell polymer sponges with advanced properties by PPX CVD coating. *Polym. Chem.* **2016**, *7* (15), 2759–2764.
- (20) Jiang, S.; Duan, G.; Kuhn, U.; Mörl, M.; Altstadt, V.; Yarin, A. L.; Greiner, A. Spongy Gels by a Top-Down Approach from Polymer Fibrous Sponges. *Angew. Chem., Int. Ed.* **2017**, *56* (12), 3285–3288.
- (21) Haynes, R. K.; Fugmann, B.; Stetter, J.; Rieckmann, K.; Heilmann, H.-D.; Chan, H.-W.; Cheung, M.-K.; Lam, W.-L.; Wong, H.-N.; Croft, S. L.; Vivas, L.; Rattray, L.; Stewart, L.; Peters, W.; Robinson, B. L.; Edstein, M. D.; Kotecka, B.; Kyle, D. E.; Beckermann, B.; Gerisch, M.; Radtke, M.; Schmuck, G.; Steinke, W.; Wollborn, U.; Schmeer, K.; Römer, A. Artemisone—A Highly Active Antimalarial Drug of the Artemisinin Class. *Angew. Chem., Int. Ed.* **2006**, *45* (13), 2082–2088.
- (22) Aditya, N. P.; Vathsala, P. G.; Vieira, V.; Murthy, R. S. R.; Souto, E. B. Advances in nanomedicines for malaria treatment. *Adv. Colloid Interface Sci.* **2013**, *201–202*, 1–17.
- (23) Schmuck, G.; Haynes, R. K. Establishment of an In Vitro screening model for neurodegeneration induced by antimalarial drugs of the artemisinin-type. *Neurotoxic. Res.* **2000**, *2* (1), 37–49.
- (24) Schmuck, G.; Roehrdanz, E.; Haynes, R. K.; Kahl, R. Neurotoxic mode of action of artemisinin. *Antimicrob. Agents Chemother.* **2002**, *46* (3), 821–827.
- (25) Wakinine-Grinberg, J. H.; Hunt, N.; Bentura-Marciano, A.; McQuillan, J. A.; Chan, H.-W.; Chan, W.-C.; Barenholz, Y.; Haynes, R. K.; Golenser, J. Artemisone effective against murine cerebral malaria. *Malar. J.* **2010**, *9* (1), 227.
- (26) Obaldia, N.; Kotecka, B. M.; Edstein, M. D.; Haynes, R. K.; Fugmann, B.; Kyle, D. E.; Rieckmann, K. H. Evaluation of artemisone combinations in Aotus monkeys infected with Plasmodium falciparum. *Antimicrob. Agents Chemother.* **2009**, *53* (8), 3592–3594.
- (27) Dunay, I. R.; Chan, W. C.; Haynes, R. K.; Sibley, L. D. Artemisone and artemiside control acute and reactivated toxoplasmosis in a murine model. *Antimicrob. Agents Chemother.* **2009**, *53* (10), 4450–4456.
- (28) Mazuz, M. L.; Haynes, R.; Shkap, V.; Fish, L.; Wollkomirsky, R.; Leibovich, B.; Molad, T.; Savitsky, I.; Golenser, J. Neospora caninum: in vivo and in vitro treatment with artemisone. *Vet. Parasitol.* **2012**, *187* (1), 99–104.
- (29) Gold, D.; Allan, M.; Domb, A.; Karawani, Y.; Jbarien, M.; Chollet, J.; Haynes, R. K.; Wong, H. N.; Buchholz, V.; Greiner, A. Elimination of Schistosoma mansoni in infected mice by slow release of artemisone. *Int. J. Parasitol.: Drugs Drug Resist.* **2017**, *7* (2), 241–247.
- (30) Gravett, A. M.; Liu, W. M.; Krishna, S.; Chan, W.-C.; Haynes, R. K.; Wilson, N. L.; Dalglish, A. G. In vitro study of the anti-cancer effects of artemisone alone or in combination with other chemotherapeutic agents. *Cancer Chemother. Pharmacol.* **2011**, *67* (3), 569–577.
- (31) Guiguemde, W. A.; Hunt, N. H.; Guo, J.; Marciano, A.; Haynes, R. K.; Clark, J.; Guy, R. K.; Golenser, J. Treatment of murine cerebral malaria by artemisone in combination with conventional antimalarial drugs: antiplasmodial effects and immune responses. *Antimicrob. Agents Chemother.* **2014**, *58* (8), 4745–4754.
- (32) Duan, G.; Koehn-Serrano, M.; Greiner, A. Highly Efficient Reusable Sponge-Type Catalyst Carriers Based on Short Electrospun Fibers. *Macromol. Rapid Commun.* **2017**, *38*, 1600511.
- (33) Wu, J.; Zhu, Y.-J.; Cao, S.-W.; Chen, F. Hierarchically Nanostructured Mesoporous Spheres of Calcium Silicate Hydrate: Surfactant-Free Sonochemical Synthesis and Drug-Delivery System with Ultrahigh Drug-Loading Capacity. *Adv. Mater.* **2010**, *22* (6), 749–753.
- (34) Muñoz, B.; Rámila, A.; Pérez-Pariente, J.; Díaz, I.; Vallet-Regí, M. MCM-41 Organic Modification as Drug Delivery Rate Regulator. *Chem. Mater.* **2003**, *15* (2), 500–503.
- (35) Horcajada, P.; Rámila, A.; Pérez-Pariente, J.; Vallet-Regí, M. Influence of pore size of MCM-41 matrices on drug delivery rate. *Microporous Mesoporous Mater.* **2004**, *68* (1–3), 105–109.
- (36) Zhao, F.; Li, G.; Wang, X.; Sun, D.; Jin, C. Loading and release of ibuprofen on mesoporous molecular sieve Ti-HMS. *J. Porous Mater.* **2010**, *17* (5), 629–634.
- (37) Horcajada, P.; Márquez-Alvarez, C.; Rámila, A.; Pérez-Pariente, J.; Vallet-Regí, M. Controlled release of Ibuprofen from dealuminated faujasites. *Solid State Sci.* **2006**, *8* (12), 1459–1465.
- (38) Yufang, Z.; Jianlin, S.; Weihua, S.; Hangrong, C.; Xiaoping, D.; Meilin, R. Preparation of novel hollow mesoporous silica spheres and their sustained-release property. *Nanotechnology* **2005**, *16* (11), 2633.
- (39) Horcajada, P.; Serre, C.; Maurin, G.; Ramsahye, N. A.; Balas, F.; Vallet-Regí, M.; Sebban, M.; Taulelle, F.; Férey, G. Flexible Porous Metal–Organic Frameworks for a Controlled Drug Delivery. *J. Am. Chem. Soc.* **2008**, *130* (21), 6774–6780.

F

DOI: 10.1021/acs.biomac.7b00852  
Biomacromolecules XXXX, XXX, XXX–XXX

- (40) Horcajada, P.; Serre, C.; Vallet-Regí, M.; Sebban, M.; Taulelle, F.; Férey, G. Metal–Organic Frameworks as Efficient Materials for Drug Delivery. *Angew. Chem.* **2006**, *118* (36), 6120–6124.
- (41) Bag, P. P.; Wang, D.; Chen, Z.; Cao, R. Outstanding drug loading capacity by water stable microporous MOF: a potential drug carrier. *Chem. Commun.* **2016**, *52* (18), 3669–3672.
- (42) Yang, Y.; Hu, Q.; Zhang, Q.; Jiang, K.; Lin, W.; Yang, Y.; Cui, Y.; Qian, G. A Large Capacity Cationic Metal–Organic Framework Nanocarrier for Physiological pH Responsive Drug Delivery. *Mol. Pharmaceutics* **2016**, *13* (8), 2782–2786.
- (43) Sun, C.-Y.; Qin, C.; Wang, C.-G.; Su, Z.-M.; Wang S.; Wang, X.-L.; Yang, G.-S.; Shao, K.-Z.; Lan, Y.-Q.; Wang, E.-B. Chiral Nanoporous Metal–Organic Frameworks with High Porosity as Materials for Drug Delivery. *Adv. Mater.* **2011**, *23* (47), 5629–5632.
- (44) McMaster, W. A.; Wang, X.; Caruso, R. A. Collagen-Templated Bioactive Titanium Dioxide Porous Networks for Drug Delivery. *ACS Appl. Mater. Interfaces* **2012**, *4* (9), 4717–4725.
- (45) Ma, Z.; Ji, H.; Teng, Y.; Dong, G.; Tan, D.; Guan, M.; Zhou, J.; Xie, J.; Qiu, J.; Zhang, M. Engineering and optimization of medically multi-functional mesoporous SiO<sub>2</sub> fibers as effective wound dressing material. *J. Mater. Chem.* **2011**, *21* (26), 9595–9602.
- (46) Sadeghi, M.; Shafei, F.; Mohammadinasab, E.; Sadeghi, H.; Shasvari, H. Biosuperabsorbent Hydrogel Based on Alginate-g-PolyAA/kaolin Composite for Releasing Cefalexin Drug. *Orient. J. Chem.* **2014**, *30* (1), 285–290.
- (47) Tsai, H.-C.; Lin, J.-Y.; Maryani, F.; Huang, C.-C.; Imae, T. Drug-loading capacity and nuclear targeting of multiwalled carbon nanotubes grafted with anionic amphiphilic copolymers. *Int. J. Nanomed.* **2013**, *8*, 4427.
- (48) Moazzen, E.; Ebrahimzadeh, H.; Amini, M. M.; Sadeghi, O. A novel biocompatible drug carrier for oral delivery and controlled release of antibiotic drug: loading and release of clarithromycin as an antibiotic drug model. *J. Sol-Gel Sci. Technol.* **2013**, *66* (2), 345–351.
- (49) Tang, Q.-L.; Zhu, Y.-J.; Wu, J.; Chen, F.; Cao, S.-W. Calcium phosphate drug nanocarriers with ultrahigh and adjustable drug-loading capacity: One-step synthesis, in situ drug loading and prolonged drug release. *Nanomedicine* **2011**, *7* (4), 428–434.
- (50) Mosharraf, M.; Nyström, C. The effect of particle size and shape on the surface specific dissolution rate of micro-sized practically insoluble drugs. *Int. J. Pharm.* **1995**, *122* (1), 35–47.
- (51) Berkland, C.; King, M.; Cox, A.; Kim, K.; Pack, D. W. Precise control of PLG microsphere size provides enhanced control of drug release rate. *J. Controlled Release* **2002**, *82* (1), 137–147.
- (52) Soppimath, K. S.; Tan, D. C. W.; Yang, Y. Y. pH-Triggered Thermally Responsive Polymer Core–Shell Nanoparticles for Drug Delivery. *Adv. Mater.* **2005**, *17* (3), 318–323.
- (53) Chan, J. M.; Zhang, L.; Yuet, K. P.; Liao, G.; Rhee, J.-W.; Langer, R.; Farokhzad, O. C. PLGA–lecithin–PEG core–shell nanoparticles for controlled drug delivery. *Biomaterials* **2009**, *30* (8), 1627–1634.
- (54) Sperling, L. E.; Reis, K. P.; Pranke, P.; Wendorff, J. H. Advantages and challenges offered by biofunctional core–shell fiber systems for tissue engineering and drug delivery. *Drug Discovery Today* **2016**, *21* (8), 1243–1256.
- (55) Perez, R. A.; Kim, H.-W. Core–shell designed scaffolds for drug delivery and tissue engineering. *Acta Biomater.* **2015**, *21*, 2–19.
- (56) Mitschang, F.; Schmalz, H.; Agarwal, S.; Greiner, A. Tea-Bag-Like Polymer Nanoreactors Filled with Gold Nanoparticles. *Angew. Chem., Int. Ed.* **2014**, *53* (19), 4972–4975.
- (57) Tanioka, A.; Fukushima, N.; Hasegawa, K.; Miyasaka, K.; Takahashi, N. Permeation of gases across the poly(chloro-p-xylylene) membrane. *J. Appl. Polym. Sci.* **1994**, *54* (2), 219–229.
- (58) Chang, C.-W.; Guan, Z.-Y.; Kan, M.-Y.; Lee, L.-W.; Chen, H.-Y.; Kang, D.-Y. Vapor-phase synthesis of poly(p-xylylene) membranes for gas separations. *J. Membr. Sci.* **2017**, *539*, 101–107.
- (59) Hsu, J.-M.; Rieth, L.; Normann, R. A.; Tathireddy, P.; Solzbacher, F. Encapsulation of an integrated neural interface device with Parylene C. *IEEE Trans. Biomed. Eng.* **2009**, *56* (1), 23–29.
- (60) Xie, X.; Rieth, L.; Caldwell, R.; Diwekar, M.; Tathireddy, P.; Sharma, R.; Solzbacher, F. Long-Term Bilayer Encapsulation Performance of Atomic Layer Deposited Al<sub>2</sub>O<sub>3</sub> and Parylene C for Biomedical Implantable Devices. *IEEE Trans. Biomed. Eng.* **2013**, *60* (10), 2943–2951.
- (61) Mooney, D.; Park, S.; Kaufmann, P.; Sano, K.; McNamara, K.; Vacanti, J.; Langer, R. Biodegradable sponges for hepatocyte transplantation. *J. Biomed. Mater. Res.* **1995**, *29* (8), 959–965.
- (62) Widdowson, J. P.; Picton, A. J.; Vince, V.; Wright, C. J.; Mearns-Spragg, A. In vivo comparison of jellyfish and bovine collagen sponges as prototype medical devices. *J. Biomed. Mater. Res., Part B* **2017**, DOI: 10.1002/jbm.b.33959.

### 3.5 Spongy gels by a top-down approach from polymer fibrous sponges

Shaohua Jiang, **Gaigai Duan**, Ute Kuhn, Michaela Mörl, Volker Altstädt, Alexander L. Yarin, Andreas Greiner. Spongy gels by a top-down approach from polymer fibrous sponges. *Angew. Chem.* **2017**; DOI: [10.1002/ange.201611787](https://doi.org/10.1002/ange.201611787).

2017/2/14

RightsLink - Your Account

## JOHN WILEY AND SONS LICENSE TERMS AND CONDITIONS

Feb 14, 2017

This Agreement between University of Bayreuth -- Gaigai Duan ("You") and John Wiley and Sons ("John Wiley and Sons") consists of your license details and the terms and conditions provided by John Wiley and Sons and Copyright Clearance Center.

License Number	4047691447247
License date	Feb 14, 2017
Licensed Content Publisher	John Wiley and Sons
Licensed Content Publication	Angewandte Chemie International Edition
Licensed Content Title	Spongy Gels by a Top - Down Approach from Polymer Fibrous Sponges
Licensed Content Author	Shaohua Jiang, Gaigai Duan, Ute Kuhn, Michaela Mörl, Volker Altstädt, Alexander L. Yarin, Andreas Greiner
Licensed Content Date	Feb 14, 2017
Licensed Content Pages	1
Type of Use	Dissertation/Thesis
Requestor type	Author of this Wiley article
Format	Print and electronic
Portion	Full article
Will you be translating?	No
Order reference number	100
Title of your thesis / dissertation	3D porous sponges from electrospun polymer fibers and their applications
Expected completion date	Dec 2017
Expected size (number of pages)	160
Requestor Location	University of Bayreuth Universitätsstrasse 30  Bayreuth, 95440 Germany Attn: Gaigai Duan
Publisher Tax ID	EU826007151
Billing Type	Invoice
Billing Address	University of Bayreuth Universitätsstrasse 30  Bayreuth, Germany 95440 Attn: Gaigai Duan
Total	<b>0.00 USD</b>

Terms and Conditions

### TERMS AND CONDITIONS

This copyrighted material is owned by or exclusively licensed to John Wiley & Sons, Inc. or one of its group companies (each a "Wiley Company") or handled on behalf of a society with which a Wiley Company has exclusive publishing rights in relation to a particular work (collectively "WILEY"). By clicking "accept" in connection with completing this licensing transaction, you agree that the following terms and conditions apply to this transaction (along with the billing and payment terms and conditions established by the Copyright Clearance Center Inc., ("CCC's Billing and Payment terms and conditions"), at the time that you opened your RightsLink account (these are available at any time at <http://myaccount.copyright.com>).

Terms and Conditions

2017/2/14

RightsLink - Your Account

- The materials you have requested permission to reproduce or reuse (the "Wiley Materials") are protected by copyright.
- You are hereby granted a personal, non-exclusive, non-sub licensable (on a stand-alone basis), non-transferable, worldwide, limited license to reproduce the Wiley Materials for the purpose specified in the licensing process. This license, and any **CONTENT (PDF or image file) purchased as part of your order**, is for a one-time use only and limited to any maximum distribution number specified in the license. The first instance of republication or reuse granted by this license must be completed within two years of the date of the grant of this license (although copies prepared before the end date may be distributed thereafter). The Wiley Materials shall not be used in any other manner or for any other purpose, beyond what is granted in the license. Permission is granted subject to an appropriate acknowledgement given to the author, title of the material/book/journal and the publisher. You shall also duplicate the copyright notice that appears in the Wiley publication in your use of the Wiley Material. Permission is also granted on the understanding that nowhere in the text is a previously published source acknowledged for all or part of this Wiley Material. Any third party content is expressly excluded from this permission.
- With respect to the Wiley Materials, all rights are reserved. Except as expressly granted by the terms of the license, no part of the Wiley Materials may be copied, modified, adapted (except for minor reformatting required by the new Publication), translated, reproduced, transferred or distributed, in any form or by any means, and no derivative works may be made based on the Wiley Materials without the prior permission of the respective copyright owner. **For STM Signatory Publishers clearing permission under the terms of the STM Permissions Guidelines only, the terms of the license are extended to include subsequent editions and for editions in other languages, provided such editions are for the work as a whole in situ and does not involve the separate exploitation of the permitted figures or extracts**. You may not alter, remove or suppress in any manner any copyright, trademark or other notices displayed by the Wiley Materials. You may not license, rent, sell, loan, lease, pledge, offer as security, transfer or assign the Wiley Materials on a stand-alone basis, or any of the rights granted to you hereunder to any other person.
- The Wiley Materials and all of the intellectual property rights therein shall at all times remain the exclusive property of John Wiley & Sons Inc, the Wiley Companies, or their respective licensors, and your interest therein is only that of having possession of and the right to reproduce the Wiley Materials pursuant to Section 2 herein during the continuance of this Agreement. You agree that you own no right, title or interest in or to the Wiley Materials or any of the intellectual property rights therein. You shall have no rights hereunder other than the license as provided for above in Section 2. No right, license or interest to any trademark, trade name, service mark or other branding ("Marks") of WILEY or its licensors is granted hereunder, and you agree that you shall not assert any such right, license or interest with respect thereto
- NEITHER WILEY NOR ITS LICENSORS MAKES ANY WARRANTY OR REPRESENTATION OF ANY KIND TO YOU OR ANY THIRD PARTY, EXPRESS, IMPLIED OR STATUTORY, WITH RESPECT TO THE MATERIALS OR THE ACCURACY OF ANY INFORMATION CONTAINED IN THE MATERIALS, INCLUDING, WITHOUT LIMITATION, ANY IMPLIED WARRANTY OF MERCHANTABILITY, ACCURACY, SATISFACTORY QUALITY, FITNESS FOR A PARTICULAR PURPOSE, USABILITY, INTEGRATION OR NON-INFRINGEMENT AND ALL SUCH WARRANTIES ARE HEREBY EXCLUDED BY WILEY AND ITS LICENSORS AND WAIVED BY YOU.
- WILEY shall have the right to terminate this Agreement immediately upon breach of this Agreement by you.
- You shall indemnify, defend and hold harmless WILEY, its Licensors and their respective directors, officers, agents and employees, from and against any actual or threatened claims, demands, causes of action or proceedings arising from any breach of this Agreement by you.
- IN NO EVENT SHALL WILEY OR ITS LICENSORS BE LIABLE TO YOU OR ANY OTHER PARTY OR ANY OTHER PERSON OR ENTITY FOR ANY SPECIAL, CONSEQUENTIAL, INCIDENTAL, INDIRECT, EXEMPLARY OR PUNITIVE DAMAGES, HOWEVER CAUSED, ARISING OUT OF OR IN CONNECTION WITH THE DOWNLOADING, PROVISIONING, VIEWING OR USE OF THE MATERIALS REGARDLESS OF THE FORM OF ACTION, WHETHER FOR BREACH OF CONTRACT, BREACH OF WARRANTY, TORT, NEGLIGENCE, INFRINGEMENT OR OTHERWISE (INCLUDING, WITHOUT LIMITATION, DAMAGES BASED ON LOSS OF PROFITS, DATA, FILES, USE, BUSINESS OPPORTUNITY OR CLAIMS OF THIRD PARTIES), AND WHETHER OR NOT THE PARTY HAS BEEN ADVISED OF THE POSSIBILITY OF SUCH DAMAGES. THIS LIMITATION SHALL APPLY NOTWITHSTANDING ANY FAILURE OF ESSENTIAL PURPOSE OF ANY LIMITED REMEDY PROVIDED HEREIN.
- Should any provision of this Agreement be held by a court of competent jurisdiction to be illegal, invalid, or unenforceable, that provision shall be deemed amended to achieve as nearly as possible the same economic effect as the original provision, and the legality, validity and enforceability of the remaining provisions of this Agreement shall not be affected or impaired thereby.
- The failure of either party to enforce any term or condition of this Agreement shall not constitute a waiver of either party's right to enforce each and every term and condition of this Agreement. No breach under this agreement shall be deemed waived or excused by either party unless such waiver or consent is in writing signed by the party granting such

<https://s100.copyright.com/MyAccount/web/jsp/viewprintablelicensefrommyorders.jsp?ref=deb7e0b8-31bf-4cc3-8e92-e735deb233d7&email=>

2/3

2017/2/14

RightsLink - Your Account

waiver or consent. The waiver by or consent of a party to a breach of any provision of this Agreement shall not operate or be construed as a waiver of or consent to any other or subsequent breach by such other party.

- This Agreement may not be assigned (including by operation of law or otherwise) by you without WILEY's prior written consent.
- Any fee required for this permission shall be non-refundable after thirty (30) days from receipt by the CCC.
- These terms and conditions together with CCC's Billing and Payment terms and conditions (which are incorporated herein) form the entire agreement between you and WILEY concerning this licensing transaction and (in the absence of fraud) supersedes all prior agreements and representations of the parties, oral or written. This Agreement may not be amended except in writing signed by both parties. This Agreement shall be binding upon and inure to the benefit of the parties' successors, legal representatives, and authorized assigns.
- In the event of any conflict between your obligations established by these terms and conditions and those established by CCC's Billing and Payment terms and conditions, these terms and conditions shall prevail.
- WILEY expressly reserves all rights not specifically granted in the combination of (i) the license details provided by you and accepted in the course of this licensing transaction, (ii) these terms and conditions and (iii) CCC's Billing and Payment terms and conditions.
- This Agreement will be void if the Type of Use, Format, Circulation, or Requestor Type was misrepresented during the licensing process.
- This Agreement shall be governed by and construed in accordance with the laws of the State of New York, USA, without regards to such state's conflict of law rules. Any legal action, suit or proceeding arising out of or relating to these Terms and Conditions or the breach thereof shall be instituted in a court of competent jurisdiction in New York County in the State of New York in the United States of America and each party hereby consents and submits to the personal jurisdiction of such court, waives any objection to venue in such court and consents to service of process by registered or certified mail, return receipt requested, at the last known address of such party.

#### WILEY OPEN ACCESS TERMS AND CONDITIONS

Wiley Publishes Open Access Articles in fully Open Access Journals and in Subscription journals offering Online Open. Although most of the fully Open Access journals publish open access articles under the terms of the Creative Commons Attribution (CC BY) License only, the subscription journals and a few of the Open Access Journals offer a choice of Creative Commons Licenses. The license type is clearly identified on the article.

##### The Creative Commons Attribution License

The [Creative Commons Attribution License \(CC-BY\)](#) allows users to copy, distribute and transmit an article, adapt the article and make commercial use of the article. The CC-BY license permits commercial and non-

##### Creative Commons Attribution Non-Commercial License

The [Creative Commons Attribution Non-Commercial \(CC-BY-NC\) License](#) permits use, distribution and reproduction in any medium, provided the original work is properly cited and is not used for commercial purposes.(see below)

##### Creative Commons Attribution-Non-Commercial-NoDerivs License

The [Creative Commons Attribution Non-Commercial-NoDerivs License \(CC-BY-NC-ND\)](#) permits use, distribution and reproduction in any medium, provided the original work is properly cited, is not used for commercial purposes and no modifications or adaptations are made. (see below)

##### Use by commercial "for-profit" organizations

Use of Wiley Open Access articles for commercial, promotional, or marketing purposes requires further explicit permission from Wiley and will be subject to a fee.

Further details can be found on Wiley Online Library <http://olabout.wiley.com/WileyCDA/Section/id-410895.html>

#### Other Terms and Conditions:

v1.10 Last updated September 2015

Questions? [customer-care@copyright.com](mailto:customer-care@copyright.com) or +1-855-239-3415 (toll free in the US) or +1-978-646-2777.

## Spongy Gels by a Top-Down Approach from Polymer Fibrous Sponges

Shaohua Jiang<sup>†</sup>, Gaigai Duan<sup>†</sup>, Ute Kuhn, Michaela Mörl, Volker Altstädt, Alexander L. Yarin,<sup>\*</sup> and Andreas Greiner<sup>\*</sup>

**Abstract:** Ultralight cellular sponges offer a unique set of properties. We show here that solvent uptake by these sponges results in new gel-like materials, which we term spongy gels. The appearance of the spongy gels is very similar to classic organogels. Usually, organogels are formed by a bottom-up process. In contrast, the spongy gels are formed by a top-down approach that offers numerous advantages for the design of their properties, reproducibility, and stability. The sponges themselves represent the scaffold of a gel that could be filled with a solvent, and thereby form a mechanically stable gel-like material. The spongy gels are independent of a time-consuming or otherwise demanding *in situ* scaffold formation. As solvent evaporation from gels is a concern for various applications, we also studied solvent evaporation of wetting and non-wetting liquids dispersed in the sponge.

Ultralight-weight scaffolds with open cell fibrous structures are known for a variety of materials prepared by different methods.<sup>[1]</sup> One of the most common methods is the use of a dispersion of a solid scaffold material in a solution followed by a freeze-drying step.<sup>[2]</sup> This method has also been successfully used recently for dispersions of short electrospun polymer fibers.<sup>[3]</sup> The resulting polymer scaffolds are termed as aerogels or sponges. In contrast to classic aerogels, the sponges are made directly from fibers and not from gels. The solid scaffold of the sponges is pre-formed by electrospun fibers, while the shape and dimension of the solid scaffold of the aerogel is formed during the gelation process. Typically, the sponges made from electrospun fibers have very low densities (10 mg cm<sup>-3</sup>) and show very high porosities (> 99.5%) like classic aerogels, but much larger pore size in

the range of several 10 μm, while aerogels are mostly mesoporous.<sup>[3a,4]</sup> The sponges are water-repelling but oleophilic, which makes them perfect materials for membranes for separation of organic compounds (such as oil or organic solvents) from water.<sup>[3a,5]</sup> An amazing feature of these sponges is the absorption of huge amounts of oily liquids while keeping their shape, in spite of a tiny mass of the solid scaffold of the sponges.<sup>[3a,b]</sup> The huge capacity can be understood by the large pore volume of 200–300 mL g<sup>-1</sup> of the sponges derived from their densities. With a liquid of a density of 1 g cm<sup>-3</sup>, 30 mg of polymer spongy scaffold (Figure 1a)

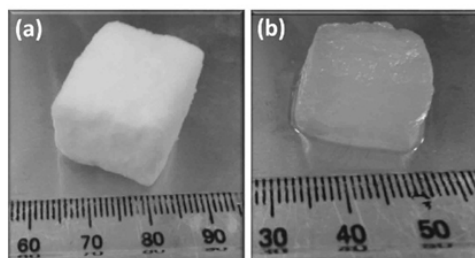


**Figure 1.** Sponge made of electrospun fibers with mass of 0.03 g (a) and the sponge after uptake of 30 g of mineral oil (b).

keeps 30 g of liquid in a shape that is 1000-times the mass of the spongy scaffold. The appearance of the sponge/liquid mixture after uptake of the liquid is gel-like (Figure 1 b). This type of gel-like material represents a new paradigm for gels and is defined here as spongy gels. Essentially, the mixture shows all of the characteristics of a thixotropic gel: a liquid phase, a 3D network, and practically no flow.

A similar relation, but in a reverse fashion, can be found in the so-called organogels (also referred to as molecular gels), which consist of a solid self-assembled 3D fibrous network (in some cases it could be also platelets) and a nonpolar liquid.<sup>[4,6]</sup> Organogels are formed by self-assembly of an organogelator to an entangled fibrous 3D network in a nonpolar liquid (Figure 2a). The self-assembly process could be initiated by different stimuli, such as temperature, concentration, pH, light, and current. The organogelators can possess different chemical nature ranging from low-molecular weight to polymer organogelators, and even coordination compounds. The chemical nature of the organogelators and apolar liquid could lead to a variety of different applications including drug delivery, sensors, lubrication, templates, oil recovery, and optical media.<sup>[4,6]</sup> An important feature for drug delivery applications of organogels is that they are thermodynamically stable but could also disintegrate under certain conditions.

[\*] Dr. S. Jiang,<sup>[†]</sup> G. Duan,<sup>[†]</sup> Prof. A. Greiner  
Macromolecular Chemistry, Bavarian Polymer Institute  
University Bayreuth  
Universitätsstrasse 30, 95440 Bayreuth (Germany)  
E-mail: greiner@uni-bayreuth.de

U. Kuhn, M. Mörl, Prof. V. Altstädt  
Polymer Engineering, University Bayreuth  
Universitätsstrasse 30, 95440 Bayreuth (Germany)

Prof. A. L. Yarin  
Department of Mechanical and Industrial Engineering  
University of Illinois at Chicago  
842 W. Taylor Street, Chicago, IL 60607 (USA)  
E-mail: ayarin@uic.edu

Dr. S. Jiang<sup>[†]</sup>  
College of Materials Science and Engineering  
Nanjing Forest University  
Nanjing 210037 (China)

[†] These authors contributed equally to this work.

Supporting information for this article can be found under:  
<http://dx.doi.org/10.1002/anie.201611787>.

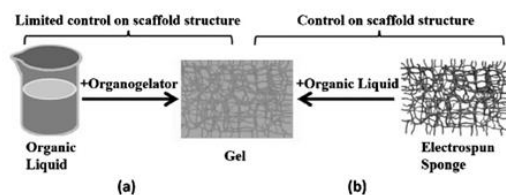


**Figure 2.** Drawing of the formation of organogels by action of organogelators on liquids (a) and by filling of electrospun fiber sponges with liquids (b).

Similar to spongy gels, organogels are thixotropic gels from the rheological point of view. Spongy gels obtained by contact of electrospun sponges with organic liquids show essentially the same features as an organogel: the formation of a 3D fibrous network, commonly assigned as self-assembled fibrillary network, filled with an apolar liquid. Even the disintegration of spongy gels is possible as reported previously.<sup>[3b]</sup> In contrast to organogels, the 3D fibrous network of spongy gels is pre-formed and then filled with the apolar liquid (Figure 2b). To avoid any misunderstanding or confusion of scientific terminology, it should be emphasized here that spongy gels are not organogels, as organogels are based on self-assembly of low- or high-molecular weight molecules,<sup>[4,6]</sup> while spongy gels are based on fibrous scaffolds. The appearance of organogels and spongy gels are very similar, but the spongy gels have the distinct advantages of fine control over the nature and structure of the 3D fibrous network, no shrinkage, no sensitivity to impurities on gel formation, and provide a wide range of possibilities for functionalization owing to the wealth of modifications of electrospun fibers. Although a wide variety of beautiful examples for the functionalization of organogels has been shown, their realization is often laborious, in particular as far as the synthesis of the organogelators is concerned, which makes organogels quite expensive.<sup>[4,7]</sup> Another disadvantage of organogels is their sensitivity to impurities in conjunction with the gelation process, which hampers technical applications.<sup>[4,7]</sup> With this set of differences, spongy gels offer completely new possibilities but also raise several questions that we want to discuss in this paper. We report here on the preparation of spongy gels by a top-down process. We obtained the spongy gels by filling of macroporous ultralight polymer sponges with wetting and non-wetting liquid. We show that spongy gels behave in many respects similar to organogels. It is important to note that the sponges used here were made from dispersions of short electrospun fibers that can disintegrate upon contact with solvents. As recently shown, the sponges could be stabilized by an additional conformal coating by poly(*p*-xylylene) (PPX) by deposition from the vapor phase.<sup>[3b]</sup> This PPX coating makes the sponges highly stable against solvents, which enables the formation of gels according to Figure 2b. To gain understanding of organogels based on spongy gels, we discuss here the mechanical properties of the spongy gels and the evaporation of wetting and non-wetting liquids from the spongy gels backed by theoretical considerations.

The PPX-coated sponges under investigation were made according to a previously published procedure with densities of 16.2 (P-SG1) and 30.6 (P-SG2) mg cm<sup>-3</sup>, respectively.<sup>[3b]</sup> The cross-section morphologies of the sponges showed for P-SG1 much higher pore size than those of P-SG2 (Figure 3).

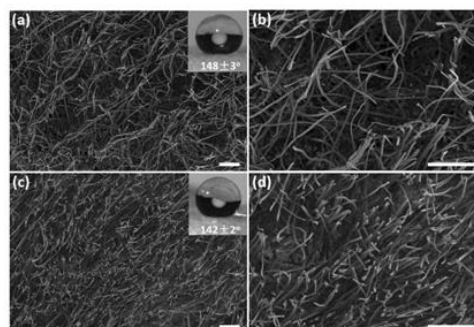


**Figure 3.** Cross-section morphology of the P-SG1 (a, b) and P-SG2 (c, d). Scale bar: 100 μm. Insert of (a) and (c) are the water contact angle of the corresponding sponges.

The differences in the density and the pore size lead to the different porosity ( $P$ ), which was determined according to Equation (1).

$$P = \left(1 - \frac{\rho_{SG}}{\rho_{bulk}}\right) \times 100\% \quad (1)$$

Herein,  $\rho_{SG}$  and  $\rho_{bulk}$  are the density of the sponges and the corresponding bulk density, respectively. The bulk densities for the P-SG1 and P-SG2 are 953 and 1457 mg cm<sup>-3</sup>, respectively. The calculated corresponding porosities for the P-SG1 and P-SG2 are 98.3% and 97.9%, respectively, which are slightly smaller than the porosity (99.5%) of the original fibrous sponges due to the additional PPX coating.

The sponges P-SG1 and P-SG2 were hydrophobic, with water contact angles (WCA) of 148 ± 3° and 142 ± 2°, respectively. Consequently, water is a non-wetting liquid for both sponges. In contrast, ethanol is a wetting liquid for the sponges, with contact angles of 0° (Supporting Information).

For a variety of applications, the evaporation behavior of liquids from the sponges could be of major importance. Therefore, we investigated the evaporation of different liquids and differentiated between wetting and non-wetting liquids, sponges of different densities, and methods of liquid delivery into the sponges. The evaporation of a wetting liquid from the sponges was analyzed with ethanol while water was used as a non-wetting liquid. The results clearly showed that the evaporation was very similar, with ethanol, for the sponges P-SG1 and P-SG2 with different densities (Figure 4). The evaporation was also independent of the sponge density for ethanol injected into the sponge and water, but the evaporation rate differed significantly for the wetting and non-wetting liquid that could not be only due to the different vapor pressures of ethanol and water. Therefore, we

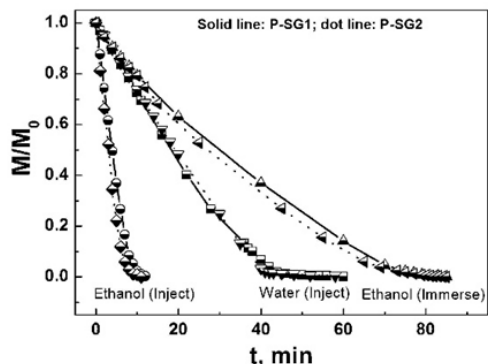


Figure 4. Evaporation of ethanol and water from P-SG1 and P-SG2.

developed a model for the evaporation of ethanol and water from spongy gels.

The so-called  $d^2$ -law for spherical drop evaporation predicts that the drop diameter  $d$  decreases linearly in time.<sup>[8]</sup> Accordingly, the drop volume and thus its mass decreases in time as per Equation (2).

$$M = M_0 \left[ 1 - \frac{2\rho_{av}D}{\rho a_0^2} \ln(1+B)t \right]^{3/2} \quad (2)$$

Herein,  $B = (c_w - c_\infty)/(\rho_{av} - c_w)$  is the Spalding number,  $M$  is the current mass of water in the sample,  $M_0$  is the initial mass of liquid in the sample,  $a_0$  is the initial radius (or a characteristic length) of liquid body,  $D$  is the diffusion coefficient of the liquid vapor in air,  $c_w$  is the saturated liquid vapor concentration over the liquid surface (depending on surface temperature  $T_s$ ),  $c_\infty$  is the liquid vapor concentration in air determined by humidity,  $\rho_{av}$  is the density of the air–vapor mixture,  $\rho$  is the liquid density, and  $t$  is time.

For liquid evaporation in air at room temperature, as in the present case, the vapor concentration is small, which implies that  $(c_w - c_\infty) \ll \rho_{av}$  and  $c_w \ll \rho_{av}$ . Then, the Spalding number  $B \ll 1$ , which means that the Stefan flow is negligibly small and vapor diffusion is dominant compared to the convective transport. Therefore, Equation (2) reduces to Equation (3).

$$M = M_0 \left[ 1 - \frac{2D(c_w - c_\infty)}{a_0^2 \rho} t \right]^{3/2} \quad (3)$$

The surface temperature of evaporating levitating droplets can be calculated quite accurately.<sup>[9]</sup> However, in the present case, the sponge with the evaporating liquid was supported by a metal holder, which inevitably increased the droplet surface temperature due to the high thermal conductivity of metal. Therefore, when calculating the saturated liquid vapor concentration over the liquid surface, the surface temperature  $T_s$  was taken as the values listed in the caption to Figure 5, which illustrates the comparisons of the predictions of [Eq. (2)] for the four experimental cases. Two panels in Figure 5a and 5b correspond to evaporation of a non-wettable liquid (water) from the sponge, while two other panels (Figure 5c and 5d) correspond to evaporation of a wettable liquid (ethanol). In all of the cases, [Eq. (3)] describes the data quite accurately, which ascertains that liquid evaporating from sponge can always be considered as a shrinking-in-time blob. Note also that sample porosities are of the order of  $\varepsilon = 0.9$ . The diffusion coefficient  $D$  decreases with porosity  $\varepsilon$  as  $D = D_0 \varepsilon^{4/3}$ , where  $D_0$  is the value of the vapor diffusion coefficient in open space ( $\varepsilon = 1$ ).<sup>[10]</sup> Because the sample

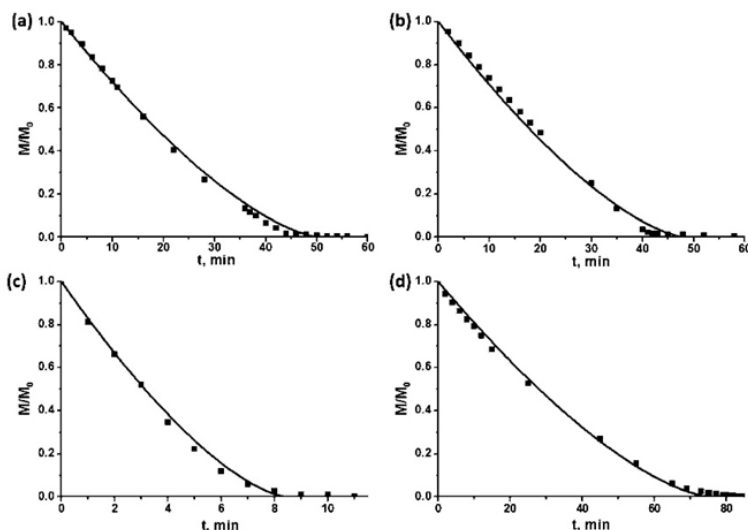
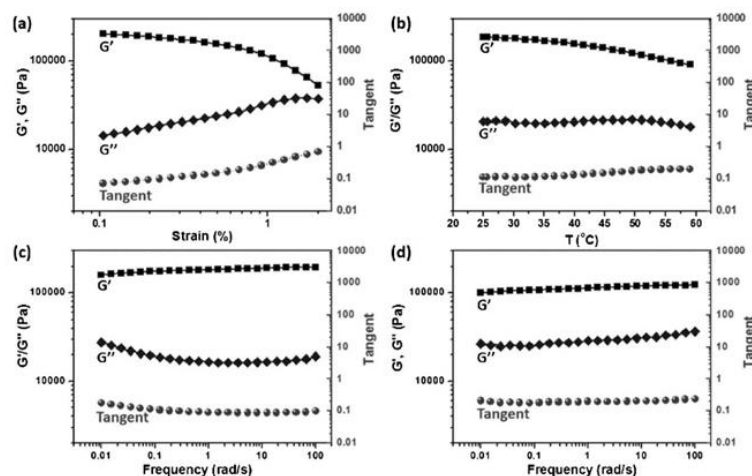


Figure 5. Evaporation from the sponges. a) Non-wettable sponge, 7.57 mg of water;  $T_s = 12^\circ\text{C}$ . b) Non-wettable sponge, 6.38 mg of water;  $T_s = 11^\circ\text{C}$ . c) Wettable sponge, 4.2 mg of ethanol;  $T_s = 12^\circ\text{C}$ . d) Wettable sponge, 190.66 mg of ethanol;  $T_s = 18^\circ\text{C}$ . In all of the cases, the humidity was assumed to be zero.

porosity is at least  $\varepsilon = 0.9$ , the presence of the sponge structure practically does not restrict diffusion of vapor molecules, and accordingly, the value of the diffusion coefficient  $D$  can be taken approximately as  $D_0$ .

Gels are liquid/solid mixtures that show essentially no flow but should display a larger storage modulus  $G'$  than a loss modulus  $G''$ . Dynamic oscillatory shear experiments were carried out with P-SG2 in gel state filled with ethylene glycol (Figure 6). The strain sweep test for P-SG2 filled with ethylene glycol is shown in Figure 6a. The storage modulus



**Figure 6.** Dynamic oscillatory shear rheological properties of P-SG2 gel loaded with ethylene glycol as functions of strain (a), temperature (b), and frequency at 25 (c) and 50 °C (d).

is almost constant at low strains and shows a clear decrease at strains higher than 1 %, whereas  $G''$  shows an increase up to 2 % strain.  $G'$  is higher than  $G''$  in the entire range that has been investigated. For the following measurements (frequency sweep and temperature sweep), a strain of 0.2 % was chosen to ensure that the deformation is within the linear regime. Similar measurements have already been performed on hydrogels in the literature.<sup>[11]</sup> In Figure 6b, the temperature-dependent behavior of the materials shows a much higher storage modulus than the loss modulus over the entire temperature range. This indicates a highly elastic behavior of the material, which is typical for a gel. The frequency tests of the materials at 25 °C and 50 °C can be found in Figure 6c and 6d. The elastic modulus is almost constant and much higher than the storage modulus over the entire frequency range, which is another characteristic gel behavior.

The rheological measurements of the dry sponges can be found in the Supporting Information (Figure S2). The behavior of the dry materials is in general very similar to the ones filled with ethylene glycol. The decrease in storage modulus at higher strains and higher temperatures is, however, a little less pronounced in the dry materials. The loss modulus in all the measurements is lower for the dry materials. This indicates a lower plastic deformation of the dry materials compared to the ethylene-glycol-filled ones.

In conclusion, ultraporous fibrous polymer sponges with tunable porosity and density have been successfully applied to load organic solvents for the formation of spongy gels. These spongy gels were mechanically stable and presented similar rheological behavior to classic organogels. The evaporation behavior of nonwetable and wettable solvents from the spongy gels are successfully described by the  $d^2$  evaporation model, and the evaporation of both solvents could be considered as shrinking-in-time blobs. These spongy gels could find potential applications in drug delivery, bioengi-

neering, catalysts, sensors, lubrication, templates, oil recovery, and optical media, which makes them of particular interest for future materials development.

#### Acknowledgments

We acknowledge financial support from the Deutsche Forschungsgemeinschaft (DFG, SFB 840).

#### Conflict of interest

The authors declare no conflict of interest.

**Keywords:** electrospinning · gels · sponges

- [1] a) S. J. Hollister, *Nat. Mater.* **2005**, *4*, 518–524; b) F. T. Moutos, L. E. Freed, F. Guilak, *Nat. Mater.* **2007**, *6*, 162–167; c) Q. L. Loh, C. Choong, *Tissue Eng. Part B* **2013**, *19*, 485–502.
- [2] a) J. Wu, J. C. Meredith, *ACS Macro Lett.* **2014**, *3*, 185–190; b) M. Y. Kim, J. Lee, *Carbohydr. Polym.* **2011**, *84*, 1329–1336; c) L. Qian, H. Zhang, *J. Chem. Technol. Biotechnol.* **2011**, *86*, 172–184.
- [3] a) G. Duan, S. Jiang, V. Jérôme, J. H. Wendorff, A. Fathi, J. Uhm, V. Altstädt, M. Herling, J. Brec, R. Freitag, *Adv. Funct. Mater.* **2015**, *25*, 2850–2856; b) G. Duan, S. Jiang, T. Moss, S. Agarwal, A. Greiner, *Polym. Chem.* **2016**, *7*, 2759–2764; c) T. Xu, J. M. Miszuk, Y. Zhao, H. Sun, H. Fong, *Adv. Healthcare Mater.* **2015**, *4*, 2238–2246; d) W. Chen, J. Ma, L. Zhu, Y. Morsi, H. El-Hamshary, S. S. Al-Deyab, X. Mo, *Colloids Surf. B* **2016**, *142*, 165–172; e) Y. Si, J. Yu, X. Tang, J. Ge, B. Ding, *Nat. Commun.* **2014**, *5*, 5802.
- [4] R. G. Weiss, *J. Am. Chem. Soc.* **2014**, *136*, 7519–7530.
- [5] Y. Si, Q. Fu, X. Wang, J. Zhu, J. Yu, G. Sun, B. Ding, *ACS Nano* **2015**, *9*, 3791–3799.
- [6] V. Ajay Mallia, R. G. Weiss, *Soft Matter* **2016**, *12*, 3665–3676.
- [7] D. J. Abdallah, R. G. Weiss, *Adv. Mater.* **2000**, *12*, 1237–1247.
- [8] a) L. P. Yarin, G. Hetsroni, *Combustion of Two-phase Reactive Media*, Springer Science & Business Media, Berlin, **2004**; b) W. A. Sirignano, *Fluid Dynamics and Transport of Droplets and Sprays*, Cambridge University Press, Cambridge, **2010**.
- [9] A. L. Yarin, G. Brenn, O. Kastner, D. Rensink, C. Tropea, *J. Fluid Mech.* **1999**, *399*, 151–204.
- [10] E. A. Davidson, S. E. Trumbore, *Tellus Ser. B* **1995**, *47*, 550–565.
- [11] F. Liu, J. Seuring, S. Agarwal, *Macromol. Chem. Phys.* **2014**, *215*, 1466–1472.

Manuscript received: December 4, 2016

Revised: January 18, 2017

Final Article published: ■■■■■■■■■■

## Zuschriften

## Gele

S. Jiang, G. Duan, U. Kuhn, M. Mörl,  
V. Altstädt, A. L. Yarin,\*  
A. Greiner\* 

Spongy Gels by a Top-Down Approach  
from Polymer Fibrous Sponges



**Gel-artige Materialien** entstehen, wenn ultraleichte Schwämme, die aus kurzen, durch Elektrosponnen erhaltenen Fasern aufgebaut sind, mit Lösungsmittel gefüllt

werden. Diese Schwämme bieten zahlreiche neue Möglichkeiten für das Design und die Verarbeitung von Gelen.

**Angewandte**  
Eine Zeitschrift der Gesellschaft Deutscher Chemiker **Chemie**

Supporting Information

**Spongy Gels by a Top-Down Approach from Polymer Fibrous Sponges**

*Shaohua Jiang<sup>+</sup>, Gaigai Duan<sup>+</sup>, Ute Kuhn, Michaela Mörl, Volker Altstädt, Alexander L. Yarin,\*  
and Andreas Greiner\**

ange\_201611787\_sm\_miscellaneous\_information.pdf  
ange\_201611787\_sm\_SI-Video.mp4

## Experimental Section

### Preparation of the P-SG

The PPX coated fiber sponges (P-SG) were prepared according to our previous report.<sup>[1]</sup> 13.5 mL of methyl methacrylate (MMA, Aldrich, 99%), 17.3 mL of methyl acrylate (MA, Aldrich, 99%), 4.6810 g of 4-methacryloyloxybenzophenone (MABP, synthesized according to our previous work<sup>[2]</sup>) and 0.2930 g of 2, 2'-Azobis(isobutyronitrile) (AIBN, Fluka, 98%, purified by recrystallized from methanol) were reacted in DMSO at 70 °C for 5 hours. After that, the copolymer poly(MA-co-MMA-MABP) was precipitated by methanol and dried at 40 °C for 2 days in vacuum oven. The solution for electrospinning was prepared by dissolving 26.20 g of poly(MA-co-MMA-MABP) solution (20 wt%) in dimethyl sulfoxide (DMSO, Fisher Chemical, 99.99%), 2 g of PAN solution (13.2 wt%) in dimethyl formamide (DMF, Fisher Chemical, 99.99%) and 2.68 g of acetone. During electrospinning, a high voltage of 9 kV, a flow rate of 1.5 ml h<sup>-1</sup> and a humidity of 40-60% were applied. The electrospun fibers were collected by an alumina foil and dried in vacuum oven at 40 °C for 24 h. The obtained fibers were firstly cross-linked by UV light (UV lamp 250GS) with a distance of 15 cm for 5 h and then processed into short fiber dispersion with concentration of 7 and 14 mg mL<sup>-1</sup> in dioxane, respectively by a razor blade at a rotation of 5000 rpm for 45 s. 100 mL of the dispersions (7 and 14 mg mL<sup>-1</sup>) were filled in cylindrical glass tubes and freeze-dried at 0.03 mbar for 48 h. The obtained sponges were coated with PPX by chemical vapor deposition (CVD) of 2.20 g of [2.2]paracyclophane with procedure of firstly sublimation at 150 °C and then pyrolysis at 650 °C in pyrolysis oven of the coater under reduced pressure. In deposition chamber, the pyrolysed monomer was formed a PPX film on the surface of the fibers of the sponges at 20 °C under 35 mtorr. The average thickness of the PPX layer was about 1.042 μm, which was measured by analyzing the step height with the profilometer. The densities of the above two P-SG made from 7 and 14 mg mL<sup>-1</sup> dispersions were 16.2 and 30.6 mg cm<sup>-3</sup>, respectively. The P-SG with densities of 16.2 and 30.6 mg cm<sup>-3</sup> were denoted as P-SG1 and P-SG2 respectively.

### Evaporation of water and ethanol from P-SG

The P-SG was cut into small pieces with a size of 0.8 cm × 0.8 cm × 1.0 cm. One small water/ethanol droplet was injected inside of the P-SG by a 1 ml syringe equipped with tiny needle (0.40 mm diameter). The initial weight and the evaporated weight of the liquids were measured by a highly precise analytical balance with readability of 0.01

mg. In another experiment, P-SG1 (0.4 cm × 0.4 cm × 0.6 cm and P-SG2 (0.4 cm × 0.5 cm × 0.7 cm) were immersed into ethanol and completely wetted by the ethanol. The weight of the adsorbent ethanol and the evaporation weight of the ethanol were monitored by the precise analytical balance. The P-SG with small droplet or after immersing in the ethanol were put on a metal holder or fixed by a stainless steel wire as shown in Figure S1. All the measurements were carried out in a constant environment with temperature of 21 °C and humidity of 27%.

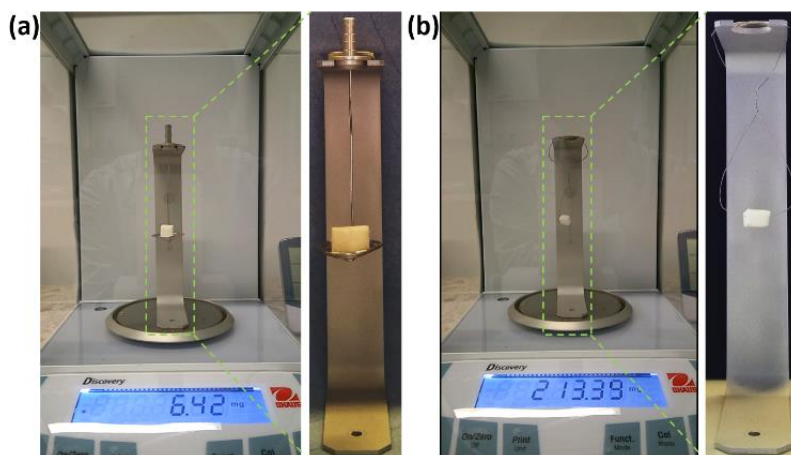


**Figure S1.** Set-up for measurement of liquid evaporation from P-SG. (a) Small liquid droplet was injected in the P-SG and the sample was held by a metal holder; (b) The P-SG was immersed in the ethanol and the sample was fixed by a stainless steel wire.

### Cross-section morphology and porosity of P-SG

The cross-section morphology of the P-SG were observed by scanning electron microscopy (Zeiss Leo 1530). Before the measurement, the samples were sputtered with platinum for 120 s.

### Dynamic oscillatory shear rheological measurement

Dynamic oscillatory shear rheological properties were measured on a MCR 702 from Anton Paar with plate/plate geometry. The strain sweep was carried out in a deformation range from 0.001 to 2% strain at a temperature of 25 °C and a frequency of 1 rad s<sup>-1</sup>. Frequency sweeps were carried out from 100 to 0.01 rad s<sup>-1</sup> at 25 °C and 50 °C with 0.2% strain. Temperature sweeps were carried out from 25 °C to 60 °C with a heating rate of 1 °C min<sup>-1</sup>, 0.2% strain and 1 rad s<sup>-1</sup>. All measurements were carried out in a nitrogen atmosphere.

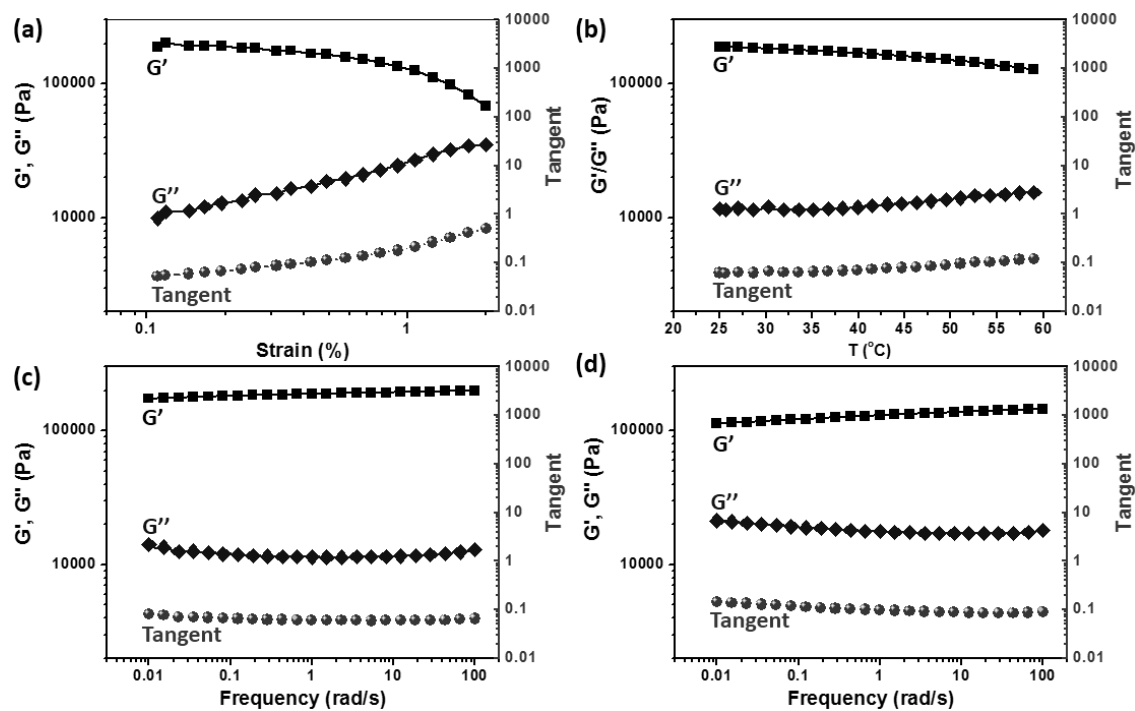


**Figure S2.** Dynamic oscillatory shear rheological properties of P-SG2 in dry state as functions of strain (a), temperature (b), and frequency at 25 (c) and 50 °C (d).

### SI-video

SI-video shows the wetting behavior of ethanol with P-SG.

### References

- [1] G. Duan, S. Jiang, T. Moss, S. Agarwal, A. Greiner, *Polym. Chem.* **2016**, *7*, 2759-2764;
- [2] G. Duan, S. Jiang, V. Jérôme, J. H. Wendorff, A. Fathi, J. Uhm, V. Altstädt, M. Herling, J. Breu, R. Freitag, *Adv. Funct. Mater.* **2015**, *25*, 2850-2856;

## 4 Outlook

Recently, more and more groups are focusing on the research of fibrous sponge from electrospun fibers due to the highly porous structures. The lab scale fabrication of the sponges is nearly perfectly completed and the current applications of the fibrous sponges include tissue engineering, oil/water separation, energy fields, liquid absorption, thermal/acoustic insulations, drug release, and catalysts. However, for this relatively new area of fibrous sponges from electrospun fibers, more investigations are highly required in different aspects.

- (1) Large scale fabrication. Recent studies always prepared the sponges by freeze-drying in lab scale due to the production limitation of the applied freeze-drier. In the future, novel techniques should be developed to satisfy the industrial applications of the sponges, for example, changing the drying procedure, and applying big freeze-drier.
- (2) Solvent problems. The current technique to produce the sponges involved large amounts of solvents, in most cases, organic solvents. In the future, developing new systems with green solvents, such as water, or even without solvents to prepare the fibrous sponges is highly required.
- (3) Wetting behavior. The wetting behavior of the fibrous sponges is very important for practical applications of the sponges. Therefore, detailed investigations on the wetting behavior between sponges and liquid are highly interesting.
- (4) Functionalized sponges. The development of the world requires more and more materials with single or multi functions. In the future, how to prepare functionalized fibrous sponges with single or multi functions will be a big challenge and a hot topic for the scientists from polymer engineering and polymer chemistry.

## 5 Acknowledgements

Herein I want to give my best appreciation to all the people around and thank for their endless help and support for my life during my PhD period.

First I would like to send my thanks to Prof. Dr. Andreas Greiner for the support during my doctor research including the guidance on the projects, financial support, and attending conferences. It is really a pleasure to work with him. Then I want to thank Prof. Dr. Seema Agarwal for her useful suggestions and discussions on my projects.

I would like to present my thanks to Prof. Dr. Haoqing Hou in College of Chemistry and Chemical Engineering, Jiangxi Normal University, for recommending me to Prof. Greiner's group.

I also thank the Deutsche Forschungsgemeinschaft (DFG) and the University of Bayreuth Graduate School for financial support.

Many thanks to the colleagues and cooperators who helped me a lot during my PhD work: Dr. Shaohua Jiang, Dr. Valérie Jérôme, Prof. Dr. Joachim H Wendorff, Dr. Amir Fathi, Jaqueline Uhm, Prof. Dr. Volker Altstädt, Markus Herling, Prof. Dr. Josef Brey, Prof. Dr. Ruth Freitag, Tobias Moss, Dr. Mellisa Koehn-Serrano, Amir Reza Bagheri, Markus Langer and Dr. Roland Dersch.

In particular, I want to thank Dr. Roland Dersch, Annette Krökel, Rika Schneider, Bianca Uch, Martina Heider, Dr. Beate Foerster, Melanie Förtsch and Annika Pfeppenberger for their technical supports.

Many thanks to my colleagues, who provided nice atmosphere around me for my life and study, Dr. Ilka E. Paulus, Dr. Holger Pletsch, Dr. Peter Ohlendorf, Dr. Hui Wang, Dr. Zhicheng Zheng, Dr. Hadi Bakhshi, Lisa Hamel, Florian Käfer, Martin Pretscher, Oliver Hauenstein, Holger Pletsch, Dr. Holger Schmalz, Paul Pineda, Amanda Pineda, Viola Buchholz, Judith Schöbel, Markus Langner, Steffen Reich, Matthias Burgard, Marius Feldmann, Julia Kronawitt, Michael Mader, Pin Hu, Lu Chen, Ziyin Fan, Yinfeng Shi, Li Liu, Xiaojian Liao, Jian Zhu, Minde Jin and Dr. Fangyao Liu.

Special thanks to Cornelia Nicodemus, previous member from Welcome Center,

University of Bayreuth for her help at the beginning of my enrollment at the University of Bayreuth and for the given opportunity to travel to many beautiful towns in Germany.

Appreciations to Tobias Moss and Judith Schöbel for helping me to translate the summary of my PhD thesis into German, to Oliver Hauenstein, Judith Schöbel, Matthias Burgard and Dr. Shaohua Jiang for proof-reading of my thesis.

Last but not least, I would like to deeply thank my family for the endless help and encourages for my life and my study during my PhD studies, especially my husband, Dr. Shaohua Jiang and my son, Zhenhao Jiang.

## 6 List of publications

- (1) **Gaigai Duan**, Amir Reza Bagheri, Shaohua Jiang, Jacob Golenser, Seema Agarwal, Andreas Greiner. Exploration of Macroporous Polymeric Sponges As Drug Carriers. *Biomacromolecules*. **2017**; DOI: 10.1021/acs.biomac.7b00852.
- (2) Jiang S, **Duan G**, Kuhn U, Mörl M, Altstädt V, Yarin AL, Greiner A. Spongy gels by a top-down approach from polymer fibrous sponges. *Angewandte Chemie* **2017**; DOI: 10.1002/ange.201611787.
- (3) **Duan G**, Jiang S, Jérôme V, Wendorff JH, Fathi A, Uhm J, Altstädt V, Herling M, Breu J, Freitag R, Agarwal S, Greiner A. Ultralight, Soft Polymer Sponges by Self-Assembly of Short Electrospun Fibers in Colloidal Dispersions. *Advanced Functional Materials* **2015**, 25(19): 2850-2856.
- (4) **Duan G**, Jiang S, Moss T, Agarwal S, Greiner A. Ultralight open cell polymer sponges with advanced properties by PPX CVD coating. *Polymer Chemistry* **2016**, 7: 2759-2764.
- (5) **Duan G**, Mellisa Koehn-Serrano, Andreas Greiner. Highly Efficient Reusable Sponge-Type Catalyst Carriers Based on Short Electrospun Fibers. *Macromolecular Rapid Communications* **2017**, 38: 1600511.
- (6) Jiang S, **Duan G**, Zussman E, Greiner A, Agarwal S. Highly flexible and tough concentric triaxial polystyrene fibers. *ACS Applied Materials & Interfaces* **2014**, 6(8): 5918-5923.
- (7) Jiang S, **Duan G**, Hou H, Greiner A, Agarwal S. Novel layer-by-layer procedure for making nylon-6 nanofiber reinforced high strength, tough, and transparent thermoplastic polyurethane composites. *ACS Applied Materials & Interfaces* **2012**, 4(8): 4366-4372.
- (8) Jiang S, **Duan G**, Schöbel J, Agarwal S, Greiner A. Short electrospun polymeric nanofibers reinforced polyimide nanocomposites. *Composites Science and Technology* **2013**, 88: 57-61.

---

**(Eidesstattliche) Versicherungen und Erklärungen**

(§ 8 S. 2 Nr. 6 PromO)

*Hiermit erkläre ich mich damit einverstanden, dass die elektronische Fassung meiner Dissertation unter Wahrung meiner Urheberrechte und des Datenschutzes einer gesonderten Überprüfung hinsichtlich der eigenständigen Anfertigung der Dissertation unterzogen werden kann.*

(§ 8 S. 2 Nr. 8 PromO)

*Hiermit erkläre ich eidesstattlich, dass ich die Dissertation selbständig verfasst und keine anderen als die von mir angegebenen Quellen und Hilfsmittel benutzt habe.*

(§ 8 S. 2 Nr. 9 PromO)

*Ich habe die Dissertation nicht bereits zur Erlangung eines akademischen Grades anderweitig eingereicht und habe auch nicht bereits diese oder eine gleichartige Doktorprüfung endgültig nicht bestanden.*

(§ 8 S. 2 Nr. 10 PromO)

*Hiermit erkläre ich, dass ich keine Hilfe von gewerblichen Promotionsberatern bzw. -vermittlern in Anspruch genommen habe und auch künftig nicht nehmen werde.*

.....  
Ort, Datum, Unterschrift